THE D.C. DISC ARMATURE TRACTION MOTOR

Research into the design and performance of d.c. axial-field machines for use in battery electric traction

by

C.S. Roerig

A thesis submitted to the University of Warwick for the degree of Doctor of Philosophy based upon research conducted in the Department of Engineering

March 1981

CONTENTS

	Page
List of tables	iv
List of figures	v
Acknowledgements	ix
Summary	xi
List of principal symbols	xii
1: Introduction	1
2: Principles of machine operation	4
2.1 Considerations for the magnetic circuit	12
2.1.1 Magnetic circuit parameters	17
2.1.2 Magnetic field in the airgap	22
2.2 General machine considerations	28
3: Use of the motor in traction applications	35
3.1 The 930W traction motor	38
3.2 The 1.1kW traction motor	42
3.3 The 2.5kW traction motor	45
3.4 The 1.9kW traction motor	50
3.5 Considerations for a further prototype	56
3.5.1 Considerations for the vehicle specification	56
3.5.2 Considerations for the motor specification	57
3.6 Other axial-field traction machines	62
3.6.1 Flinders university electric vehicle project	62
3.6.2 Cambridge university electric bicycle	64
3.6.3 T.R.R.L. electric moped	65
4: Machine design and performance prediction	66
4.1 Considerations for magnet material choice	68
4.1.1 Manufacture of different materials	73
4.1.2 Effect of magnet choice on motor design	77

4.2 Initial requirements for the design procedure 77
4.3 Development of the software 80
4.3.1 Initial considerations for design stage 1 82
4.3.2 Operation of design stage 1 85
4.3.3 Performance prediction by design stage 1 93
4.3.4 Operation of design stage 2 100
4.3.4.1 Generation of numerical results 100
4.3.4.2 Generation of graphical results 105
4.4 Analysis of armature windings 106
4.4.1 Initial considerations for armature windings 107
4.4.2 Calculation of e.m.f.s induced in armature paths 109
4.4.3 Application to the duplex wave winding 121
5: Construction and performance of a duplex wave motor 131
5.1 Construction of stator and armature 133
5.2 Performance of the magnetic circuit 144
5.3 Performance of the motor 149
5.4 Rating of disc armature motors 159
6: Application to battery electric vehicles 167
6.1 The electric vehicle system model 168
6.1.1 Consideration of the road losses 169
6.1.2 Consideration of the transmission 173
6.1.3 Consideration of the electric traction motor 180
6.1.3.1 Series wound motor 181
6.1.3.2 Disc armature motor 188
6.1.4 Consideration of the controller 191
6.1.5 Consideration of the traction battery 197
6.2 Application of the vehicle model 204
7: Preparation and testing of road vehicle 212
7.1 Vehicle conversion and instrumentation 212
7.2 Road testing procedure 220
7.3 Results from road testing 221
8: Conclusions and suggestions for further work 227

6: References 231

Appendix I: An alternative ferrite design 238

Appendix II: Further traction applications 243

A2.1 The 130W, 2000 rev/min motor 243

A2.2 The 130W, 4000 rev/min motor 243

A2.3 The 20kW motor 249

Appendix III: Further application of the e.m.f. analysis 256

Appendix IV: Selected published papers 262

LIST OF TABLES

		Page
2.1	Physical properties of different magnet materials	18
2.2	Magnetic properties of different magnet materials	18
3.1	Design parameters for 930W motor	39
3.2	Design parameters for 1.1kW motor	46
3.3	Design parameters for 1.9kW motor	53
3.4	Design parameters for 7.5kW motor	59
4.1	Original C.A.D. input data sheet	67
4.2	Predicted and measured values of mechanical loss	99
4.3	New C.A.D. input data sheet	101
5.1	Specification of epoxy resin for encapsulation	141
5.2	Voltages measured between like brushes	152
5.3	Predicted voltages between like brushes	152
6.1	Efficiency map - E.D.C. series wound motor	189
6.2	Efficiency map - 7.5kW disc armature motor	190
6.3	Results of computer simulation - E.D.C. motor	208
6.4	Results of computer simulation - E.D.C. motor	209
6.5	Results of computer simulation - disc armature motor	210
6.6	Results of computer simulation - disc armature motor	211
7.1	Test results for electric vehicle	222
7.2	Theoretical results corresponding to Table 7.1	224
7.3	Theoretical results corresponding to Table 7.1	226
A1.1	Design parameters for 7.5kW ferrite motor	239
A2.1	Design parameters for 130W, 2000 rev/min motor	244
A2.2	Design parameters for 130W, 4000 rev/min motor	247
A2.3	Design parameters for each 'half' of 20kW motor	253

LIST OF FIGURES

		Page
1.1	Comparative efficiency curves	2
2.1	Schematic of Faraday's disc	5
2.2	Schematics of conventional and disc armature motors	5
2.3	Typical disc armature motor	7
2.4	Schematics of alternative magnetic arrangements	8
2.5	Printed circuit motor	10
2.6	Schematic of a typical magnetic circuit	13
2.7	Typical intrinsic and normal demagnetisation curves	14
2.8	Demagnetisation curves of different materials	16
2.9	Recoil operation of a magnet material	20
2.10	Magnet segment for field distribution	23
2.11	Normal demagnetisation curve for Hycomax III	25
2.12	Average airgap flux density in Hycomax III system	27
2.13	Schematic of magnets with single-turn coil	29
3.1	Disc motor features	36
3.2	Schematic of 930W motor	41
3.3	Performance curves of 930W motor	43
3.4	Application of 930W motor	44
3.5	Schematic of 1100W motor	48
3.6	Performance curves of 1100W motor	49
3.7	Schematic of 2.5kW motor	51
3.8	Schematic of 'wheel motor' unit	54
3.9	Prototype wheel motor unit	55
3.10	Reliant Robin vehicle	55
3.11	Predicted performance of 7.5kW motor	61
3.12	Mechanical layout of 7.5kW motor	63
4.1	Computer-produced curves	69

4.2 Demagnetisation curves for various Alnico materials 75
4.3 Remote computer terminal 81
4.4 Flowchart of design stage 1 86
4.5 Mechanical loss versus speed 96
4.6 Flowchart of design stage 2 103
4.7 Diagram for typical 8 pole, 40 coil lap winding 111
4.8 Diagram for typical 8 pole, 41 coil wave winding 112
4.9 Representation of lap winding by coil sides 113
4.10 Representation of lap winding after rotation 115
4.11 Representation of wave winding (8 brushes) 116
4.12 Representation of wave winding (2 brushes) 117
4.13 Representation of winding pattern 120
4.14 Diagram for 7.5kW motor - winding option 1 123
4.15 Representation of winding option 1 by coil sides 124
4.16 Diagram for 7.5kW motor - winding option 2 125
4.17 Representation of winding option 2 by coil sides 126
4.18 E.m.f.s generated in both winding options (2 brushes) 127
4.19 E.m.f.s generated in both winding options (4 brushes) 128
4.20 E.m.f.s generated in both winding options (8 brushes) 129
5.1 Assembly drawing for 7.5kW motor 132
5.2 Magnets used in 7.5kW motor 135
5.3 Half stator assembly of 7.5kW motor 135
5.4 Winding formers 136
5.5 Coils and commutator 136
5.6 Complete set of armature coils 138
5.7 Coils connected to commutator 138
5.8 Encapsulation mould 139
5.9 Armature windings positioned in mould 140
5.10 Complete armature 140
5.11 7.5kW motor - disassembled 143
5.12 7.5kW motor - assembled 143

4.2 Demagnetisation curves for various Alnico materials 75
4.3 Remote computer terminal 81
4.4 Flowchart of design stage 1 86
4.5 Mechanical loss versus speed 96
4.6 Flowchart of design stage 2 103
4.7 Diagram for typical 8 pole, 40 coil lap winding 111
4.8 Diagram for typical 8 pole, 41 coil wave winding 112
4.9 Representation of lap winding by coil sides 113
4.10 Representation of lap winding after rotation 115
4.11 Representation of wave winding (8 brushes) 116
4.12 Representation of wave winding (2 brushes) 117
4.13 Representation of winding pattern 120
4.14 Diagram for 7.5kW motor - winding option 1 123
4.15 Representation of winding option 1 by coil sides 124
4.16 Diagram for 7.5kW motor - winding option 2 125
4.17 Representation of winding option 2 by coil sides 126
4.18 E.m.f.s generated in both winding options (2 brushes) 127
4.19 E.m.f.s generated in both winding options (4 brushes) 128
4.20 E.m.f.s generated in both winding options (8 brushes) 129
5.1 Assembly drawing for 7.5kW motor 132
5.2 Magnets used in 7.5kW motor 135
5.3 Half stator assembly of 7.5kW motor 135
5.4 Winding formers 136
5.5 Coils and commutator 136
5.6 Complete set of armature coils 138
5.7 Coils connected to commutator 138
5.8 Encapsulation mould 139
5.9 Armature windings positioned in mould 140
5.10 Complete armature 140
5.11 7.5kW motor - disassembled 143
5.12 7.5kW motor - assembled 143

5.13 Actual demagnetisation curve of Hycomax III magnets 145
5.14 Flux density in airgap at grid points 147
5.15 Average airgap flux density in 7.5kW motor 148
5.16 Measurement of e.m.f.s generated at non-powered brushes 151
5.17 Schematic of Ward Leonard testing apparatus 154
5.18 Performance curves of 7.5kW motor - winding option 1 155
5.19 Performance curves of 7.5kW motor - winding option 2 156
5.20 Computer predicted curves for 7.5kW motor 157
5.21 Armature temperature/time curves for traction motor 163
5.22 Armature temperature/time curves for various motors 164
6.1 Block diagram of electric vehicle system 170
6.2 Coefficient of rolling resistance versus speed 172
6.3 Efficiency versus output speed and torque - 1st gear 175
6.4 Efficiency versus output speed and torque - 2nd gear 176
6.5 Efficiency versus output speed and torque - 3rd gear 177
6.6 Efficiency versus output speed and torque - top gear 178
6.7 Efficiency versus output speed and torque - differential 179
6.8 Performance curves of E.D.C. series wound motor 182
6.9 Idealised linear flux/current relationship 183
6.10 Effective flux versus current (E.D.C. motor) 184
6.11 Performance of E.D.C. motor as predicted by model 187
6.12 Operation of chopper controller 192
6.13 Typical chopper circuit 193
6.14 Model of chopper controller 196
6.15 Normalised battery capacity versus normalised current 201
6.16 Cell voltage versus normalised discharge current 202
6.17 Cell voltage versus depth of discharge 203
6.18 Flowchart of vehicle simulation program 206
7.1 E.D.C. series wound traction motor 213
7.2 E.D.C. motor in Reliant vehicle 213
7.3 Fitting the motor into the vehicle 215

7.4 Typical chopper controller 217

A1.1 Predicted performance of 7.5kW ferrite motor 241

A2.1 Predicted performance of 130W, 2000 rev/min motor 245

A2.2 Measured performance of 130W, 2000 rev/min motor 246

A2.3 Predicted performance of 130W, 4000 rev/min motor 250

A2.4 Measured performance of 130W, 4000 rev/min motor 251

A2.5 Mechanical layout of 20kW motor 252

A2.6 Predicted performance of 20kW motor at 96V 255

A2.7 130W motors 248

A3.1 Connection diagram for 31 coil, 10 pole motor 257

A3.2 E.m.f.s generated in 31 coil, 10 pole armature (2 brushes) 259

A3.3 E.m.f.s generated in 31 coil, 10 pole armature (4 brushes) 260

A3.4 E.m.f.s generated in 31 coil, 10 pole armature (10 brushes) 261

7.4 Typical chopper controller 217

A1.1 Predicted performance of 7.5kW ferrite motor 241

A2.1 Predicted performance of 130W, 2000 rev/min motor 245

A2.2 Measured performance of 130W, 2000 rev/min motor 246

A2.3 Predicted performance of 130W, 4000 rev/min motor 250

A2.4 Measured performance of 130W, 4000 rev/min motor 251

A2.5 Mechanical layout of 20kW motor 252

A2.6 Predicted performance of 20kW motor at 96V 255

A2.7 130W motors 248

A3.1 Connection diagram for 31 coil, 10 pole motor 257

A3.2 E.m.f.s generated in 31 coil, 10 pole armature (2 brushes) 259

A3.3 E.m.f.s generated in 31 coil, 10 pole armature (4 brushes) 260

A3.4 E.m.f.s generated in 31 coil, 10 pole armature (10 brushes) 261

ACKNOWLEDGEMENTS

One of the pleasures of writing this thesis has been to record the assistance (practical and otherwise) of many people who have been involved in the research.

My sincere gratitude is extended to my academic supervisor, Mr. A.E. Corbett, for encouragement, assistance and patience over the last few years, and for many helpful comments and suggestions.

Along with other research projects requiring the construction of hardware, the research described here would not have been possible without the skill and dedication of the staff in the departmental workshops. Although many have contributed in various ways, I would particularly like to thank David Thompson, Ron Fathers and Mike Legg for valuable assistance with construction of the disc armature motor and the electric vehicle conversion.

To my friends and colleagues (past and present) in the Electrical Machines Group at Warwick, I wish to express my thanks for not only taking a genuine and helpful interest in the research, but also providing an excellent working (and social!) environment.

The electric vehicle conversion project was made much easier by the close involvement of two industrial companies. I wish to thank Mr. J.V. Woods and Colin Wolfe of the Electro Dynamic Construction Co. Ltd. for supplying the series wound motor and much helpful advice, and John Morton and Cliff Watson of Cableform Ltd. for assistance with the electronic controller and the supply of prototypes. For financial support during the research, I thank the

Science Research Council, and Cableform Ltd.

While it is impossible to mention everyone by name, I further thank all who have contributed in any way to the work described here.

Most of the writing has been carried out after leaving the University and I would like to thank my present company, Moore Reed and Co. Ltd., and in particular Mr. R.J. Smith, for patience, understanding of the problems involved and many helpful suggestions.

Finally, my particular thanks go to Mrs. Loraine Birch for converting my unintelligible hieroglyphics into readable prose.

SUMMARY

With growing interest in battery electric vehicles, the use of the disc armature motor, with its inherent high efficiency and power density, is investigated for such applications. With the need to establish an optimum design for a given specification a computer-aided design procedure is developed with due regard to the motor operating principles and the performance of existing prototypes. This procedure presents a large number of alternative designs to meet a specification in terms of the voltage, power and speed requirement. The magnet material to be used is the only other necessary input to the program, although various restrictions may be applied if desired. With the use of a duplex wave winding sometimes called for, and in certain cases alternative methods of connection available, a study is made of a particular winding in terms of the e.m.f.s generated in the primary armature paths and those short-circuited by the brushes. It is shown that an optimum arrangement exists and if this is not specified,significant deterioration in motor performance results as verified experimentally. The thermal performance of the motor is discussed and appropriate rating conditions are proposed as an aid to future design. Finally the use of the motor in a practical application is studied with the aid of a simulation model of an electric vehicle and practical road testing. It is shown that improvements in overall vehicle performance result when a disc armature motor is specified in place of a comparable series wound machine.

LIST OF PRINCIPAL SYMBOLS

Symbols represented as strings of capital letters usually refer to those used in a computer program or associated output.

a	number of parallel paths in a d.c. machine.
A	brush contact area
A_F	frontal area of road vehicle
α,ALPHA	ratio of pole arc to pole pitch
ARMCRT	armature current
$B_{i,j}$	flux density at position (i,j) in polar co-ordinates.
B_g	airgap flux density
B_m,BM	magnet flux density
BMS	maximum allowable flux density in mild steel
B_r	remanance, on demagnetisation curve
C,CRTDSY	current density in armature conductors
C_B	battery capacity
C_D	vehicle drag coefficient
COILS	number of coils in a d.c. machine
D	duty cycle for electronic controller
d_1,D1	inner active diameter of disc armature motor
d_2,D2	outer active diameter of disc armature motor
D_s	percentage discharge of battery
η,EFF	efficiency
E,ER	generated e.m.f.
e_j	e.m.f. induced in conductor at angular position j
F_a	retarding force due to aerodynamic drag
F_r	total retarding force

FRR	flux-return ring
G, GAUGE	gauge of wire used in armature
GAP	magnetic airgap length
H_g	magnetising force in airgap
H_m,HM	magnetising force in magnet
I	(armature) current
I_B	current drawn from battery
I_{BA}	average current drawn from battery
I_M	motor current
I_N	normalised battery current) see text
I_R	rated battery current) see text
K_1	coefficient of rolling resistance
K_2	coefficient of aerodynamic retarding force
L, LAY	number of layers of armature conductors
LC,LCOEFF	leakage coefficient
LF,LFACT	loss factor
lg	length of magnetic airgap
l_m,LMAG	length of magnet
LOSS	electrical losses in disc armature motor
M	intrinsic magnetisation
MAGDSY	density of magnet material
MECHLO	mechanical loss
M_s	pole strength on magnet face
M_v	mass of road vehicle
μ_o	permeability of free space
n	rotational speed, rev/min.
ω	rotational speed, rad/sec.
p, POLES	number of poles in a d.c. machine
P	power output (gross)

PATHS	number of parallel paths in a d.c. machine
Ø, PHI	flux per pole
$Ø_{eff}$	effective working flux
$Ø_s$	saturation flux
p_r, PR	power output (net)
PWRWGT	ratio of motor power to motor weight, power density
Ψ	magnetic potential
ρ	density of air
Ra, RARM	armature resistance
R_c	resistance of a single coil
r_1	inner active radius of disc armature motor
r_2	outer active radius of disc armature motor
SF	space factor
T	mechanical torque
TEMP	armature temperature at which motor performance is calculated
THICK	thickness of flux-return ring
T_m	discharge time for a battery
T_r	rated torque
TURNS	turns per coil
TOTWGT	total weight of motor
t_1	on time for electronic chopper controller
t_2	off time for electronic chopper controller
v	speed of road vehicle
V	voltage
V_{av}	average voltage from electronic controller
V_b	brush voltage drop
V_B	battery voltage
V_{D1}	voltage across a diode
V_M	motor voltage

V_{MA}	average motor voltage
V_N	voltage between negative brushes
V_P	voltage between positive brushes
V_S	supply voltage
V_T	voltage across a thyristor
WGTFRR	weight of flux-return ring
WGTMAG	weight of magnets
WGTNAP	weight of 'non-active parts' (see text)
WGTWIR	weight of copper used in armature winding
W_m	mechanical loss
z,Z	number of conductors in an armature
z_i	ideal number of conductors

1: INTRODUCTION

Events of the past decade have led to much uncertainty over the availability and security of the oil supplies upon which this and other industrialised nations depend. Together with the tenfold increase in the price of crude oil in the period from January 1970 to July 1979, this has led to an increasing awareness of the finite nature of the world's natural energy resources, and many studies have been initiated[1-7] to try and determine how long these resources are likely to last. It is in the transport sector, and in particular road transportation where 79% of petroleum is used[4], that shortages and price increases are quickly felt. This has led to a resurgence of interest in battery electric vehicles which many think will form a large proportion of future transportation. Much recent research and development effort, a great deal funded by various governments, has been expended in this area[8-17] to try and achieve an economic vehicle with acceptable performance. A recent study[18] predicted that if care is taken over vehicle component selection, aerodynamics and the like, dramatic increases in range would be possible. One of the major contributing factors to this improvement in vehicle performance is the specification of a permanent magnet d.c. disc armature motor in place of the more conventional series wound machine. This motor has found varied applications[19] but its use in battery electric traction is not widespread. The motor has a high working efficiency and Fig. 1.1 shows efficiency curves for a disc armature motor and a comparable series wound motor. The improvement in efficiency is most apparent at the lower values of input current.

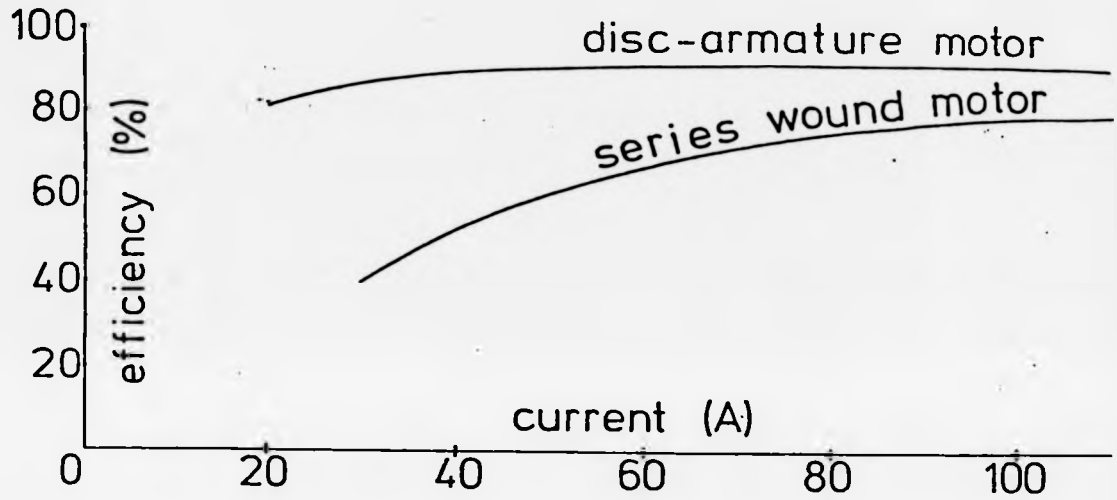

Fig. 1.1 : Comparative Efficiciency Curves

The reasons for this improved machine performance are the use of an ironless armature which eliminates hysteresis and eddy-current loss, and the use of a permanent magnet field system.

Since the invention of the wire-wound version of the machine in 1967[20], much research effort has been expended on the motor with the result that a growing interest in its production has been shown by several manufacturers. Although the motor was originally intended for traction use, it is not in this field that it has found most application and only limited experience in traction has been gained. To rectify this, several projects have been initiated at Warwick University involving the design, construction and performance assessment of disc armature motors for use in battery electric and hybrid vehicles. The principles of the machine have been studied at great length[21,22] and comparable attention needs to be paid to the design procedures involved and their relation to the performance of the machine especially when applied to electric traction. There have been no quick and reliable methods of determining the optimum design parameters for a given application and much design has been done on a trial and error basis. Thus, it was felt necessary to reappraise the design methods available and highlight aspects of design and performance peculiar to this type of machine. Although the research was primarily directed towards traction machines, much of the work relates to disc armature motors generally and results can easily be applied to motors for any application.

2: PRINCIPLES OF MACHINE OPERATION

The concept of an axial-field machine is not a new one. Michael Faraday used exactly this principle to demonstrate the first rotating electromagnetic machine (Fig. 2.1). To produce maximum useful torque from a machine of this type the 'armature' current must flow in a radial direction across the magnetic field. It is also apparent that as it stands the machine would need to be operated at a low voltage while supplying high currents. Thus, to be of more general use, a multipolar arrangement would be necessary with the ability to incorporate an armature winding more closely related to those used today. Developments in d.c. motor design have resulted in the now familiar construction employing longitudinal conductors embedded in a laminated iron core and interacting with a radial magnetic field. Manufacturing techniques have been established to support large-scale production of such motors and thus any radical departure from conventional designs, such as an axial field arrangement, would rarely be able to compete economically unless similar techniques were made available. For these reasons, relatively little research and development has been carried out on axial field machines, although several different types have been proposed over the years, including the superconducting homopolar motor and the printed circuit motor. Of these, only the latter has found commercial application with a range of machines available. The essential differences between a conventional d.c. machine and an axial field d.c. machine are shown in Fig. 2.2. The conventional layout is

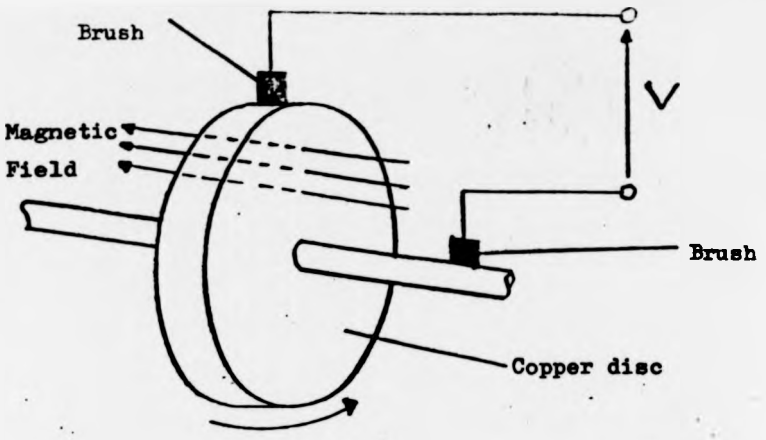

Fig. 2.1 : Schematic of Faraday's Disc

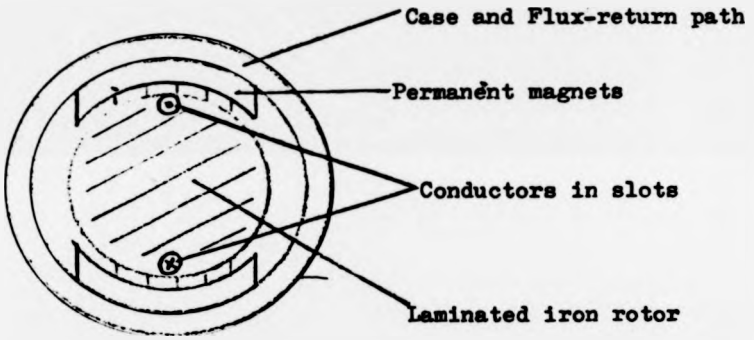

Fig. 2.2(a): Schematic of conventional motor

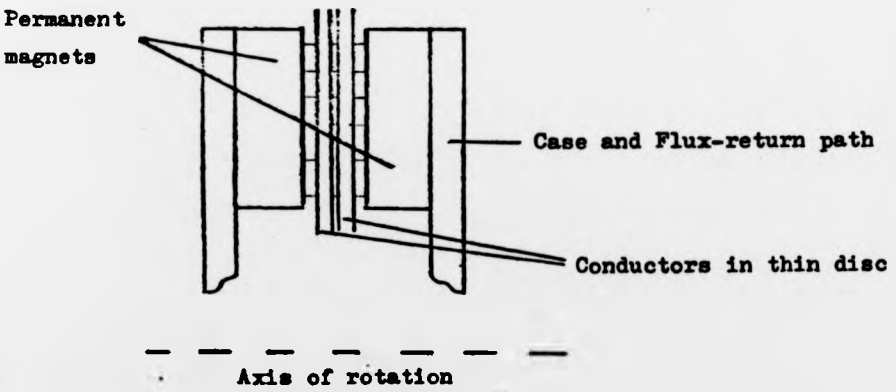

Fig. 2.2(b) : Schematic of disc armature motor

shown schematically in Fig. 2.2(a), a section across the machine, and the flux produced by the stationary poles is seen cutting the armature conductors situated in the rotor slots - for clarity, only two conductors are shown. For good magnet utilisation, the rotor must be constructed of a magnetic material, and since it rotates in the magnetic field, it must be laminated to reduce hysteresis and eddy-current loss. A typical axial field schematic is given in Fig. 2.2(b) which is a section along the machine showing a pair of poles and again two conductors. The armature conductors are located in or on a thin disc which rotates in the gap between opposite poles. It is not essential to have iron in the armature and in most cases an iron-free construction is used. The airgap will therefore be relatively long and this must be considered when specifying the field system - permanent magnets being the only feasible choice. The magnetic circuit is completed by mild steel rings onto which the magnets are bonded and which provides a path to adjacent magnets which will be of opposite polarity. These flux-return rings can often form part of the motor case as can be seen in Fig. 2.3 which is an exploded view of a typical wound-armature axial-field motor. To include rotating iron in the armature, thus reducing the effective magnetic airgap and therefore the amount of magnet material needed, is not a straightforward process. A laminated structure would be very thin, and as radial teeth would need to be impressed to accommodate the conductors, it would also be very fragile. The use of iron powder in the disc has been investigated[23] either as a rotating flux return path, Fig. 2.4(b), or filling the disc completely, Fig. 2.4(c). The latter method may still necessitate the use of a

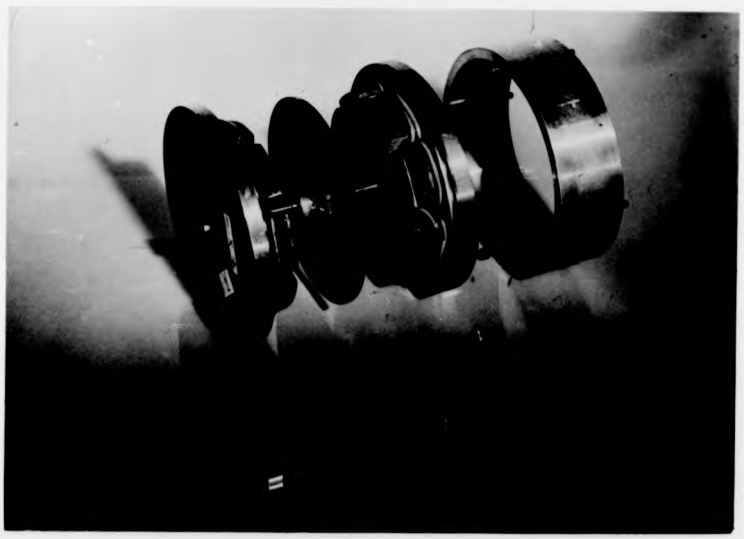

Fig. 2.3 : Typical disc armature motor

Fig. 2.3 : Typical disc armature motor

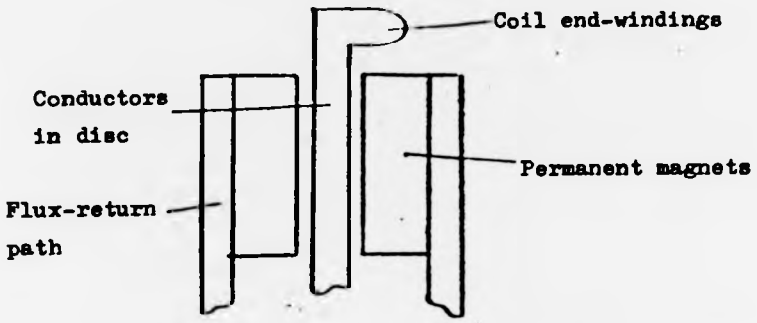

Fig. 2:4(a) : Schematic of iron-free encapsulation

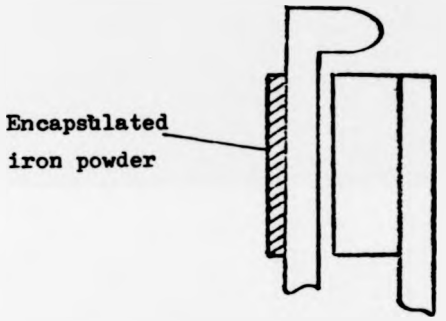

Fig. 2.4(b) : Schematic of rotating flux-return ring

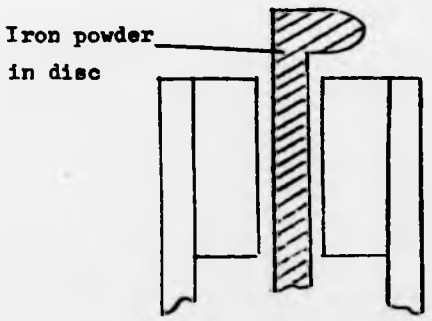

Fig. 2.4(c) : Schematic of iron-loaded encapsulation

second stationary magnet (or steel ring) depending on the detailed construction. As indicated earlier, the layout illustrated in Fig. 2.4(a) is generally used in axial field or 'disc-armature' d.c. machines which has the advantage of eliminating all iron losses.

In the above discussion, it has been assumed that it is possible to construct an armature winding equivalent to that used in conventional d.c. machines. There are, at present, two methods of achieving such an arrangement, namely that used in the printed circuit motor mentioned earlier, and the wound armature version for which a patent was applied in 1967 (granted in 1971) and which is the subject of this research. The armature of a printed circuit motor consists of a thin insulating disc onto both sides of which are bonded copper conductors. At the periphery of the disc, conductors from either side are joined. Power to the armature is supplied by brushes bearing directly onto the inner ends of the conductors. Fig. 2.5 shows an exploded view of a printed circuit motor with all the component parts clearly visible. It will be noted that the magnetic poles are circular, for ease of manufacture, and that in this case windings are employed for magnetisation after assembly. Such windings are also apparent in Fig. 2.3 and their need is discussed later. This type of machine has established itself in applications where good efficiency, short axial length or low armature inertia are advantageous. In spite of these advantages, a more robust and reliable motor has been developed that is more suited to applications involving conditions of overload, for example, electric traction. This is the wound armature axial field d.c. motor and it is more conventional in that copper wire is used to

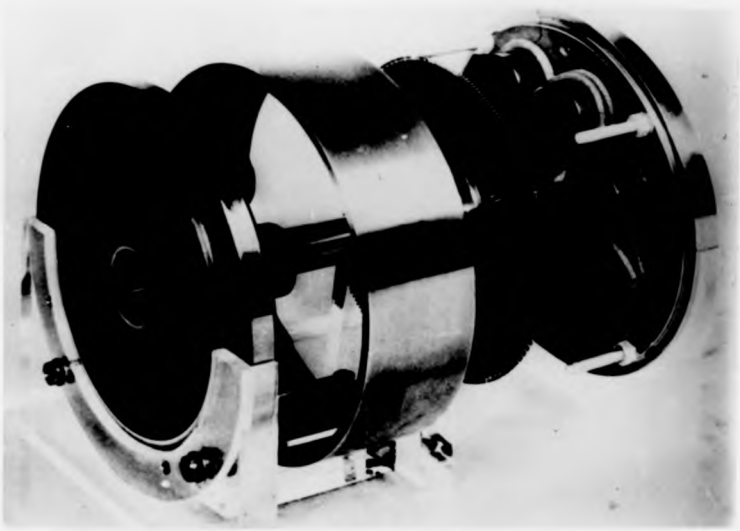

Fig. 2.5 : Printed circuit motor

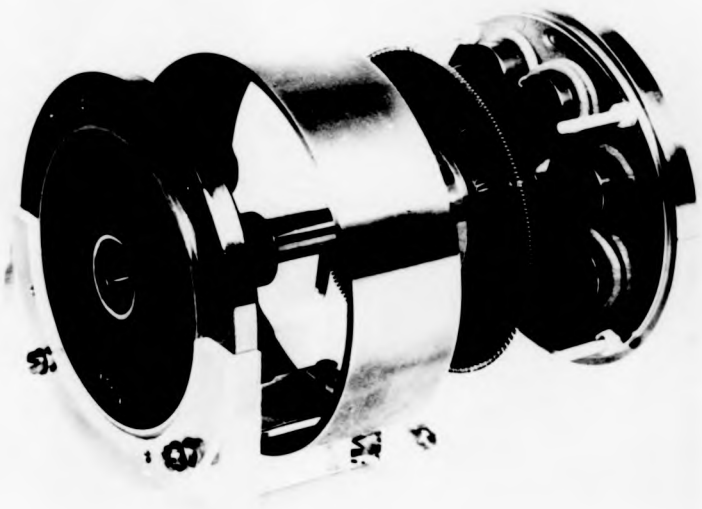

Fig. 2.5 : Printed circuit motor

form multi-turn coils. The coils themselves are individually wound (for prototypes) and then nested together to form generally a two-layer winding (although four layers and even a single layer version have been used). After connecting the coil ends to a conventional commutator, in any of the usual lap or wave configurations, the complete assembly is then encapsulated in an epoxy resin for mechanical strength and rigidity. A typical motor has been shown in Fig. 2.3 and it will be noted that the magnetic poles are shaped as segments (c.f. circular magnets in Fig. 2.5) as it is possible to get a more uniform flux distribution in the airgap using this shape. Advantages of this construction over the printed circuit motor include the protection of the winding and associated connections from the elements, the ability to use conventional brushgear on the commutator and the potential of the machine for use in applications such as traction. Printed circuit motors have been investigated for traction use (see section 3.6.1) but the overload current has been limited with special control/transmission arrangements. The inventors of the wound armature version of the motor (henceforth designated the d.c. disc-armature motor) originally intended that it should be used to drive electric vehicles, and this aspect will be covered in Chapter 3. Although any rotating electrical machine is dependent on common physical laws, there are certain operating principles of the d.c. disc-armature motor that warrant separate attention and these will be detailed in the following sections.

2.1 Considerations for the magnetic circuit

In the disc armature motor the magnetic airgap is relatively large, comprising the total disc thickness and a suitable running clearance between it and the pole faces. With reference to Fig. 2.6, the magnetising force in the airgap, Hg, can be related to the magnet and airgap lengths and the magnetising force of the magnet, Hm, by:-

$$Hg.lg = Hm.lm/LF \qquad (2.1)$$

where LF (the loss factor) allows for the non-infinite permeability in the remainder of the magnetic circuit, and here is greater than one. Thus it can be seen that to accommodate a large airgap while maintaining a given field strength in it requires either a long magnet or one with a high coercive force. In order that the machine weight does not become excessive the latter course is usually chosen with suitable materials being the common and inexpensive ferrites, or in exceptional cases, exotic and highly expensive rare-earth magnets. However, the ferrite material does have a significant disadvantage in its low specific energy content (J/m^3), and the relatively low values of flux density available.

Fig. 2.7 shows the normal and intrinsic demagnetisation curves for a magnetic material - for the purpose of machine design/ operation it is only necessary to consider the normal curve. Marked on the curve is the point where the product of the remanance and coercivity is a maximum. This BH_{max} point corresponds to the maximum energy available from the material and thus to optimum

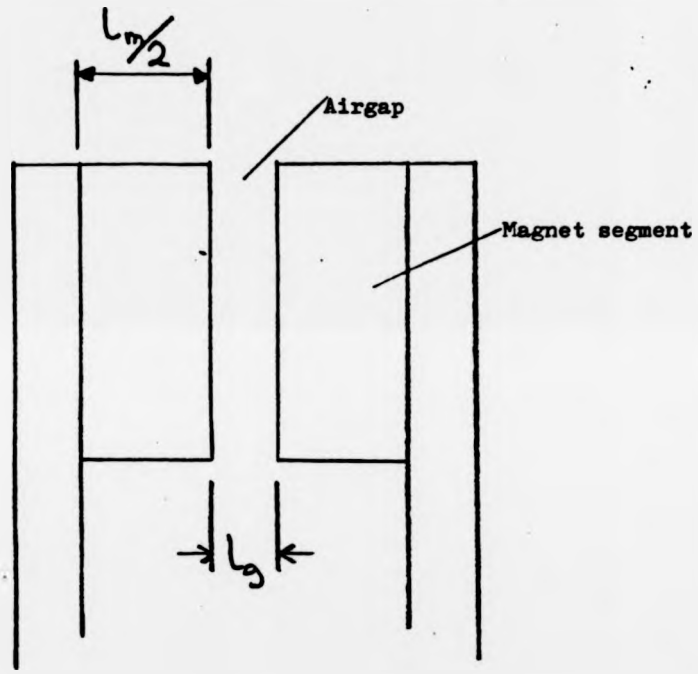

Fig. 2.6 : Schematic of a typical magnetic circuit for the disc armature motor

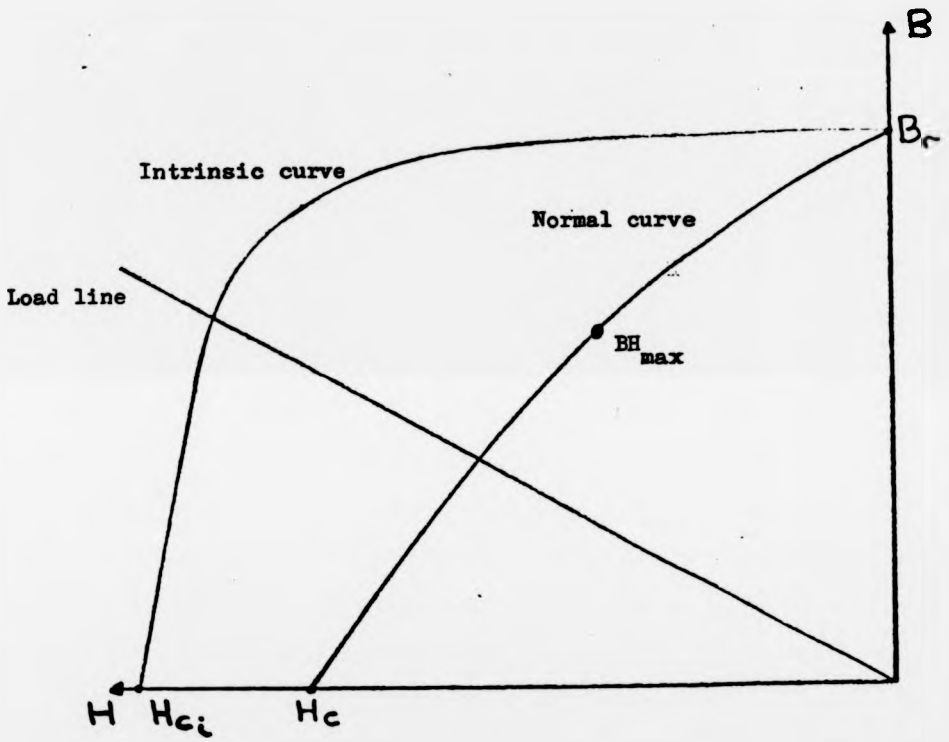

Fig. 2.7 : Typical intrinsic and normal demagnetisation curves

usage. A load line is also illustrated, and neglecting the loss factor in equation (2.1) and any leakage effects this line may be defined as having a slope:-

$$\frac{B}{H} = - \frac{4\pi \times 10^{-7} \times l_m}{l_g} \qquad (2.2)$$

Thus,knowing the characteristics of the magnet material under consideration, it is possible to specify magnet dimensions that will ensure optimum usage of the material - the load line intersecting the demagnetisation curve at BH_{max}. It can be seen that reducing the airgap will increase the slope of the load line thus increasing the flux density in the airgap. Often it is required that this should be the case, for example, a magnet is specified to be longer than would correspond to BH_{max} either to increase the flux density or provide a greater resistance to demagnetisation forces. On the other hand, magnets for simple devices that work on 'open-circuit' (no steel return path) would have a load line that intersects the demagnetisation curve well below the BH_{max} point. As described earlier, the magnets used in disc armature motors are shaped as segments and these may be situated on one or both sides of the armature disc. The choice between the two cases is made from manufacturing considerations and also the desire to reduce the leakage between adjacent segments. For many materials, however, there is a minimum magnet length that can be economically produced. Although Fig. 2.7 is useful in outlining the principles involved when considering the magnetic circuit, a wide range of materials with totally unrelated characteristics are available today. A selection is shown in Fig. 2.8 which shows the normal

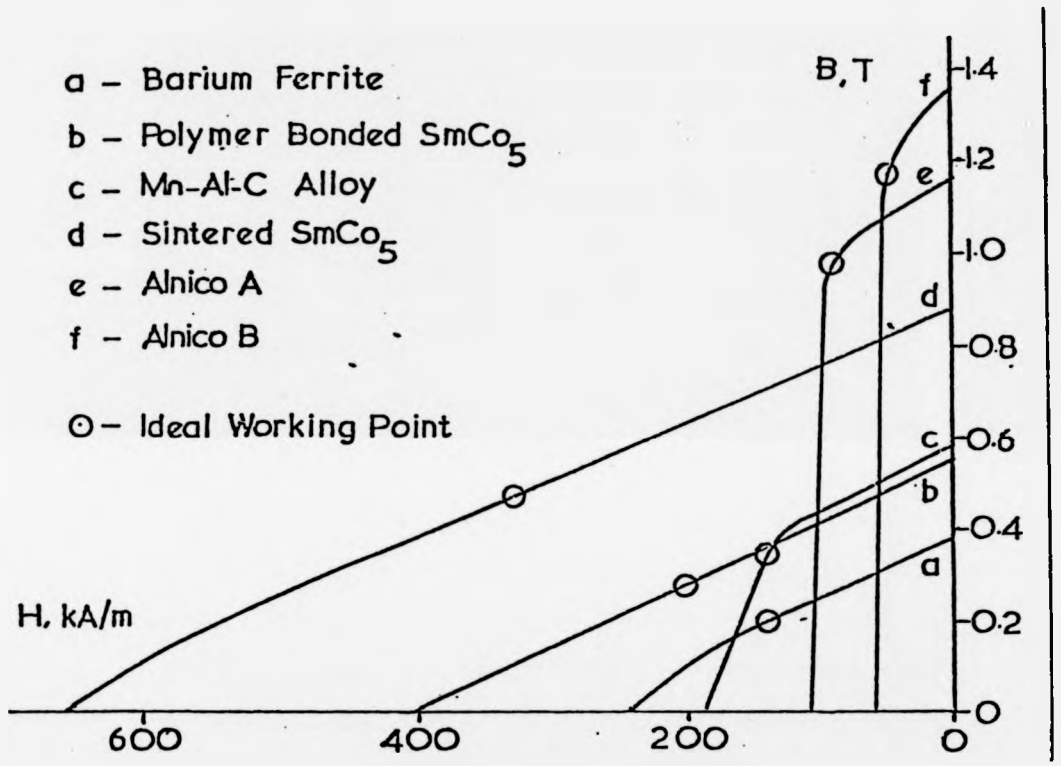

Fig. 2.8 : Demagnetisation curves of different materials

demagnetisation curve of each along with the BH_{max} point. They range in order of increasing remanance from the ferrite mentioned earlier, through the rare-earths to the high remanance Alnico materials. A point worth noting is that grades b and c are easily machined whereas all of the others are extremely brittle. A comparison of physical and magnetic properties of these materials is given in Tables 2.1 and 2.2 while further consideration of their use in disc armature motor design will be found in reference 24. Since the characteristics of the materials are so different, it is important to consider aspects of motor operation that depend on the choice of material.

2.1.1 Magnetic circuit parameters

One of the most important parameters of any magnetic material is the working flux density available. Assuming that operation at BH_{max} is always possible then it is clear from Fig. 2.8 that any Alnico material will have a higher working flux density than a ferrite. Thus, for a given motor power output from a given size of motor, the low value of flux available when specifying a ferrite would have to be compensated for by an increased copper content in the armature. However, to produce a given magnetising force in an airgap will require a shorter length of ferrite than Alnico simply because of the higher coercivity available. The choice between materials is, therefore, not a straightforward one and it is further complicated by the non-linear characteristic of many of the materials. This can be most apparent when considering initial magnetisation, assembly or reassembly after dismantling as will now

Material	Density, kg/m^3	Machineability
Barium Ferrite	4700	Hard, Brittle-Grinding Only
Polymer $SmCo_5$	5200	Easily Machined and Drilled
Mn-Al-C	5100	Easily Machined and Drilled
$SmCo_5$	8200	Brittle - Grinding Only
Alnico A	7300	Hard, Brittle - Grinding Only
Alnico B	7300	Hard, Brittle - Grinding Only

Table 2.1 : Physical properties of different magnet materials

Material	Br, Tesla	Hc, kA/M	BH max, kJ/m^3	Max. temp, ^oC	Reversible coeff. of temperature
Barium Ferrite	0.37	240	26	200	0.20%
Polymer $SmCo_5$	0.55	400	55	100	0.03%
Mn-Al-C	0.57	185	44	300	0.12%
$SmCo_5$	0.87	660	152	250	0.04%
Alnico A	1.15	110	89	200	0.02%
Alnico B	1.35	59	60	200	0.02%

Table 2.2 : Magnetic properties of different magnet materials

be shown. Fig. 2.9 illustrates a further normal demagnetisation curve with a load line OP corresponding to some initial condition - a fully magnetised material working into an airgap, for example. Now, suppose these conditions are changed - the airgap is increased - so that some new load line OQ now represents the system with the operating point moving down the curve to Q. Evidently, the flux density will take a new lower value represented by B_Q. If the initial conditions are now restored the operating point will not, in general, return to P, but will move to a point R on the original load line OP. The line QR will be approximately parallel to the tangent of the demagnetisation curve at Br. Thus, only a reduced flux density, B_R, is available. These are known as conditions of recoil and close attention should be paid to magnetic circuits where such conditions are likely to exist - the demagnetising effect of a wound armature, for example. In the disc armature motor such problems will only usually be apparent when assembling a machine. If the magnets are magnetised before assembly, there is always the possibility that on removal from the magnetisation jig and installation in the machine they will be operating under recoil. Fortunately, the problem is not equally apparent in all materials. The straight line characteristic of ferrite and rare-earth magnets ensures that recoil occurs along the original BH curve and therefore it is quite permissible to magnetise them before assembly. It is the Alnico types that are most susceptible and when these are specified it is not unusual to include magnetising windings within the machine itself (Figs. 2.3 and 2.5) so that the magnets may be energised initially after assembly, and also re-energised if ever the motor is dismantled.

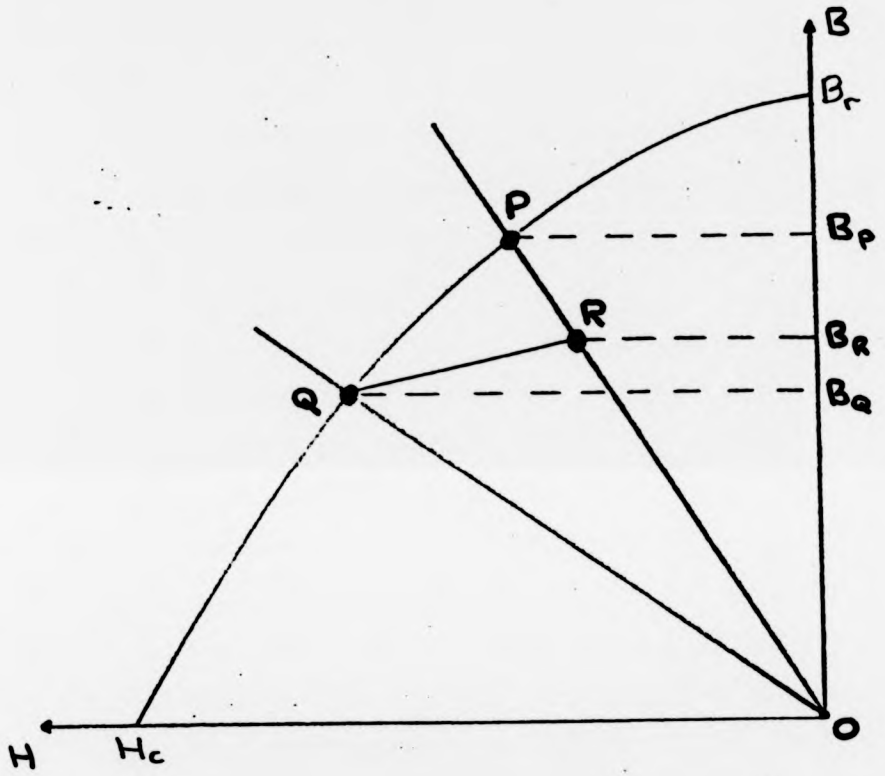

Fig. 2.9 : Recoil operation of a magnet material

It has been found that with Alnico magnets used without such magnetising windings, the working flux density is reduced. To assess whether recoil is likely, it is necessafy to consider both the normal demagnetisation characteristic and the expected conditions of operation. For example, with some Alnicos operating some way above the BH_{max} point, there may exist a small range of operating conditions where recoil operation coincides with the BH curve. Material e in Fig. 2.8 is an example of this.

Once a permanent magnet electrical machine has been assembled, the only demagnetisation effects likely to be experienced are those due to armature reaction and temperature. With conventional machines the former effect can be significant and serious with several techniques available to reduce or compensate for it. In the disc armature motor, the air-cored coils in a large airgap produce an extremely small demagnetising force, and this is spread over a relatively large number of poles. Armature reaction demagnetisation is thus negligible in machines of this type and such effects have never been experienced in any of the prototypes. The effect again depends on the magnet material specified and in traction applications where high-coercivity ferrite is almost exclusively used it would be even less pronounced than with Alnico. Although reduction of flux density with temperature is apparent in all materials to varying degrees (Table 2.2), most motor operating conditions lie in the reversible temperature range and thus no permanent demagnetisation occurs. Obviously, if continuous operation at an elevated temperature is to be catered for,the modified value of flux density must be used in design calculations. Magnet manufacturers

supply BH curves taken at different temperatures and these can prove extremely useful.

2.1.2 Magnetic field in the airgap

Having considered general aspects of magnet materials for these machines, attention must now be paid to the magnetic flux distribution in the airgap. This is an area where much analysis has been carried out in order to predict the distribution associated with such an array of magnet segments. With reference to Fig. 2.10, it is possible to show[25] that the magnet potential ψ at a distance x from some permanent magnet material can be expressed as:-

$$4\pi.\psi = \int \frac{\text{div } M.}{q}\, dV + \int \frac{M_s.dA}{q} \qquad (2.3)$$

where M is the intrinsic magnetisation, M_s the pole strength on the magnet face, q the distance from the point of interest to the area element dA, and dV is an element of magnet volume. For the majority of disc armature motor applications, the magnet materials used are homogeneous and anisotropic - the material is given a preferred direction of magnetisation in the manufacturing process. In the case of materials with a linear demagnetisation characteristic, it is postulated[22] that uniform magnetisation is apparent, i.e. M is constant in magnitude and direction and thus the R.H.S. of equation (2.3) reduces to the second term. By taking the gradient of this modified equation and considering the axial direction only, it has been found[22] that if radial and angular positions are denoted

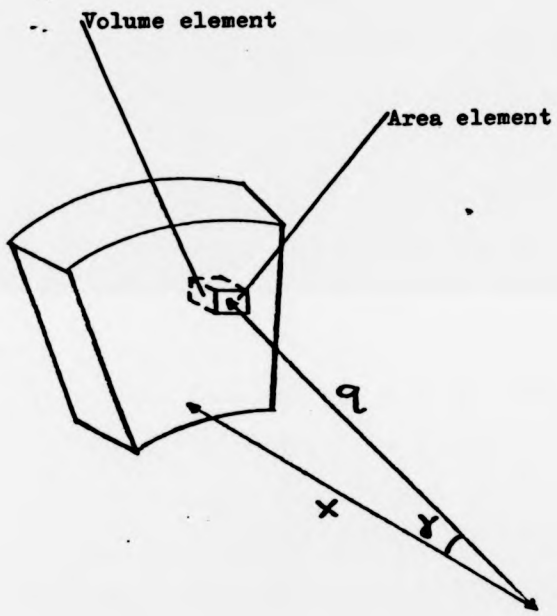

Fig. 2.10 : Magnet segment for field distribution

by subscripts i and j respectively then the airgap flux density in the axial direction at the point of interest is given by:-

$$B_{i,j} = \frac{\mu_o M_s}{4\pi} \int \frac{\cos\gamma}{q^2} \, dA \qquad (2.4)$$

where γ is the angle between the normal at dA and a line drawn from dA to the point of interest. This has been evaluated for the pole shape under consideration[22] and the results compared with those obtained by practical measurement of the flux produced by a set of segmented ferrite magnets with close agreement shown. It has been further postulated that it may not be reasonable to assume that the intrinsic demagnetisation in Alnico materials is uniform. This would not allow the assumption that div M = 0 to be made when simplifying equation (2.3). If this is the case, it is predicted[26] that a considerable field reduction would occur near the edges of the magnet face. However, comprehensive flux measurements in the Alnico field system of the 7.5 kW motor described in Chapter 5 show that a very uniform and extended field pattern is apparent. This is maintained with only slight reduction at the magnet edges. The grade of material used in this motor (Hycomax III) has a normal demagnetisation characteristic as illustrated in Fig. 2.11. The Hycomax material has a much greater coercivity and the non-linearity of the BH curve is not as pronounced as in many other grades of Alnico material. Specific design considerations dictate that magnet operation significantly above BH_{max} should occur, and as this dictates that the slope of the tangent at the operating point must move closer to that of the tangent at B_r, it is proposed that relatively uniform magnetisation would be apparent. That this is a reasonable assumption to make is borne out by actual

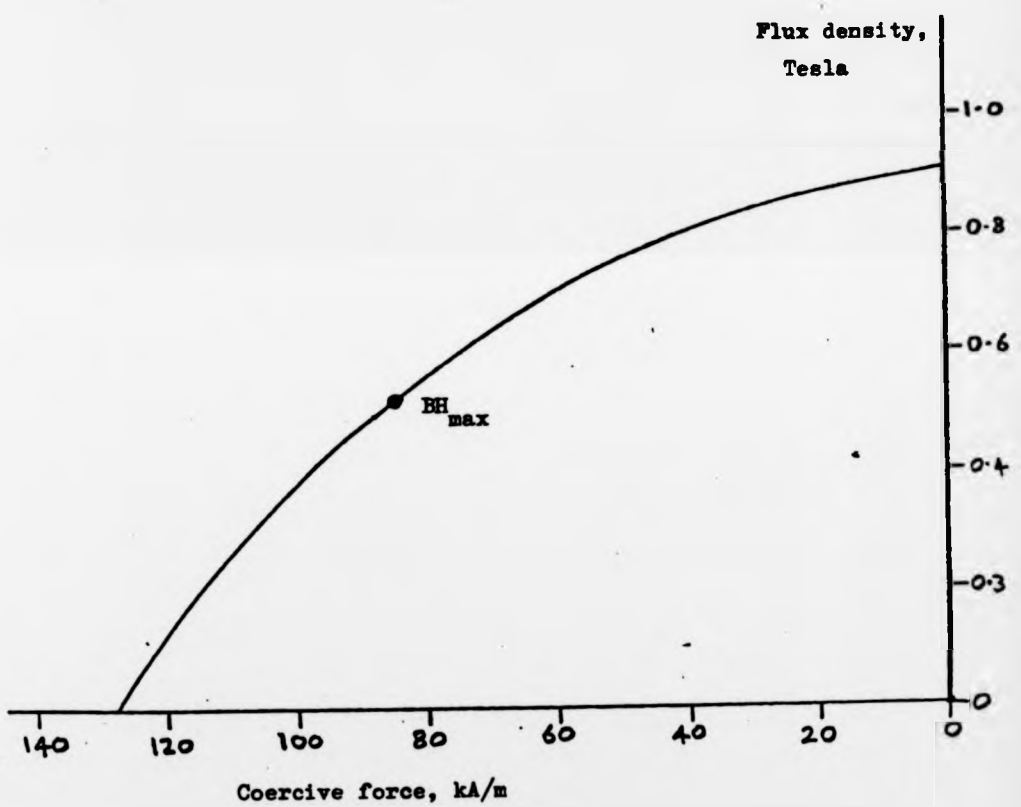

Fig. 2.11 : Normal demagnetisation curve for Hycomax III

flux measurements as described above and illustrated for convenience in Fig. 2.12. Thus, for this field system, the term M in equation (2.3) may be taken as constant and equation (2.4) applies.

If the flux density of the permanent magnet system can therefore be expressed by equation (2.4), the e.m.f. induced in a conductor at angular position j may be evaluated from:-

$$e_j = \omega \int_{r_1}^{r_2} B_{ij}.r_i \, dr \qquad (2.5)$$

where r_2 and r_1 are the outer and inner radii of the magnet ring, ω the angular velocity and dr an element of radius. This may be applied to all disc-armature motors.

For practical design purposes, it is inconvenient to continually evaluate equation (2.5) and then sum the results through the machine to determine the total e.m.f. produced - especially as the evaluation of B_{ij} is not itself straightforward. It has been found sufficient to define an average airgap flux density, B_g, which is related to the magnet flux density, B_m, by:-

$$B_g = B_m/LC \qquad (2.6)$$

where LC is greater than 1 and represents the leakage paths in the magnetic circuit. It is chosen with reference to both calculated and measured values of airgap flux density and for the magnet configuration used in these motors, with a high degree of similarity from machine to machine a value of LC between 1.25 and 1.3 is considered most suitable. It is also closely related to the ratio of pole arc to pole pitch, α , as a large value of this ratio will

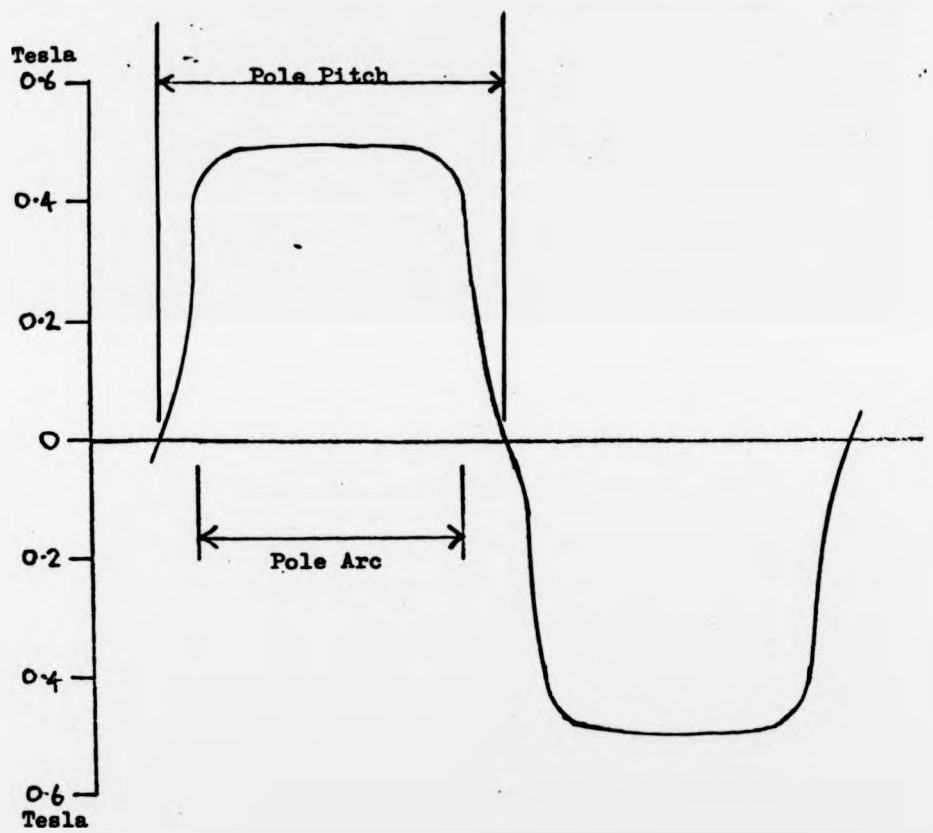

Fig. 2.12 : Average airgap flux density in Hycomax III system

increase the leakage and also reduce the neutral region in which commutation takes place. Investigation of the dependent parameters has shown that a good compromise is achieved with α in the range 0.75 to 0.8 although a motor with a high value of α is discussed in appendix III.

2.2 General machine considerations

Although the magnetic circuit has, for convenience, been treated in isolation in the preceeding discussion, more general aspects of machine operation will now be covered. The airgap flux distribution will be assumed to be constant although a treatment of actual flux density in the airgap and its effect on different winding arrangements will be considered in Chapter 4. Fig. 2.13 shows a schematic of a pair of magnets with a single-turn coil. The active portion of the conductors (AB or CD) corresponds to the difference in radii r_1 and r_2. It will be assumed that no conductors laying outside of r_2 or within r_1 play any part in torque generation in the machine and thus r_2 and r_1 may be considered the outer and inner active radii, respectively. The length of conductor BC forms an outer end winding and as most coils are multi-turn there will be inner end windings situated approximately along AD. In practice, one of the coil sides will be longer than the other to allow additional coils to be nested inside it, although this will not change either the outer or inner active radius. It will be noted that the end windings form a large part of the total coil length and this is especially true when a small number of poles is specified. In order to prevent excessive copper loss in the end windings, the number of poles in

Fig. 2.13 : Schematic of magnets with a single-turn coil

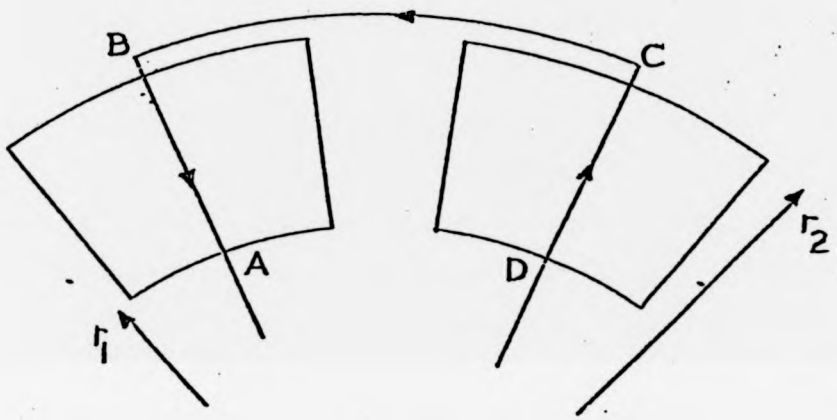

a disc armature motor tends to be quite high when compared with conventional machines - 10 or 12 pole arrangements are not uncommon.

Although a conventional commutator is used in the machine, the term 'slot' has no meaning and coil sides are aligned with respect to the appropriate commutator segment when the winding is being constructed - it is assumed that after encapsulation the coil sides do not move with respect to the commutator. The armature may, of course, be connected in any of the usual wave, lap or duplex arrangements. It is also feasible to connect two separate armatures in parallel, or even to connect coils of one winding one by one in series with those of another thus doubling the effective turns/coil. In both cases, this will result in a four-layer winding with double the power output over the two-layer version. Examples of four layer armatures are given in Chapter 3, and appendix II.

It is well known that the number of parallel paths through the armature of a d.c. machine is equal to 2 for a wave winding and the number of poles for a lap winding. Because of the relatively large number of poles employed in the disc armature motor, the situation has often arisen where a wave winding has too few parallel paths and a lap winding would have too many. To overcome this, a duplex wave winding has been specified on a number of occasions. This has four parallel paths and presents a suitable compromise although care must be taken is specifying the winding arrangement especially when multiple brush sets are used to carry high traction currents.

Having considered the basic magnetic and electrical circuits, attention must now be paid to the torque and e.m.f. generation within the machine together with the relationsip between r_1 and r_2 for optimum machine performance. The total armature e.m.f., E can be expressed as:-

$$E = B.l.v.z_s \qquad (2.7)$$

where B is the machine's average working flux density, l the active length of a conductor, v the average conductor velocity, and z_s the number of conductors in series between the brushes. However, l, v, and z_s may be written:-

$$l = (r_2 - r_1) \qquad (2.8)$$

$$v = \frac{\omega(r_2 + r_1)}{2} \qquad (2.9)$$

$$z_s = z/a \qquad (2.10)$$

where a is the number of parallel paths through the armature and z the total number of armature conductors. Thus:-

$$E = \frac{B.(r_2-r_1).\ \omega.(r_2 + r_1).z}{2a}$$

$$= \frac{B.\omega.z.\ (r_2^{\,2} - r_1^{\,2})}{2a} \qquad (2.11)$$

Equation (2.11) is often the most useful for determining the e.m.f. generated in a disc armature machine. However, the flux per pole, ϕ, may be written as:-

$$\phi = \frac{B.\pi.(r_2^{\,2} - r_1^{\,2})}{p} \qquad (2.12)$$

where p is the number of poles, and also:-

$$\omega = \frac{2\pi.n}{60} \qquad (2.13)$$

where n is the rotational speed in rev/min. Therefore, the e.m.f. may be further expressed as:-

$$E = \frac{\emptyset.n.p.z}{60.a} \qquad (2.14)$$

which is the more familiar equation for any d.c. machine. If T is the gross torque developed in Nm and I the armature current in amps, then the gross electromechanical power in watts is given by:-

$$EI = \frac{2\pi.n.T}{60} \qquad (2.15)$$

and from (2.14):-

$$T = \frac{\emptyset.p.z.I}{2\pi.a} \qquad (2.16)$$

Combining equations (2.11) and (2.12) gives:-

$$E = \frac{\emptyset.p.z.\omega}{2\pi.a} \qquad (2.17)$$

illustrating that the torque and e.m.f. constants are identical when S.I. units are used. No assumptions have yet been made concerning the relationship between r_1 and r_2 (except $r_2 > r_1$) and the condition for maximum power will now be derived. As the conductors are more tightly grouped towards the inner active radius and as end windings exist at a radius less than r_1, a space factor, SF, is defined to ensure that it will be possible to accommodate the end windings. SF is kept approximately constant and less than 1 for all disc armature motors and it is defined as:-

$$SF = \frac{z.G}{2\ L.\pi.r_1} \qquad (2.18)$$

where G is the gauge of wire used and L the number of layers in the armature winding. Multiplying equation (2.11) by I gives the total mechanical power, P:-

$$EI = P = \frac{B.\omega.z.(r_2^2 - r_1^2).I}{2a} \qquad (2.19)$$

and substituting from (2.18):-

$$P = \frac{B.\omega.SF.L.\pi.r_1(r_2^2 - r_1^2).I}{a.G} \qquad (2.20)$$

$$= \kappa.r_1.(r_2^2 - r_1^2)$$

where κ is a constant. Let r_1 be some fraction of r_2 so that $r_1 = \beta r_2$ where $\beta \leq 1$. Then:-

$$P = \kappa.r_2^3.(\beta - \beta^3) \qquad (2.21)$$

Equation (2.21) is now differentiated w.r.t.β to find a maximum.

$$\frac{dP}{d\beta} = \kappa.r_2^3.(1-3\beta^2) \qquad (2.22)$$

and this is zero when $\beta = \pm 1/\sqrt{3}$. To check that a maximum exists, equation (2.22) is differentiated:-

$$\frac{d^2P}{d\beta^2} = -6\beta.\kappa.r_2^3 \qquad (2.23)$$

which is negative for $\beta = 1/\sqrt{3}$. Therefore, for maximum power from a disc armature motor:-

$$r_2 = \sqrt{3}\ r_1 \qquad (2.24)$$

Substituting (2.24) into (2.20) gives:-

$$P = \frac{B.\omega.SF.L.\pi.r_2/\sqrt{3}.(r_2^2 - r_2^2/3).I}{a.G}$$

$$= \frac{2B.\omega.SF.L.\pi.I.r_2^3}{3\sqrt{3}\ a.G} \qquad (2.25)$$

Thus for a disc armature motor with a given number of layers, the gross power output is proportional to the cube of the outer active radius (or diameter). This may be compared with the familiar product of square of diameter and length for a conventional machine.

Having established the operating principles of the machine, it is now appropriate to review briefly the previous traction applications that have been considered as results from this work are of considerable importance to the comprehensive design procedure developed in Chapter 4, and performance evaluation (Chapter 5).

3: USE OF THE MOTOR IN TRACTION APPLICATIONS

In the 1971 patent granted for the d.c. disc armature motor, mention was made of the use of the machine in 'wheel motor' units to drive an electric car. The potential advantages for battery electric traction were thus appreciated at an early stage of the development program, although the motor has now found numerous applications elsewhere[19]. The advantage of a high operating efficiency is immediately apparent, but further benefits result from the methods of construction used. As the magnetic field is provided by permanent magnets and no rotating iron is used in the armature the power density (ratio of power to weight) is significantly improved over comparable series wound machines - an important consideration in battery electric traction. The lightweight construction of the armature lends itself to low inertia drives where this feature is desirable and the short axial length of the machine is often advantageous when space is limited, for example. The extremely low inductance of the armature winding allows higher operating speeds to be considered as the upper limit defined by the onset of under-commutation is effectively raised. A diagram of how these specific advantages affect the overall machine performance is presented in Fig. 3.1.

It is to the construction of the armature that the patent is most applicable and although this is complex when compared to a conventional d.c. machine, the large number of wound armature disc motors marketed today show that volume production on a commercial basis is possible.

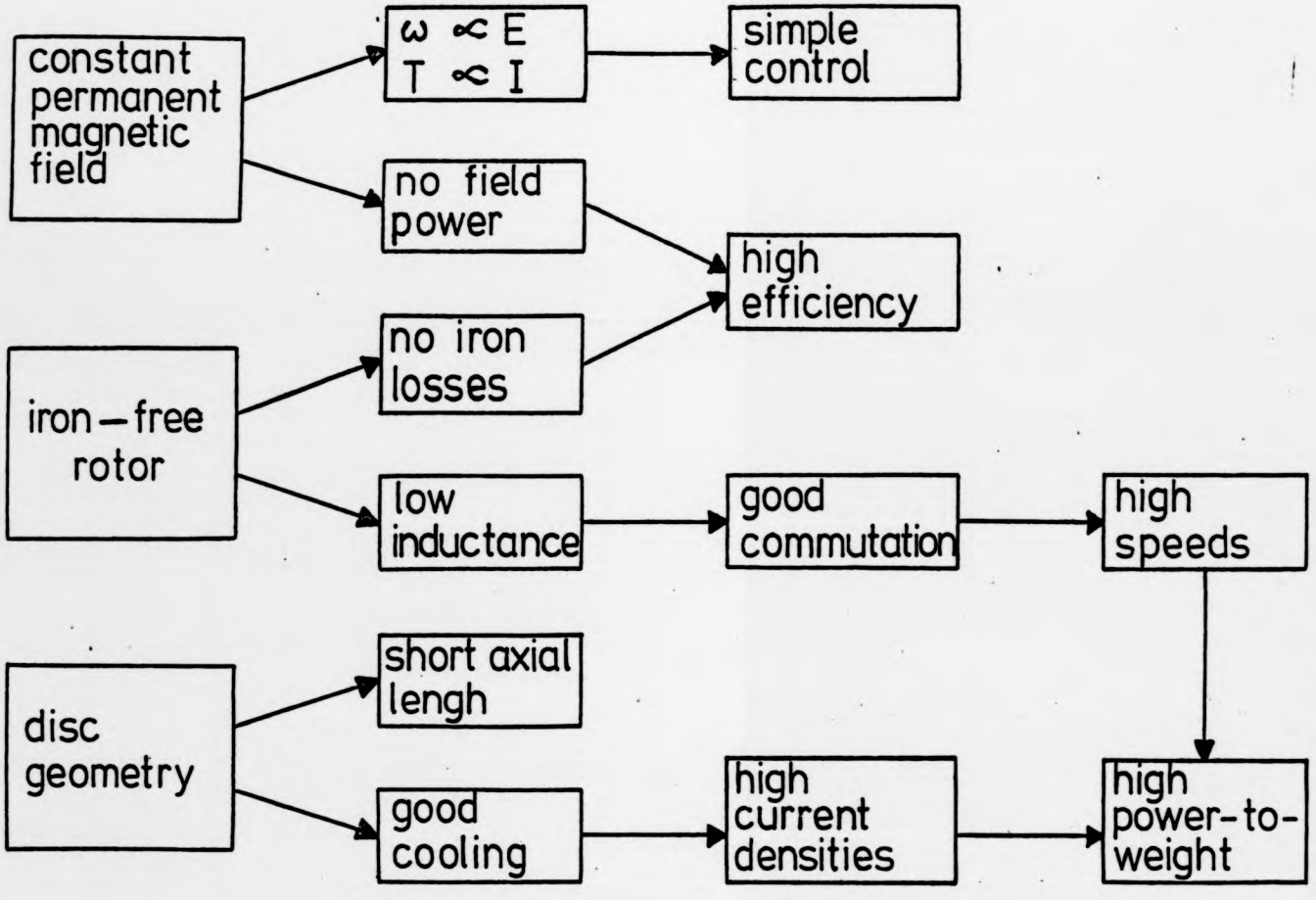

Fig. 3.1 : DISC MOTOR FEATURES

Strength is added to the thin disc of copper conductors by locating the coils' circumferential end windings 90° out of the plane of the disc, and by the encapsulation process. The quality of the encapsulating material obviously has considerable bearing on the resulting product - it must be sufficiently strong, but also be able to accommodate expansion of the copper it contains. As a conventional commutator is used in the motor, conventional winding patterns and brushgear may also be specified and further consideration of armature windings is given in Chapter 4.

The concept of wheel motor units resulted from the postulated high speed capability of the machine. Any motor located in the wheel of a vehicle becomes part of the unsprung weight, and from vehicle handling considerations should be as light as possible. Thus, in order to obtain sufficient output power from an electric motor, it must operate at a high speed with suitable reduction gearing between it and the driven road wheel. As this is a specialised application (see Section 3.4) it was decided to construct the initial prototypes to a more conservative speed specification in order to gain a general assessment of motor performance without the need to consider problems arising from high speed operation. The sections below will briefly describe the various traction prototypes as results obtained are used to define important design and performance criteria in Chapters 4 and 5.

In addition to the construction and evaluation of prototypes, consideration was given at an early stage to the design facilities available. As experience of the motors developed, it was found

possible to develop a digital computer program incorporating routines which, when given the design parameters of a motor, would calculate the performance[27]. This allowed designs to meet a given specification to be produced much more quickly as tedious and repetitive calculations are removed from the designer. The program itself is described in Chapter 4 as developments from it have led to the comprehensive facilities available today.

3.1 The 930W traction motor

This was the first prototype permanent-magnet d.c. disc armature motor built and tested at the University of Warwick. The work was sponsored by a lawnmower manufacturer who intended to build a ride-on type lawnmower for use in conditions where low noise-levels are important - hospital grounds, for example. The mower would need to have a good working range - hence the interest in the disc armature motor with its inherently high efficiency. A suitable specification was drawn up after consultation with the manufacturer and work on the motor commenced in November 1968. It was based around a power requirement of 930W, an operating speed of 2500 rev/min and a working voltage of 12V, power to be derived from four lead-acid heavy duty starter batteries. The design parameters of the machine are given in Table 3.1 which is in the form of a computer printout and should be read in conjunction with the symbols list. A schematic diagram of the motor is given in Fig. 3.2 which illustrates the general mechanical layout. The motor is 300 mm in diameter and 105 mm in length (excluding the shaft extension). The magnetic field is provided by a 12 pole

DISC-ARMATURE MOTOR DESIGN

DESIGN NO: 12

DESIGN SPECIFICATION

OUTPUT: 930.0 WATTS
VOLTS: 12V
SPEED: 2500 R.P.M.

DESIGN DATA

D2 = 230 MM
D1 = 140 MM
NO OF POLES = 12
TERMINAL VOLTAGE = 12 VOLTS

MAGNETIC CIRCUIT DATA

BM = .286 TESLA
HM = 50500.0 A/M
LEAKAGE COEFFICIENT = 1.27
LOSS FACTOR = 1.27
USEFUL FLUX/POLE= .000368WEBERS
POLE PITCH/POLE ARC = .75
MAGNET LENGTH = 16.9 MM
MAGNET WEIGHT = 1.56 KGMS
THICKNESS OF FRR = 3.46 MM
FRR WEIGHT = 1.41 KGMS
AIR GAP = 5.00 MM
MAGNET DENSITY = 4.70 GMS/CC
MAXIMUM FLUX DENSITY OF MILD STEEL = 1.50 TESLA
DOUBLE OR SINGLE MAGNETS = 1

WEIGHT OF NON ACTIVE PARTS = 9.00 KGMS
TOTAL WEIGHT = 12.60 KGMS
MECHANICAL LOSS= 132 WATTS
SPEED = 2376.6 R.P.M.
POWER = 897.4 WATTS
TORQUE= 3.61NM
POWER/WEIGHT = 71.25 WATTS/KGM
EFFICIENCY = .763

Table 3.1 : Design parameters for 930W motor

ELECTRIC CIRCUIT DATA

NO OF PARALLEL PATHS	= 12
NO OF COILS	= 60
NO OF TURNS/COIL	= 6
NO OF CONDUCTORS	= 720
WIRE DIAMETER	= 1.02 MM
WIRE WEIGHT	= .625 KGMS
CURRENT DENSITY	= 10.0 AMPS/MM*2
ARMATURE CURRENT	= 98.06 AMPS
I*2R LOSSES	= 147.3 WATTS
SPACE FACTOR	= .84
NO OF LAYERS	= 2
TEMPERATURE	= 75.0 DEGREES C.
ARMATURE RESISTANCE	= .015 OHMS
INDUCED EMF	= 10.50 VOLTS

Table 3.1 (continued) : Design parameters for 930W motor

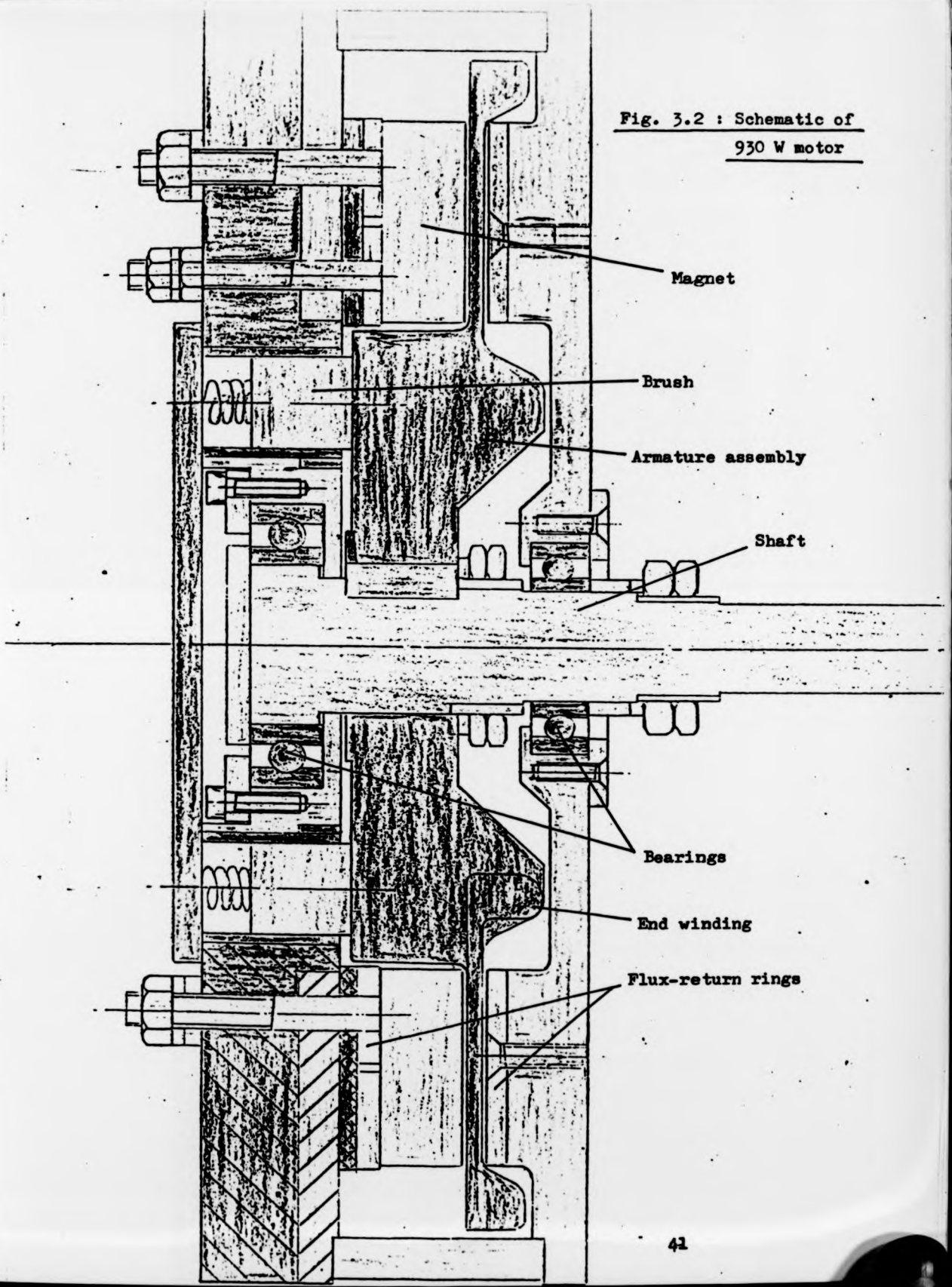

Fig. 3.2 : Schematic of 930 W motor

system of ferrite magnets and the armature has 60 coils, is lap wound (12 parallel paths), and has 5 equaliser rings with every other commutator segment connected to an equaliser. The performance characteristics of the motor are given in Fig. 3.3. These are substantially as expected and the motor has been successfully tested in a 24 inch ride-on lawnmower (Fig. 3.4).

Temperature rise tests were also carried out on the motor to gain some assessment of the thermal characteristics under running conditions. These are considered alongside similar tests on other machines in Chapter 5, where thermal rating of the motors is discussed.

Although the results from this project were very encouraging, the limited demand for lawnmowers of this type made volume production uneconomic. Valuable experience was gained, however, and further details of the design, construction and performance of the machine may be found in references 28 and 29.

3.2 The 1.1 kW traction motor

The construction of this prototype resulted from an interest shown by the South of Scotland Electricity Board (SSEB) in battery electric traction. It was intended to evaluate the performance of a disc armature motor in an electric car and the motor specifications were chosen to be 72V (six 12V traction batteries), 2100 rev/min and 1.1 kW, which would enable the vehicle to travel at speeds between 25 and 30 m.p.h. The project was commended in February 1970, and it was found possible to design a machine with

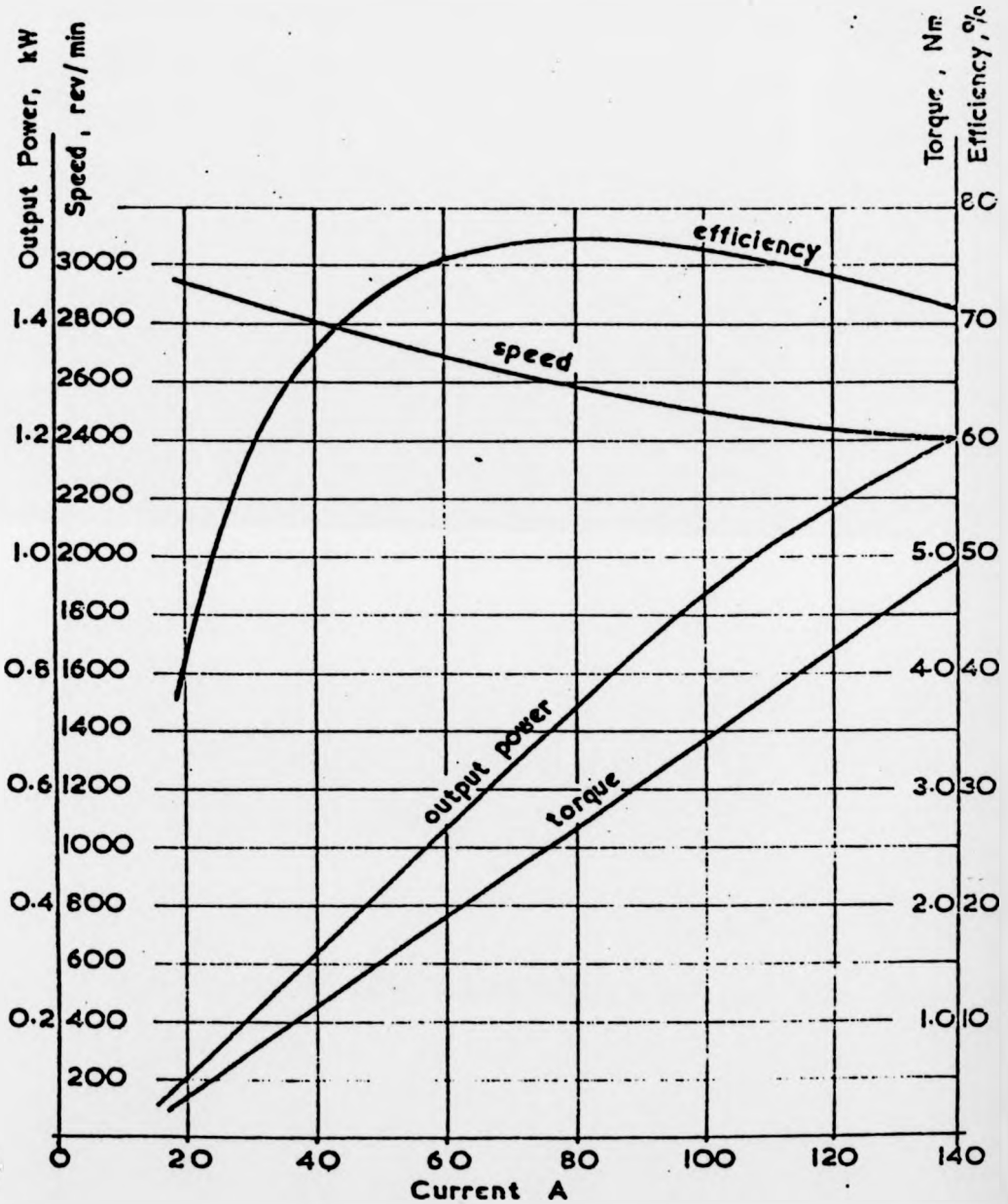

Fig. 3.3 PERFORMANCE CURVES OF PROTOTYPE DISC ARMATURE MOTOR : SUPPLY VOLTAGE = 12 V

Fig. 3.4 : Application of 930W motor

Fig. 3.4 : Application of 930W motor

mechanical specification very similar to that of the 930 W motor described above. The stator assembly is exactly the same, but the armature is now a 61 coil wave winding as dictated by the higher operating voltage. Table 3.2 details the design parameters and the mechanical layout is shown schematically in Fig. 3.5. Performance curves for the machine are shown in Fig. 3.6. Although the motor was successfully and extensively tested, the SSEB found that they could no longer support any further development work on either electric vehicles or disc armature motors. This decision was taken before delivery of the prototype and thus the motor has never been used in its intended application. Further details of the machine may be found in reference 30.

3.3 The 2.5 kW traction motor

The development of this machine followed from the University of Warwick Engineering Society expressing an interest in an electric vehicle motor after the cancellation of the SSEB project. The armature represented a departure from previous practice in that a four-layer arrangement was used for the first time. This was achieved by connecting a pair of two-layer windings in parallel so that each commutator segment has four connections to it rather than the usual two. The disc thickness is now doubled along with the output power capability although this 'back to back' arrangement required a new encapsulation mould to be constructed. The specification of the motor was to be 2.5 kW, 84 V and 3000 rev/min, and again it was found possible to design a machine with similar dimensions to the existing prototypes. Each half of the armature

DISC-ARMATURE MOTOR DESIGN

DESIGN NO: 31

DESIGN SPECIFICATION

OUTPUT: 1100 WATTS
VOLTS: 72V
SPEED: 2700 R.P.M.

DESIGN DATA

D2 = 230 MM
D1 = 140 MM
NO OF POLES = 12
TERMINAL VOLTAGE = 72 VOLTS

MAGNETIC CIRCUIT DATA

BM = .286 TESLA
HM = 50500.0 A/M
LEAKAGE COEFFICIENT = 1.27
LOSS FACTOR = 1.27
USEFUL FLUX/POLE= .000368WEBERS
POLE PITCH/POLE ARC = .75
MAGNET LENGTH = 16.9 MM
MAGNET WEIGHT = 1.56 KGMS
THICKNESS OF FRR = 3.94 MM
FRR WEIGHT = 1.61 KGMS
AIR GAP = 5.00 MM
MAGNET DENSITY = 4.70 GMS/CC
MAXIMUM FLUX DENSITY OF MILD STEEL = 1.32 TESLA
DOUBLE OR SINGLE MAGNETS = 1

WEIGHT OF NON ACTIVE PARTS = 9.00 KGMS
TOTAL WEIGHT = 12.93 KGMS
MECHANICAL LOSS= 100 WATTS
SPEED = 2915.9 R.P.M.
POWER = 1201 WATTS
TORQUE= 3.93NM
POWER/WEIGHT = 92.93 WATTS/KGM
EFFICIENCY = .839

Table 3.2 : Design parameters for 1.1kW motor

ELECTRIC CIRCUIT DATA

NO OF PARALLEL PATHS	= 2
NO OF COILS	= 61
NO OF TURNS/COIL	= 5
NO OF CONDUCTORS	= 610
WIRE DIAMETER	= 1.22 MM
WIRE WEIGHT	= .762 KGMS
CURRENT DENSITY	= 8.50 AMPS/MM**2
ARMATURE CURRENT	= 19.87 AMPS
I**2R LOSSES	= 129.7 WATTS
SPACE FACTOR	= .84
NO OF LAYERS	= 3
TEMPERATURE	= 75.0 DEGREES C.
ARMATURE RESISTANCE	= .328 OHMS
INDUCED EMF	= 65.47 VOLTS

Table 3.2 (continued) : Design parameters for 1.1kW motor

ELECTRIC CIRCUIT DATA

NO OF PARALLEL PATHS	= 2
NO OF COILS	= 61
NO OF TURNS/COIL	= 5
NO OF CONDUCTORS	= 610
WIRE DIAMETER	= 1.22 MM
WIRE WEIGHT	= .762 KGMS
CURRENT DENSITY	= 8.50 AMPS/MM**2
ARMATURE CURRENT	= 19.87 AMPS
I**2R LOSSES	= 129.7 WATTS
SPACE FACTOR	= .84
NO OF LAYERS	= 3
TEMPERATURE	= 75.0 DEGREES C.
ARMATURE RESISTANCE	= .328 OHMS
INDUCED EMF	= 65.47 VOLTS

Table 3.2 (continued) : Design parameters for 1.1kW motor

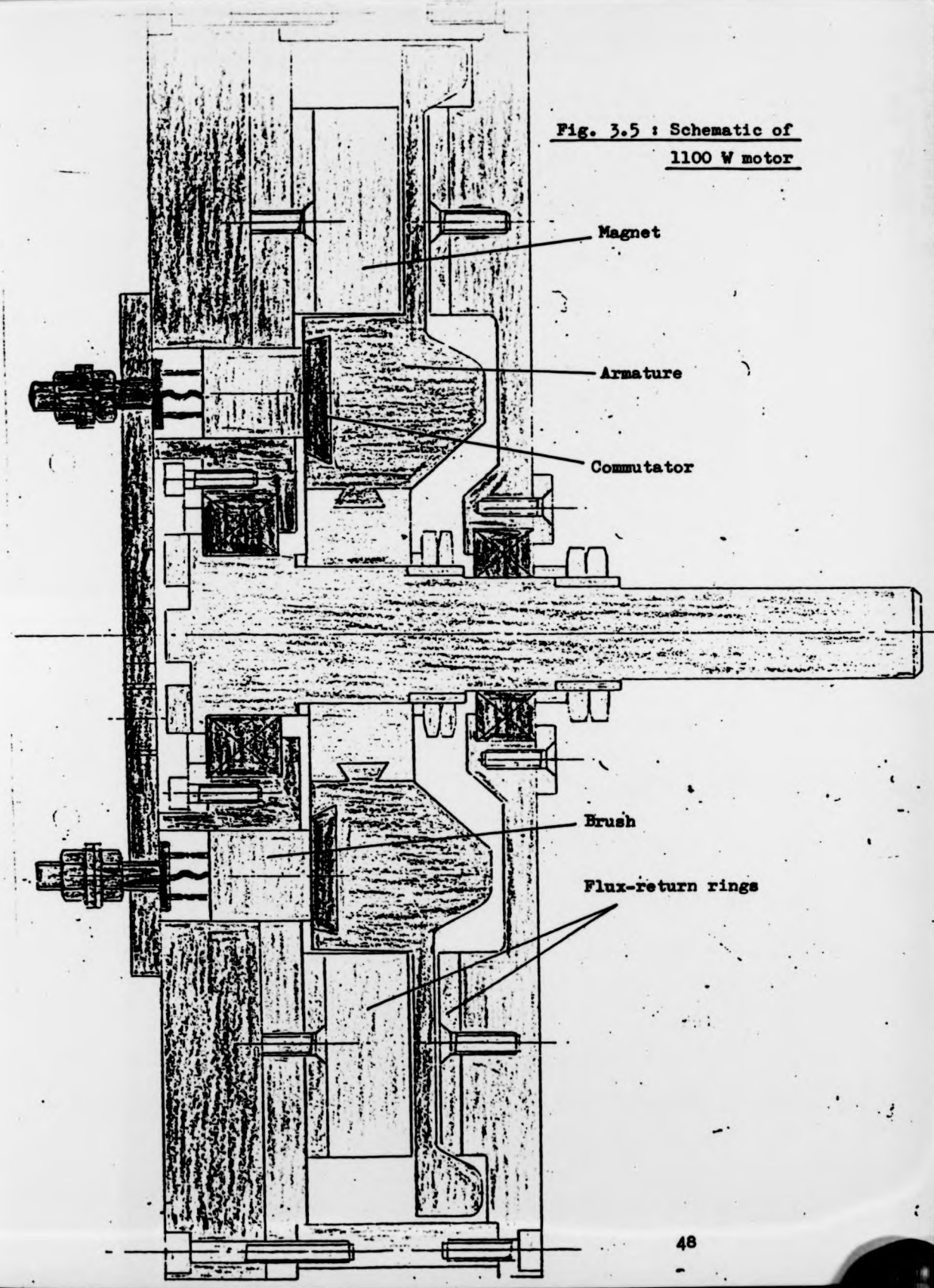

Fig. 3.5 : Schematic of 1100 W motor

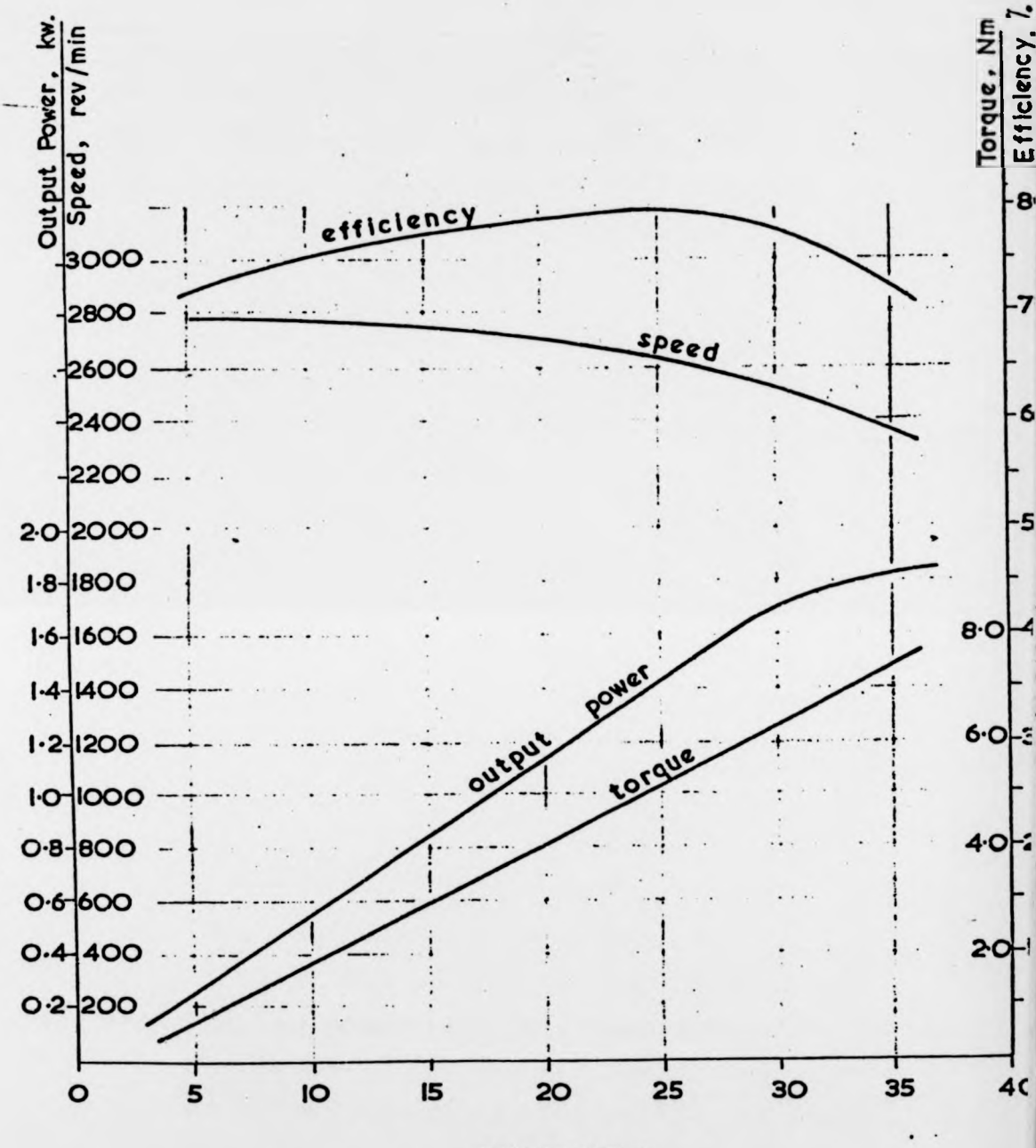

Fig. 3.6 : PERFORMANCE CURVES OF 1100W MOTOR

SUPPLY VOLTAGE = 72 v.

is in fact identical to that used in the 1.1 kW motor (61 coils, wave wound) and the stator consists of a double-sided magnet assembly with each half again identical to those previously used. A schematic is shown in Fig. 3.7 and a 30% increase in length over the 1.1 kW motor is required.

After the armature had been encapsulated, it was found that a fault existed in the winding making it impossible to use, and the motor was not completed. Although disappointing, the results did show that great care must be taken with the winding and encapsulating processes. Mistakes obviously cannot be rectified after encapsulation and it may not always be possible to test the winding beforehand. This is often the case when a suitable 'off-the-shelf' commutator is not available and a purpose-built component has to be constructed. An example of this is the 7.5 kW motor described in Chapter 5. Full details of the design parameters of the 2.5 kW machine are given in reference 31.

3.4 The 1.9 kW traction motor

With the experience gained from prototype disc armature motors, it was decided to return to the concept of an electric wheel motor. It was stated above that this would have to be operated at a relatively high speed to enable sufficient power to be derived from the machine, and therefore some form of reduction gearing would need to be incorporated in the mechanical design. Because of the severe limitation on diameter, particular attention would need to be paid to the selection of the magnet

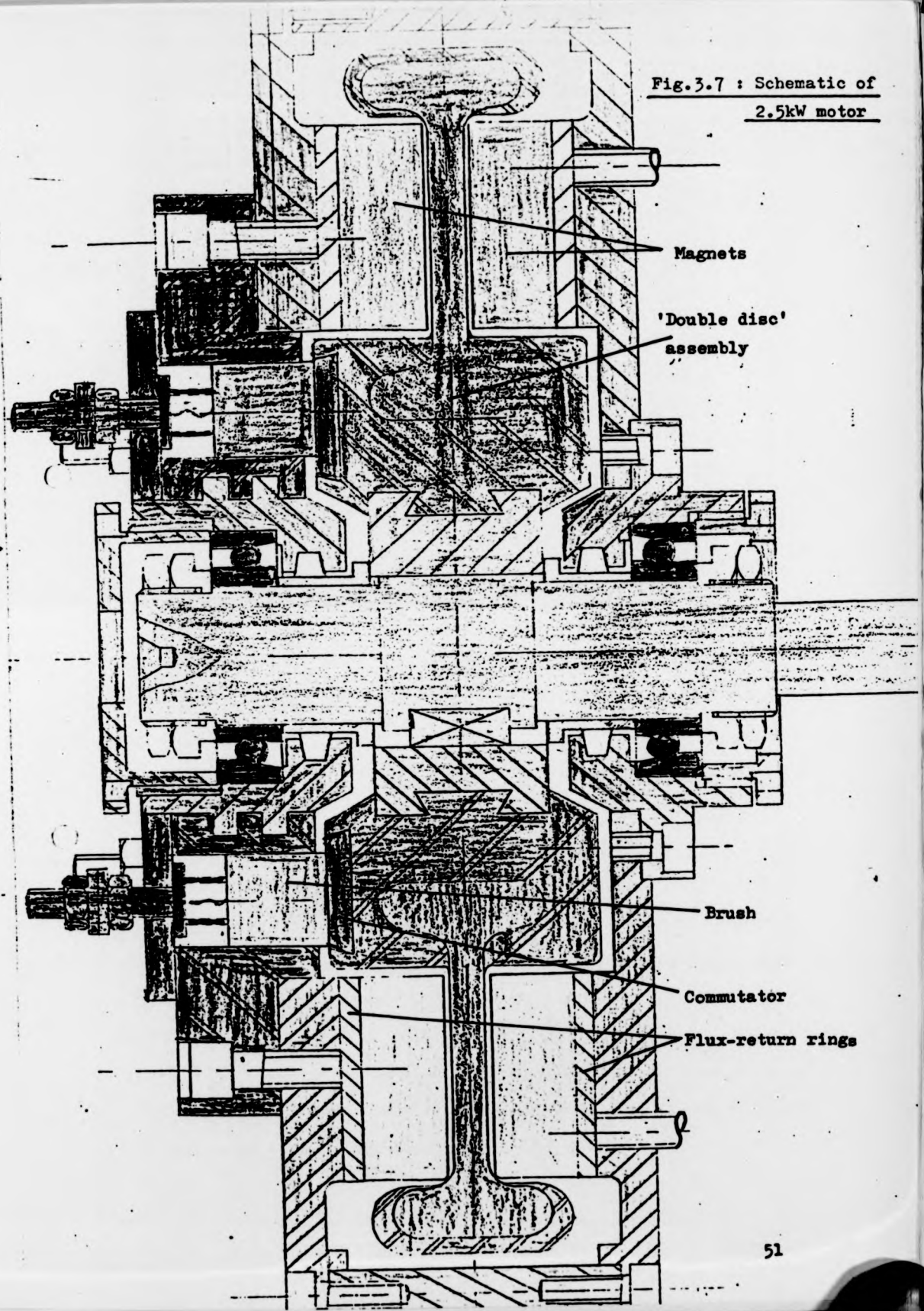

Fig.3.7 : Schematic of 2.5kW motor

material so that a good working flux is obtained.

To propel a small vehicle at 40 m.p.h., it was considered that around 3.6 kW would be required. This is most easily achieved by the use of two identical units, one incorporated in each driven wheel of the vehicle. With this arrangement, the motors could be connected either in series or parallel. The former has a particular advantage in that differential action, necessary for correct cornering ability, would be accomplished automatically and electrically. With a system voltage of 72 V each motor was designed to operate at 36 V, and for the cruising speed of 40 m.p.h., the use of a 2-stage 16:1 epicyclic gearbox corresponds to a motor speed of 10500 rev/min.

Instead of the ferrite material used in all previous prototypes, Alnico magnets of the grade Hycomax III were specified in order to give a good working flux in the limited space available. The computer listing of the design parameters is given in Table 3.3 and it will be noted that a four-layer, parallel-connected armature winding is again employed. The machine has 10 poles, 40 coils and is lap wound. The overall diameter is 180 mm and a schematic of the assembly, including gearing and road wheel is shown in Fig. 3.8. Two prototypes were constructed (Fig. 3.9) but excessive heating and high currents were encountered on light load with both machines failing after a very short time. Investigations into this failure were not conclusive and no further work on high-speed wheel motor units has been carried out. Further details of the machine may be found in references 21 and 32.

DESIGN NO: 91

DESIGN SPECIFICATION

OUTPUT: 1860. WATTS
VOLTS: 36. V
SPEED: 10300. RPM

DESIGN DATA

D2: 142. MM
D1: 82. MM
POLES: 10.

MAGNETIC CIRCUIT DATA

BM 0.500 TESLA
HM 80000. A/M
LCOEFF 1.24
LFACT 1.27
PHI .000332 WEBERS
ALPHA .78
LMAG 22.9 MM
WGTMAG 1.38 KG
THICK 3.81 MM
WGTFRR 0.63 KG
GAP 4.50 MM
MAGDSY 7300. KG/M**3
BMS 1.80 TESLA

WGTNAP 2.00 KG
TOTWGT 4.25 KG
MECHLO 200. WATTS
SPEED 10843.8 RPM
POWER 1811.0 WATTS
TORQUE 1.59 NM
PWRWGT 425.81 WATTS/KG
EFF .841

ELECTRIC CIRCUIT DATA

PATHS 20
COILS 80.
TURNS 7.
Z 1120.
GAUGE 0.63 MM
WGTWIR 0.25 KG
CRTDSY 9.6 A/MM**2
ARMCRT 59.85 AMPS
LOSS 143.59 WATTS
LAY 4
TEMP 75. DEGREES.
SF .80
RARM 0.015 OHMS
ER 33.60 VOLTS

OUTPUT DATA

Table 3.3 : Design parameters for 1.9kW motor

ELECTRIC VEHICLE TRACTION MOTOR

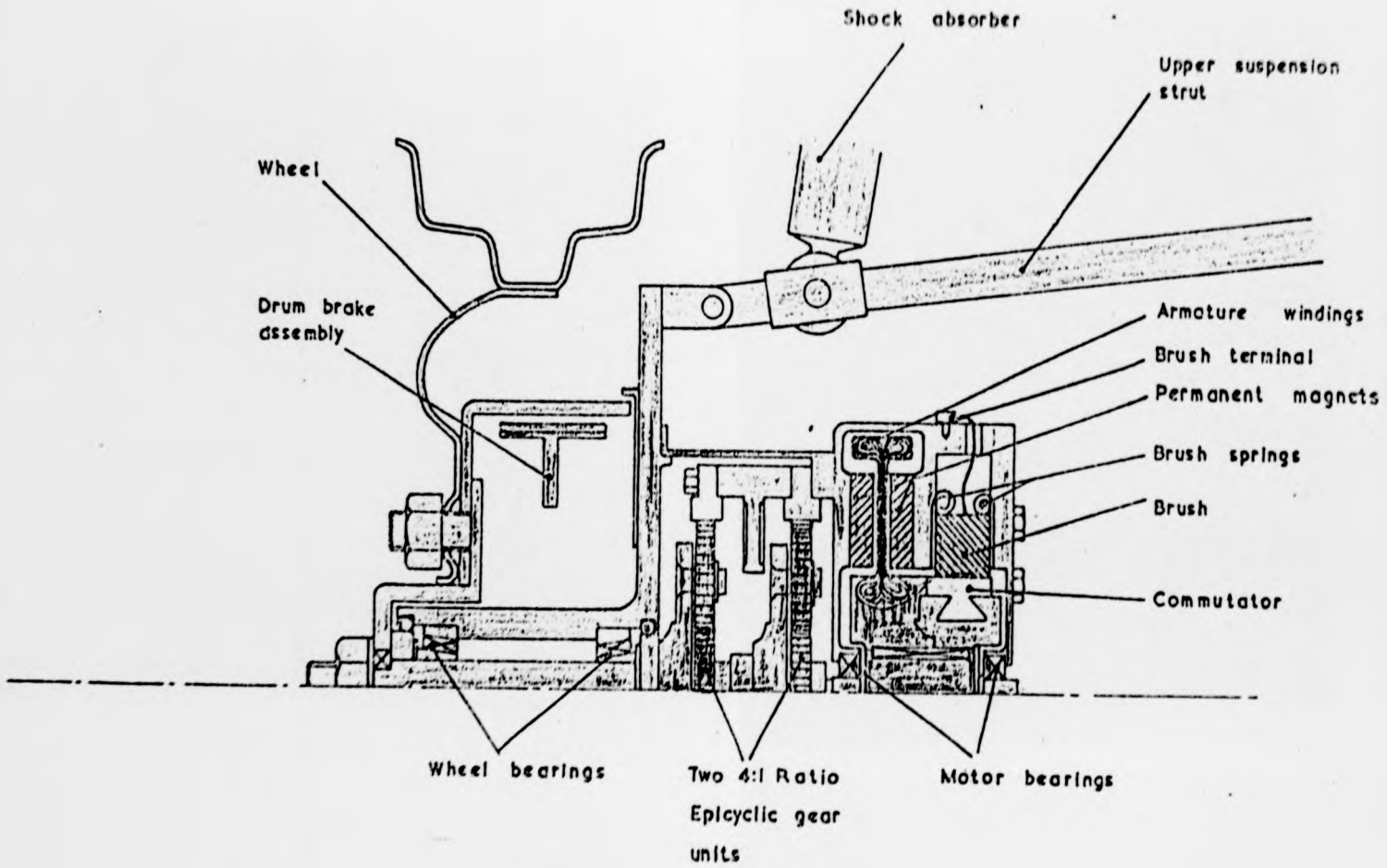

Fig. 3.8 : Schematic of 'Wheel motor' unit

ELECTRIC VEHICLE TRACTION MOTOR

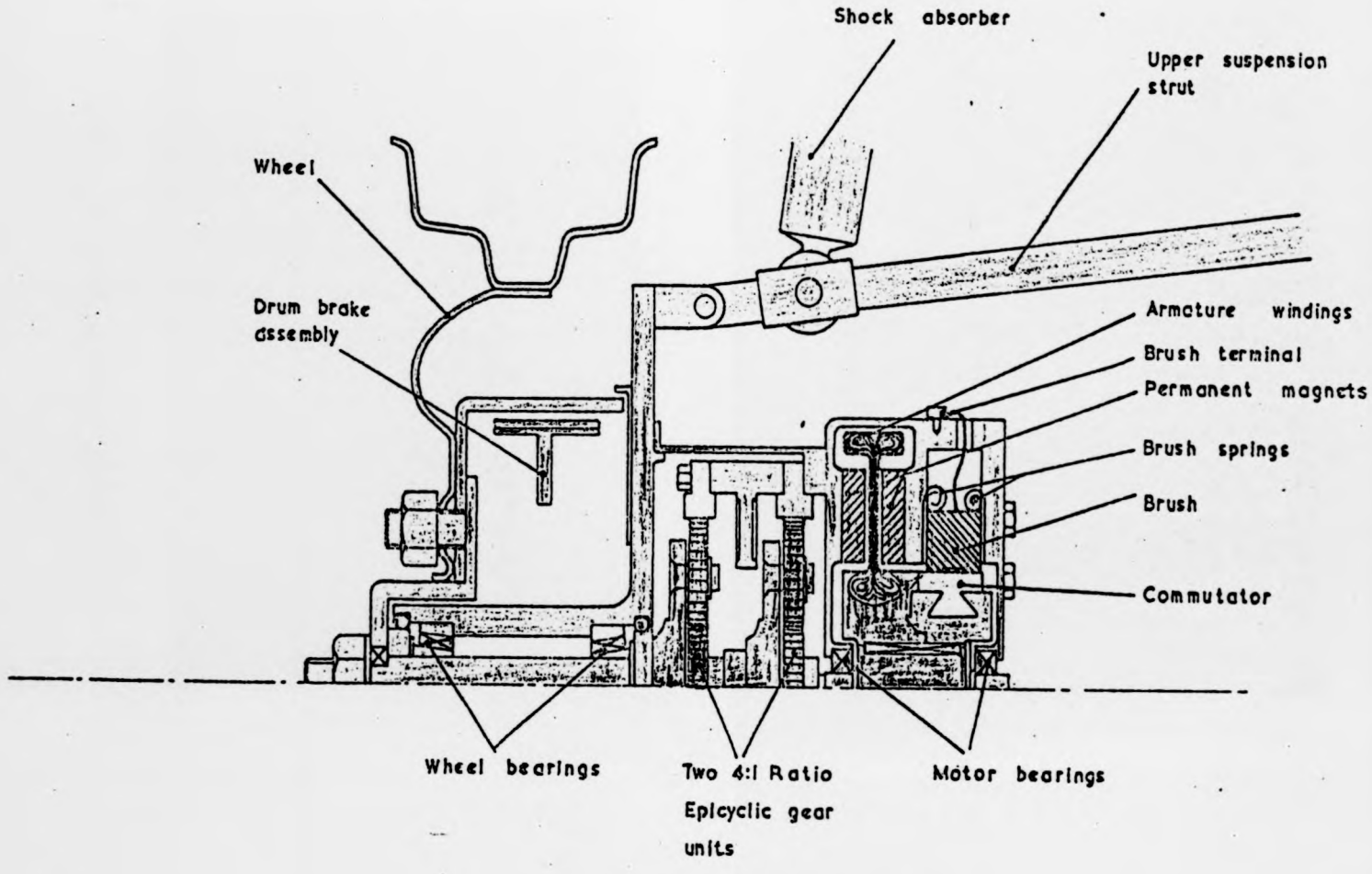

Fig. 3.8 : Schematic of 'Wheel motor' unit

Fig. 3.9 : Prototype wheel motor unit

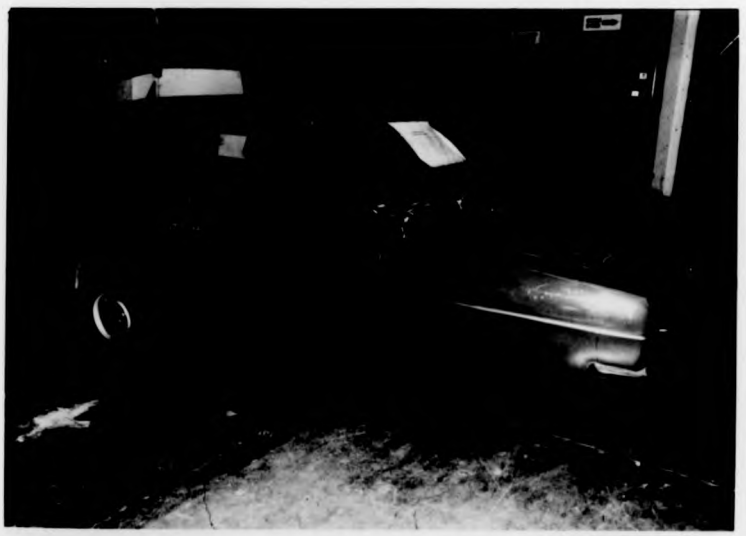

Fig. 3.10 : Reliant Robin vehicle

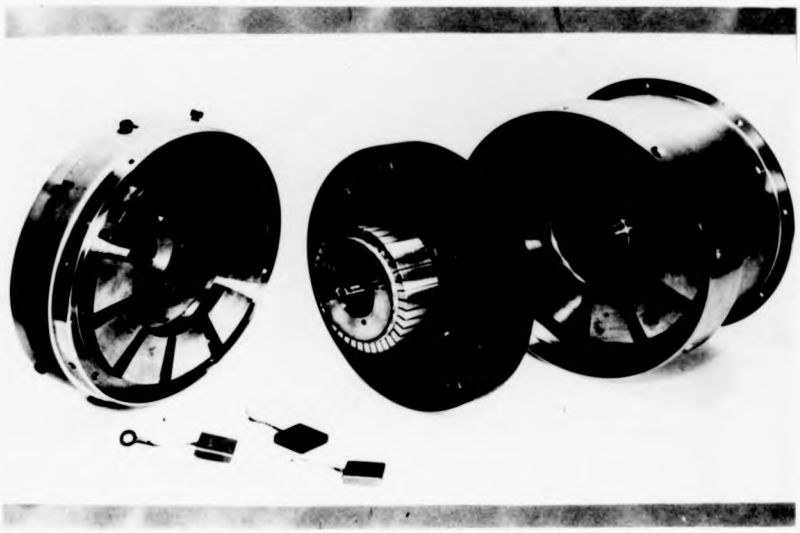

Fig. 3.9 : Prototype wheel motor unit

Fig. 3.10 : Reliant Robin vehicle

3.5 Consideration for a further prototype

The above sections conclude a review of the work at Warwick University on disc armature traction machines to 1975. Despite the setbacks mentioned,the initial results were encouraging with further design and construction envisaged. However, the next two motors were built for totally different applications - a low inertia drive and a car radiator cooling-fan motor. Although the results are extremely valuable in connection with a general design and performance assessment of disc armature motors, they are not considered in detail here[33,34]. It need only be said that several new features were incorporated in these machines and the results from the successful testing and evaluation programme were most encouraging.

3.5.1 Considerations for the vehicle specification

With a growing interest in battery electric traction, it was decided that the advantages of the disc armature motor could best be demonstrated by its use in an electric vehicle, and in particular by a direct comparison with a series wound machine that would usually be specified for this application. It is possible to undertake such a project at the University engineering department using a small car as a suitable testbed. Road testing may be carried out along with static tests on a rolling road or similar facility with experimental results complimented by a theoretical analysis. An immediate choice was between the construction of a purpose-built prototype or the conversion of an existing car to electric drive. In view of the time and facilities needed to pursue

the former option, the latter was chosen for this initial work. The vehicle selected was a Reliant Robin three-wheeled car (Fig. 3.10). Its strong but lightweight construction makes it ideal for the application - vehicles of this type have been a popular choice for many similar conversion projects[35,36]. The car was supplied from the manufacturer without the internal combustion engine and associated components (petrol tank, radiator, heater, etc.) although the four-speed manual gearbox and final drive were retained. A discussion on other components, including the series d.c. motor, and the conversion of the vehicle is given in Chapters 6 and 7.

3.5.2 Considerations for the motor specification

Initial calculations suggested that to propel the vehicle at speeds of 45-50 m.p.h. a motor output power of approximately 7.5 kW is required. The system voltage was determined by a survey of the capacities and dimensions of a wide range of batteries. The Lucas 66 Ah CP11 heavy-duty 12 V starter battery was eventually chosen as information from Lucas indicated that the energy density of this type of battery would be equivalent to that available from their future lightweight traction battery. Considerable experience of the charge/discharge performance of this particular model had been gained in previous work in the department[37]. It was feasible to consider using eight such batteries mounted over the rear axle of the vehicle and thus a nominal system voltage of 96 V was established. With the experience of the wheel motor units, a more conventional drive arrangement was proposed and as the vehicle's

existing final drive was already in place, direct coupling to the mechanical differential was a possibility - for a vehicle speed of 50 m.p.h. the motor would need to operate at 3400 rev/min. However, to adopt this approach would have entailed considerable mechanical modification to the vehicle, especially to allow for the use of both series wound and disc armature motors. Further, more general results on the drive system itself would be available if the conventional gearbox, with four different gear ratios, was retained. It was also easier to consider locating the motor in the space originally occupied by the i.c. engine. As the top gear on most conventional gearboxes is a 1:1 ratio, the motor speed of 3400 rev/min remained. Having determined the basic requirements (7.5 kW, 96 V, 3400 rev/min) any physical limitations on size should next be considered. In terms of overall diameter, the space available immediately forward of the gearbox dictated that this should be no greater than 350 mm. With a suitable allowance for motor case, end windings and running clearances, this corresponded to a value of 280 mm for d_2, the outer active diameter. Because of this diameter restriction, and also to demonstrate the extremely high efficiency of the motor, Hycomax III magnets were chosen to give a high working flux density. This enabled an armature winding to be specified which has a relatively low copper loss associated with it. The design parameters are given in the usual computer printout format in Table 3.4 with the predicted performance curves in Fig. 3.11. It will be noted that the armature is a two-layer duplex wave winding employing 42 coils. The magnetic circuit consists of 8 poles of length 30 mm situated on either side of the armature disc with the steel flux-return

DESIGN NO: 236

DESIGN SPECIFICATION

OUTPUT: 7500. WATTS
VOLTS: 96. V
SPEED: 3400. RPM

DESIGN DATA

D2: 280. MM
D1: 171. MM
POLES: 8.

MAGNETIC CIRCUIT DATA

B1 0.686 TESLA
H1 62975. A/M
LCOEFF 1.30
LFACT 1.20
PHI .001935 WEBERS
A_PHA .75
LMAG 60.0 MM
WGTMAG 12.85 KG
THICK 12.82 MM
WGTFER 7.72 KG
GAP 7.50 MM
MAGDSY 7300. KG/M**3
B1S 1.80 TESLA

ELECTRIC CIRCUIT DATA

PATHS 4.
COILS 42.
TURNS 5.
Z 420.
GAUGE 1.80 MM
WGTWIR 1.66 KG
CRTDSY 3.0 A/MM**2
ARMCRT 31.43 AMPS
LOSS 372.52 WATTS
LAY 2
TEMP 75. DEGREES
SF .85
RARM 0.038 OHMS
ER 91.43 VOLTS

Table 3.4 : Design parameters for 7.5kW motor

[illegible] 13.55 KG
TOTAL 33.79 KG
MECHLO 284. WATTS
SPEED 3374.7 RPM
POWER 7147.6 WATTS
TORQUE 20.23 NM
PWRWGT 199.72 WATTS/KG
EFF .914

PERFORMANCE SPECIFICATIONS

CURRENT DENSITY AMP/MM**2	ARMATURE CURRENT AMPS	SPEED RPM	POWER WATTS	TORQUE NM	EFFICIENCY
1.	10.16	3474.0	649.4	1.78	.665
2.	20.32	3459.8	1601.2	4.42	.819
3.	30.54	3445.6	2545.1	7.05	.868
4.	40.72	3431.4	3481.3	9.69	.891
5.	50.89	3417.2	4409.6	12.32	.903
6.	61.07	3403.1	5330.1	14.96	.909
7.	71.25	3388.9	6242.8	17.59	.913
8.	81.43	3374.7	7147.6	20.23	.914
9.	91.6.	3360.5	8044.6	22.86	.915
10.	101.79	3346.3	8933.8	25.49	.914
11.	111.97	3332.1	9815.2	28.13	.913
12.	122.15	3317.9	10688.7	30.76	.912
13.	132.32	3303.7	11554.4	33.40	.910
14.	142.50	3289.6	12412.3	36.03	.907
15.	152.68	3275.4	13262.3	38.67	.905
16.	162.86	3261.2	14104.6	41.30	.902

Table 3.4 (continued) : Design parameters for 7.5kW motor

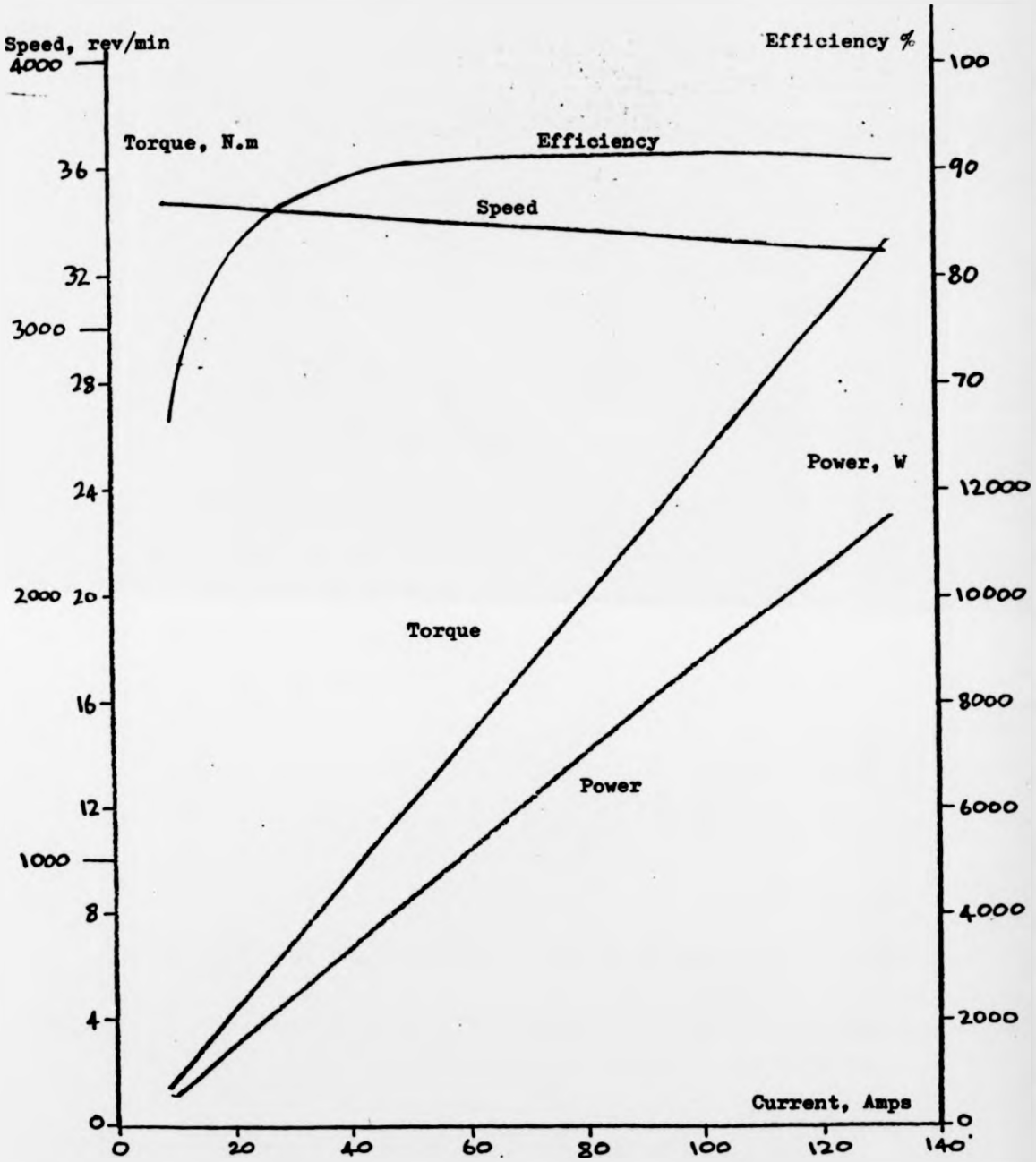

Fig. 3.11 : Predicted performance of 7.5kW motor

Supply voltage = 96V

rings integral with the motor casing. In order to carry the armature current, a full set of 8 brushes is used, bearing on a face-type commutator. The mechanical layout of the motor coupled to the gearbox is shown in Fig. 3.12 and construction and performance details of this machine are covered in Chapter 5. Important considerations relating to the duplex winding chosen are discussed in Chapter 4.

3.6 Other axial-field traction machines

Although the wound-armature d.c. disc motor originated at Warwick University, the use of axial-field traction motors is also being investigated elsewhere. These machines may either be developments of the original (patented) design or the printed circuit motor. In both cases, the attraction of high operating efficiencies and power densities is apparent, although in terms of reliability in this application, the wound rotor machine with its conventional commutator is considered to have the advantage. Principal areas of research are described below.

3.6.1 Flinders University electric vehicle project

In 1972, the electric vehicle group at Flinders University in Southern Australia commenced a project aimed at producing an improved electric vehicle. Their main philosophy is that the high currents required for starting and accelerating a vehicle could be reduced if the electric motor is run at a constant speed with a torque converter in the mechanical drive. Reduced currents lead to better battery utilisation and improve the range of a vehicle.

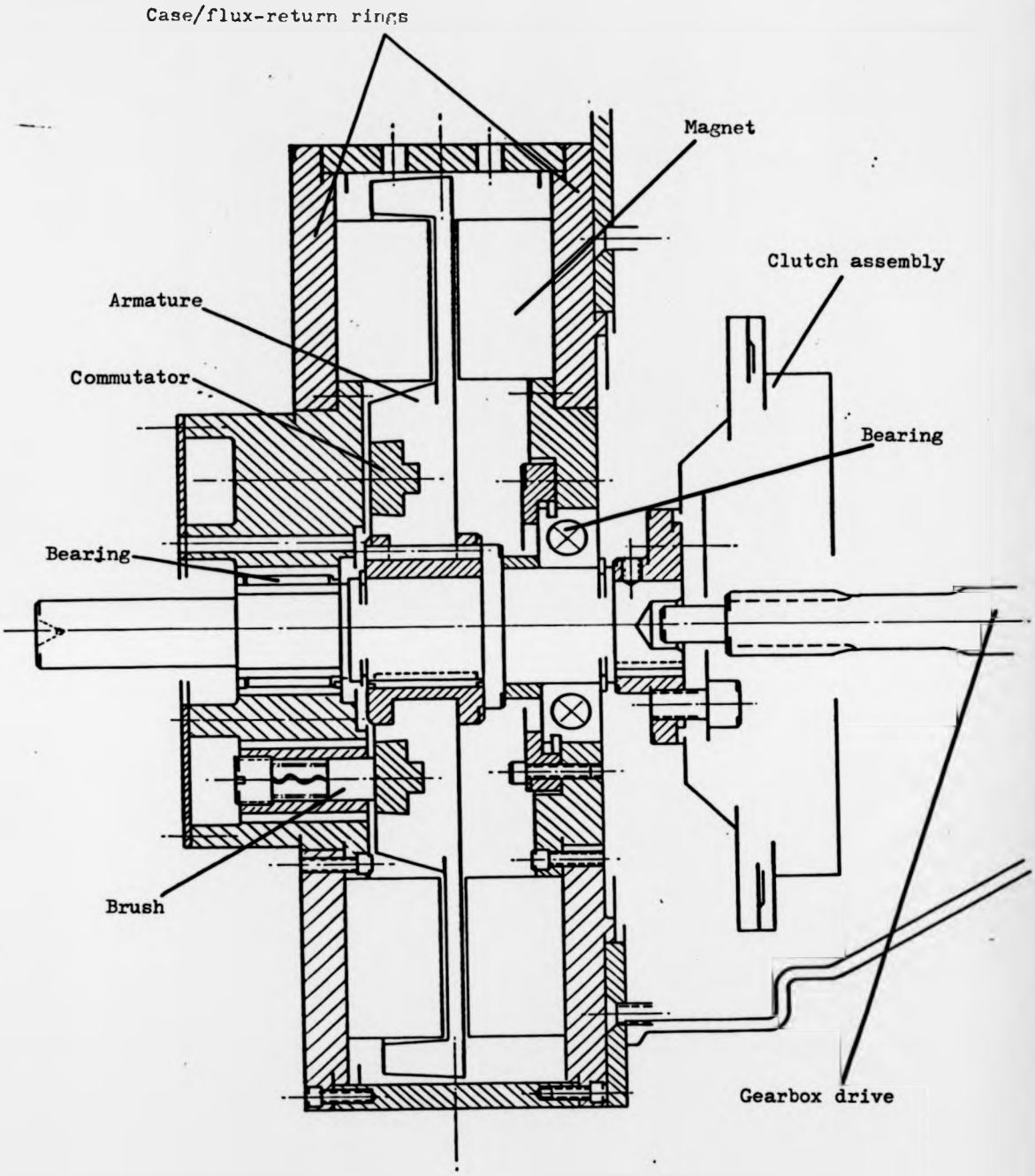

Fig. 3.12 : Mechanical layout of 7.5kW motor

The technique is denoted as 'impedance matching' of the load to the motor and the control system is the subject of a patent. The motors used in the experimental vehicle are printed circuit machines rated at 5 kW. If a higher power output is required, more of these 5 kW 'modules' may be added. As the motor is running at a constant speed, it is less susceptible to overload conditions and tests carried out by the group have indicated that good performance may be obtained using these techniques. Their prototype based on a Fiat 127 has a top speed of 45 m.p.h. and a range of between 38 and 50 miles in urban traffic. Work is progressing in the area of light commercial vehicles where the group consider that EV's will make their first impact. Full details of the technology involved in this research can be found in references 38 and 39.

3.6.2 Cambridge University electric bicycle

This is a development of the Warwick research with the objective of building a motor into the wheel of a bicycle thus employing direct drive[40,41]. The very low motor speed (750 rev/min) leads to a heavy and relatively inefficient machine to produce 400 W output from a 12 V supply. Although the peak motor efficiency is only 57% there is no additional transmission loss to be considered. As the design of this motor involves significant departures from established practice, further discussion is reserved for appendix III.

3.6.3 TRRL electric moped

An investigation into the feasibility of using wheel motor units in an electric moped comparable to such vehicles of today was instigated by the Transport and Road Research Laboratory (TRRL). Direct drive was again highly favoured and this method was employed in a development project using designs based on the Cambridge wheel motor. A specification of 750 W, 600 rev/min and 24 V was established and one motor was to be mounted in each wheel of the moped. Although results have not been published, it is understood that relatively low efficiencies are apparent accompanied by sparking at the brushes, a phenomenon also observed in the motor of Section 3.6.2. At present, new designs are being prepared at Warwick University based on a higher speed motor with reduction gearing. It is intended to evaluate prototypes built to this new design.

4: MACHINE DESIGN AND PERFORMANCE PREDICTION

The design of the early prototype disc armature motors was achieved by selecting the various design parameters by intuition/ experience based on the fundamental operating principles discussed in Chapter 2. Restrictions on available time did not allow any extensive investigation of the effects of parameter change on either predicted or actual performance of the machine. Predicted performance itself could only be based upon trial calculations incorporating expected losses, etc. as no operating experience of machines of this type was available. Because the concept of the machine was a relatively new one, it was felt that the facility to enable rapid assessment and comparison of parameter changes would be extremely useful, and would help to produce an optimum design (in terms of efficiency or power density, say) for any given application. With the availability of a powerful digital computer the design processes were incorporated into a computer program which had the advantage of eliminating repetitive calculation and enabled results to be obtained much more quickly. The first program[27] was written in 1970 using the language Algol 60 and it enabled the designer to specify the majority of the motor design parameters as input data with the program calculating other design parameters and the predicted performance. The input data sheet is illustrated in Table 4.1 and when values are assigned to the listed parameters, the program performs the calculations and outputs the results as shown in Tables 3.1 to 3.4. Unique results are calculated from each set of input data although there is no

Table 4.1 : Printout C.A.D. input data sheet

U N I V E R S I T Y O F W A R W I C K

Department of Engineering

DISC-ARMATURE MOTOR DESIGN - DATA SHEET.

Design specification	Machine design No.	
	Output power, watts	
	Voltage, volts	
	Speed, rev/min	
Design	Internal diameter, d_1 mm	
	External diameter, d_2 mm	
	No. of poles.	
Magnetic circuit data	B_m, Tesla	
	H_m A/M	
	Double or single magnets	
	Leakage coefficient	
	Loss factor	
	Pole-arc/pole-pitch	
	Airgap, mm	
	Magnet density	
	Max flux density in MS, T	
Electric circuit data	No. of parallel paths	
	No. of coils	
	No. of turns/coil	
	Diameter of wire (bare) mm	
	Current density, A/mm^2	
	Space factor	
	Armature temperature, ^oC.	
	Wt. of non-active parts, kg	
	Mechanical loss, watts	
	Performance graphs (T or F)	

guarantee that the predicted performance will match the original specification, or that an optimum design has been produced. Several attempts are usually needed to achieve the desired result. As well as the results presented in tabular form, there is also the option of graphical representation on a plotting device. Examples of this form of output are shown in Fig. 4.1 which illustrates the performance curves of a motor. Although this program was of great value, it had the obvious limitation that as it was only a calculating routine, the majority of design parameters had to be specified at the start and thus it was still a time-consuming process to investigate a wide range of parameter variation. No detailed description of this program is given here as an extended and modified version now forms the second stage of the two-stage design routine which is described later and which is able to encompass parameter variation. However, it is first necessary to consider the effect of the choice of magnet material as this has a great influence on motor performance, size and cost.

4.1 Considerations for magnet material choice

In spite of the advantages of improved efficiency and power density that the use of permanent magnets can bring, it is only within the past two decades that permanent magnets generally have achieved great economic importance in d.c. electric motors[42] and in particular, machines for electric traction. The basic choice for motors is between ferrite, Alnico and rare-earth magnets, although there are many different grades of these materials available today and a wider consideration is necessary for detailed

Fig. 4.1(a) : Computer-produced curve

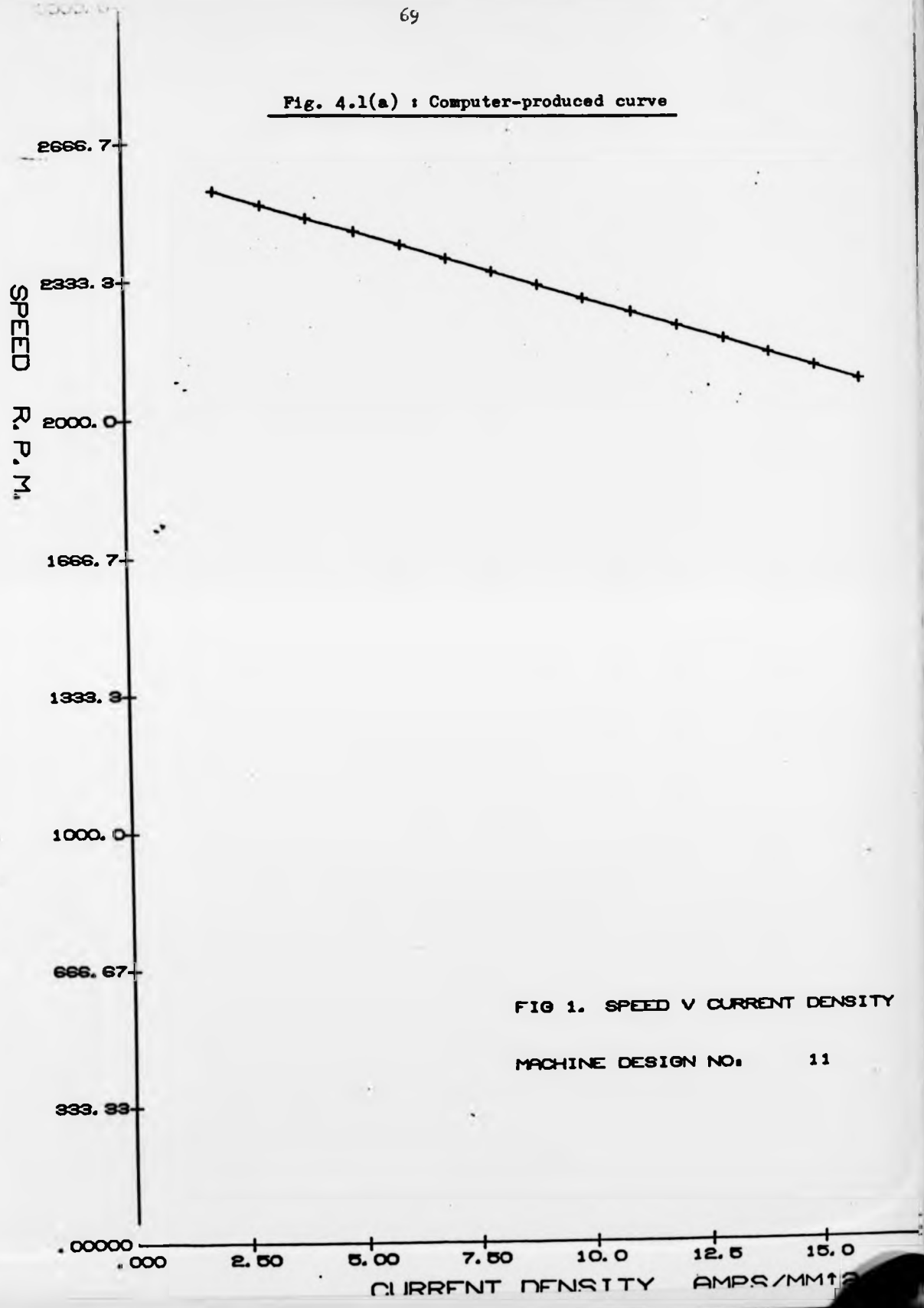

FIG 1. SPEED V CURRENT DENSITY

MACHINE DESIGN NO: 11

Fig. 4.1(b) : Computer-produced curve

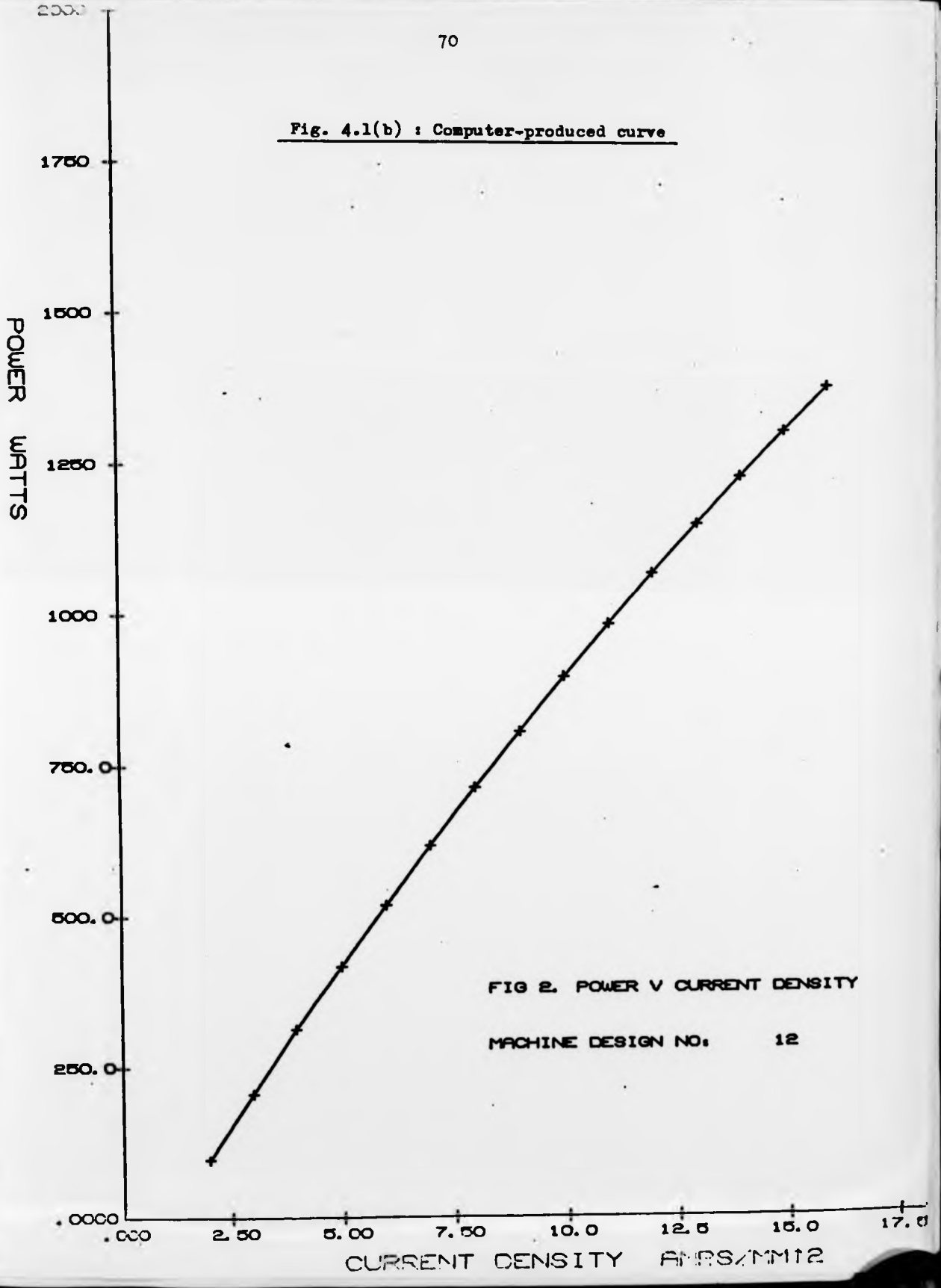

Fig. 4.1(c) : Computer-produced curve

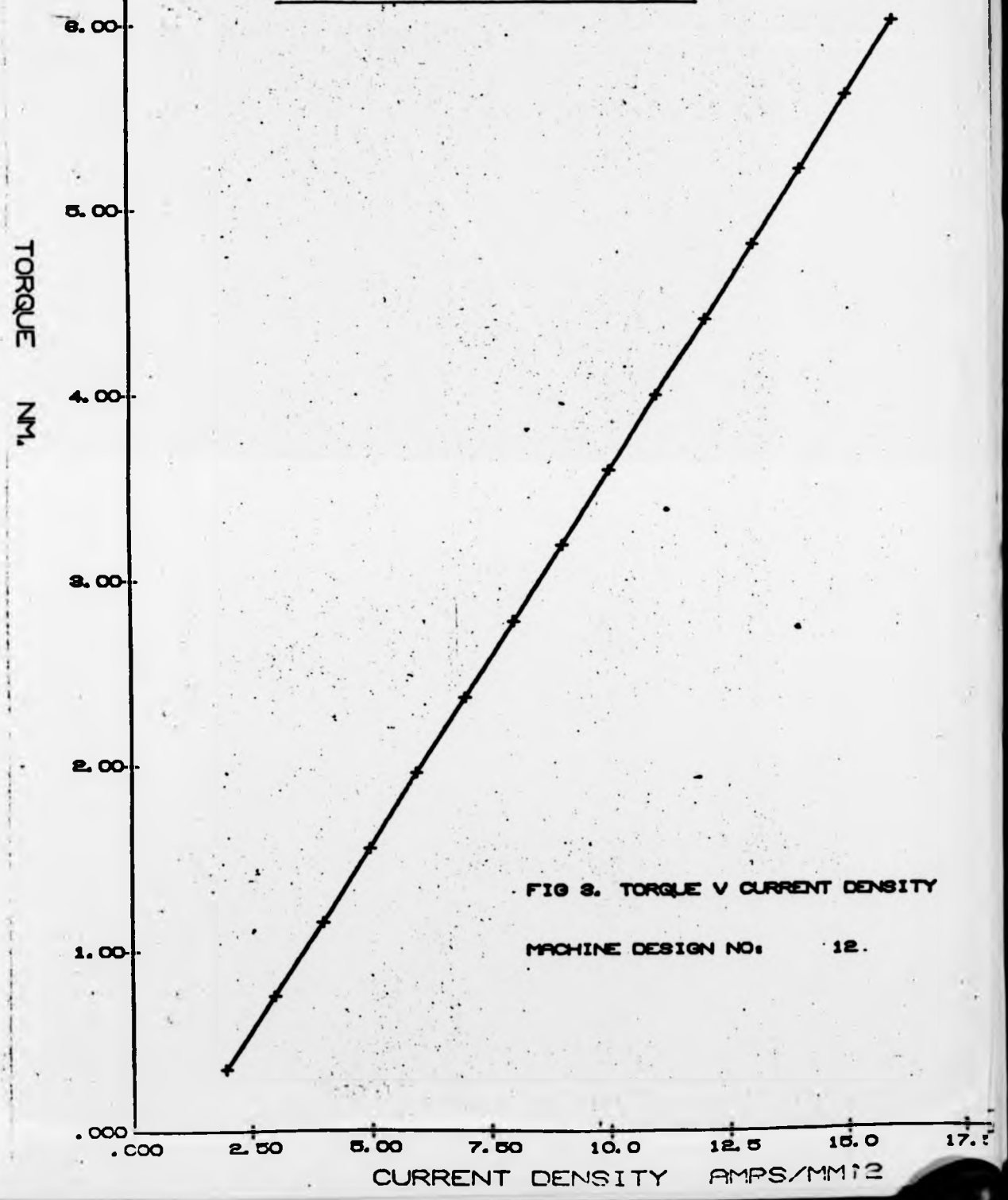

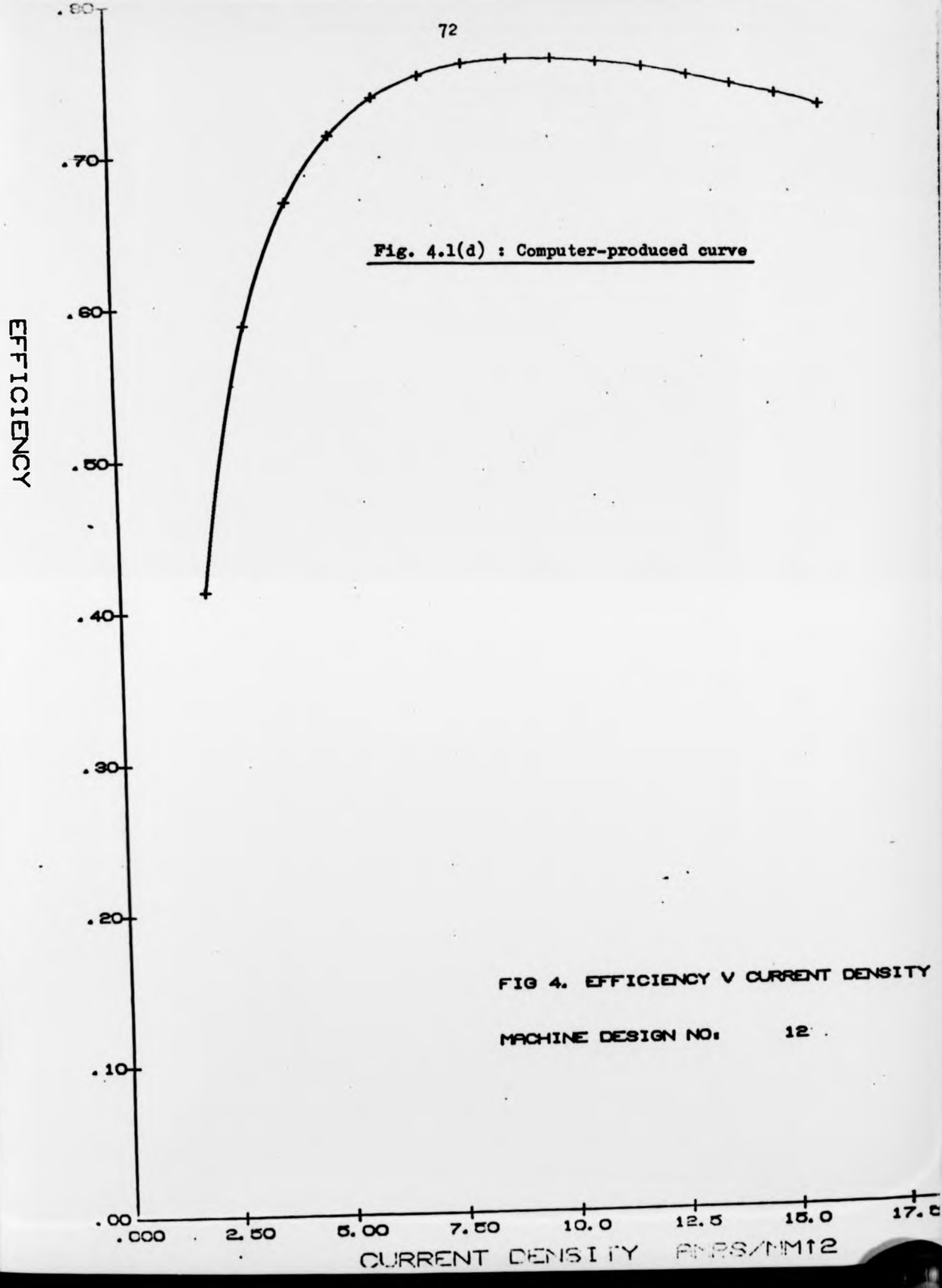

Fig. 4.1(d) : Computer-produced curve

FIG 4. EFFICIENCY V CURRENT DENSITY

MACHINE DESIGN NO: 12

design work. The three types have been considered for use in disc armature motors and several design studies have been carried out which illustrate the differences between selected magnet materials on a size, cost and performance basis.[24,43]

4.1.1 Manufacture of different materials

As well as the basic material cost, the method of production of permanent magnets can have a significant effect on both the final cost and performance of the material. Most magnetic materials can be made with or without a preferred direction of magnetisation (anisotropy) and although specifying an anisotropic material enhances the magnetic performance (in the direction of interest), it adds complexity to the manufacturing process as a strong magnetic field has to be applied at some stage. Ferrite materials are ceramics consisting of mixed oxides including barium or strontium. The resulting compound is powdered, pressed in a magnetic field (aligns the magnetic domains and leads to an anisotropic material) and then fired. The resulting material is very brittle and some shrinkage usually occurs whcih has to be allowed for in the initial specification. As indicated earlier, this is the cheapest available material and although there is scope for improvement of magnetic characteristics most effort is being expended to reduce the relatively high manufacturing costs.

Alnico materials are metallic alloys with constituents in typical ratios of 8% aluminium, 14% nickel, 25% cobalt with the balance made up or iron. The alloy may be cast, after heating to

1400°C, or pressed and sintered, after reduction to a powdered form. In both cases, the anisotropic material is produced by the application of a magnetic field while the material is cooling. Many different grades of Alnico material are available today and Fig. 4.2 shows the BH curves for a range of these. They result from variation in the proportions of the constituent metals - for example, increasing the cobalt content from 25% to 35% yields a material with a higher coercivity and reduced remnance, the 'Hycomax' grade.

A development over the last 10 years has been the increased use of magnets made with combinations of the rare-earths - the most favoured to date being an alloy of samarium and cobalt $SmCo_5$. These materials have an extremely high coercivity and energy product although the remanance is not as high as Alnico types. They are produced by pressing the powdered alloy in a magnetic field, sintering, and finally a heat treatment process is used. The $SmCo_5$ alloy typically contains 35% samarium although a greater percentage is used initially to allow for oxidisation in the manufacturing process. An extremely high magnetising field is needed either to magnetise or demagnetise $SmCo_5$ magnets and they are usually supplied to a customer in a magnetised condition in contrast to ferrites and Alnicos which are normally unmagnetised.

The grades of material just described are also available in 'bonded form'. This is where the base material in powdered form is mixed with a bond material (rubber, polymer, plastic, etc.) to from a magnet which is no longer brittle and which can easily be machined. It can also be made flexible if required - magnetic gaskets for refrigerators are an obvious example. Such magnets do

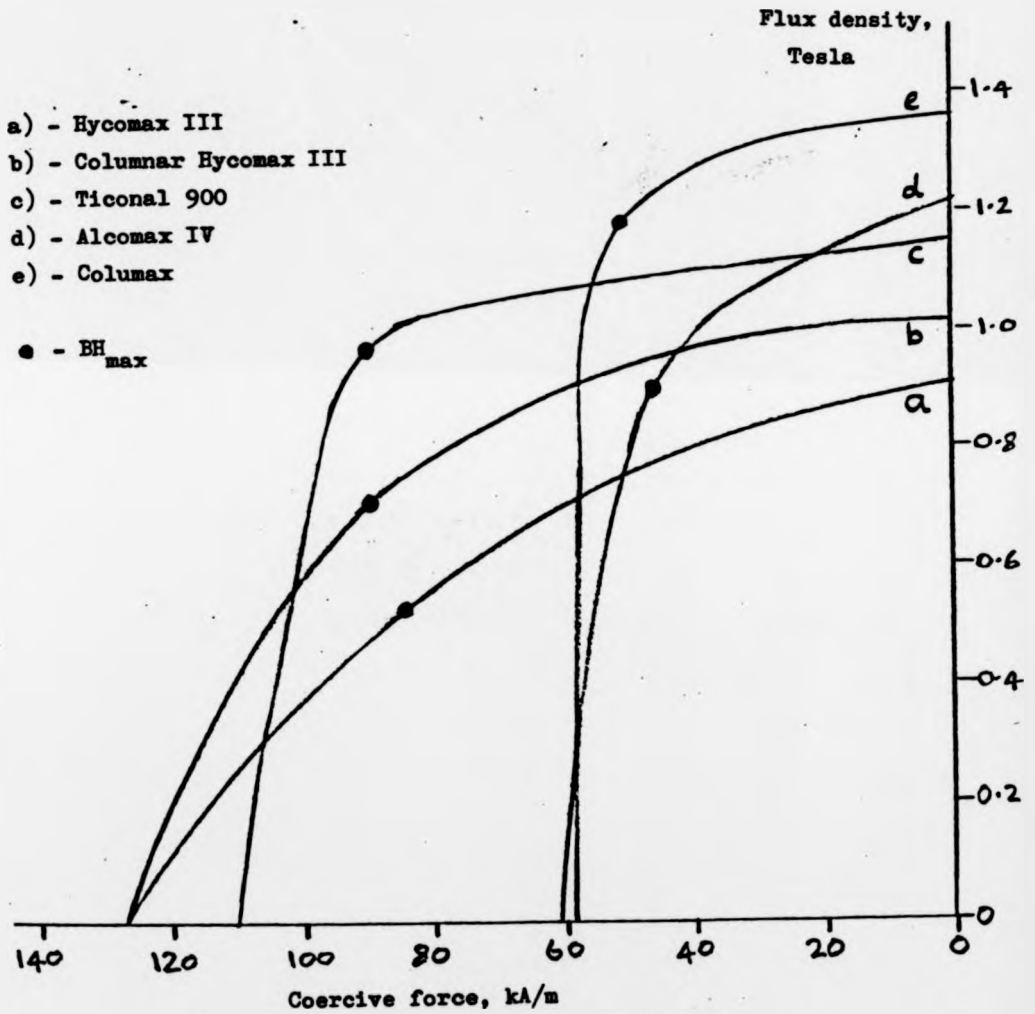

Fig. 4.2 : Demagnetisation curves for various Alnico materials

however have a limited temperature range, the upper limit determined by the characteristics of the bond material. In addition, permanent degrading of the magnetic properties of polymer-bonded $SmCo_5$ results when working at temperatures much above $60^{o}C$. While the mechanism behind this is not fully understood, it is believed that at elevated temperatures a reaction occurs between the samarium and the bond material. A further general disadvantage of bonded magnets is that the energy product is reduced, sometimes by as much as 50%. In spite of these limitations, such materials have found wide application - particularly for prototype work where a new or complex shape can be made relatively cheaply and easily as expensive tooling is not required.

As indicated earlier, there are many variants of the basic grades of material, and research also continues into new materials - an example being the alloy of chromium, iron and cobalt (Chrofeco). However, with the increasing worldprice of cobalt, materials that do not depend on this element have a great attraction. A recent development is the alloy of manganese, aluminium and carbon[44,45] and although this material is not yet commercially available elsewhere, its use in Japanese loudspeakers has been reported. Fig. 2.8 illustrates the BH curves for representative samples of the materials considered in this section. Two grades of Alnico are included as the range of these materials is so large. Information on mechanical and physical properties is given in Tables 2.1 and 2.2.

4.1.2 Effect of magnet choice on motor design

Having assessed the range of magnetic materials available the machine designer is faced with the often difficult problem of choosing between them. Sometimes a restriction imposed by the motor specification or a specialised application will lead easily to a particular material, but generally the selection of magnet material and in particular the associated flux density is fundamental to the design process. As well as the cost and performance of the machine, the specification of the armature winding depends heavily on this choice, and thus in the computer-aided design procedures that are described in Section 4.3 the magnet material is the first parameter to be decided, and this by the designer - not by any program subroutine. A particularly relevant example is the development of a low inertia disc armature motor[34]. This is to satisfy the requirement for an extremely rapid-response drive-acceleration from rest to 6000 rev/min in 300 ms being necessary. As the acceleration of a d.c. motor's armature is proportional to the product of armature current and flux density, the use of a high-remanance magnetic material is most appropriate. However for a given motor output an increase in working flux density will generally require a smaller amount of armature copper and in this particular case it was possible to construct a light, thin armature disc - precisely the requirement for a low inertia system. If, on the other hand, a ferrite material had been chosen, the low flux density would have led to a comparatively heavy armature, exactly the opposite condition.

Another factor that must be carefully considered is the

relatively long magnetic airgap. This condition makes the use of a high-coercivity material most appropriate, and the penalty to be paid for specifying an Alnico grade with its low coercivity is the much larger quantity of material that will be needed. The motor application is of prime importance here and the acceleration characteristics required of the low inertia motor can only be met by using the highest remanance material available.

In battery electric traction applications, the efficiency of the motor is a very important factor and any way of reducing the motor losses will be of great benefit. Although in the disc armature motor the iron losses are eliminated, the copper loss still remains and this may be reduced by specifying a high flux-density magnet material which in turn will require less armature copper. Unfortunately, the use of such magnets in disc armature traction motors has become prohibitively expensive because of the price of cobalt. It is possible, however, to obtain some degree of compromise by working a ferrite material well above the BH_{max} point on the demagnetisation curve. Although this represents an inefficient use of the magnet, generally requiring a far greater length than for optimum conditions, the resulting higher flux density allows an increase in the motor efficiency with only a small increase in overall motor costs. A recent design study[43] has compared such a machine with those using Alnico or rare-earth magnets and has found that only a small reduction in efficiency occurs with considerable cost saving. A disc armature motor using ferrite material under conditions of relatively high flux density is detailed in Appendix II.

The magnetisation of the selected material needs to be considered at an early stage along with the possibility of recoil operation. As discussed earlier with ferrite and rare-earth magnets, it is possible to magnetise the segments before assembling the motor as the linear demagnetisation characteristic will ensure operation at the desired operating point. If Alnico magnets are specified magnetising windings are usually specified to allow energisation of the field system after assembly.

4.2 Initial requirements for the design procedure

The basis of the new disc armature motor design program is that the predicted performance of a machine should be accurately calculated to allow meaningful comparison of the various design options. In addition all design options presented should meet the original specification to within a given tolerance. It was also felt desirable to introduce a number of other enhancements to the program. As indicated above, the need to change parameter values in the search for an optimum design was considered along with the ability to place restrictions on selected parameters if necessary. Instead of having to specify all the design data, as in the 1970 program, the only input required is the power, speed and voltage specification along with the choice of magnet material. Perhaps the greatest benefit resulting from the new program is the inclusion of the 'interactive' computing facility. The operation of the earlier program required the Algol instructions to be supplied on punched cards with the actual run supervised by a member of the computer unit staff. The output from the program generated on the

lineprinter and/or plotter would be returned after a short time. With the interactive facility a remote terminal (Fig. 4.3) is used with the design program stored in the computer disc memory. Inputs to the program (power requirements, design limitations, etc.) are entered via the terminal and the resulting output is displayed at the terminal and printed on the lineprinter if desired. The advantage of this method is that the results can be seen very quickly and this is particularly useful when design parameters are restricted or modified in some way. Many of the design parameters can only be varied in discrete steps (number of poles, coils or turns per coil, etc.) and this must also be allowed for. On the other hand, the magnet dimensions and operating point may be varied continuously and it has been found useful to allow the program access to a data file on which a suitable portion of the BH curve is stored. More generally, the program must be capable of modification as experience allows greater sophistication, and all of the hard copy must have sufficient information on it to allow easy reference at a later stage. With the inexperienced computer user in mind, the operation of the program should be as straightforward as possible with prompts in plain English displayed at the terminal where appropriate. This 'user friendliness' is considered to be a major requirement of computer operating systems today, especially with the increasing usage of desk-top microcomputers.

4.3 Development of the software

The ability of the digital computer to perform extremely fast mathematical computation lends it admirably to programs based on an iterative procedure where the same set of calculations is performed

Fig. 4.3 : Remote computer terminal

Fig. 4.4 : Remote computer terminal

many times over. Design and optimisation programs may be based on such a technique with combined variation of the design parameters until a satisfactory result is obtained. The design parameters of a motor, for example, could be given some initial values; from these the expected performance is calculated and compared with the required performance, and finally the design parameters modified to try and improve the agreement between required and predicted performance. The whole procedure is then repeated until the agreement is close enough for all practical purposes. In the design program for the disc armature motor, the iteration is performed until the power and speed lie within given limits of the required values with other performance characteristics then calculated. This is the first and most powerful stage of a two-stage process and it produces alternative designs to a given power, speed and voltage specification. The second stage allows modification of the major design parameters if required and is described later.

4.3.1 Initial considerations for design stage one

With just the specification of the power, voltage and speed of a motor, it is clear that a large number of design alternatives are possible encompassing wide variation of the physical and electrical design parameters. Of all the factors influencing the final specification, it is the choice of magnet material that has the most dramatic effect. The selection of a ferrite, for example, will tend to lead to a motor of a larger diameter to try to achieve a high working flux. The high flux-density Alnicos will generally give a machine of a higher efficiency as the copper content of the armature

(and therefore the copper loss) will be reduced. As the selection of magnet material is thus so fundamental to machine design, the designer is allowed to choose a material from a wide range whose characteristics are stored as data. This choice is based on experience although it would, of course, be possible to run the program again with the specification of an alternative material.

Having specified the power, speed, voltage and magnet choice, a suitable starting point for the design process is a consideration of the diameter of the machine. It was shown in Chapter 2 that the power output from a disc armature motor is proportional to the cube of the diameter and the equation expressing this relationship is used in the consideration of the most appropriate diameter. It will, however, be found more convenient to express the flux density in terms of the flux density in the magnet rather than that in the airgap. This may be achieved by incorporating the leakage coefficient, LC, and the ratio of pole arc to pole pitch, α. Accordingly equation (2.25) is now written:-

$$P = \frac{B_m . \alpha . \omega . SF . L . \pi . I . d_2^3}{12 \sqrt{3} \; a . G . LC} \qquad (4.1)$$

where d_2 is the outer active diameter and B_m the magnet flux density. All other symbols remain as previously defined. As the speed of a motor is usually given in rev/min, ω may be replaced by $2\pi . n/60$ where n is the rotational speed in rev/min. The equation is also rearranged to bring d_2 to the left-hand side. Thus:-

$$d_2 = \left[\frac{360 \sqrt{3} \; P . a . G . LC}{B_m . \alpha . \pi^2 . n . SF . L . I} \right]^{1/3} \qquad (4.2)$$

which is the fundamental equation for design stage one. The power and speed are known and as discussed in Chapter 2, the values of LC, α and SF remain approximately constant from machine to machine. Suitable values are assigned, and L is initially taken as 2 to simplify the construction of the machine - this may be increased if necessary, for example, if d_2 is too large. This leaves only the number of parallel paths, gauge of wire, magnet flux density and armature current to be determined for the evaluation of d_2. Optimum magnet utilisation is initially specified with the flux density chosen corresponding to BH_{max} for the material in question. The current may be determined from the relationship:-

$$P = E.I \tag{4.3}$$

ignoring for the moment mechanical losses. E may be represented as some fraction of V, the applied voltage, and the initial value of I found. The number of parallel paths, gauge of wire, armature current and current density (current per unit area of armature conductor) are related by the equation:-

$$I = \frac{a.C.\pi.G^2}{4} \tag{4.4}$$

where C is the current density in A/mm^2 as G is specified in mm. C is given a preset value depending on rating conditions (see Chapter 5) and this leaves the wire gauge and number of parallel paths to be determined. The program initially assigns a the lowest possible value (2 for a two-layer wave winding), the corresponding ideal value of G is calculated, and the standard wire gauge above this value is selected. The value of d_2 may now be calculated and a small subroutine compares this with the value of G selected to check that the wire gauge is not unreasonably large. If it is the value of a is increased which will tend to require a smaller gauge

of wire, chosen from a wide range of wire gauges stored as data in the program. The program is biased towards two-layer windings (unless overridden by the designer) and a will first be increased to 4 - a duplex wave winding, then made equal to the number of poles (simple lap) and finally twice the number of poles - duplex lap. In practice, this final option has never arisen.

Having established d_2, equation (2.24) may be used to find d_1 and thus the two principal dimensions of the machine are known. Occasionally a limit on the overall diameter is specified and this is catered for by allowing a restriction to be placed on d_2. The program chooses the lesser of the calculated value and the restricted value with suitable modifications to a and G. As the program runs, many of these initial values can be, and often are, changed. The generation of alternative designs and the choice of an optimum in terms of efficiency and power density will now be described.

4.3.2 Operation of design stage one

The easiest way of describing the operation of a computer program is by the use of a flowchart and the following description applies to the diagram presented in Fig. 4.4. The procedure will be outlined as if it were being run from a computer terminal. Initially a message is output to the screen asking for the power, speed and voltage to be typed in. A list of magnet materials is then presented and one of these is selected - the relevant magnet characteristics are read in from a separate disc file. Possible restrictions are then considered. As well as the limitation on d_2, it is possible to select the number of poles, minimum number of coils per pole, the

Fig. 4.4 : Flowchart of program phase 1

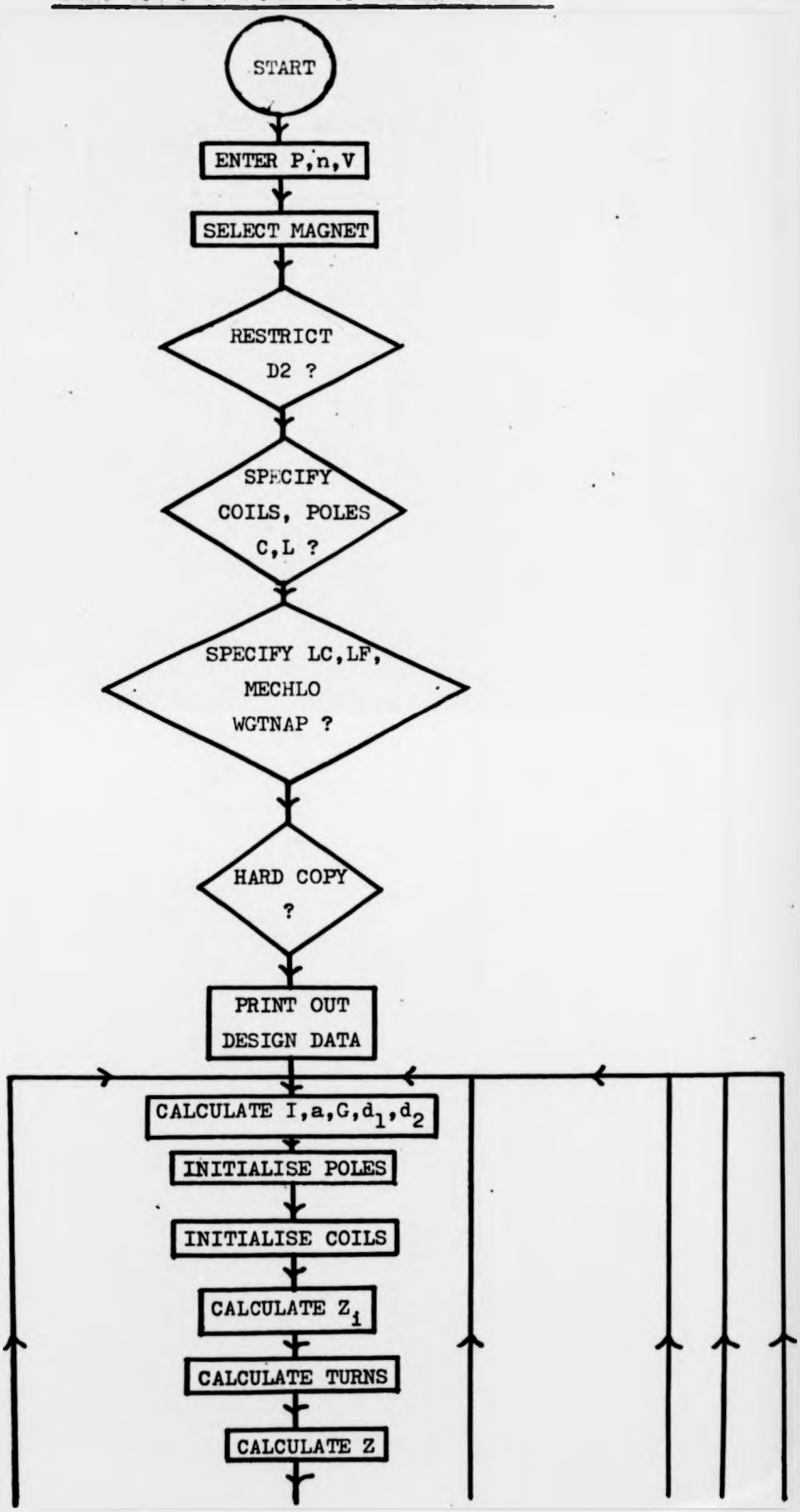

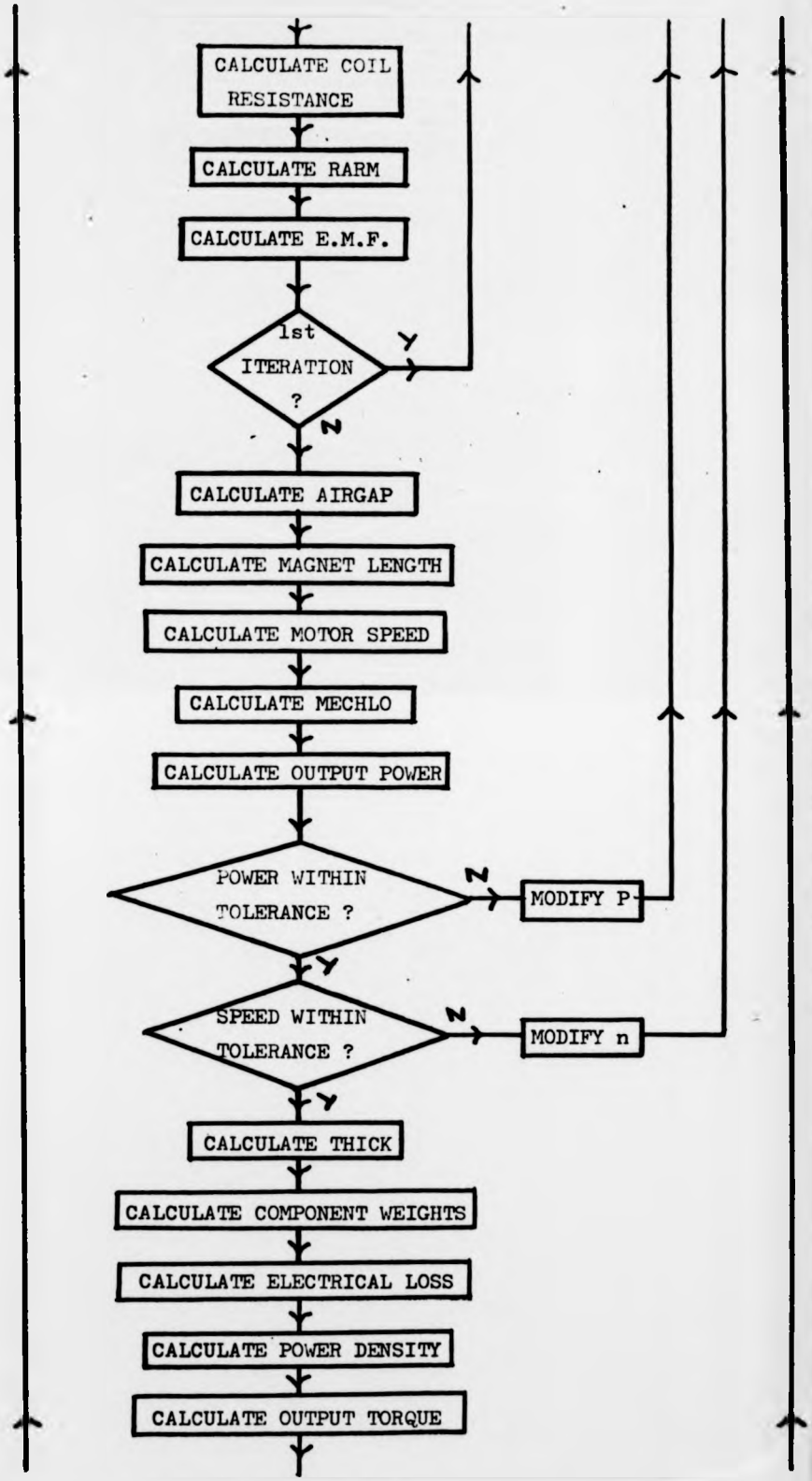
CALCULATE COIL RESISTANCE
CALCULATE RARM
CALCULATE E.M.F.
1st ITERATION ?
Y
N
CALCULATE AIRGAP
CALCULATE MAGNET LENGTH
CALCULATE MOTOR SPEED
CALCULATE MECHLO
CALCULATE OUTPUT POWER
POWER WITHIN TOLERANCE ?
N
MODIFY P
Y
SPEED WITHIN TOLERANCE ?
N
MODIFY n
Y
CALCULATE THICK
CALCULATE COMPONENT WEIGHTS
CALCULATE ELECTRICAL LOSS
CALCULATE POWER DENSITY
CALCULATE OUTPUT TORQUE

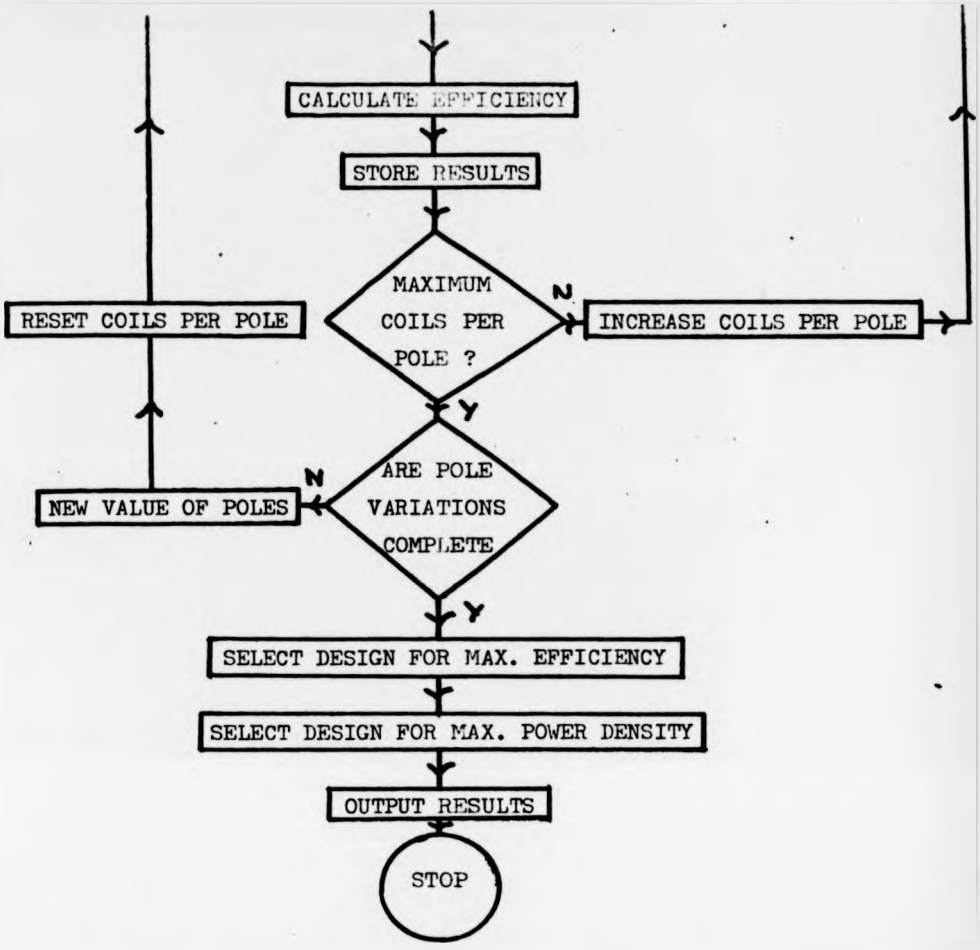

Fig. 4.4 (continued) : Flowchart of design stage 1

current density or initial number of layers. If selected, these override the values set in the program. In the same way, the leakage coefficient, loss factor, mechanical loss and the weight of the 'non-active parts' (resin, casing, bearings, etc.) may also be specified. If they are not, then values are again set or calculated within the program.

The final decision to be made by the designer is whether or not a hard copy of the results should be produced. Once these options have been dealt with, the information input so far is displayed on the screen as a check and then the calculation routines commence. It will be appreciated that all remaining calculations/ decisions covered in this sub-section are performed within the program and do not require any further external action.

The armature current, number of parallel paths, wire gauge, d_2 and d_1 are found as described in the preceeding section. if unspecified at the start, the current density assumes a value corresponding to continuous running of the motor (see Chapter 5). The next step is to set an initial number of poles. This is allowed to increase with the diameter of the machine, but the actual value is not critical as a wide variation in the number of poles is allowed at a later stage. Experience has shown that eight or ten poles represents a suitable starting point with a minimum of six for most applications. The minimum number of coils is then found by taking the minimum number of coils per pole. This is primarily for commutation reasons (see section 4.4 and Appendix II) and is set to 5 unless already specified. The type of winding under consideration (wave, lap or duplex) is also taken into account when

selecting the number of coils. An ideal number of conductors for the machine may be calculated from:-

$$n = \frac{E.a.60}{\emptyset.Z.p} \qquad (4.5)$$

where $\emptyset$ is calculated from B_m, d_2, d_1, α and p. This ideal value, Z_i may be expressed:-

$$Z_i = \frac{360a.\ E.LC.10^{-6}}{n.\alpha.\bar{b}_m.\pi.d_2^2} \qquad (4.6)$$

with d_2 expressed in mm. This will generally be a non-integral value and it is used, along with the number of coils, to find the number of turns per coil which will yield the number of armature conductors closest to Z_i. The actual relation used is:-

$$\text{Turns/coil} = \text{INT}\left(\frac{Z_i}{2\text{xcoils}} + 0.5\right) \qquad (4.7)$$

where the function INT means 'take the integer portion of'.

The armature resistance is the next parameter to be considered. First, the resistance of a coil is calculated from d_2, d_1, p, turns/coil and G. The procedure used makes an allowance for the unequal length of the coil sides and end windings, and also includes a suitable length of conductor for connection to the commutator. The total armature resistance is found from:-

$$R_a = \frac{\text{Coils.}\ R_c}{a^2} \qquad (4.8)$$

where R_c is the previously found coil resistance and R_a the total resistance. R_a is calculated at a temperature of 75^oC as this is a

specified temperature for performance characteristics according to B.S. 1727. A new value for the generated e.m.f. is calculated from:-

$$E = V - IR_a - V_b \qquad (4.9)$$

where V_b is the voltage drop due to the brushes and is given a suitable value from manufacturers' data. At this point during the first iteration, the new value for E is substituted in place of the initial estimate in equation (4.3) and the entire set of calculations is repeated. On the second and subsequent iterations, the airgap is determined from the gauge of wire, number of layers and suitable allowances for the encapsulation material and running clearances. The magnet length is found using a modified version of equation (2.2) and the rated motor speed found directly from equation (4.5). Before the rated power output can be calculated the mechanical losses in the machine have to be determined. Until recently, an estimate of these losses based on experience was made by the designer. The new program contains an empirical formula for mechanical losses which has been found quite accurate and will be described in more detail in the next section. The rated power output of the motor, Pr, may now be calculated from:-

$$P_r = E.I - W_m$$

where W_m is the mechanical loss in watts. P_r is then compared with the specified power which is given a modified value depending on whether P_r is greater than or less than that required. The modified value is used in the next iteration although P_r is compared with the original specified power each time. Iteration continues until P_r lies between the specified power and 15% above the specified

power. When this occurs, the number of layers in the machine is rechecked and then the speed is compared with the required value and modified until it lies within ± 5% of that specified. Each time the program changes the speed specification, the power iteration is reworked. When studying the operation of the program it has been found that while the power assumes an acceptable value after 4 or 5 iterations, the speed will either do likewise or will possibly alternate between two values, one above and one below the allowable speed range. If this occurs during a run, the program will allow modification of the magnet flux density, moving B_m further up the demagnetisation curve until a predetermined value is reached. While this represents a departure from the BH_{max} ideal, it allows designs to be considered that might otherwise have been lost. Once the power and speed are acceptable, the remaining design calculations may be performed. These include the thickness and weight of the flux return ring (the steel must not saturate), the weight of copper and magnets and the weight of the 'non-active parts'. As with the mechanical loss this was originally specified by the designer but in the new program, it is related with good accuracy to a function of the ratio of motor power to motor speed. The total weight is now calculated along with the electrical losses (copper and brushloss) and the power density. Finally, the torque and efficiency are found from:-

$$T_r = \frac{60P_r}{2.\pi.n} \tag{4.10}$$

and

$$\eta = 1 - \frac{W_m + I^2.R_a + V_b.I}{V.I} \tag{4.11}$$

where T_r is the rated torque in N_m and η the efficiency of the motor. The information relating to this design is stored and the number of

coils per pole increased by one. The entire procedure is repeated with this new number of coils and the results are again stored. When the number of coils per pole reaches a preselected maximum, usually ten, the number of poles is changed to two above the value originally selected and the number of coils to the preselected minimum. The procedure is repeated with increments applied to the number of coils per pole as before. The total variation in pole number is from 4 above to 4 below the value initially selected in the program. With all the results stored as output data, the design which has the highest efficiency and that with the highest power density are selected and output in a similar fashion to Table 3.4. The remaining designs are output in abbreviated form on the lineprinter for assessment by the designer at a later stage.

This represents the end of a single run of the program although it may easily be re-run with the same motor specification but using an alternative magnet material or incorporating restrictions on the design process.

4.3.3 Performance prediction by design stage one

The accurate prediction of the performance of a motor is necessary, both as a check against the original specification and to be able to assess the motor's behaviour under a range of operating conditions. Thus as well as the rated power, speed, torque and efficiency these parameters are also provided over the range from no load to around twice the rated output (depending on rating conditions). In order to carry out such a performance prediction, the losses within the machine must be taken into account and routines within

the design program are provided to calculate to a suitable accuracy the magnitudes of the various losses. With an iron free encapsulation material eddy current and hysteresis losses are eliminated. Armature reaction effects can be considered negligible in machines of this type which leaves only the copper loss, brush voltage drop loss and mechanical loss to be estimated. The copper loss is taken as the I^2R heating loss within the armature and may easily be evaluated; similarly a constant voltage drop per brush pair may be assumed and this is multiplied by the armature current to give the power loss here. The assessment of mechanical loss is more complex, however, as it consists of brush friction, bearing friction and windage, and therefore its direct evaluation is not a straightforward process. This was recognised in the 1970 program and was overcome by allowing the designer to specify a suitable value of mechanical loss from experience. For the new and more general design program, an alternative approach is required which enables a reasonable assessment of mechanical losses to be made within the program itself. It is necessary, however, that any routine developed to achieve this does not require a detailed specification of the mechanical layout. Fortunately, experience gained in the operation of earlier machines may be used to advantage in this situation and it has been found possible to develop an empirical equation which will predict mechanical losses.

In order to establish the correlation between the mechanical losses of a machine and the size, power,rotational speed, etc., it is first necessary to investigate the magnitudes of such losses under various operating conditions in prototypes that have already been built and tested. This can best be achieved by a collation of

the 'light-run' or 'no-load' test results. These relate to conditions of varying speed and applied voltage where the motor does not drive any additional load. Thus, all the power supplied to the motor is used to overcome copper, brush and mechanical losses; further since the values of armature current under these conditions are relatively small, the majority of the input power is dissipated as mechanical loss. In light-run tests, the voltage, current and speed are recorded for a range of values between zero and maximum speed. The input power is calculated from the product of current and voltage. From this is subtracted the I^2R loss and the brush voltage drop loss with the remaining power taken as the mechanical loss for the particular machine at this operating speed. The light run test results from the previously described prototypes are used in this analysis along with those from other disc armature motors not specifically built for traction purposes. Fig. 4.5 illustrates typical curves of mechanical loss, as deduced above, plotted against rotational speed and -for reasons that will become apparent later, a logarithmic plot is used. Results are presented for the 930 W motor, the 1.1 kW motor with various numbers of brushes, and the motor designed for a low-inertia drive. It is now assumed that brush friction, windage and bearing friction are the only mechanical losses to be considered. For the thin rotating disc used in a disc armature motor the windage losses under normal atmospheric conditions are related to the rotational speed and the diameter of the disc. Similarly, the bearing loss depends on the motor speed and the size of the bearing (itself generally dependent on motor size). The brush friction losses may be related to the brush area, diameter

Fig. 4.5 : Mechanical loss versus speed

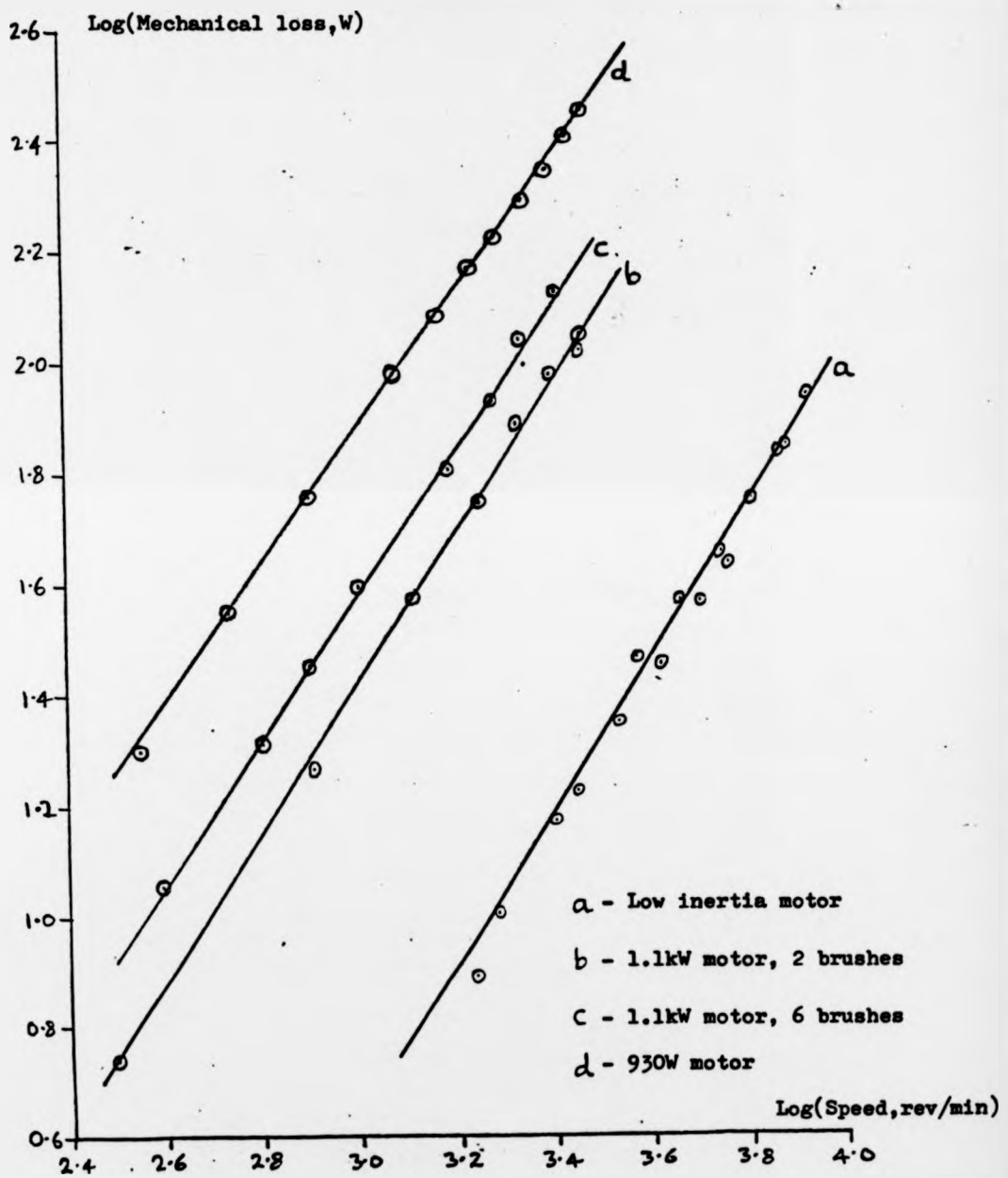

of the commutator, brush pressure and again rotational speed. For the majority of brush grades used in these motors very similar brush pressures are used and it will be assumed that no significant variation occurs from motor to motor. In addition, the diameter of the commutator will be assumed to depend on the machine diameter. The mechanical loss in a disc armature motor may therefore be expressed without loss of generality as:-

$$W_m = f(d_2, A, n) \tag{4.12}$$

where W_m is the mechanical loss, A the brush contact area and d_2 and n as already specified. From Fig. 4.5, the dependence of W_m on n is apparent from the straight line logarithmic plot and is remarkably consistent from motor to motor. The average slope is calculated as 1.304 and thus:-

$$W_m = k.n^{1.304} \tag{4.13}$$

where k contains the dependence on d_2 and A. By consideration of machines which have the same value of d_2 but differing numbers of brushes the proportion of k made up of brush loss may be assessed. At the same time, it is desirable to simplify the procedure by replacing brush area with the rated armature current. The latter's value has already been calculated within the program and the brush area specified is usually proportional to the rated armature current of the machine. The remaining term in k contains the dependence of W_m on d_2 and this is evaluated to yield the final expression for mechanical loss in a disc armature motor.

$$W_m = \left(\frac{d_2^{2.64}}{59600} + \frac{0.0496I}{0.155}\right) \times 10^{-4} \times n^{1.304} \tag{4.14}$$

where d_2 is in mm, I the rated current in amps and n the rotational speed in rev/min. W_m will then be expressed in watts. Although certain simplifications have been made in deriving this formula, any dependence of mechanical loss on machine diameter, rotational speed or armature current (thus brush area) has been allowed for. The formula may easily be incoprorated into the iterative design procedure in order to accurately predict the performance of any disc armature motor. To illustrate the accuracy, Table 4.2 gives predicted and measured values of mechanical loss for various disc armature motors operated at their rated speeds. The 'fan motor' is that described in references 21 and 33 while the 7.5 kW motor is fully described in Chapter 5. None of the last five motors in Table 4.2 were used in determining equation (4.14) and good agreement in the results is apparent.

Having determined the expected losses in a motor,the efficiency may be found from equation (4.11) and is presented with the other performance parameters on the computer printout. In design stage one only the rated conditions are considered and thus a single efficiency figure is given. Design stage two, described below, covers a wide range of operating conditions and equation (4.14) is used repeatedly as the motor speed varies.(Obviously the values of rated current and d_2 will remain constant once a design is specified and thus mechanical loss will only be dependent on n. The copper and brush loss will, however, depend on the actual armature current.) Design stage two which is directed towards a single design specification will now be described.

Motor	Predicted mechanical loss	Actual mechanical loss
930W motor	162 Watts	220 Watts
1.1kW motor	104 Watts	100 Watts
Low inertia	52 Watts	48 Watts
Fan motor	26 Watts	26 Watts
7.5kW motor	284 Watts	340 Watts
130W motor*	25 Watts	27 Watts
130W motor*	47 Watts	44 Watts
20kW motor*	484 Watts	516 Watts

*see appendix II

Table 4.2 : Predicted and measured values of mechanical loss

4.3.4 Operation of design stage two

This is based on the earlier CAD program in which every design parameter was specified and the computer then used to predict the mtoor performance. The limitations of this procedure were discussed earlier but it may now be used to modify any parameter of a working design produced by the stage one program, i.e. as a 'fine tune' on a given design. As previously indicated, it will provide the necessary data for the motor performance curves to be drawn up. However, to be of greatest use certain modifications to the 1970 program are necessary, the most important of which are the inclusion of the interactive facility and the rewriting of the graphics routine. Instead of punching the design parameters on cards, they are entered via a computer terminal with the results output to the terminal and also to the lineprinter if desired. The design parameters to be input are shown in Table 4.3 which is similar in format to Table 4.1. It will be noted, however, that several of the design parameters are listed as optional. If these are not specified then suitable values are selected by the program as in design stage one. Another important facility included in this particular program is the ability to repeat the entire procedure with a change in one or more of the design parameters. This is a quick and easy method of assessing the effect of such a change and allows a final design specification to be produced in a relatively short time.

4.3.4.1 Generation of numerical results

The operation of the program is described with reference to the

UNIVERSITY OF WARWICK

Department of Engineering

DISC-ARMATURE MOTOR- COMPUTER AIDED DESIGN

Project:-

Design Paramters		1	2	3
1	Machine Design Number			
2	Output Power, Watts			
3	Voltage, volts			
4	Speed, r.p.m.			
5	External Diameter D2, mm			
6	Internal Diameter D1, mm			
7	Number of Poles			
8	Bm, Tesla			
9	Hm, A/m			
10	Airgap, mm			
11	Magnet Density, Kg/m^3			
12	Number of Parallel Paths			
13	Number of coils			
14	Number of Turns/Coil			
15	Gauge of Wire, mm			
16	Current Density, A/mm^2			
Optional Design Paramters				
17	Leakage Coefficient			
18	Loss Factor			
19	Pole-Arc/Pole-Pitch			
20	Space Factor			
21	Armature Temp. ^oC			
22	Weight of Non-Active Parts, Kg			
23	Mechanical Loss, Watts			
	Actual Power			
	Actual Speed			

Table 4.3 : New C.A.D. input data sheet

UNIVERSITY OF WARWICK

Department of Engineering

DISC-ARMATURE MOTOR- COMPUTER AIDED DESIGN

Project:-

Design Paramters		1	2	3
1	Machine Design Number			
2	Output Power, Watts			
3	Voltage, volts			
4	Speed, r.p.m.			
5	External Diameter D2, mm			
6	Internal Diameter D1, mm			
7	Number of Poles			
8	Bm, Tesla			
9	Hm, A/m			
10	Airgap, mm			
11	Magnet Density, Kg/m^3			
12	Number of Parallel Paths			
13	Number of coils			
14	Number of Turns/Coil			
15	Gauge of Wire, mm			
16	Current Density, A/mm^2			
Optional Design Paramters				
17	Leakage Coefficient			
18	Loss Factor			
19	Pole-Arc/Pole-Pitch			
20	Space Factor			
21	Armature Temp. ^oC			
22	Weight of Non-Active Parts, Kg			
23	Mechanical Loss, Watts			
	Actual Power			
	Actual Speed			

Table 4.3 : New C.A.D. input data sheet

flowchart in Fig. 4.6. The machine design parameters in Table 4.3 are input with any optional parameters set as necessary. The number of conductors is then calculated from the number of coils and the turns per coil. The flux per pole, magnet length, dimensions of flux-return ring and armature resistance are determined in the same way as previously described. The rated armature current is found from the specified current density, number of parallel paths and wire guage by use of equation (4.4.) and this allows the copper loss and generated e.m.f. to be calculated. The rated speed, power output, torque and efficiency are found as before including use of the equation for mechanical loss.

Having determined the performance at one particular operating point, it is necessary to calculate the data for a full set of performance curves (torque, speed, power and efficiency plotted against armature current). This is done at rated voltage and is achieved here by increasing the current density in stages from a low value to that corresponding to approximately twice rated current. Corresponding values of the dependent variables are output as shown in Table 3.4.

Once a completed design, along with predicted performance has been achieved, the complete process may be repeated with a change in any of the parameters listed in Table 4.3. Similar results will be presented, although it is possible to save time at the terminal by supressing much of the data output. For example, in many cases the effect on speed or output power of a parameter change may be all that is required and it is thus possible to select a 'shortform' version of the output at the terminal which will immediately provide

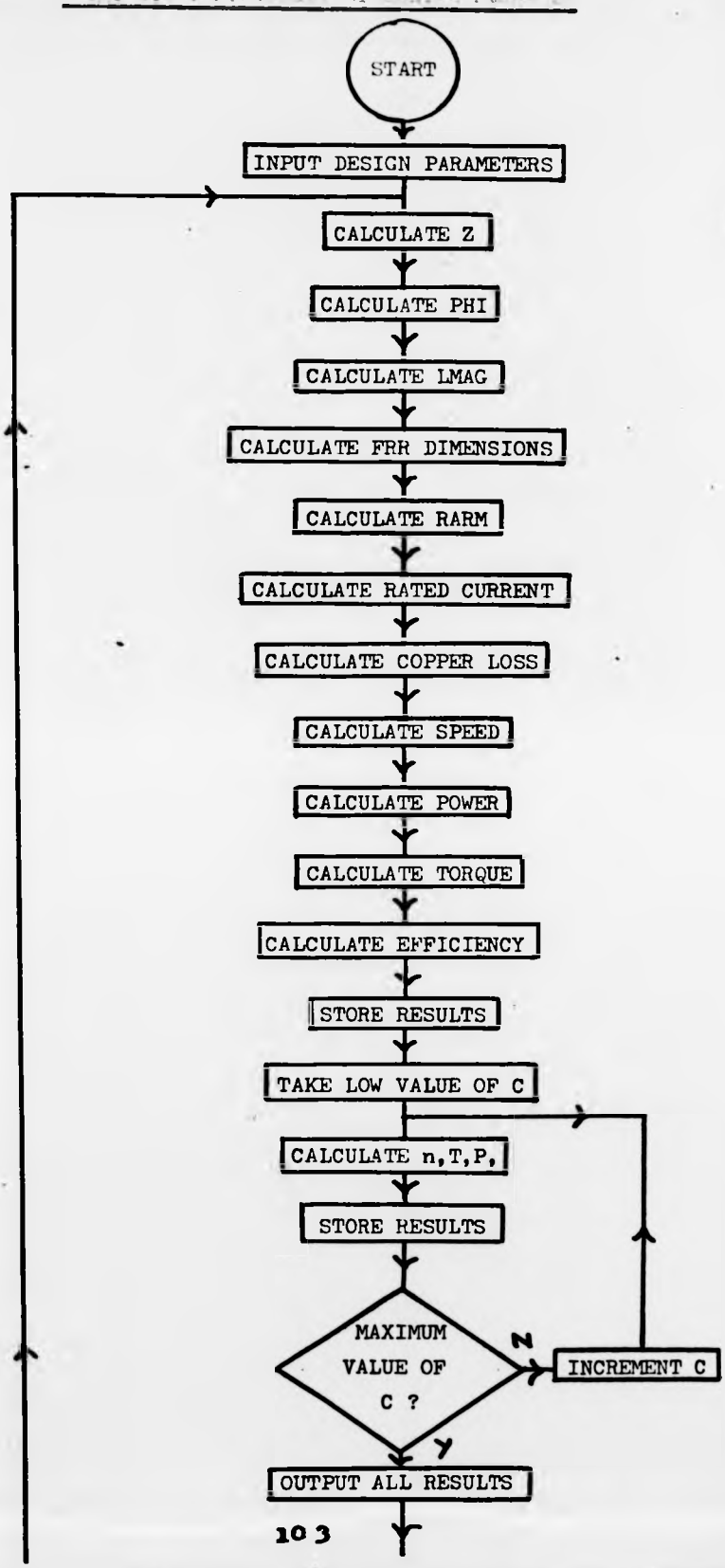
START
INPUT DESIGN PARAMETERS
CALCULATE Z
CALCULATE PHI
CALCULATE LMAG
CALCULATE FRR DIMENSIONS
CALCULATE RARM
CALCULATE RATED CURRENT
CALCULATE COPPER LOSS
CALCULATE SPEED
CALCULATE POWER
CALCULATE TORQUE
CALCULATE EFFICIENCY
STORE RESULTS
TAKE LOW VALUE OF C
CALCULATE n,T,P,
STORE RESULTS
MAXIMUM VALUE OF C ?
N
INCREMENT C
Y
OUTPUT ALL RESULTS

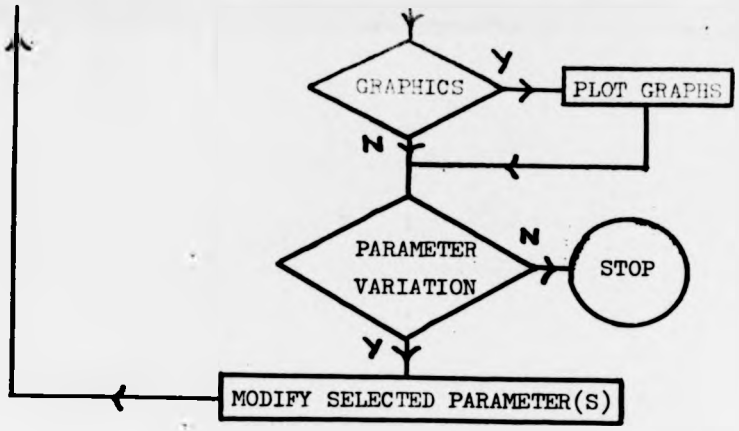

Fig. 4.6 (continued) : Flowchart of design stage 2

the most relevant results (power, torque, speed, etc.). Any hard copy specified will still consist of a full set of results. This facility can save a great deal of designer and computer time.

4.3.4.2. Generation of graphical results

As the installation of a new computer at the University necessitated the translation of the original 1970 program from Algol to the more common Fortran IV, the graphical routines were also updated to make extensive use of the 'Culham Ghost' graphical subroutines. These allow single statements to plot and annotate suitable axes and draw curves within their boundaries. Previously, every move of the plotter pen was controlled by a separate statement. Four separate graphs are produced in turn and the tabulated values of the performance curves must initially be scanned to allow suitable axes to be drawn and marked off according to the magnitudes of the variables. A curve fitting routine is then applied to the independent variable (current density) and each dependent variable in turn with each curve drawn out on its own axes. Typical examples of this output are given in Fig. 4.1. Although the use of a digital plotter has been implied, the graphical results may be displayed at any device equipped to handle them (remote terminals, line printer, etc.). It is, however, convenient to limit graphics to the plotter as this provides a permanent, good quality hard copy of the results.

4.4 Analysis of armature windings

The use of a conventional commutator in the disc armature motor makes it possible to specify winding patterns in the same way as conventional machines (lap, wave, etc.) even though the term 'slot' has no meaning. The most common arrangement is to have as many coils as there are commutator segments and arrange these so that one side of a coil is positioned over the opposite side of another and both positioned with respect to an appropriate commutator segment. This leads to a two-layer winding with each commutator segment having two coil ends connected to it. It is of course possible to consider more than two layers in the armature winding and this option may be either specified, or initiated automatically in the computer-aided design procedure. To achieve this a 'multilayer coil' may be wound so that when nested with the other coils the required number of armature layers exists. This method is best suited to smaller machines designed to operate from a relatively high voltage supply, rectified mains, for example, where many turns of a thin wire can be easily shaped and accommodated. For traction applications, an alternative approach is usually adopted whereby two two-layer armatures are wound separately and then connected in a 'back-to-back' arrangement resulting in a four-layer composite armature. The coils may be either connected in parallel (four connections to each segment of a common commutator) or in series (a series of stub joints connecting the ends of coils from each layer). The former doubles the number of armature paths and halves the armature resistance, while the latter doubles the number of turns per coil and also the armature resistance. Several motors have been constructed in this manner (see Chapter 3

and Appendix II) although this method of connection has been applied only to 4 layer windings as the production of 6 or 8 layers involves a complex nesting and connection procedure. For the same value of d_2 the power output from a motor is effectively doubled when the number of layers is doubled and this may be an advantage where space is limited.

4.4.1 Initial considerations for armature windings

Simple lap and wave windings are most usually adopted in disc armature motors and these are common and straightforward arrangements. However, as indicated earlier, there is occasionally the need for the number of parallel paths to be greater than two but less than the large number of poles. As discussed above, a wave connected back-to-back armature can yield four parallel paths but this involves added complication and also an increase in the amount of magnet material needed to maintain the same flux density in the longer airgap. An alternative solution, and one that has been adopted in the 7.5 kW motor described in the next chapter is to employ a duplex wave winding. This allows four parallel paths to be achieved from a two-layer winding by the addition of an extra coil and commutator segment over that required for a simple wave arrangement. The number of parallel paths in a duplex wave winding is always four regardless of the number of poles employed. The arrangement may best be considered as two simple wave windings, each with half the total number of coils and connected to alternate segments of a common commutator. Depending on the detailed arrangement, there may either be two independent circuits, which are effectively connected in parallel by the brushes of the machine, or a larger closed circuit. Such winding

and Appendix II) although this method of connection has been applied only to 4 layer windings as the production of 6 or 8 layers involves a complex nesting and connection procedure. For the same value of d_2 the power output from a motor is effectively doubled when the number of layers is doubled and this may be an advantage where space is limited.

4.4.1 Initial considerations for armature windings

Simple lap and wave windings are most usually adopted in disc armature motors and these are common and straightforward arrangements. However, as indicated earlier, there is occasionally the need for the number of parallel paths to be greater than two but less than the large number of poles. As discussed above, a wave connected back-to-back armature can yield four parallel paths but this involves added complication and also an increase in the amount of magnet material needed to maintain the same flux density in the longer airgap. An alternative solution, and one that has been adopted in the 7.5 kW motor described in the next chapter is to employ a duplex wave winding. This allows four parallel paths to be achieved from a two-layer winding by the addition of an extra coil and commutator segment over that required for a simple wave arrangement. The number of parallel paths in a duplex wave winding is always four regardless of the number of poles employed. The arrangement may best be considered as two simple wave windings, each with half the total number of coils and connected to alternate segments of a common commutator. Depending on the detailed arrangement, there may either be two independent circuits, which are effectively connected in parallel by the brushes of the machine, or a larger closed circuit. Such winding

arrangements are used in special machines (high speed for example) as the bar-to-bar voltage is reduced helping to prevent electrical breakdown.[46]

The simple lap winding is symmetrical about a pole-pair and thus there exist many sets of commutator segments which in theory should be at the same potential. In practice, slight discrepancies can occur due to inaccuracy in the coil positions and to avoid the possibility of excessive circulating currents being carried by the brushes 'equalising' connections are often incorporated within the armature to connect together some or all of the commutator segments at the same potential. For example, in an 8 pole 48 coil lap connected machine, each pole-pair is associated with 12 commutator segments and thus there can be a maximum of 12 equalisers, each connecting four segments - one under each pple-pair. Alternate segments only may be equalised. In this case, only six equalising rings will be required.

The same state of affairs does not exist in a simple wave winding. The extra coil introduced (or subtracted) to allow multiple tours of the armature in the winding pattern has a displacing effect on the winding as a whole and thus no two commutator segments are maintained at equal potential. Even with a duplex wave connection, with two additional coils (or two coils subtracted) only pairs of segments on opposite sides of the disc will be at the same potential and thus the maximum number of equalising connections is equal to half the number of coils employed. For these reasons, it is inappropriate to use equalisers on wave windings and thus any differences in generated e.m.f. must be tolerated. In the case of a duplex winding

there are often alternative connecting patterns available, as will be shown later, and it is only by a careful consideration of the e.m.f.s generated within the winding that the optimum pattern can be selected.

It has been found necessary to evaluate the emf.s induced in the armature conductors as the armature rotates and sum these between brush pairs as appropriate in order to determine the magnitude of the e.m.f. induced in each armature path, and also those induced in coils short-circuited by the brushgear. The number of bushes obviously has considerable bearing on the analysis and accordingly results are presented for alternative numbers of brushes. Bi-directional rotational of the machine is required and the brushes are located on the neutral axis. As no additional generated e.m.f. is necessary to assist in commutation, the e.m.f.s induced in coils undergoing commutation and short-circuited by the brushes should ideally be zero. To continually evaluate and sum the conductor e.m.f.s as the armature rotates would be an extremely tedious process and it is doubtful whether such a calculation by hand would even be attempted. It is possible, however, to write a computer program which will achieve this evaluation while taking into account changes in brush position and airgap flux as rotation occurs. The program may be used with any winding configuration but is applied here mainly to duplex wave configurations and in particular those relevant to the 7.5 kW traction motor that is being developed.

4.4.2 Calculation of e.m.f.s induced in primary and short-circuit armature paths

Assessments of the e.m.f.s induced in armature coils during

commutation and the application of digital computers to commutation analysis have already been reported[47,48,49]. However, these were directed towards the design of interpoles for d.c. machines so that a prescribed current distribution between commutator and brush could be achieved. Since the majority of the induced e.m.f.s that are considered in these analyses are negligible in disc armature motors (very small reactance voltage, no eddy current effects, end windings at 90^{o} to main flux) such treatment is inappropriate here and thus the present discussion is confined to the e.m.f.s induced by the main field in all armature conductors, and how these vary for different winding configurations.

The analysis is based on a development of the armature winding diagram that is drawn up for every different armature that is produced. These show relative positions of brushes, commutator segments, coils and poles, and examples corresponding to simple lap and simple wave windings are given in Figs. 4.7 and 4.8 respectively. The symmetrical nature of the lap winding is evident with each of the 8 brushes centred on a commutator segment, an equal number of coils between each brush and in the position shown no coils shorted by the brushes. An alternative representation is to trace through the complete winding denoting each coil side by the number of the commutator segment it is most closely aligned to. This is shown in Fig. 4.9 where the 8 parallel paths are clearly seen - the dash notation represents coil sides in another layer. The conditions illustrated in Figs. 4.7 and 4.9 will only be true for one angular position of the armature. If the armature rotates by half the pitch of a commutator segment each brush will now contact two segments and this situation is

Fig. 4.7 : Diagram for typical 8 pole, 40 coil lap winding

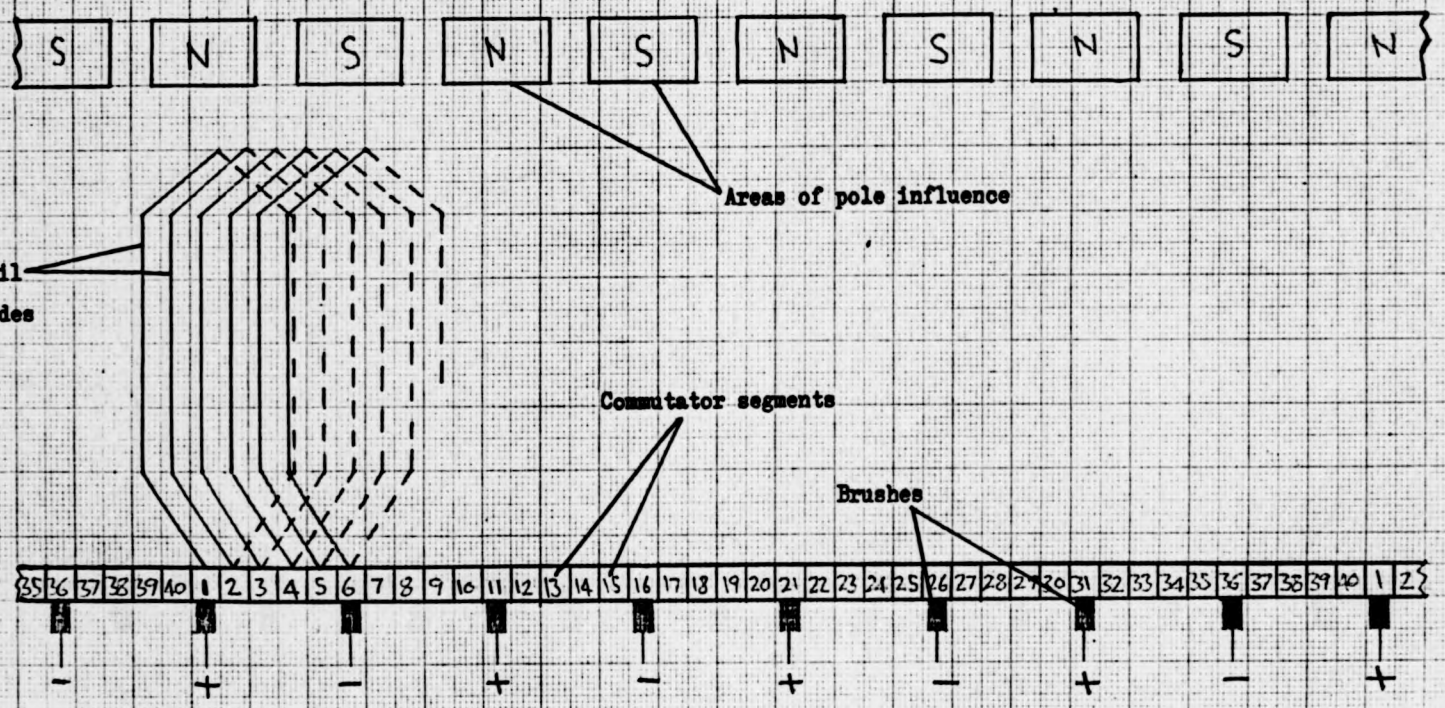

111

Fig. 4.8 : Diagram for typical 8 pole, 41 coil wave winding

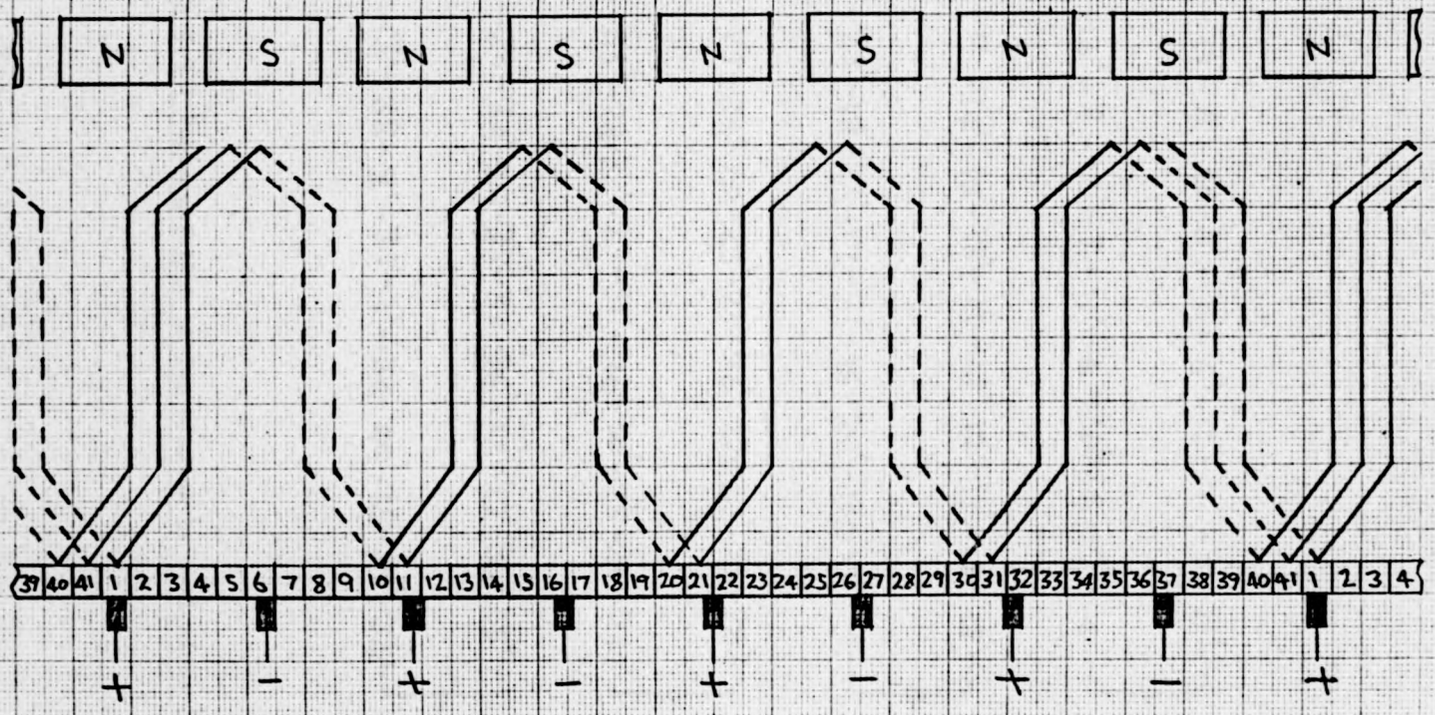

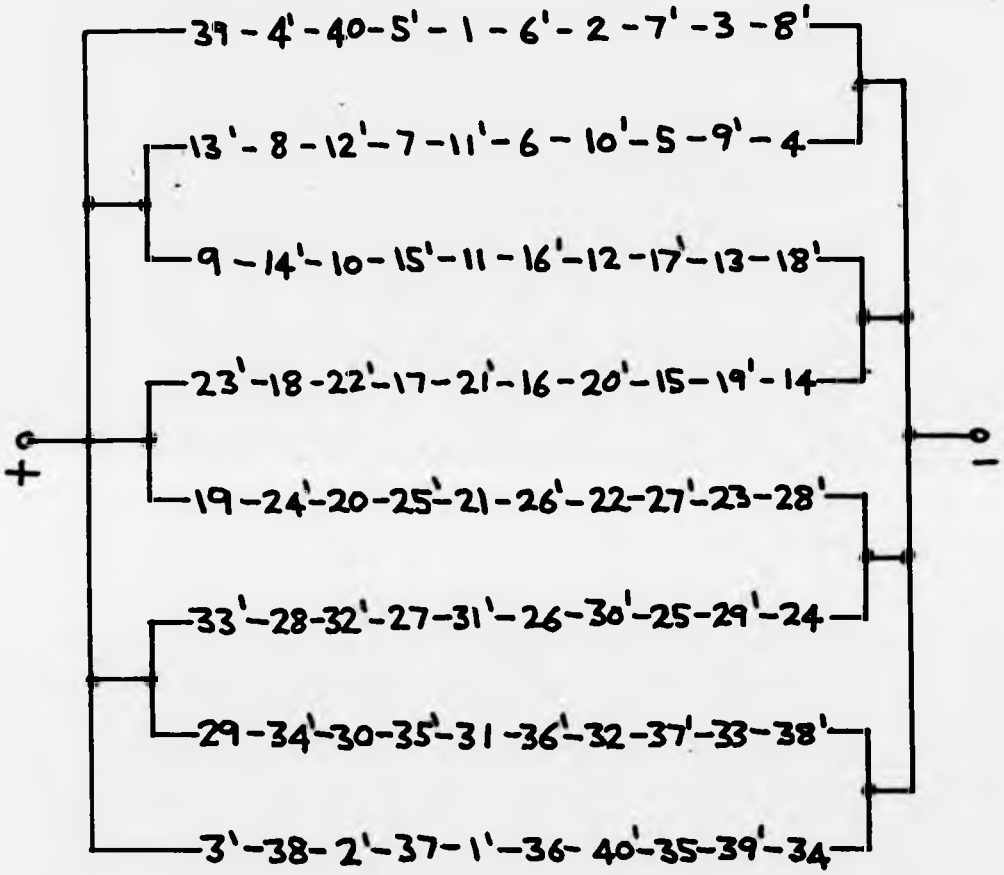

Fig. 4.9 : Representation of lap winding by coil sides

represented in Fig. 4.10. The coils that are short circuited are represented as coil sides connected to the same brush.

Fig. 4.8 shows a winding diagram having the same number of poles and brushes as Fig. 4.7 but wave connected. It can be seen that an extra coil is employed and there is no longer a symmetrical pattern relating brushes to commutator segments. Several of the brushes are thus shorting two commutator segments and this always is the case as the armature rotates. Fig. 4.11 shows this winding represented in a similar fashion to Fig. 4.9 and the two parallel paths through the armature may easily be seen although more coils are shorted by the brushes than in the lap winding. When two brushes are used an improvement in this situation is evident (Fig. 4.12) but the value of armature current often dictates that more than one brush pair is employed. With reference to Fig. 4.7 if the armature is displaced by half a commutator segment with respect to the brushes (and poles) the coil sides connected to the brushes lie in the neutral zone between the poles and therefore any e.m.f. induced in them should be extremely small. When the wave winding is considered (Fig. 4.8) it can be seen that some of the coils shorted by the brushes have sides laying more towards the sides of a pole and these will have a comparatively larger e.m.f. induced. This problem is aggravated if the ratio of pole arc to pole pitch is too large or if the number of coils per pole is too small. Experience has shown that for pole arc/pole pitch ratios of around 0.75 the minimum number of coils per pole should be about five, unless exceptional circumstances warrant otherwise.

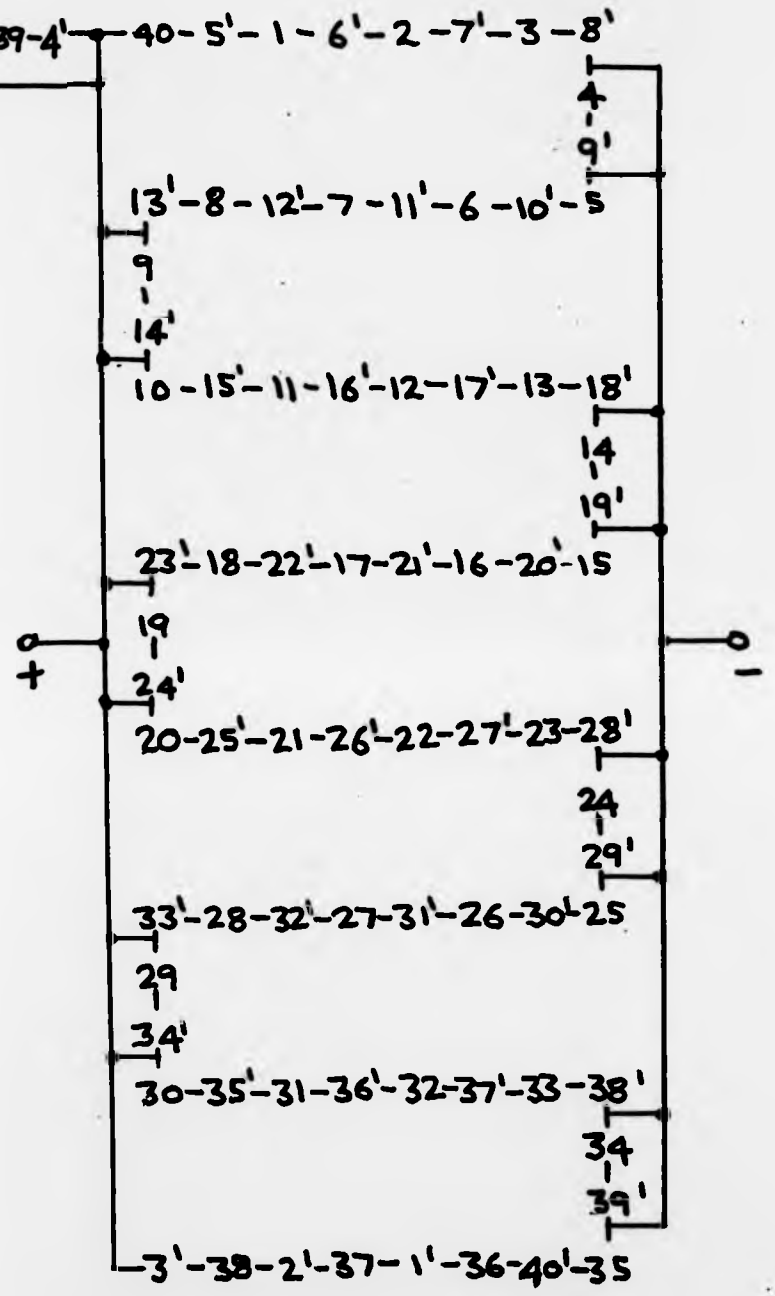

Fig. 4.10 : Representation of lap winding after rotation by half a commutator segment pitch

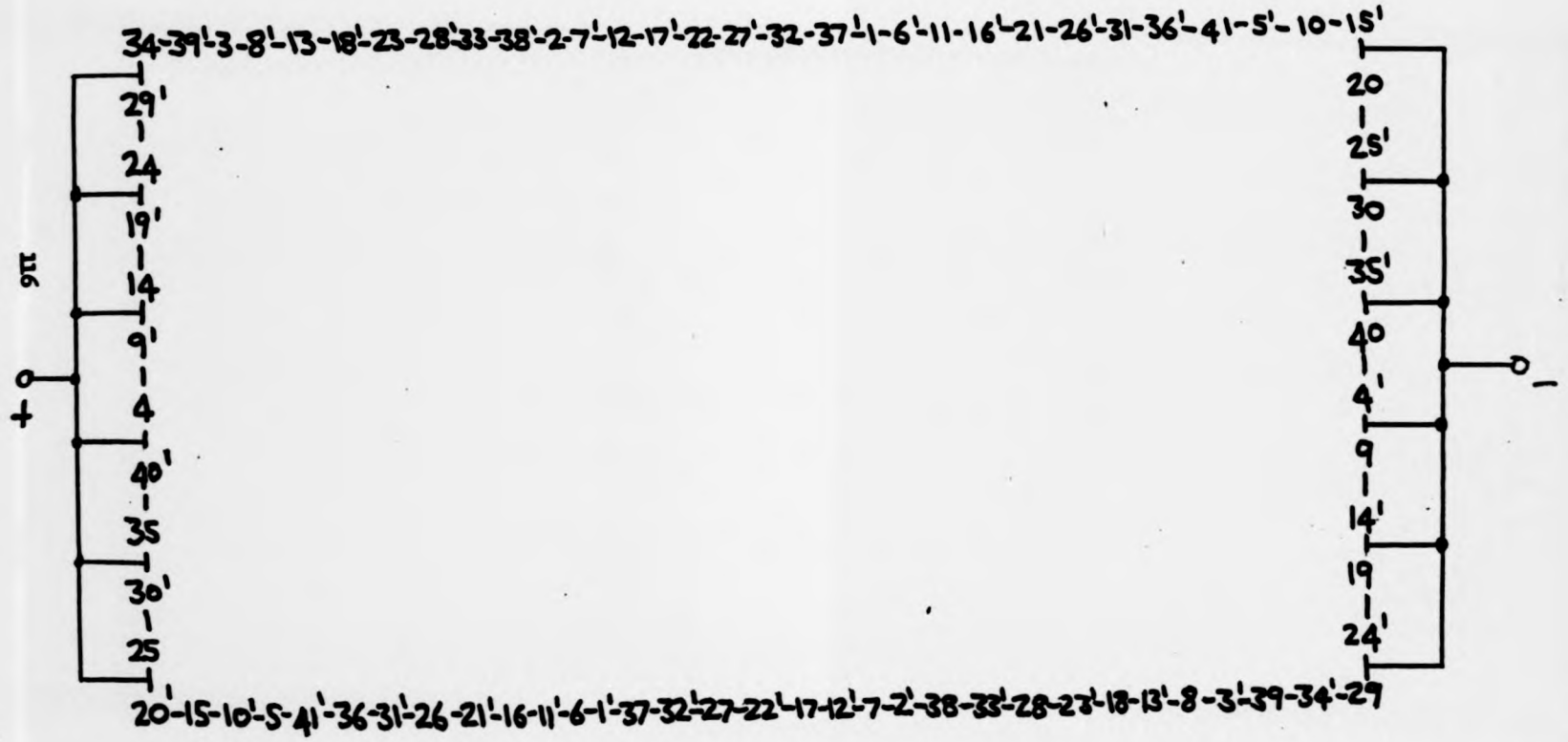

Fig. 4.11 : Representation of wave winding (8 brushes)

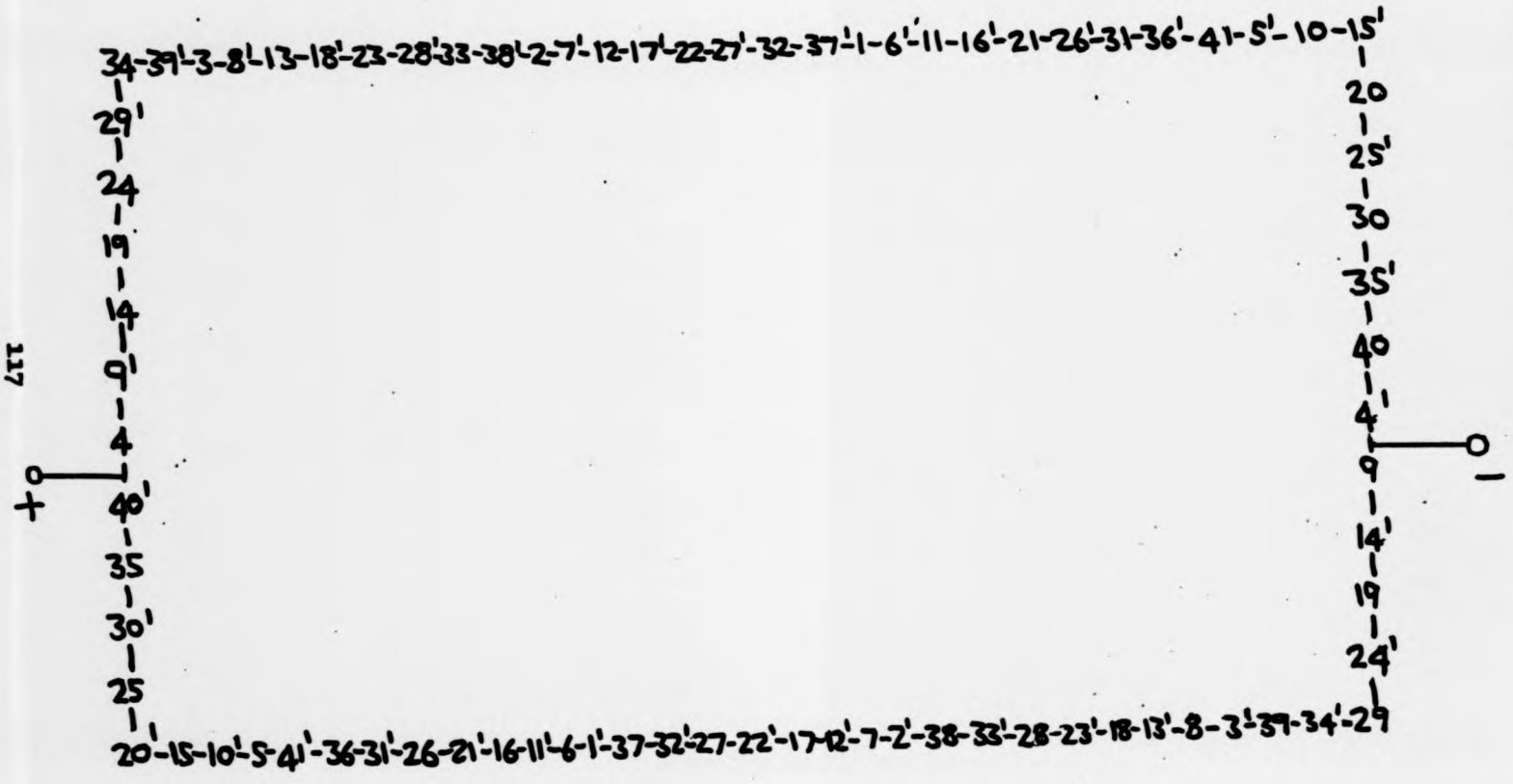

Fig. 4.12 : Representation of wave winding (2 brushes)

With reference to a diagram such as Fig. 4.8 and for a constant motor speed it is possible to calculate the induced e.m.f.s by considering the flux associated with each conductor. If a coil has five turns then each commutator segment may be divided into five smaller segments each of which will be associated with one conductor from each layer, and either lie under a pole or in a neutral region. This assumes an idealised rectangular flux distribution and thus conductors will have either a single 'unit' of e.m.f. induced in them, or zero e.m.f. The e.m.f. in a coil side may be found by summing the contributions from the five conductors and then the total e.m.f. in each armature path is found using a diagram such as Fig. 4.11. Allowance must of course be made for e.m.f.s in coil sides in the other layer or under an opposite pole to be of the appropriate sign. In addition to constant speed and rectangular flux distribution the method assumes a uniform distribution of conductors through the disc. The actual e.m.f.s induced in the armature paths may be found by multiplying the number of summed units in each case by the airgap flux density, length of conductor and average velocity.

While this method has proved useful for initial assessment or comparison of windings the limitations it imposes are quite severe. A more representative flux distribution is shown in Fig. 5.15 and although it is possible to allow for this, the summation becomes extremely time-consuming. The resulting e.m.f. values are true for only one armature position although they repeat after rotation by an integral number of commutator segments. To investigate changes in position by one conductor position would require the complete

winding diagram to be reassessed taking into account the change in brush position and flux pattern with respect to the armature. Similarly, any change in pole arc/pole pitch ratio would not be easily allowed for.

The computer program that has been developed takes into account the actual flux distribution as measured in Chapter 5, and numbers of poles, coils, turns per coil and brushes. The flux distribution is stored as numerical data within the program (one pole pitch is required) and the width of a brush in terms of a commutator segment is also required. With reference to Fig. 4.13 the winding pattern is specified by two numbers, x and y, which are selected by the designer. Together they define the coil pitch and commutator pitch in terms of commutator segments. Each commutator segment is divided into conductor positions and for each of these positions the initial flux density is calculated according to the number of poles and the specified flux distribution. They are then summed in appropriate groups to find the units of e.m.f. associated with each coil side. Each brush is taken in turn and the commutator segments contacting it are identified. Using the specified values of x and y (Fig. 4.13) the path from every segment in contact with a brush is traced through the armature, summing the coil e.m.f.s until another brush is reached. In this way, all of the armature paths are accounted for and the output consists essentially of the starting brush, the finishing brush and the units of e.m.f. generated between them. It has been found most convenient to allow one unit of e.m.f. to be equal numerically to the maximum value of the flux distribution. The actual e.m.f. is then calculated by multiplying the number of units by

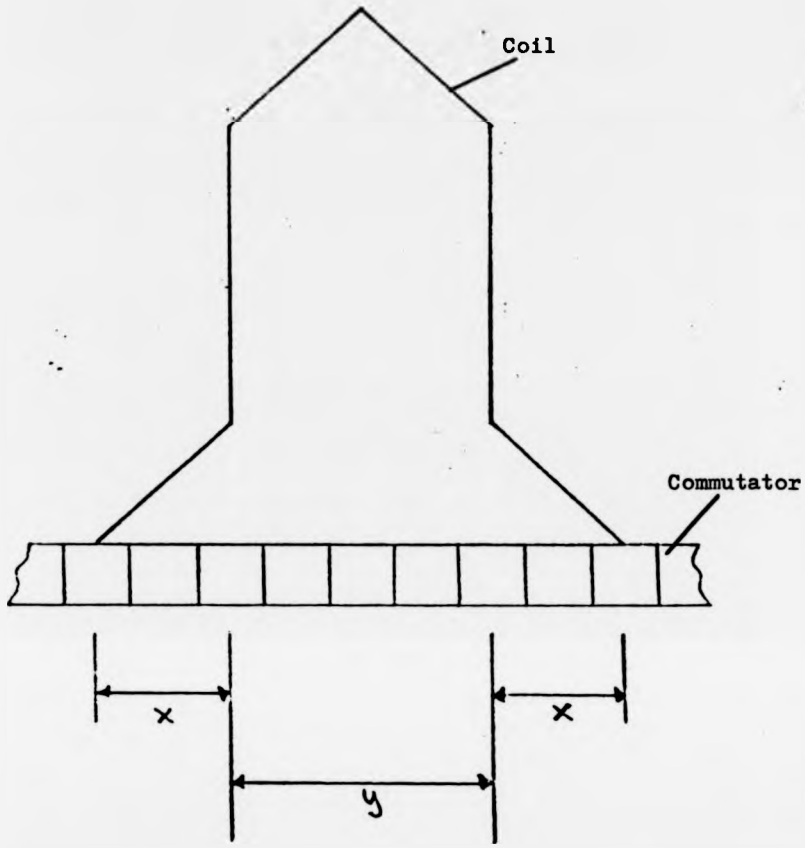

x and y in terms of commutator segment pitches
(here x=2,y=4)

y = coil pitch
2x+y = commutator pitch

Fig. 4.13 : Representation of winding pattern

conductor length and average velocity as before.

Once the initial e.m.f.s have been evaluated the armature is rotated by one conductor pitch. This requires new values of flux density to be calculated for each conductor position, and also the new position of the brushes with respect to the commutator. The induced e.m.f.s are then calculated as before.

The entire process is repeated until rotation by one commutator segment has occurred, and the results show how the e.m.f.s between the brushes vary with rotation. The program will cater for any number of coils, turns per coil or poles, and as the details of the armature winding are specified by two numbers, found from the winding diagram, any conventional arrangement may be investigated. The program has been of greatest value in comparing two alternative duplex wave arrangements and this particular aspect is considered in the next section.

4.4.3 Application to the duplex wave winding

The winding under consideration is that specified for the 7.5 kW traction motor intended for use in the Reliant Robin electric vehicle conversion. There are 8 poles in the machine and the armature has 42 coils each of 5 turns to allow for the duplex wave winding. A set of 8 brushes is employed to handle the full armature current and the remainder of the specification is given in Table 3.4. In a simple wave winding the coil and commutator pitches are easily chosen from the nearest integer to the number of coils per pole. In the 41 coil, 8 pole arrangement of Fig. 4.8 the number of coils per pole is 5.125

and thus the coil pitch must be 5 and the commutator pitch 10. With the duplex wave winding and especially with 8 poles the commutator pitch is not so well defined and could be either of two integers. The number of coils per pole in the arrangement under consideration is 5.25, and while this leads to a coil pitch of 5, the commutator pitch could be either 10 or 11. These two possibilities must be investigated to assess whether any advantage is to be gained by specifying a particular configuration. The winding diagram for the version with a commutator pitch of 10 (Option 1) is illustrated in Fig. 4.14 and is shown as a series of coil sides in Fig. 4.15. Similarly the version with a coil pitch of 11 (Option 2) is shown in Figs. 4.16 and 4.17.

It can be seen that option 1 leads to two separate circuits which are connected in parallel by the brushes, while option 2 is a continuous winding. It has been suggested[50] that the latter configuration is easier on the brushes as it does not rely on them for paralleling the two circuits.

The relevant parameters for each winding are input to the computer program and the values of e.m.f.s. for the armature circuits are output and plotted graphically in terms of units of e.m.f. for rotation by a conductor pitch. They are illustrated in Figs. 4.18, 4.19, and 4.20 which correspond to using 2, 4 and 8 brushes respectively. In Figs. 4.19 and 4.20 there exist a second set of values identical to those illustrated and thus only 2 main armature paths are shown. In Fig. 4.18 several of the e.m.f. values for the four main paths in option 1 are coincident. In all of the diagrams, the positive-going short circuit e.m.f.s are those due to the

Fig. 4.14 : Diagram for 7.5kW motor, winding option 1

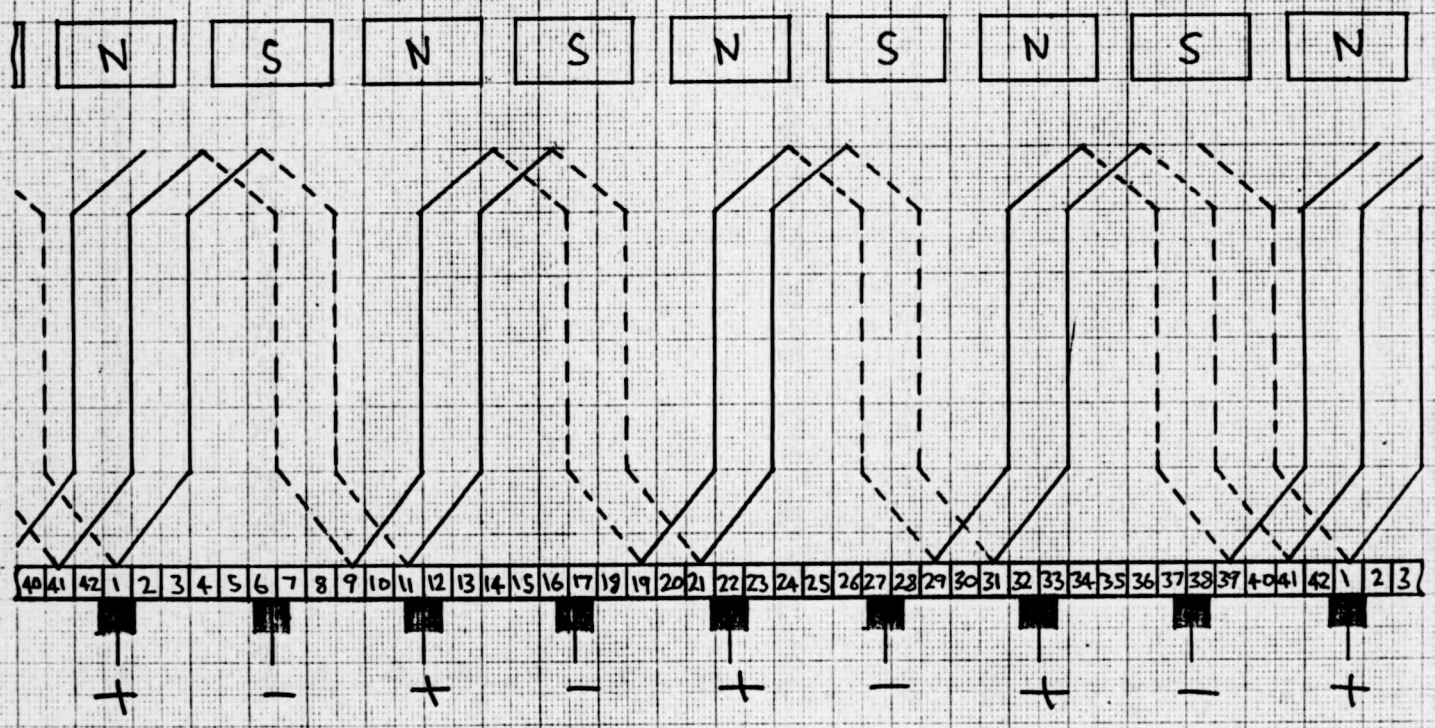

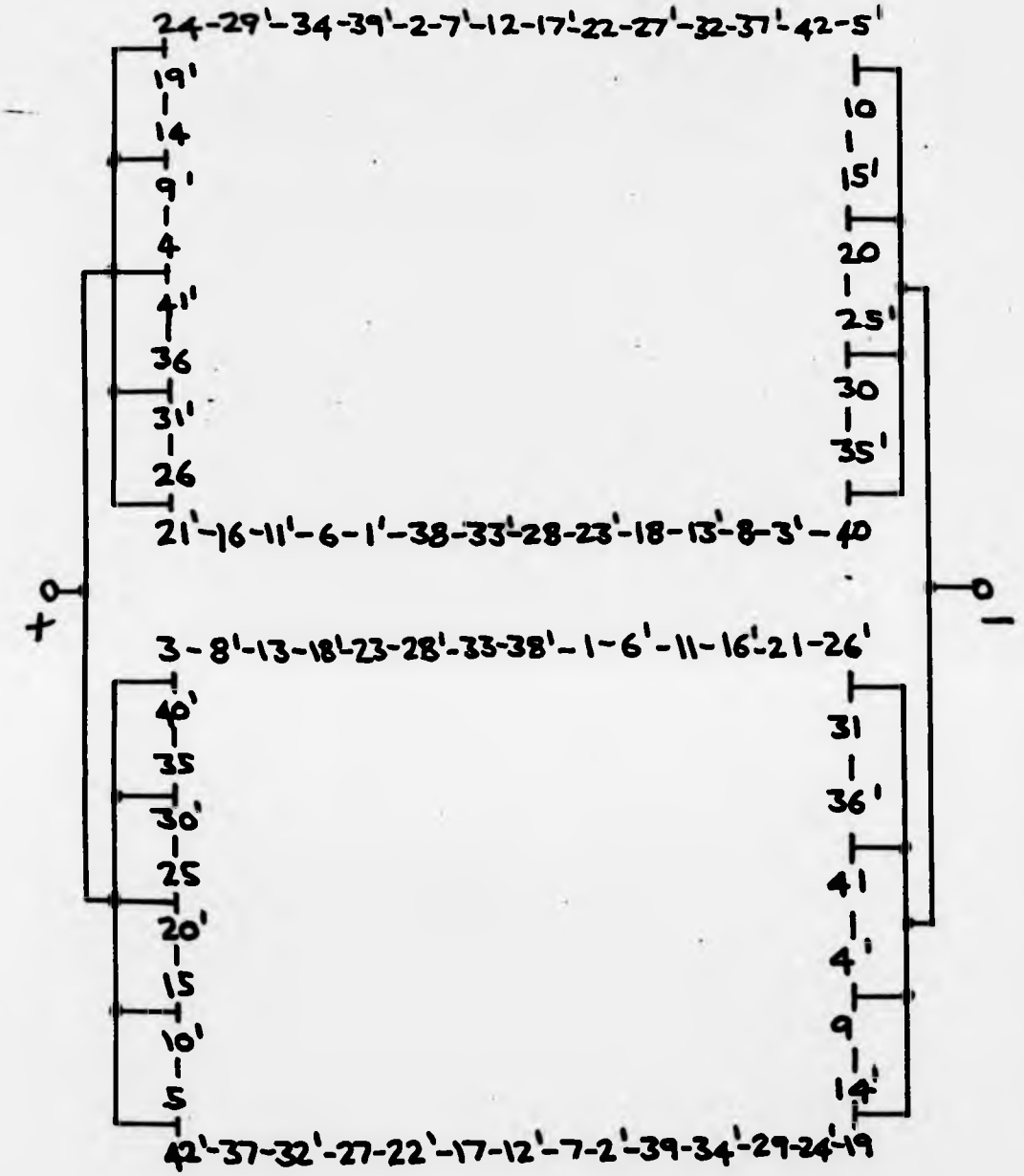

Fig. 4.15 : Representation of winding option 1 by coil sides

Fig. 4.16 : Diagram for 7.5kW motor, winding option 2

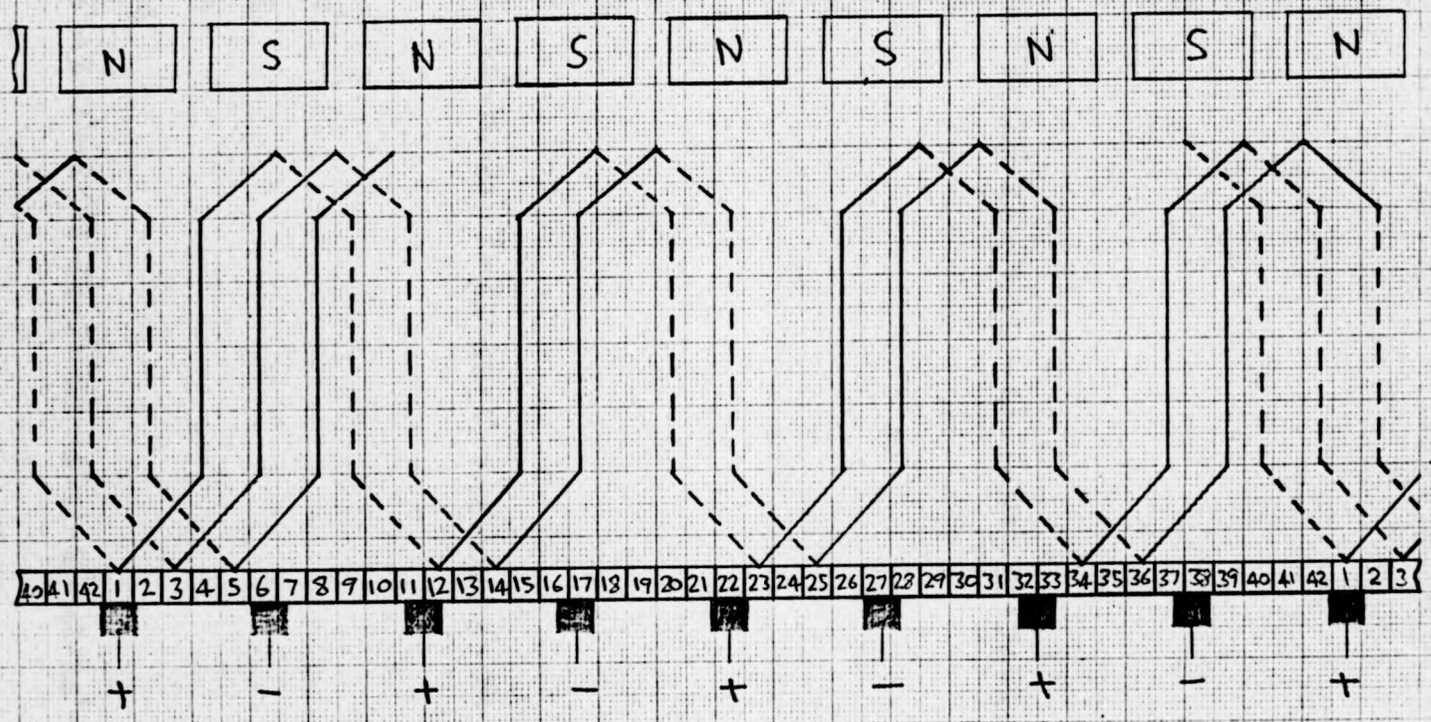

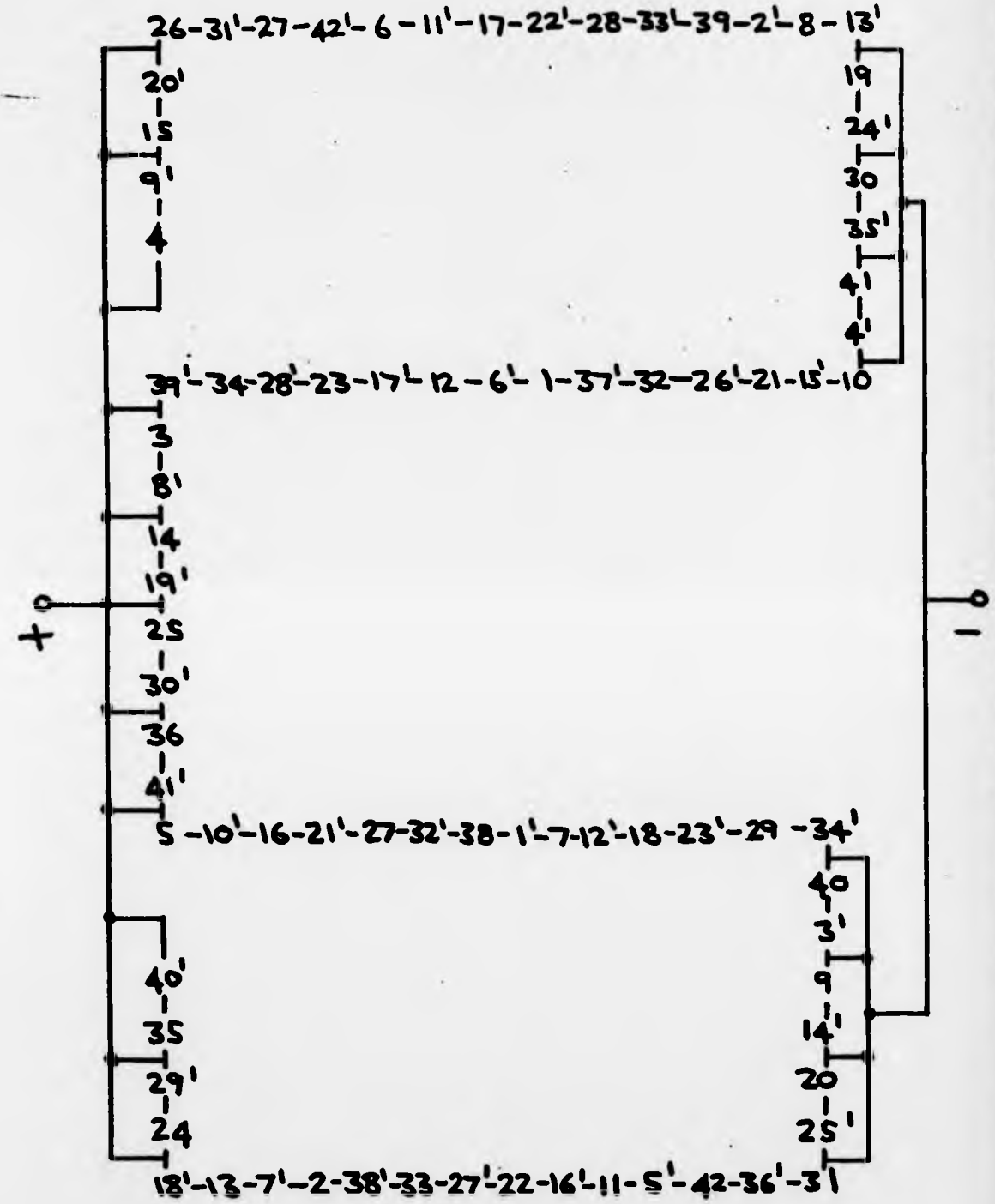

Fig. 4.17 : Representation of winding option 2 by coil sides

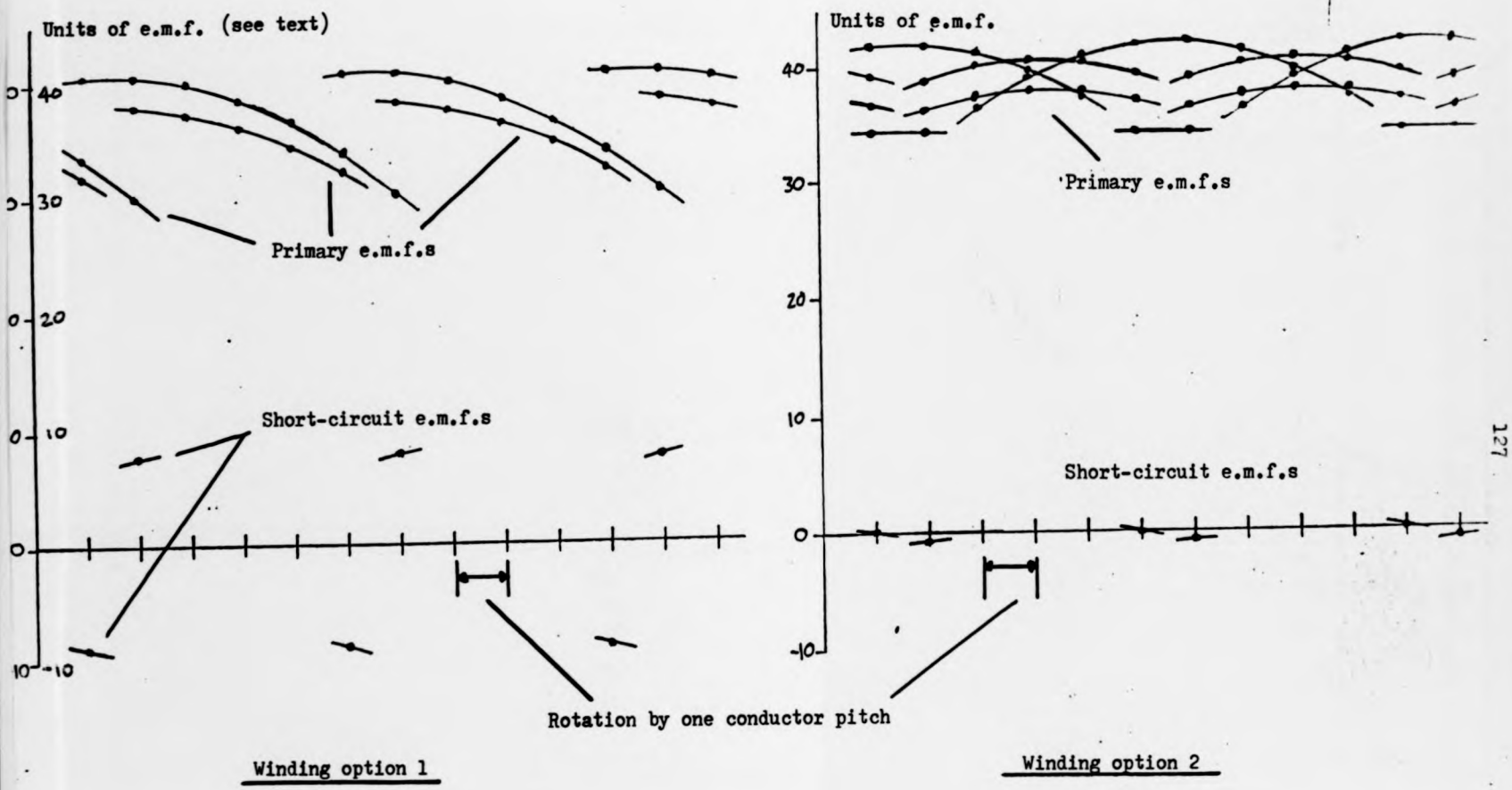

Fig. 4.18 : E.m.f.s generated in both winding options (2 brushes)

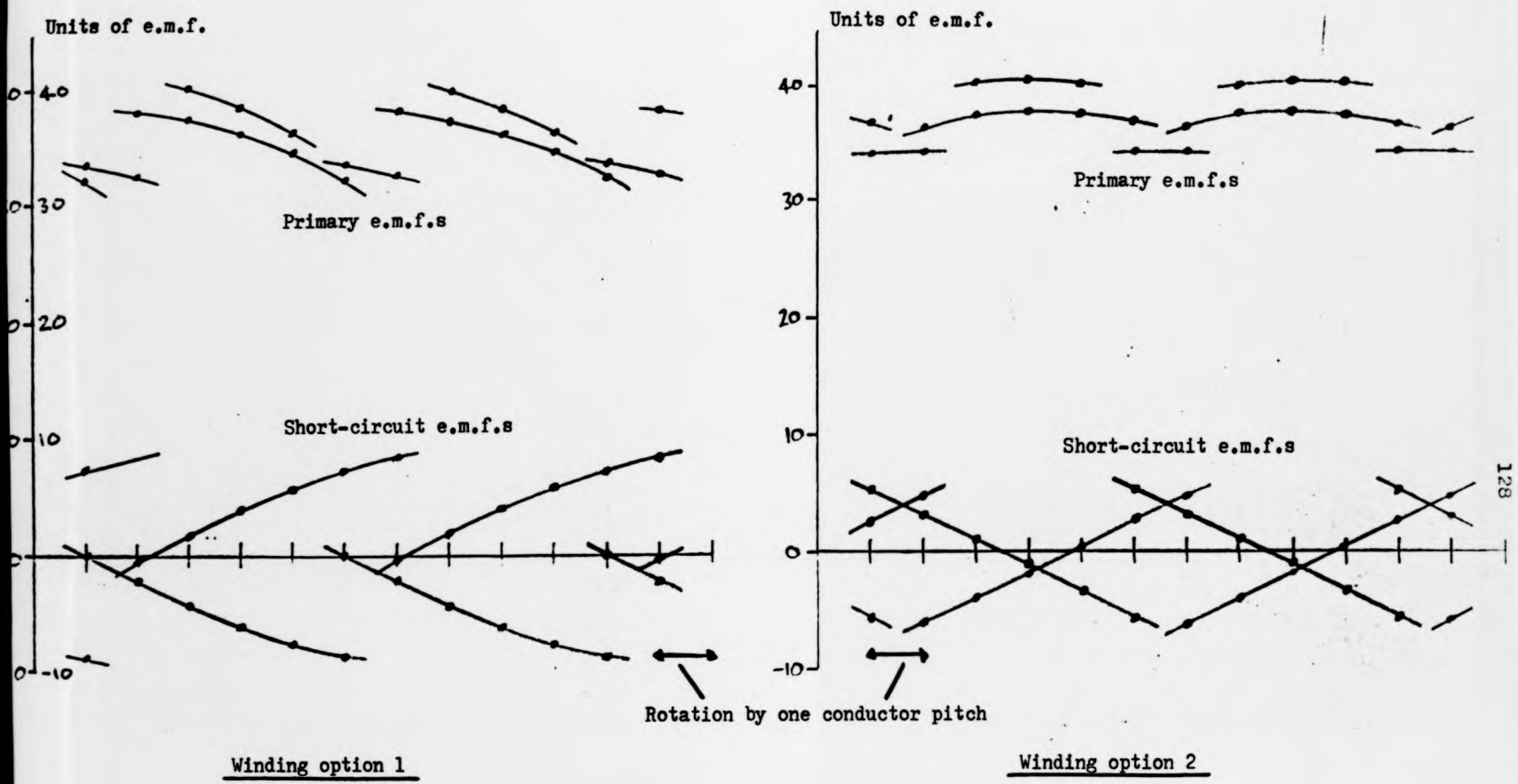

Fig. 4.19 : E.m.f.s generated in both winding options (4 brushes)

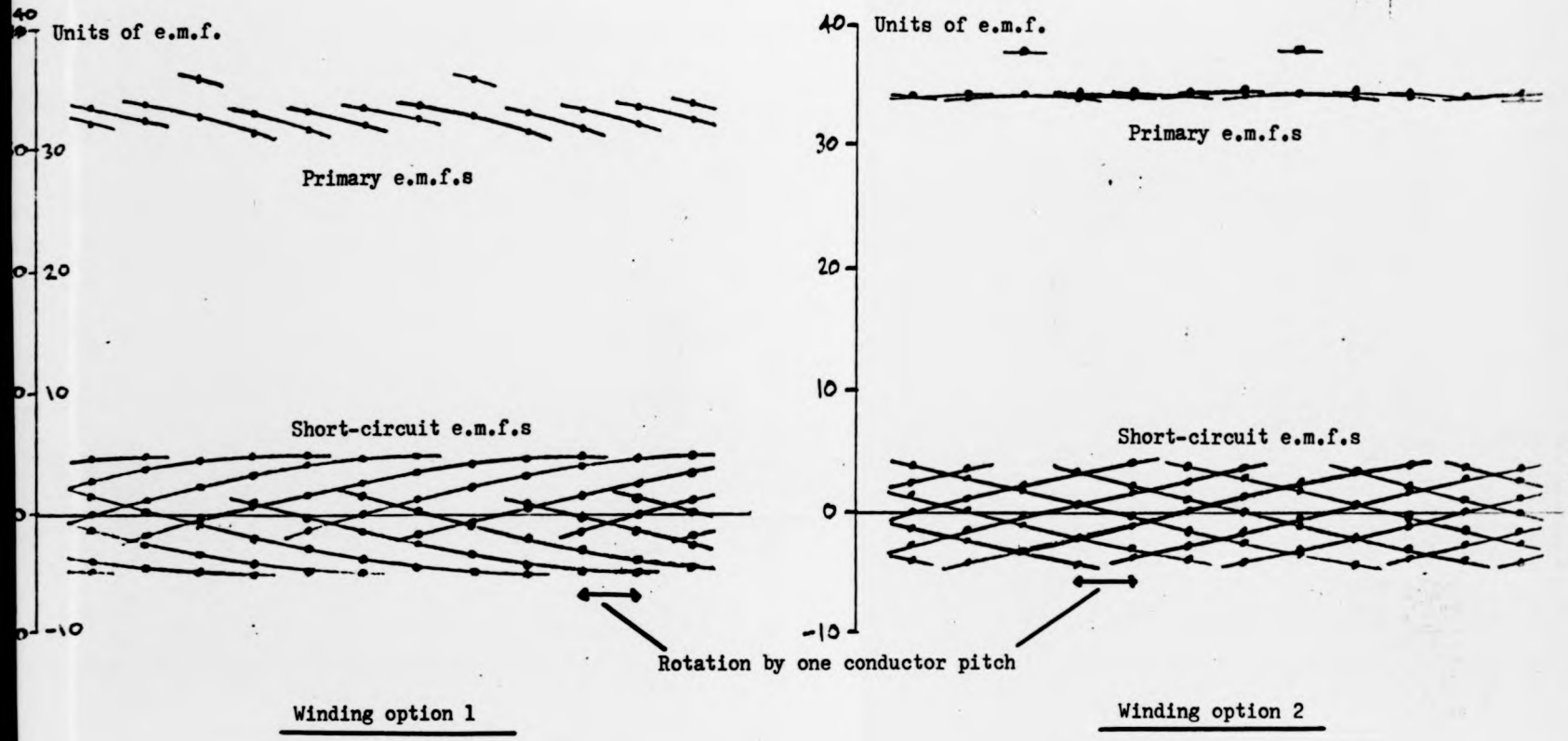

Fig. 4.20 : E.m.f.s generated in both winding options (8 brushes)

negative brush while the negative-going short circuit e.m.f.s are due to the positive brush. It is clear that as the number of brushes increases, the spread of the main e.m.f.s reduces although this is at the expense of a reduced average value of main e.m.f. with a corresponding increase in the number of short-circuit paths. It is apparent that the generally higher values of short-circuit e.m.f. in the option 1 winding exist to the detriment of the e.m.f.s in the main paths and this has been found to adversely affect the performance as will be seen later. In addition, the values of the short-circuit e.m.f.s associated with either the positive or negative brush average to approximately zero over the period of rotation by one commutator segment in the option 2 winding while this is not the case in option 1. This too has a direct bearing on motor performance. However, further discussion on the relative merits of the windings will be reserved until the performance of each in an identical stator is considered in the next chapter.

5: CONSTRUCTION AND PERFORMANCE OF A DUPLEX WAVE DISC ARMATURE TRACTION MOTOR

The motor considered in this chapter is built to the specification given in Table 3.4. Armatures using both the winding arrangements discussed in section 4.4.3 are constructed and a comparison made of their performance. The constructional details have much in common to all prototype disc armature motors and it is convenient to consider independently the stator and the armature particularly as their construction may be performed concurrently if necessary up to final assembly. The general assembly drawing for the motor is reproduced for convenience in Fig. 5.1. The dimensions of the armature are determined from D1 and D2 in Table 3.4, making a suitable allowance for the end windings at the inner and outer circumferences. Additionally, several coils may be trial-wound and nested before the final mechanical specification is drawn up and in motors involving significant departure from pervious mechanical arrangements, this is sometimes the case. The dimensions of the armature encapsulation mould are usually finalised after the first winding has been constructed. Although two different windings are being evaluated, the mechanical details of each are precisely the same and the stator parts are also common to both. Consideration must also be given to fitting the motor into the electric car and Fig. 5.1 shows details of the gearbox and input shaft.

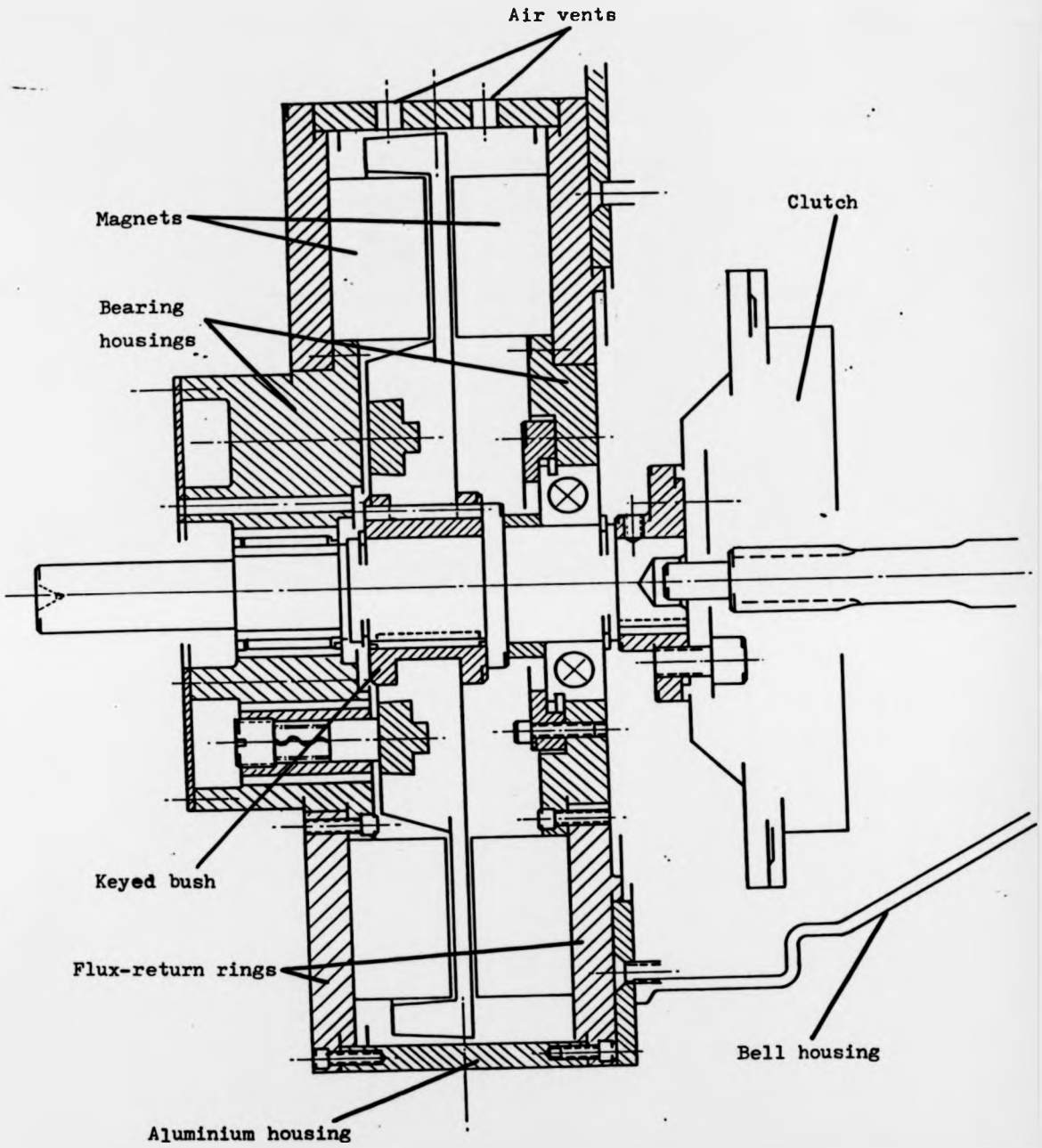

Fig. 5.1 : Assembly drawing for 7.5kW motor

5.1 Construction of stator and armature

The first task in constructing any prototype disc armature motor is the specification of the magnets as the small quantities that are generally required often take some time to be produced. Occasionally, the magnet manufacturer will have a standard shape which is close to that desired - in this situation it may be worth redesigning the motor so that this can be used. However, for the 7.5 kW motor purpose made segments of the alloy Hycomax III are specified and these are cast to the desired shape. The magnet dimensions are given by D1, D2, ALPHA and LMAG from Table 3.4. LMAG refers to the total magnet length and as can be seen from Fig. 5.1, magnets of half this total length are situated either side of the armature. The non-linear BH characteristic of the Hycomax III material makes it necessary to magnetise the segments after the motor has been assembled and the correct airgap set up. Magnetising windings will thus need to be incorporated in each stator half and brought out to external connections. The steel flux-return rings form part of the motor case and a narrow ring is incorporated onto each to allow location to the gearbox of the vehicle. The bearing housings are made of aluminium as is the cylindrical ring forming the remainder of the motor case. These components are all bolted directly to the flux-return rings and the bearing housings constructed so that the magnet segments can be located against the outer circumference of each (Fig. 5.1). The motor shaft is made with a coupling suitable for connection to the rotating clutch member in the gearbox and a bush which will be

encapsulated with the armature winding is made to key onto the centre portion of the shaft. The brush holders are integral with one of the bearing housings and as a face-type commutator is used, the brushes and holders are trapezoidal in section. As in previous prototypes, the advice of a brush manufacturer is sought regarding brush grade and size for a machine of these dimensions, power and speed - Morganite metal/graphite brushes of the grade CM12 are finally specified.

After delivery of the magnets, they are inspected and then fixed to the steel flux-return rings in the appropriate positions with an epoxy adhesive. Once this has been done, the magnetising windings can be located around the magnet segments and these are connected on each side to two threaded brass bushes fixed into, but insulated from, the steel rings. The connection to the magnetising equipment is made to the opposite ends of these bushes after assembly of the machine. Figs. 5.2 and 5.3 show photographs of the stator components.

Because of the unconventional nature of the armature prototypes are constructed completely by hand at present and this is a time-consuming procedure. (Suitable winding machines have been developed for commercial production.) Having established d_1, d_2 and the number of coils in the machine, a former is made up allowing individual coils to be wound by hand. The size of the former includes a running clearance between the end-windings and the edges of the magnets. Fig. 5.4 shows the former and several armature coils, with coils nested together and ready for connection

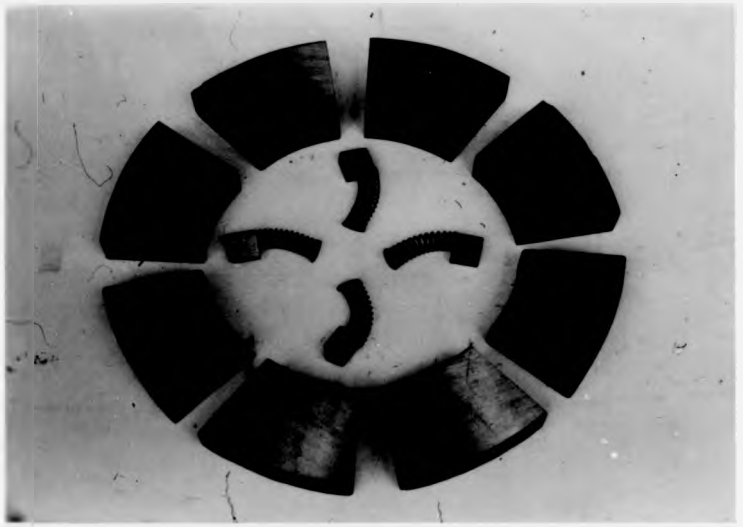

Fig. 5.2 : Magnets used in 7.5kW motor

Fig. 5.3 : Half stator assembly of 7.5kW motor

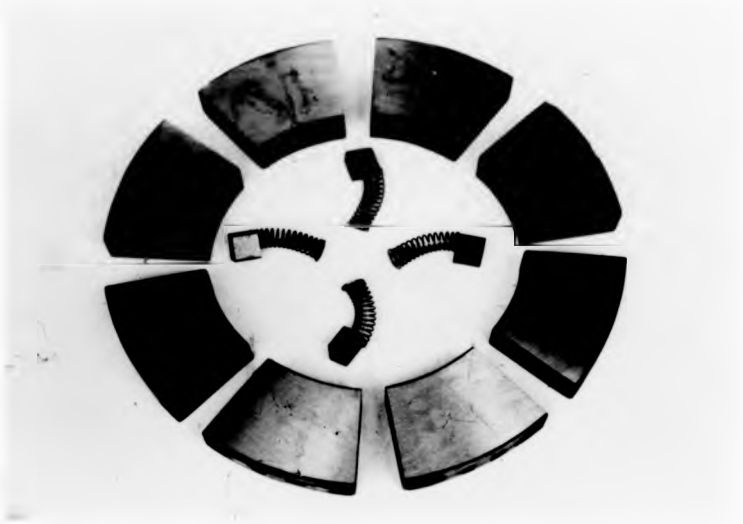

Fig. 5.2 : Magnets used in 7.5kW motor

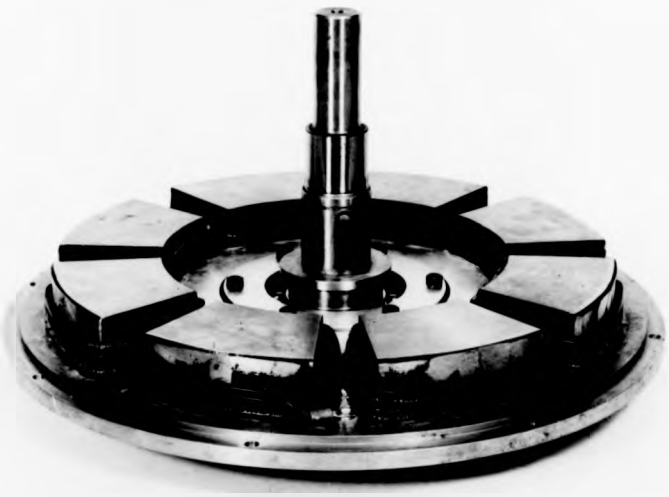

Fig. 5.3 : Half stator assembly of 7.5kW motor

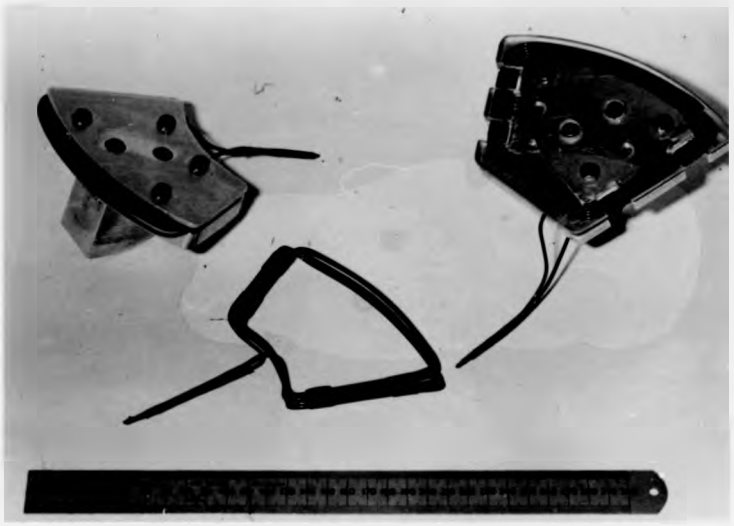

Fig. 5.4 : Winding formers

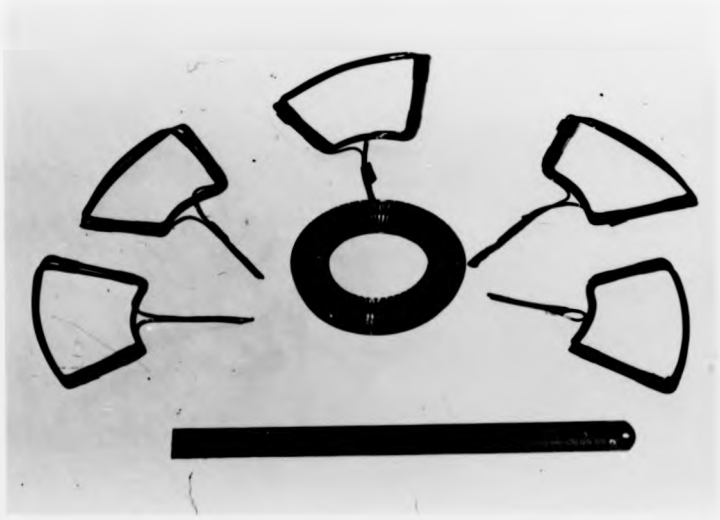

Fig. 5.5 : Coils and commutator

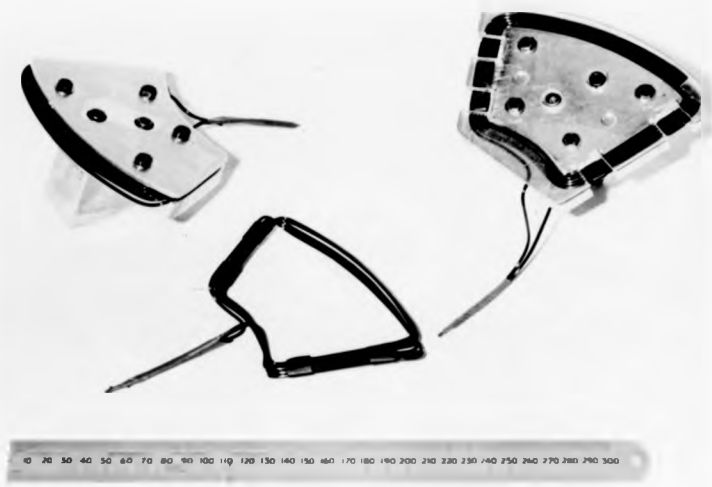

Fig. 5.4 : Winding formers

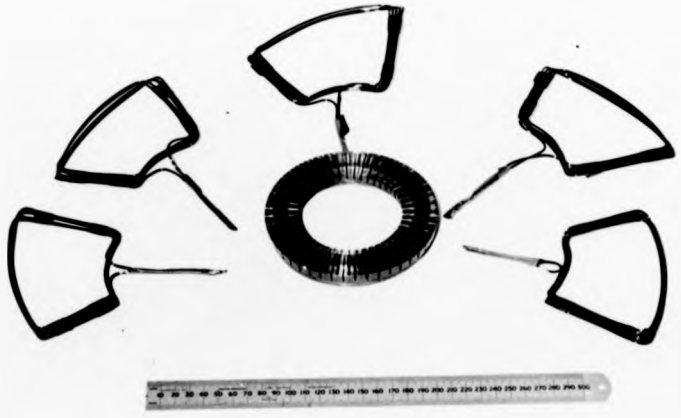

Fig. 5.5 : Coils and commutator

to the commutator illustrated in Figs. 5.5 and 5.6. As a suitable face-type commutator with 42 segments is not commercially available, a purpose-built commutator was drawn and manufactured. The design has the unusual feature that the individual segments are left connected to a copper blank for rigidity until encapsulation after which the unused copper is then machined away. Fig. 5.7 shows the armature coils connected to this commutator. A steel mould for the armature is designed and manufactured and the base and lid are shown in Fig. 5.8. The copper blank attached to the commutator serves another purpose as it may be drilled and tapped in order to locate the winding firmly in the mould with the commutator concentric to the shaft. The keyed bush which fits onto the motor shaft is positioned in the base of the mould and fixed in position by a dummy shaft which itself locates in the lid. Fig. 5.9 shows an armature about to be pressed down into the mould ready for encapsulation.

The moulding material used is an epoxy resin type PX 237C supplied by Robnorganic Systems Ltd. The specification is detailed in Table 5.1 and the resin is supplied in a twinpack form, the user mixing two constituents by hand after breaking the dividing seal of an evacuated polythene container. This method allows the resin to be mixed thoroughly with no risk of spillage or ingress of air bubbles. The encapsulation process is carried out by hand after pre-heating the armature, mould and resin to approximately 40^{o}C. Sufficient twinpacks are prepared and these mixed as required. The containers are then opened and the warm resin poured over the armature windings, commutator and centre bush. To facilitate the removal of any air bubbles that

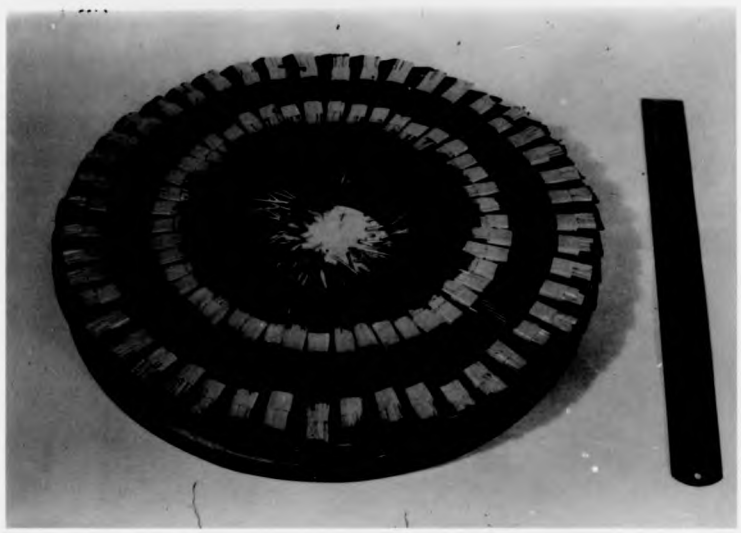

Fig. 5.6 : Complete set of armature coils

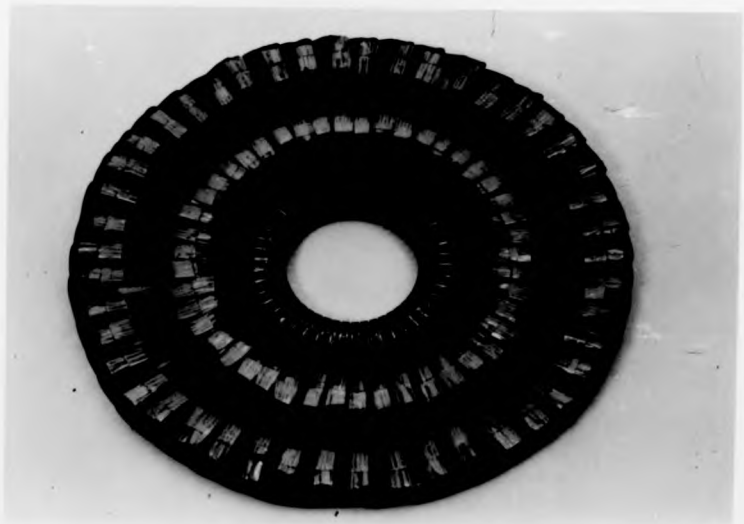

Fig. 5.7 : Coils connected to commutator

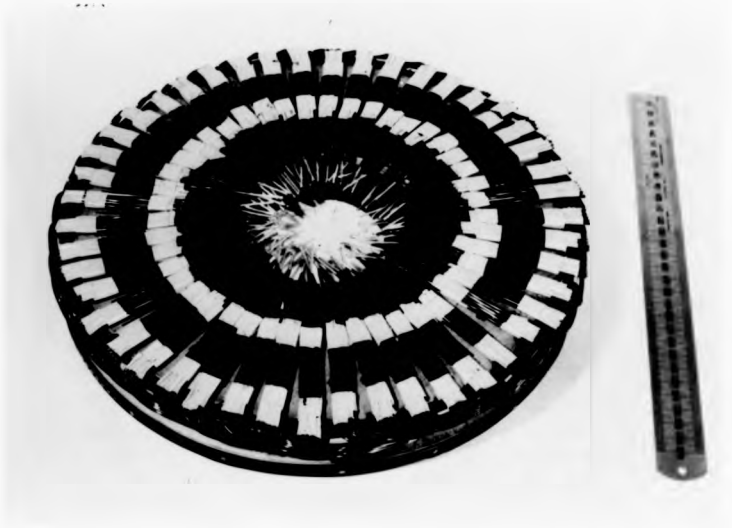

Fig. 5.6 : Complete set of armature coils

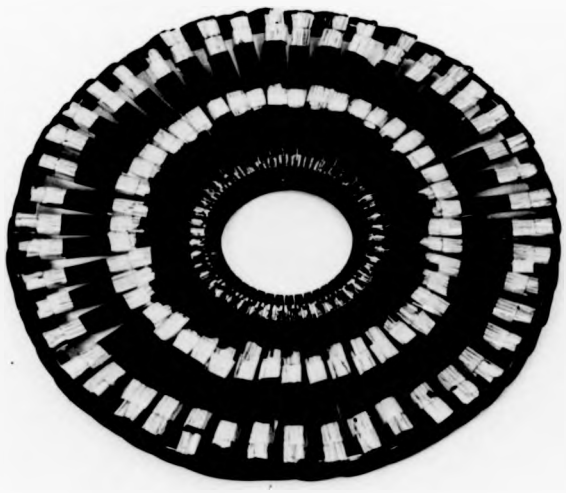

Fig. 5.7 : Coils connected to commutator

Fig. 5.8(a) : Base of encapsulation mould

Fig 5.8(b) : Lid of encapsulation mould

Fig. 5.8(a) : Base of encapsulation mould

Fig 5.8(b) : Lid of encapsulation mould

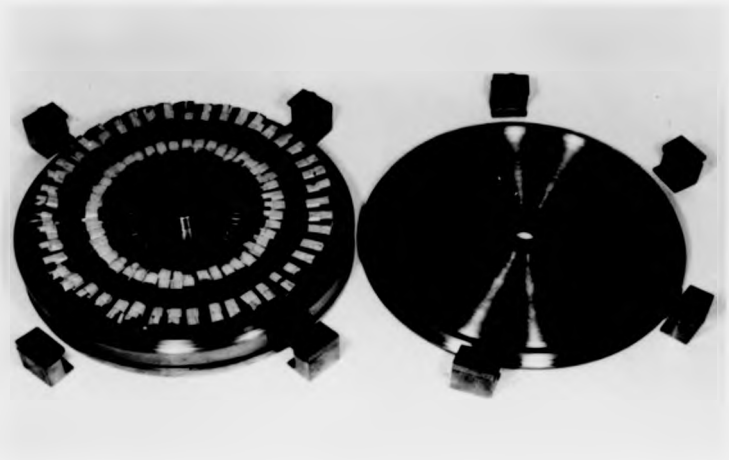

Fig. 5.9 : Armature windings positioned in mould

Fig. 5.10 : Complete armature

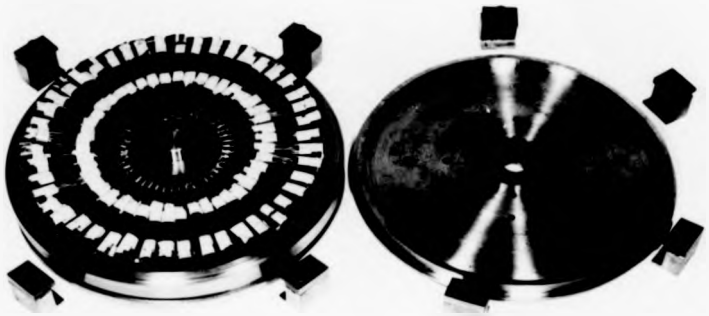

Fig. 5.9 : Armature windings positioned in mould

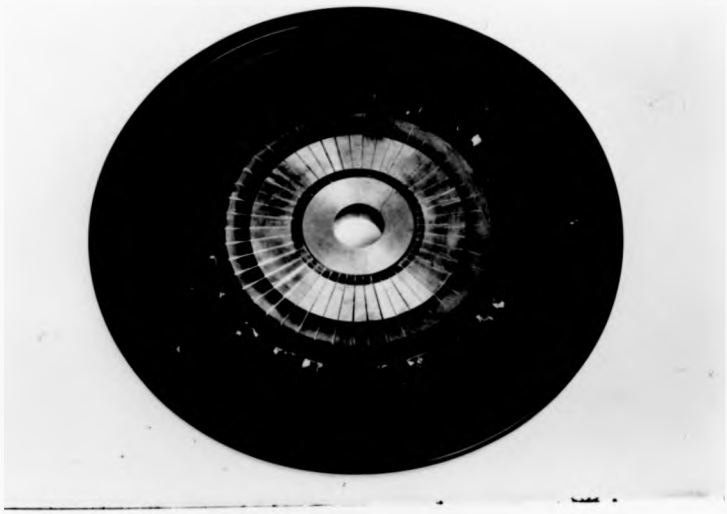

Fig. 5.10 : Complete armature

Robnor Resins
Encapsulation of Electrical and Electronic Components
Robnor Twin-Packs for Epoxy, Polyurethane, Polyester Resins and Silicone Rubbers

Highworth Road South Marston Swindon Wiltshire SN3 4TE
Telephone Stratton St. Margaret (079-382) 3741-2-3 Telex 449905

Directors: Peter Kerley G C N Snelgrove M D Hempleman

Registered in England No 664718

ROBNOR EPOXY CASTING RESIN PX 237C

This resin system is a warm curing casting system formulated for the encapsulation of electrical components. It possesses particularly good resistance to thermal cycling and to thermal shock.

It can be supplied in any of the standard range of colours or its natural colour which is a light cream.

Mixing

If in twinpack form, mixing is carried out as described in the twinpack literature. If in bulk, the resin and hardener are mixed in the ratio 17:2.

The usable life of PX 237C when mixed is as follows :-

12 hours at 20°C
4 hours at 40°C
2 hours at 60°C

Curing

Cure the system for at least :-

24 hours at 60°C
10 hours at 80°C
4 hours at 100°C
2 hours at 120°C

Properties

Initial Viscosity	50-60 poises
Specific Gravity	1.56
Resistance to Heat (continuous)	120°C
Thermal Conductivity	7×10^{-4} cal/cm °C
Electric Strength	110-120 kV/cm
Volume Resistivity	$> 15 \log_{10}$ ohm cm
Coefficient of Expansion	$4.5\text{-}5.0 \times 10^{-5}$ in/in linear/°C
Deflection Temperature	130°C improved by extended post cure.
Elasticity	270-330 kg/mm^2 (unfilled)

NOTES

Cleaning equipment

All equipment must be cleaned before the compound has hardened. Acetone or cellulose thinners are suitable cleaning agents.

Table 5.1 : Specification for epoxy resin for encapsulation

may be present, the mould is placed on a vibrating table while pouring proceeds. When the base of the mould is filled with resin, the lid is attached and extra resin added if required through the holes in the lid. Having applied the clamps, the complete mould is then transferred to an oven where the resin is cured according to the specification. When.cool, the mould is opened and the completed armature removed. The unused copper may then be machined off to expose the commutator segments and the armature is now complete (Fig. 5.10). As it is not possible to test the armature electrically before encapsulation as the commutator segments are shorted together, a voltage drop test is carried out to ensure that there are no electrical faults. Once this has been done, the commutator segments are undercut, the armature is balanced and it is then ready for installation in the motor. The machine is shown disassembled in Fig. 5.11 and complete in Fig. 5.12 where the magnetising winding connections can be seen.

Although the encapsulation process just described is a slow and time-consuming procedure, it is very suitable for prototype work. Techniques are available today to perform such operations much more quickly, and on a commercially viable basis. All the mechanical parts of this motor and the armature encapsulating mould were constructed by staff at the Engineering Department workshops at Warwick University. The armature was manufactured externally and encapsulated at the University by the author, who also assembled the magnetic circuit.

Fig. 5.11 : 7.5kW motor - disassembled

Fig. 5.12 : 7.5kW motor - assembled

Fig. 5.11 : 7.5kW motor - disassembled

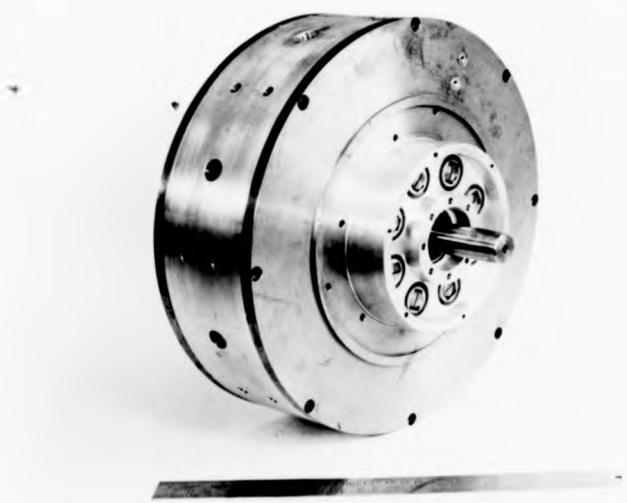

Fig. 5.12 : 7.5kW motor - assembled

5.2 Performance of the magnetic circuit

With the stator assembly complete, it is important to carry out a detailed investigation of the flux within the machine to ensure that a uniform pattern is apparent with no serious deterioration at the edges of the poles.[26] This is done without the armature present in order to facilitate the use of the measuring transducer - in this case a Hall Effect probe.

Supplied with the magnets is a demagnetisation curve with a shaded area marked within which the demagnetisation curves of the magnets lie (Fig. 5.13). A comparison of this curve with the standard curve used in the computer-aided design program, indicates that the standard curve passes quite close to the centre of the shaded area in Fig. 5.13. It may therefore be assumed that the magnets supplied are within specification and that the field will be as predicted. The stator is assembled and an impulse magnetiser connected to the magnetising windings. The magnetiser works by charging a large bank of capacitors to a high voltage and then discharging them through the magnetising windings of the motor using a thyristor switching element. Extremely high currents are caused to flow for a very short time and the magnetic field produced is sufficient to saturate the magnets and thus allow them to operate at the desired point on the BH curve. Because the saturation flux density is higher than the working flux density, the flux-return path needs to be extended while magnetisation is being carried out. This is accomplished by temporarily locating additional steel rings either side of the motor case. It is

DEMAGNETISATION CURVE FOR HYCOMAX III MAGNETS

TYPE 2235CM1, OUR ORDER NO. F55823, CUST. O/No ES/242/78

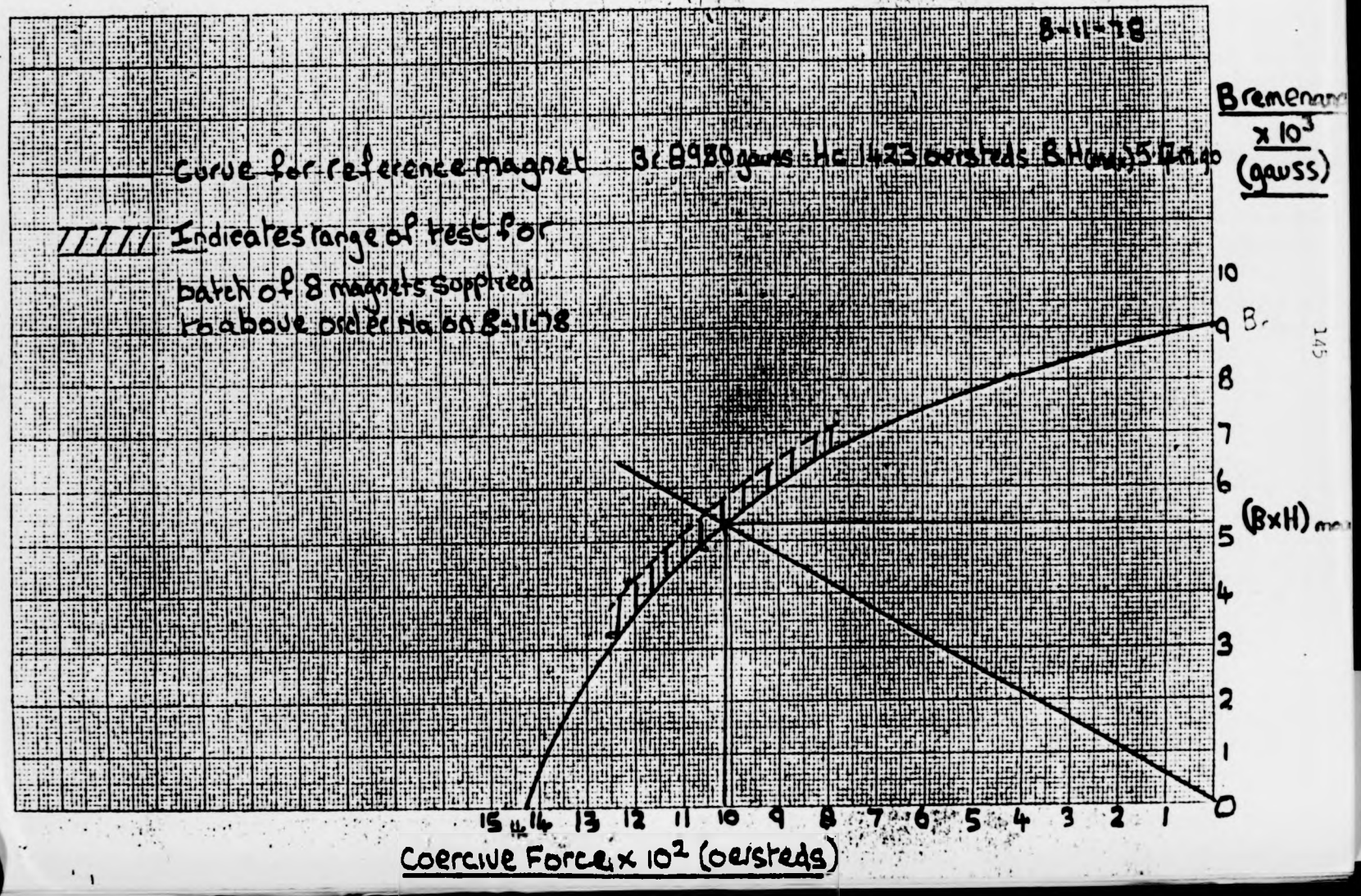

Fig. 5.13 : Actual demagnetisation curve

recommended that for the initial magnetisation of this material, the magnetising force should be increased to the maximum value in several stages as this will ensure maximum alignment of the magnetic domains. Once magnetisation is complete and the connections to the magnetising windings removed along with the auxiliary flux-return rings,measurements of the airgap flux density can be made. This is done by marking out a grid pattern over the magnet positions and then locating the Hall Effect probe at these grid points in the centre of the airgap. (The probe is inserted through the ventilation holes in the aluminium casing of the machine.) Measurements are taken at positions between opposite magnets and also between opposite neutral zones, so that a continuous assessment of the flux distribution may be made. Although some variation from pole to pole is evident, this is within the spread of BH values given in Fig. 5.13. Fig. 5.14 shows typical values of flux density for the indicated sections of the magnet segment. A slight reduction in flux is noticed towards the edge of the magnet and although this is more pronounced at the corners, the airgap flux density over most of the pole area is maintained at approximately 0.5 Tesla. With the value of B_m taken from Table 3.4 this corresponds to an actual leakage coefficient of 1.36 for this configuration of magnets. With the measurements of neutral zone flux combined with those above Fig. 5.15 gives the average airgap flux density distribution over a pole pair, and it is this particular distribution which is used in the computer program for armature winding analysis detailed in section 4.4.

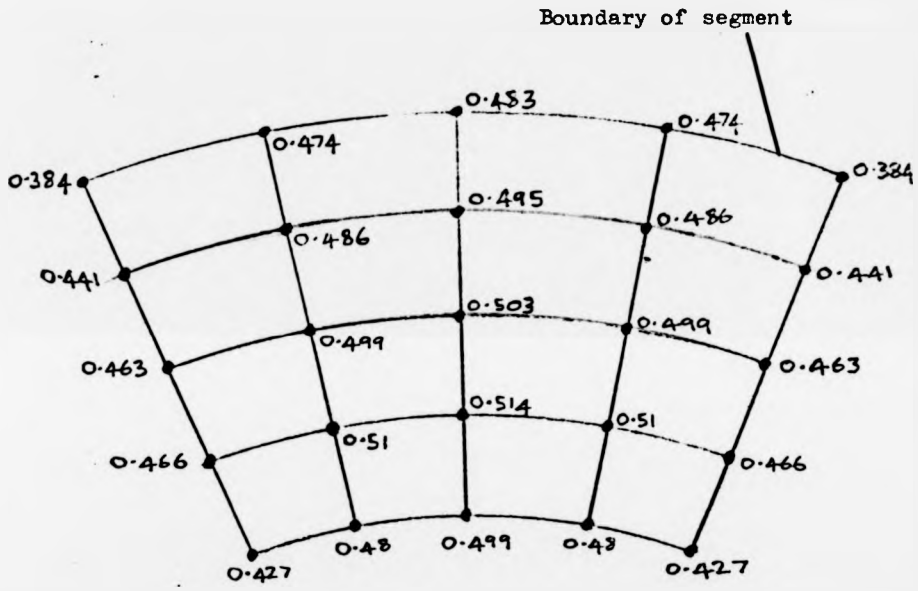

Fig. 5.14 : Flux density in airgap at grid points, Tesla

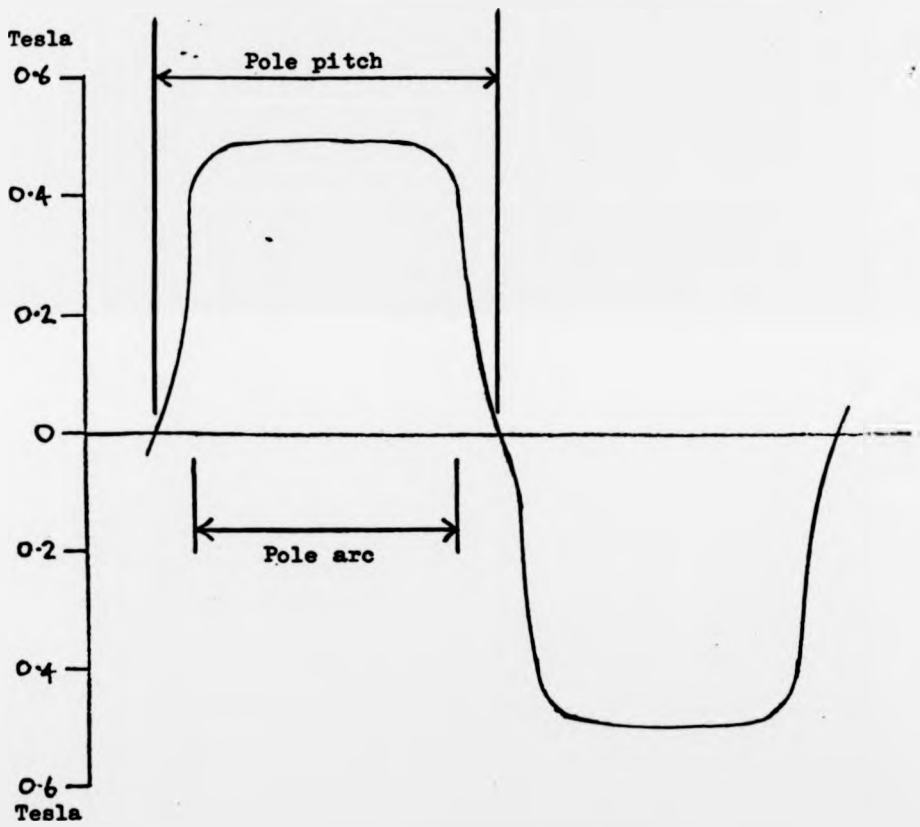

Fig. 5.15 : Average airgap flux density in 7.5kW motor

5.3 Performance of the motor

Having characterised the magnetic circuit, the motor may be assembled with the armature in place, remagnetised and run. As the surfaces of both brush and commutator are flat, no extensive bedding-in procedure is necessary, although the brush surfaces are given a light treatment with a fine abrasive cloth to remove any residual deposits. The motor is run on light load until a good patina (collecting surface) is formed on the commutator.

In section 4.4. it was shown that significant differences occur in the e.m.f.s generated in both the primary and short circuit armature paths of the two winding options considered. In particular, the generally higher short circuit e.m.f.s in winding option 1 (commutator pitch 10) exist to the detriment of those in the primary paths. Over rotation by one commutator segment these short circuit e.m.f.s average to a significant fraction of the average primary e.m.f. which is not the case in winding option 2 (commutator pitch 11) where the short circuit e.m.f.s average to approximately zero. Clearly, this effect must be investigated in a machine equipped with the alternative windings. Study of the results from the computer program relating to the e.m.f. calculations reveals that, except in the case of two brushes only in the machine, no single brush short circuits an armature path, i.e. for four and eight brushes all short circuit paths are formed between different brushes (positive or negative). It is thus feasible to measure the voltages developed between like brushes in a machine equipped with, say, four brushes, but only using two to supply

power (Fig. 5.16), thus indicating the magnitude of the e.m.f. developed between positive and negative brushes. A similar test may be carried out for the case of eight brushes. The tests are performed for both armature windings and on light load for a range of values of supply voltage. The voltages developed between positive brushes, V_P, and between negative brushes, V_N, as a fraction of the supply voltage, V_S, are given in Table 5.2 for both winding options. For each armature four brushes and eight brushes are used but with only two providing electrical power. These may be compared with similar results derived from the e.m.f. analysis (Figs. 4.18 to 4.20) and which are presented in Table 5.3. Agreement is generally good, but with a tendancy for the voltages between the positive brushes to be somewhat higher than expected - this occurs in both brush sets in the case of eight brushes used in the option 2 winding. When all brushes are powered, the e.m.f.s generated between like brushes are shorted together and it is reasonable to expect that this has greater consequence for winding option 1. This is observed in practice by a degree of sparking at the brushes when this armature is used while no significant sparking is apparent with winding option 2. When two brushes only are used in the machine any short circuits are caused by a single brush and in this particular motor occur for only relatively short periods of time (Fig. 4.18). Although there is no way of measuring this e.m.f., it is clear from Fig. 4.18 that the e.m.f.s to be expected in winding option 1 are considerably larger than those in winding option 2, with an effect on performance similar to that which has already been observed.

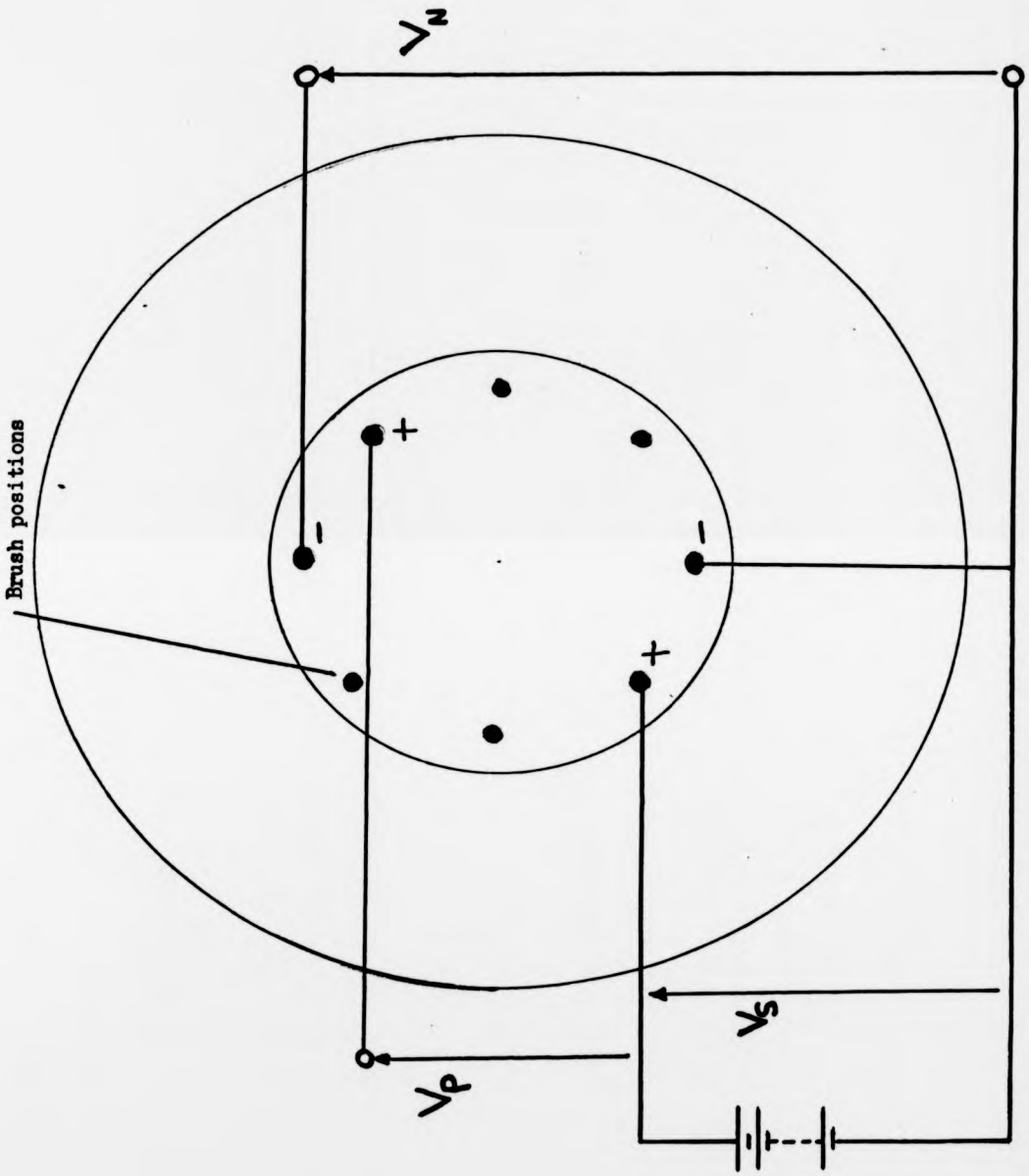

Fig. 5.16 : Measurement of e.m.f.s generated at non-powered brushes

	Winding option 1	Winding option 2
Four Brushes	$V_P = 0.178V_S$	$V_P = 0.032V_S$
	$V_N = 0.121V_S$	$V_N = 0.032V_S$
Eight Brushes	$V_P = 0.106V_S$	$V_P = 0.022V_S$
	$V_N = 0.076V_S$	$V_N = 0.017V_S$

Table 5.2 : Voltages measured between like brushes as a fraction of the supply voltage

	Winding option 1	Winding option 2
Four Brushes	$V_P = 0.135V_S$	$V_P = 0.020V_S$
	$V_N = 0.123V_S$	$V_N = 0.027V_S$
Eight Brushes	$V_P = 0.074V_S$	$V_P = 0.007V_S$
	$V_N = 0.070V_S$	$V_N = 0.001V_S$

Table 5.3 : Predicted voltages between like brushes as a fraction of the supply voltage

In addition to the measurement of short circuit e.m.f.s, it is important to assess the effect of the alternative winding arrangements when the motor is used on load. To this end, it is coupled to a Ward Leonard test set already existing in the Department (shown schematically in Fig. 5.17). As this equipment has been used and described on several previous occasions[63,64], no detailed description is given here. The generator used to load the disc armature motor is a compound wound machine and is selected to have an operating speed similar to the disc armature motor with an output voltage similar to the second d.c. machine in the test set. Power for the disc armature motor is derived from a set of traction batteries with a carbon pile stack to provide the necessary voltage variation. Output torque from the motor is measured using an ASEA 'Torductor' (type 5693-719/A) which derives the value of mechanical torque from the change in the magnetic characteristics of a shaft when it is under torsion. The motor speed is measured by a hand-held tachometer and a supply voltage of 96V is used throughout. The motor is tested under load, with four brushes, for both winding arrangements and the results are shown in Figs. 5.18 and 5.19 with the computer predicted results shown for comparison in Fig. 5.20. It will be noted that the maximum achieved armature current was, in each case, approximately 30 amps and this results from serious difficulties encountered with the mechanical stability of the discs. It was noticed that after running for a short time while drawing currents of between 20 and 30 amps, the disc came into contact with the magnets on the stator. This occurred in both armatures and after dismantling and inspecting, it became clear

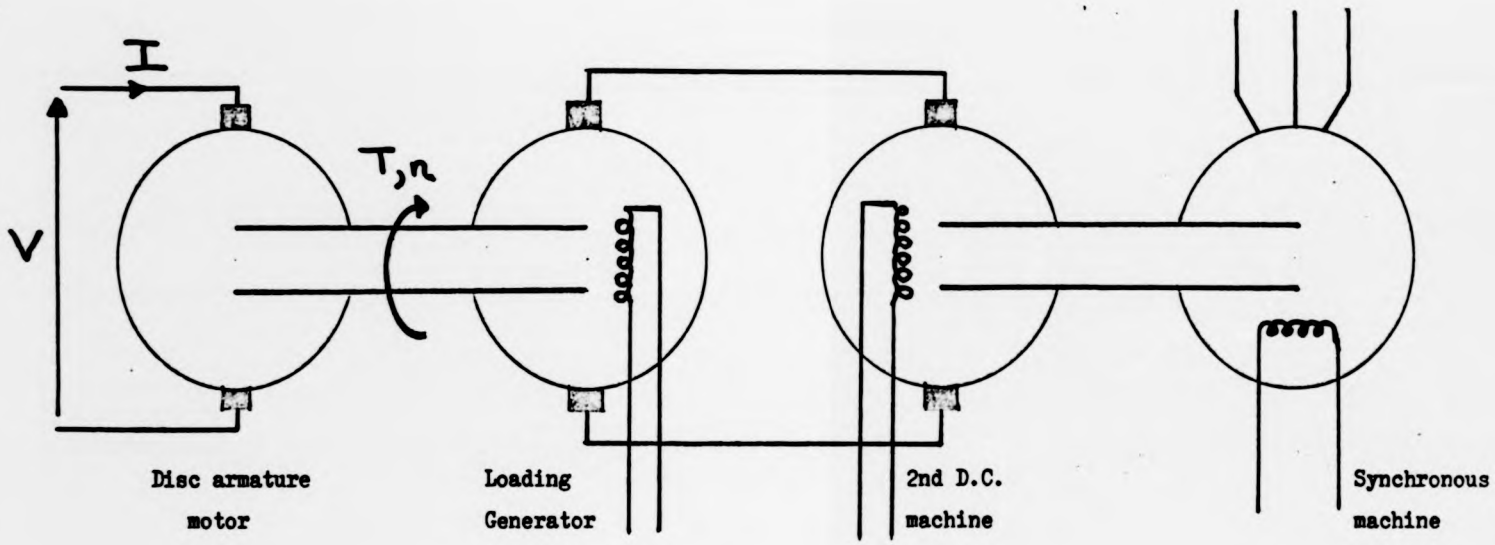

Fig. 5.17 : Schematic of Ward-Leonard testing apparatus

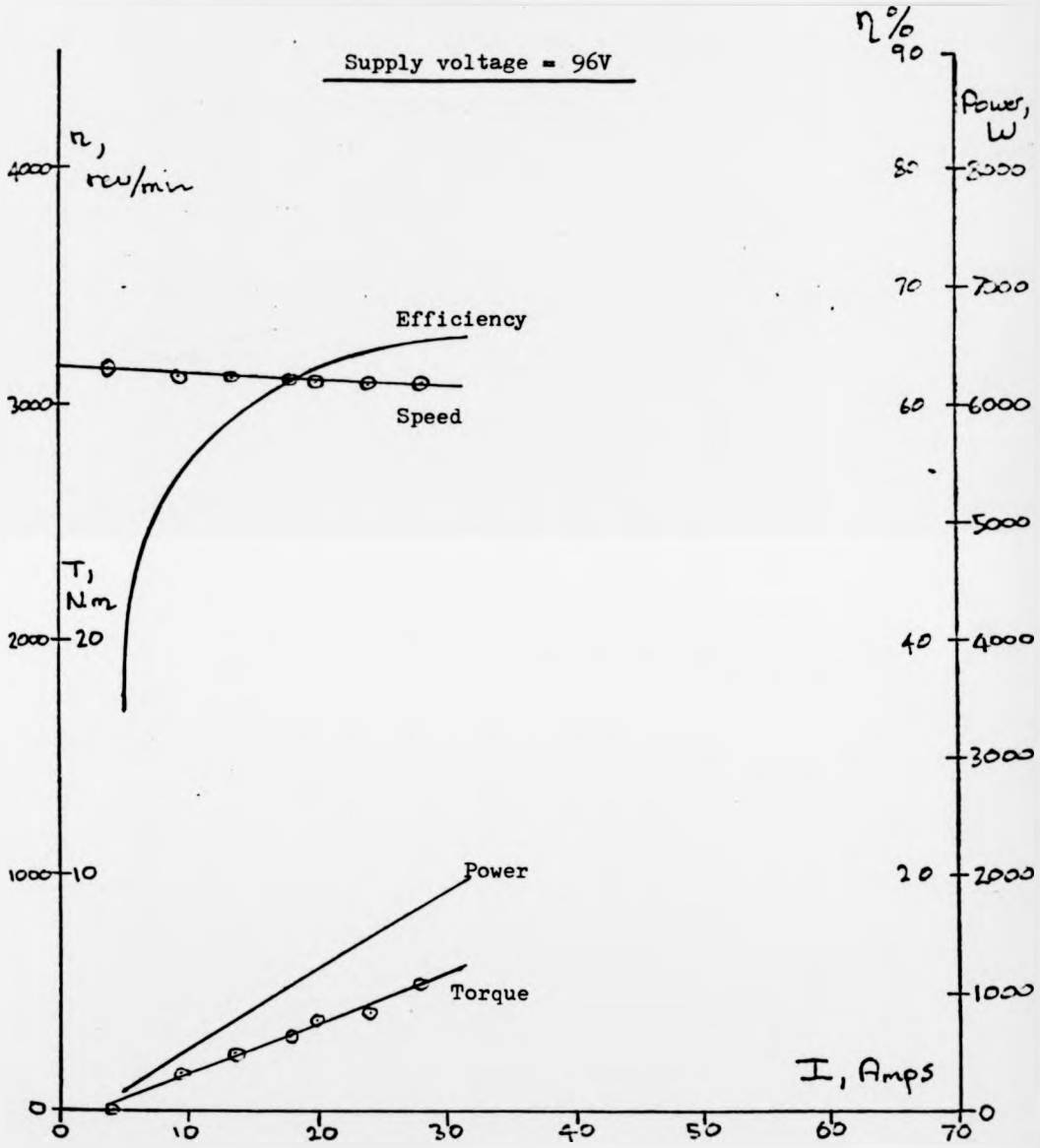

Fig. 5.18 : Performance curves of 7.5kW motor - winding option 1

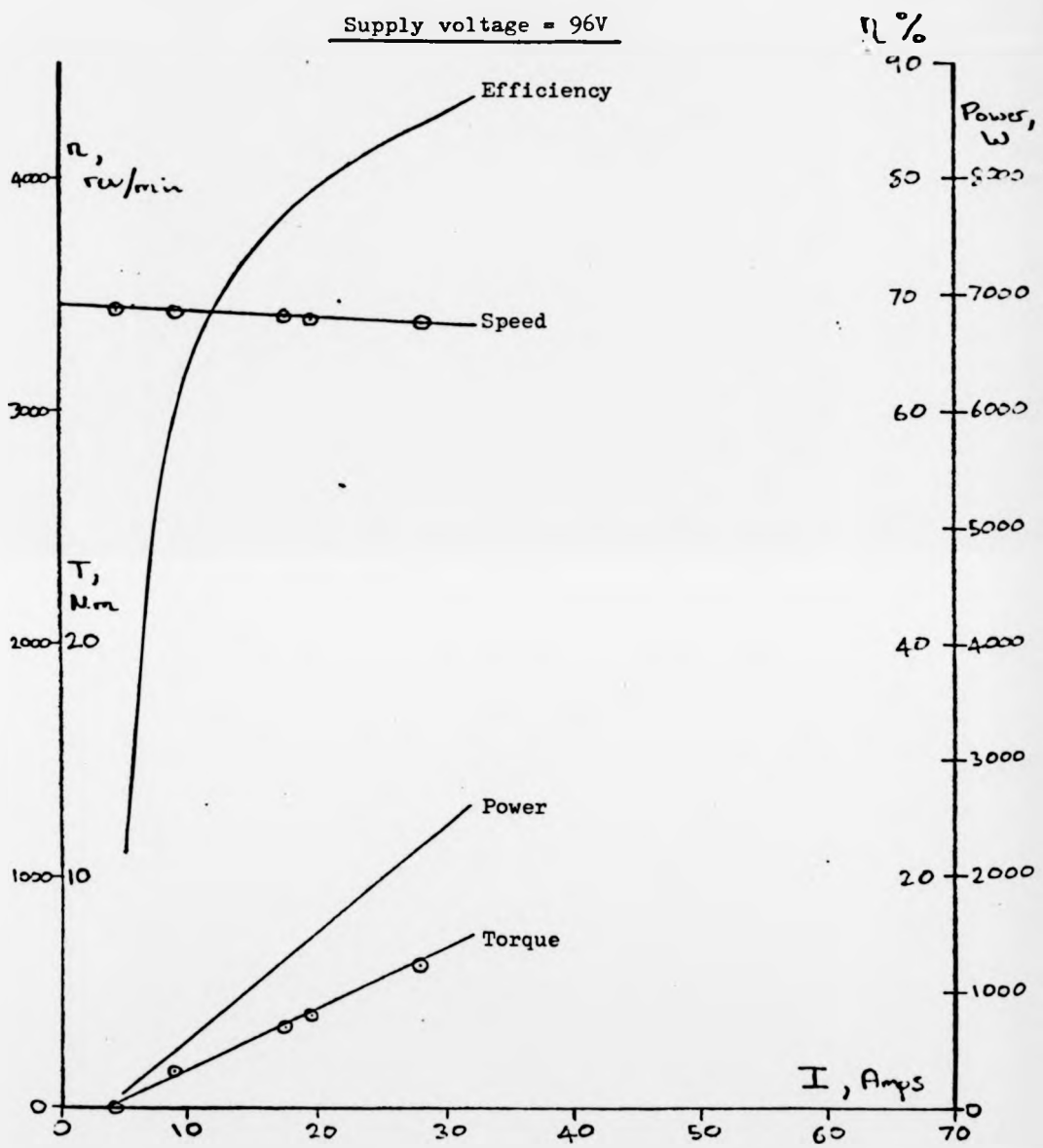

Fig. 5.19 : Performance curves of 7.5kW motor - winding option 2

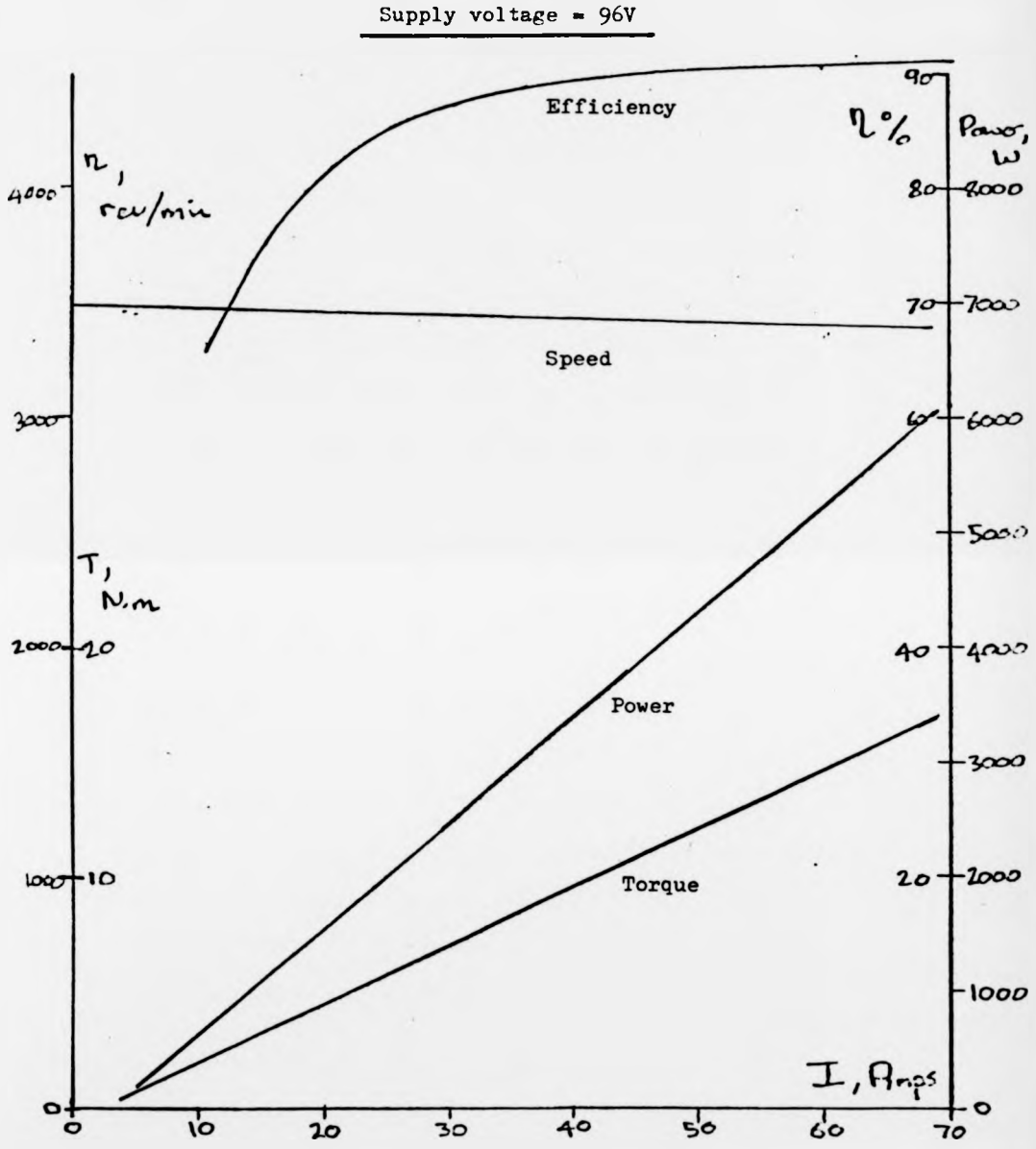

Fig. 5.20 : Computer predicted performance curves of 7.5kW motor

that the armatures were flexing at comparatively low temperatures. This eventually resulted in a circumferential fracture of the encapsulation material at a radius somewhat less than r_1 (the inner active radius) and the armature discs were eventually so distorted that they became unusable. Consultation with the resin manufacturers revealed that the specification of the material in Table 5.1 is incorrect and in particular the specified deflection temperature is 30°C and not 130°C as indicated. This explains the low temperature flexing and eventual failure of the discs, although it does place a serious limitation on the load testing possible..

However, results that are available show that a significant reduction in speed is apparent when winding option 1 is used. The value of this reduction (over option 2) is calculated from Figs. 5.18 and 5.19 to be 8.6% and this may be compared with the difference in the average values of the primary e.m.f.s for four brushes found from Fig. 4.19 - the reduction is 6.0%. In terms of overall motor efficiency, the lower speed of winding option 1 leads to a reduction in efficiency over the measured range and the results clearly show the difference in performance when the alternative armatures are used in otherwise identical machines.

Although the results from testing the motor are not as extended as was originally thought possible, they do indicate the value of the e.m.f. analysis presented in Chapter 4 as it is essential to determine the optimum winding arrangement for a given basic motor specification.

5.4 Rating of disc armature motors

An extremely important consideration for traction motors is their thermal behaviour as this will dictate the amount of overload that can be tolerated by the machine. Many such motors are required to perform arduous duty cycles which necessitate the flow of high peak currents, often for appreciable durations. For example, the motor in an electric vehicle under conditions of extreme gradient or high acceleration may be producing torques far in excess of the manufacturers continuous rating, and it is the machine's ability to withstand such overload without damage that is of prime importance. Traction machines are thus usually given load ratings - for example, the current that can be drawn for one hour or for half an hour, etc., after which overheating is likely to cause damage to the motor. More complex rating conditions may also be specified. The British Standard relating to battery electric vehicles[65] calls for the current that can be maintained for one hour followed by an increase of 200% for 5 minutes. Improvements in recent years[66] have led to a gradual raising of thermal limits, but it is important to realise that such limits exist and choose a traction motor with careful regard to the duties it will be required to perform. In applications where a vehicle will undertake known and repeatable duty cycles the specification of a suitable motor is a relatively easy task, but for general battery electric traction purposes (cars, commercial vehicles, etc.) such a choice may not be so straightforward. Ideally, typical duty cycles for such vehicles would be established and these applied

to an accurate thermal model of the traction motor. Until such methods are available, however, the forms of rating mentioned above must suffice to represent the motor's thermal performance. Conventional traction machines contain an appreciable amount of iron in the rotor which allows heat energy to be stored for a period of time before the temperature rise becomes excessive. Some heat is dissipated, especially in motors that are self-ventilated or force-cooled and under these conditions the overload tolerance of the motor will be higher than when totally enclosed. The amount of heat that can be stored depends on the size of the rotor and it is this 'thermal capacitance' which largely dictates the overload capability of a motor. By contrast, the disc motor, with its thin, iron-free armature, has considerably less capacity for thermal storage, and it is the motor's ability to dissipate heat that dictates overload capability and thermal rating. Fortunately the motor has good heat dissipation due to the proximity of the armature conductors to the surface of the disc, the relatively large disc surface area and the radially induced airflow which occurs naturally as the disc rotates. The benefit of this airflow may be enhanced by providing suitable vents in the motor casing and in prototype traction machines this has been done.

Although the thermal performance of disc armature motors is dictated by different factors, it would still be convenient to have a rating method similar to that used for conventional machines. Temperature limits have therefore to be established and these related to the armature current drawn and the time duration under consideration. It is first necessary to consider which machine

components are most susceptible to excessive temperatures. In conventional machines, the limit is imposed to protect the armature winding insulation but in the disc armature machine, it is the deflection temperature of the armature moulding compound which is the critical parameter. Although the winding insulation is Class F and thus able to withstand temperature rises of up to 155°C, typical deflection temperatures of the epoxy resin used are around 100°C which places a lower limit on armature operating temperature. This also makes it more appropriate to use the lower temperature (75°C) of the two specified in B.S. 1727 for motor performance curves.[65] Although the magnets will not reach temperatures where permanent demagnetisation is likely, the reversible coefficient of demagnetisation must be taken into account if continuous, high temperature operation is envisaged.

Once a particular motor has been constructed, it may be tested at various values of armature current and the temperature rise over a period of time recorded. Although the data thus gathered would enable a suitable rating to be given to the motor in question, it would be preferable if a parameter common to all motors could be used instead of armature current. It is therefore proposed that the current density specified for a motor (the current per unit cross-sectional area of armature conductor) would provide the means of this more general rating assessment. This is one of the fundamental parameters in the computer-aided design process and its adoption would enable motors to be designed with predetermined rating conditions. To establish the correlation between current density, temperature rise and time results from

previous and current machines involving temperature testing are investigated. The most recent of such tests were those carried out at the University by Ozpolat[67] on a low power traction motor (see Appendix II). The results relevant to this study are the temperature/time curves for the motor armature at two values of current density, 5 A/mm^2 and 10 A/mm^2. These curves are presented in Fig. 5.21 and relate to a motor which is self-ventilated. Results from the earlier prototypes covered in Chapter 3 are considered in a similar way taking into account the current density at which they are tested. Although the tests are not as extensive as those resulting in Fig. 5.21, the results compiled from all motors show a clear relationship between current density, temperature and time (Fig. 5.22). It is evident that the thermal time constant of disc armature motors tends to be much less than that in conventional d.c. machines. It must be appreciated that the size of machine in question has considerable bearing on the thermal performance available. With the heat generated within an armature dependent on its volume and heat dissipation dependent on surface area, the current density corresponding to a given rating condition will be less in large machines than in small machines unless additional cooling is specified. The present discussion is thus valid only for motors of the same order of size, which is approximately true in the motors considered. The conclusions drawn below will therefore need to be modified if machines of widely differing sizes are to be considered, and until more extensive thermal testing has been carried out rating conditions for such machines will need to be determined by experience. The results that are presented do, however, give some guidelines for an appropriate choice.

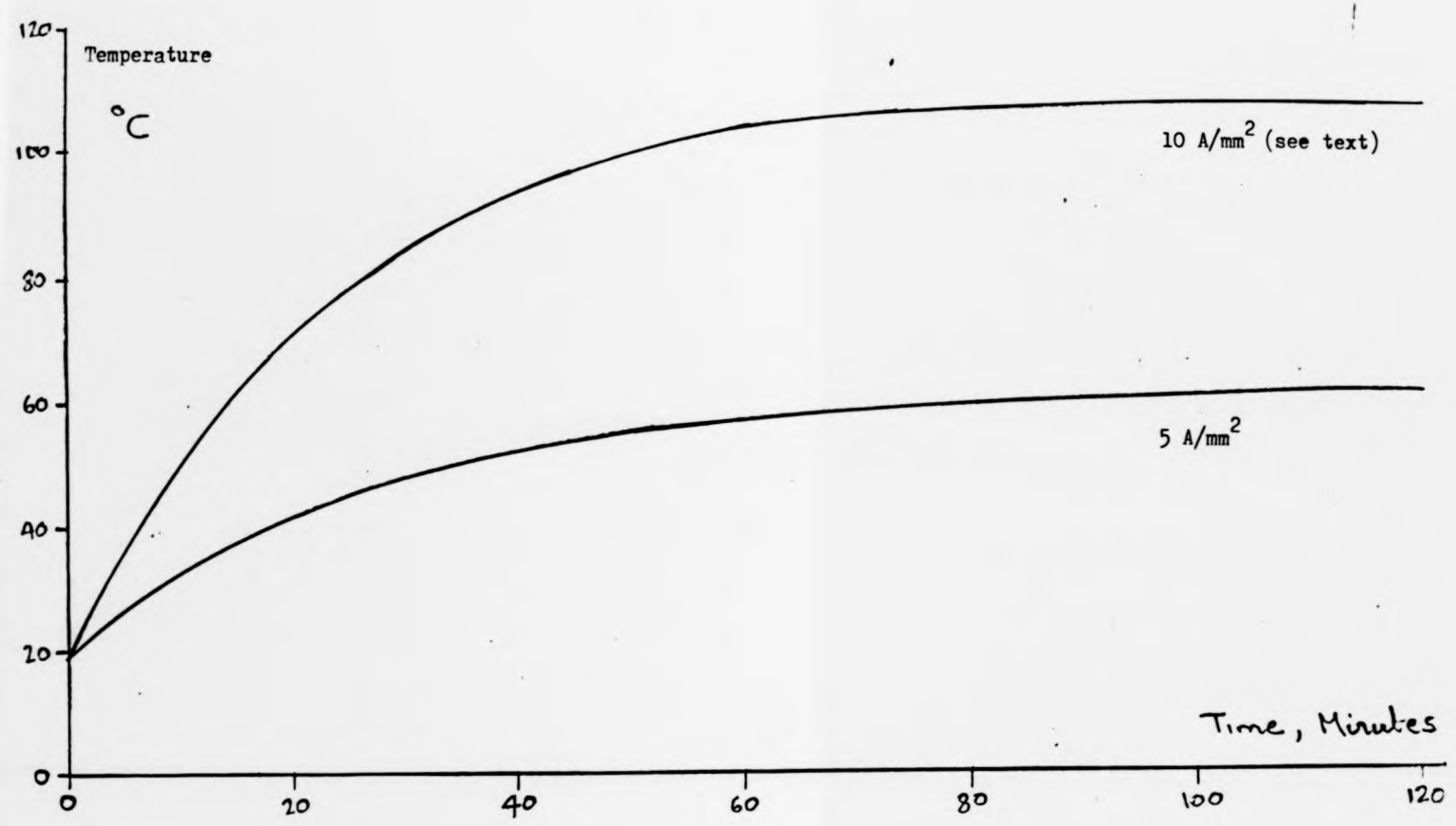

Fig. 5.21 : Armature temperature/time curves for traction motor

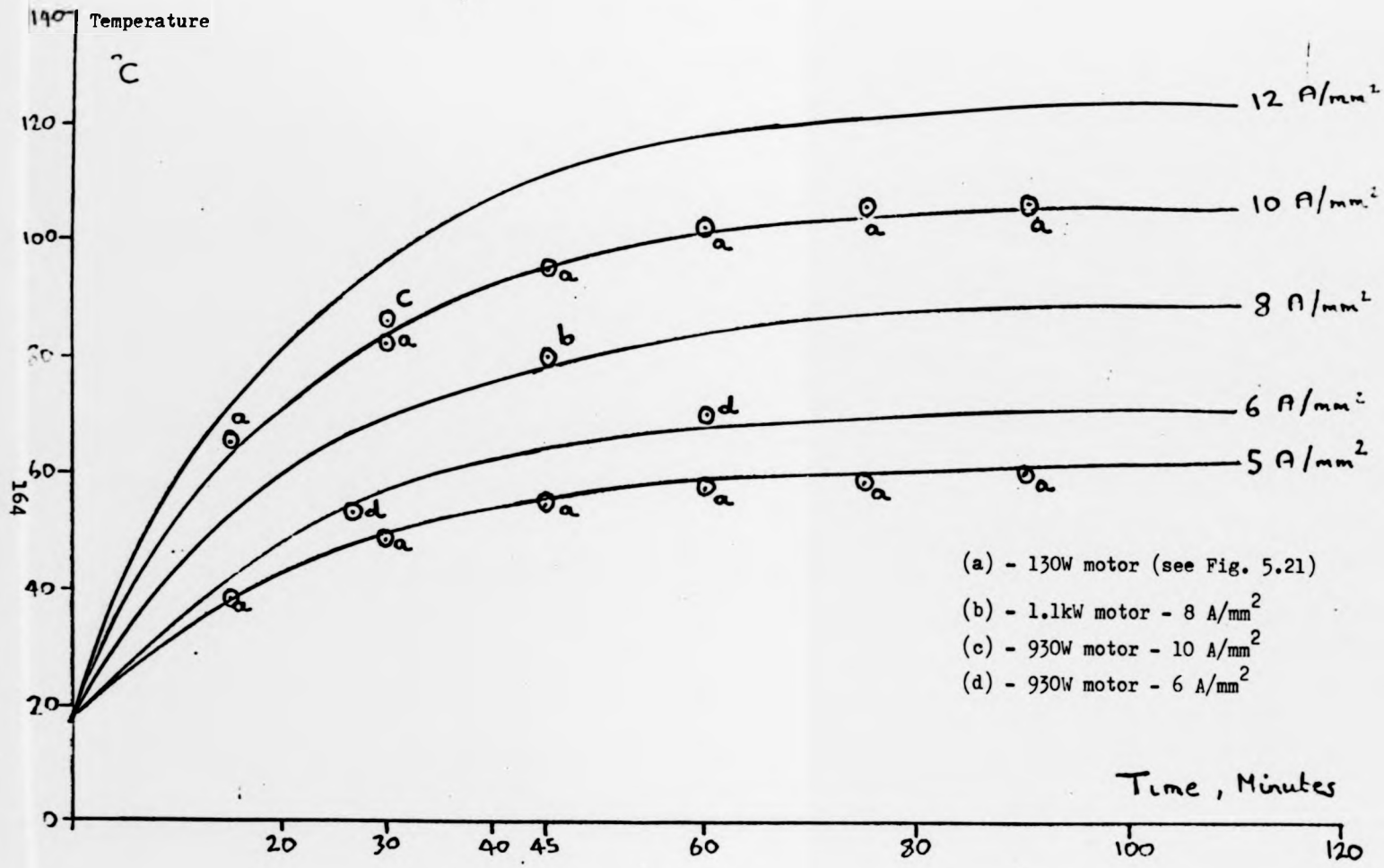

Fig. 5.22 : Armature temperature/time curves collated for various motors

Consultation with manufacturers of the moulding compound following the poor performance of the armatures discussed earlier (section 5.3) resulted in a specification of achievable deflection temperatures being more realistically assessed as between 115°C and 120°C. Information supplied by other manufacturers generally supported these figures. Allowing for a reasonable margin of safety a maximum operating temperature of 100°C is appropriate for motors of this kind, and referring to Fig. 5.22 this corresponds to a continuous operating current density of 9 A/mm^2. Because of the short thermal time constant of the machine this continuous rating is also appropriate for any rating period above one hour. Assuming the extrapolation to 12 A/mm^2 in Fig. 5.22 is valid, the following rating conditions are appropriate to machines of this type.

Continuous - 9 A/mm^2

One hour - 9.5 A/mm^2

45 minute - 10 A/mm^2

30 minute - 12 A/mm^2

Lack of short-term test results precludes specifying the 10 minute rating of B.S. 2613, or the 15 minute, 5 minute and one hour plus 200% overload for 5 minutes as specified in B.S. 1727.

It will be recalled that the computer-aided design procedure uses a default value for current density of 8 A/mm^2 and this represents an appropriately conservative limit on thermal rating for general use. However, the opportunity exists while running the program for any desired value of current density to be specified according to the envisaged motor application and working

environment. The specification of forced cooling would allow an increase in permitted current density but at present the amount of such an increase related to forced air-flow must be determined by experience as no motors with forced cooling have been tested.

6: APPLICATION TO BATTERY ELECTRIC VEHICLES

While the major limitation on electric vehicle performance remains that imposed by the lead/acid battery every effort must be made to ensure the most efficient use of the relatively small amount of energy available for vehicle propulsion. On an energy per unit weight basis, petrol has 200 times that of the lead/acid battery[51] with the obvious advantages for road transportation. Two parameters relating directly to the electric traction motor which have considerable bearing on the overall vehicle performance are the efficiency and power density. The d.c. disc armature motor is superior in both respects to the conventional series wound motor which has been an almost universal choice for battery electric traction applications. While the usual constant voltage testing of motors is extremely useful for initial comparison purposes and will provide a good indication of this improvement in efficiency, the only meaningful way of comparing two traction motors is to test both in the actual working environment i.e. when installed in a battery electric vehicle. To this end, an on-going project has been established at Warwick University involving the conversion of a three-wheeled vehicle (the Reliant Robin) to electric drive. To gain an accurate assessment of vehicle performance, it is necessary to study the power flow along the vehicle drive chain and as the working efficiency of the motor (and indeed of any vehicle sub-component) depends on the performance of the other vehicle sub-components, these must also be determined. The easiest way of studying the overall vehicle performance is to set up an accurate model of the complete system, based on suitable

models of the sub-components (transmission, motor, controller, etc.), so that this interrelation can be allowed for. Such a simulation technique is developed for use on a digital computer in parallel with the vehicle conversion work. The series wound motor is used in the vehicle to establish performance standards and to prove the simulation. The model for the disc armature traction motor is then substituted for the series machine to assess the advantages of this type of drive.

6.1 The electric vehicle system model

With recent renewed interest in electric vehicles for road transportation, much research effort has been expended in studying the performance of such vehicles under various operating conditions. This has led to the specification of several mathematical models or computer simulations to allow a more comprehensive analysis of vehicle behaviour to be carried out.[52,53] An extension of these methods to computer-controlled testing on a stationary test-bed is also becoming more popular as it allows the testing of a vehicle under precisely repeatable conditions which is useful for a direct comparison of different sub-components. Such a facilitity is being installed at Warwick University as part of the general programme of research into electric vehicle performance. Many simulation models rely on a certain amount of experimental data from the various sub-components and this approach is adopted for the electric Reliant Robin - i.e. the individual vehicle components are tested and characterised before their incorporation into the final simulation

computer program. This has the advantage of allowing substitution of any particular component as long as the new component has been characterised in a similar manner.

A block diagram of the complete vehicle model is given in Fig. 6.1. The system is considered in its widest sense here and represents the complete power flow from the lead/acid battery to the 'road power' - that used to overcome aerodynamic and tyre losses. The basis of the model is the calculation of the power into each block in Fig. 6.1 for a given value of power drawn from it. The power is determined in terms of torque and speed for mechanical systems, and voltage and current for electrical systems. After calculating the road power for the vehicle, it is possible to work back through the system until the battery voltage and current have been predicted. A useful by-product of this technique is the working efficiency of each component under particular operating conditions, and it is also possible to determine the energy flow through the vehicle for an assessment of the various loss areas involved.[54] The individual components of the block diagram in Fig. 6.1 will now be discussed separately along with the mathematical model set up to describe each.

6.1.1 Consideration of the road losses

It will be assumed that the road losses may be completely accounted for by tyre rolling resistance and aerodynamic drag. The former is proportional to the weight of the vehicle and dependent, to a certain extent, upon vehicle speed; the latter is proportional

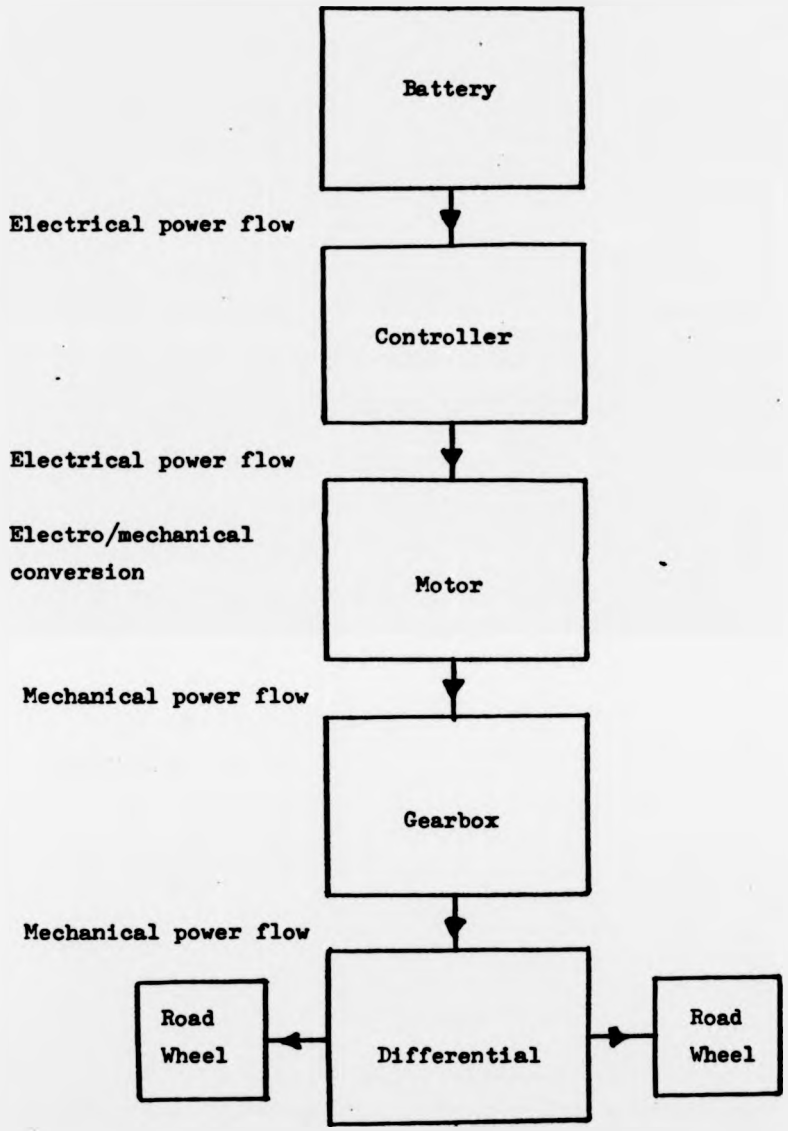

Fig. 6.1 : Block diagram of electric vehicle system

to the cube of the vehicle speed and is independent of the vehicle weight. Although methods are available for direct measurement of the coefficient of rolling resistance for a pneumatic tyre, K_1, extensive tests have been carried out by various bodies for just this purpose. For example, extremely comprehensive results are available from the American National Bureau of Standards including those related to typical crossply tyres used on the Reliant vehicle. Values of rolling resistance are presented for varying conditions of load, speed and inflation pressure and since accurate measurement of this parameter is not feasible within the present confines of the project, suitable results are drawn from the NBS data.[55] The relevant information may be shown in a single curve (Fig. 6.2) which illustrates coefficient of rolling resistance against vehicle speed - to obtain the actual value of retarding force it is only necessary to multiply by the vehicle weight. As can be seen, a slight increase in K_1 with speed is evident.

The force due to aerodynamic drag is given by:-

$$F_a = \tfrac{1}{2} C_D.\rho.v^2.A_F \qquad (6.1)$$

where F_a is the retarding force, C_D the drag coefficient, ρ the density of air, v the velocity and A_F the front area of the vehicle. A suitable value for ρ is taken from standard tables while the vehicle frontal area and the value of C_D are taken from manufacturers data, the latter found from wind-tunnel measurements on the Robin body shape. If a coefficient K_2 is expressed:-

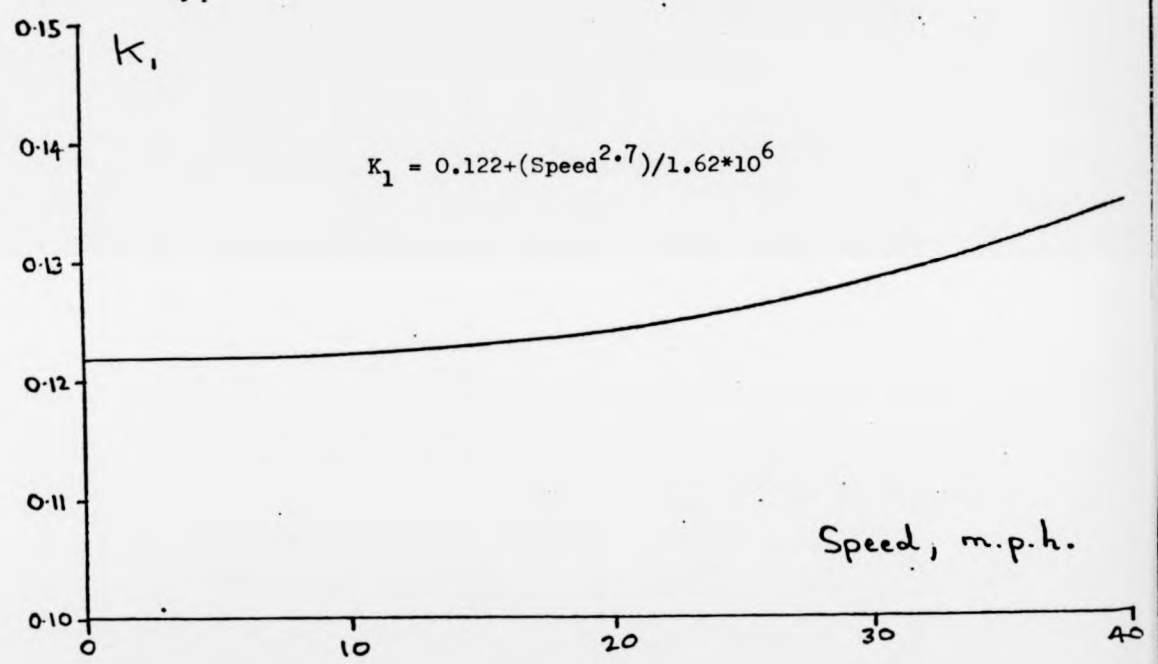

Fig. 6.2 : Coefficient of rolling resistance versus speed

$$K_2 = \tfrac{1}{2}\rho \cdot C_D \cdot A_F \qquad (6.2)$$

then the total drag force of a vehicle of mass M_V and speed v is given by:-

$$F_r = K_1 \cdot M_V + K_2 \cdot v^2 \qquad (6.3)$$

It is thus possible to calculate F_r at any given speed, and knowing the diameter of the roadwheel the output torque and speed required from the rear axle may be found.

6.1.2 Consideration of the transmission

The transmission of the vehicle consists of a change-speed gearbox to which the motor is coupled through the clutch, a propellor shaft, a differential unit and twin rear half-shafts with associated universal joints and bearings. The components are those used in the standard i.c. engined version of the vehicle, and it will be assumed that all losses between the motor output shaft and the road wheels may be accounted for by the transmission inefficiency. The change speed gearbox is retained in order to assess the merits of having different gear ratios between the motor output shaft and the final drive. If not required, top gear may be selected continuously with an allowance made for the slight inefficiency it introduces. The clutch is used only to facilitate gear-changing - any loss it introduces in normal running are assumed to be included in the gearbox losses. The transmission system is divided into its two basic components (differential and gearbox) and each is treated as a separate loss

area. It is appropriate that the efficiency of each unit is determined for the power output required from it and to this end, a series of tests on the transmission are carried out. A 3rd year undergraduate project was established to undertake this work which involved testing the transmission under various speed and torque conditions. Measurements associated with each component were taken while the transmission was being driven by an electric motor, and loaded by a band brake on the rear wheels. A theoretical approach was also applied which showed very close agreement with the results obtained by experimentation. A full description of this project with the techniques used is given in reference 56.

For the differential and each of the four forward gears, the efficiency is determined for various values of output speed at constant output torque, and various values of output torque at constant output speed. As can be seen from the graphs in Figs. 6.3 to 6.7, linear relationships may be used to describe the variation of efficiency with output torque and speed with empirical equations written to express these relations. For lst gear:-

$$\eta = 0.9252 \frac{0.0352\ (n - 263)}{387} + \frac{0.0468\ (T-14)}{51} \qquad (6.4)$$

For 2nd gear:-

$$\eta = 0.019 \frac{0.081(n-527)}{527} + \frac{0.061(T-13)}{28} \qquad (6.5)$$

For 3rd gear:-

$$\eta = 0.9725 - \frac{0.0325(n-720)}{1180} + \frac{0.0045(T-15)}{20} \qquad (6.6)$$

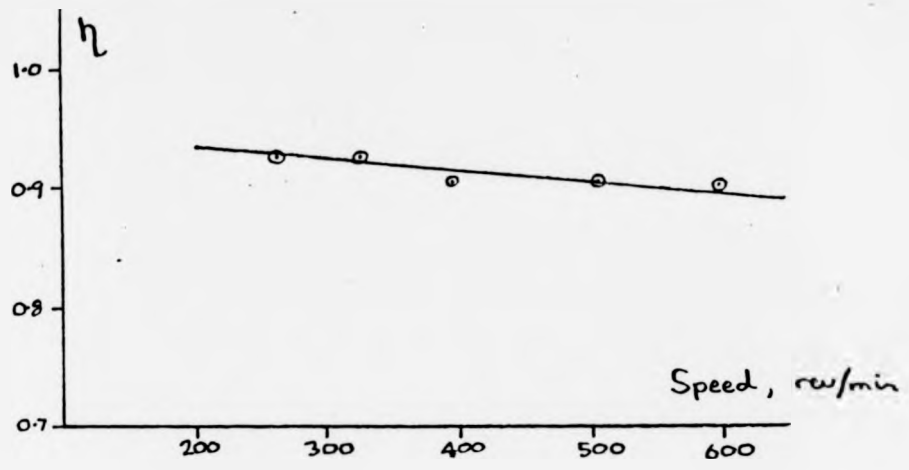

Fig. 6.3(a) : Efficiency versus output speed, 1st gear

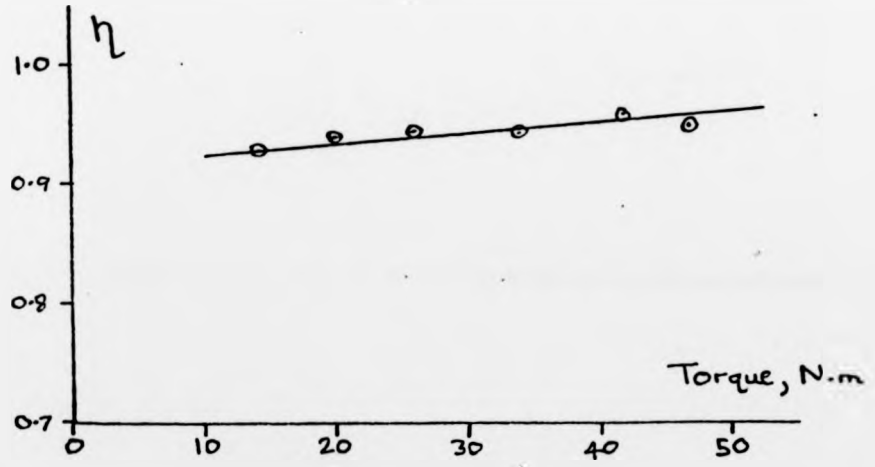

Fig. 6.3(b) : Efficiency versus output torque, 1st gear

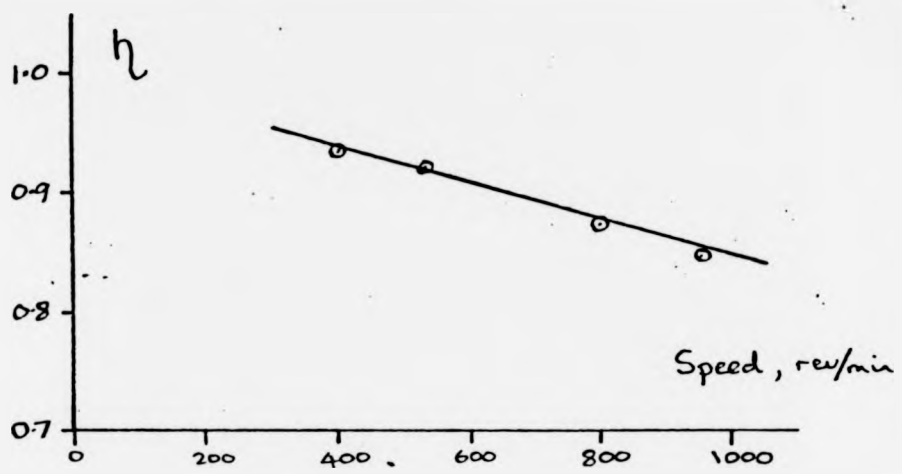

Fig. 6.4(a) : Efficiency versus output speed, 2nd gear

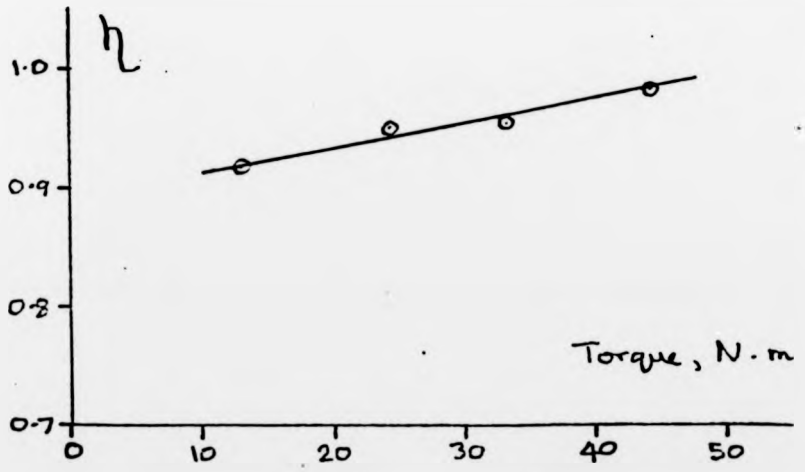

Fig. 6.4(b) : Efficiency versus output torque, 2nd gear

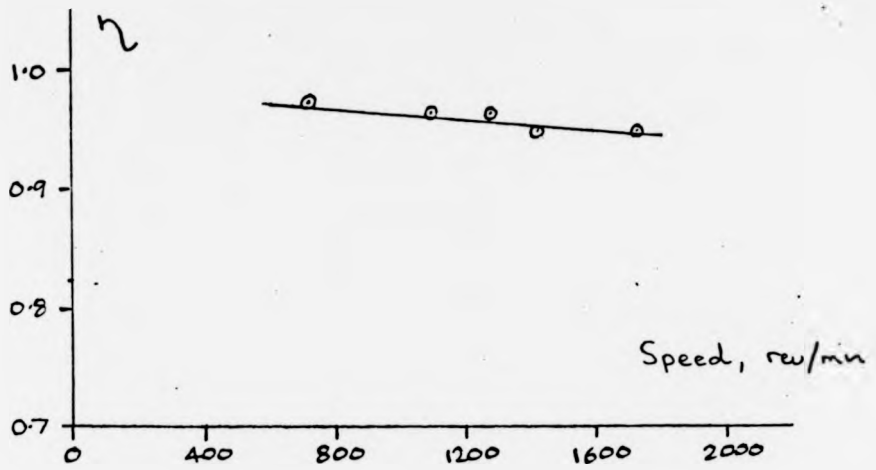

Fig. 6.5(a) : Efficiency versus output speed, 3rd gear

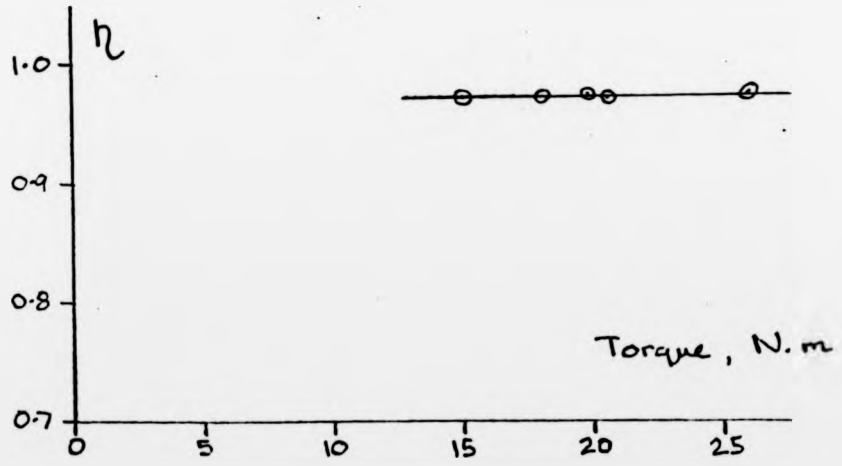

Fig. 6.5(b) : Efficiency versus output torque, 3rd gear

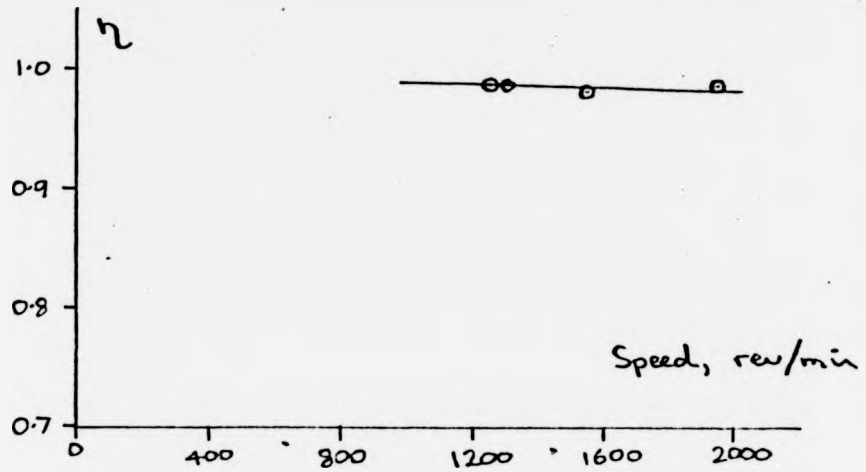

Fig. 6.6 : Efficiency versus output speed, top gear

Neglegible variation with output torque

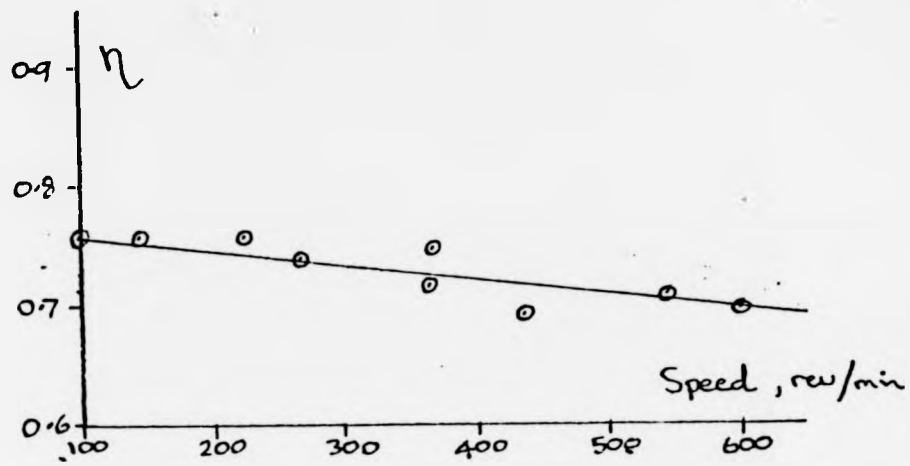

Fig. 6.7(a) : Efficiency versus output speed, differential

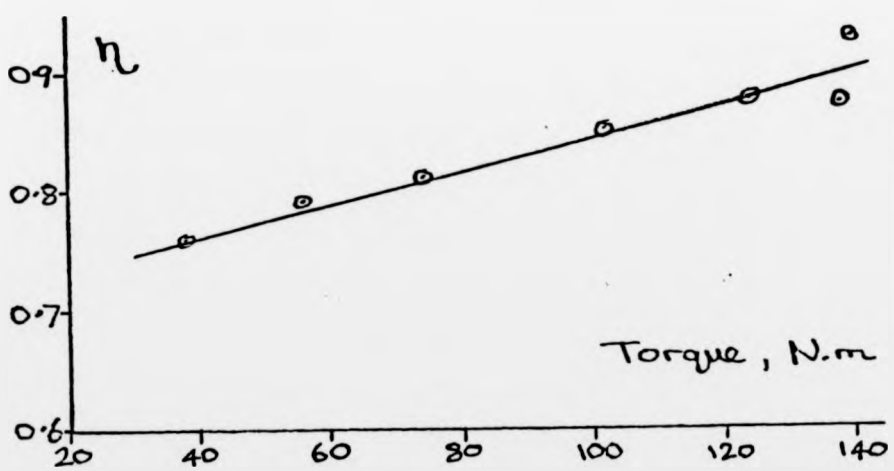

Fig. 6.7(b) : Efficiency versus output torque, differential

For top gear:-

$$\eta = 0.9877 - \frac{0.0088(n-1250)}{1250} \qquad (6.7)$$

For the differential:-

$$\eta = 0.76 - \frac{0.06(n-100)}{500} + \frac{0.1(T-38.75)}{72.15} \qquad (6.8)$$

where η is the efficiency of the unit, n the output speed in rev/min and T the output torque in Nm. Equations (6.4) to (6.8) are thus sufficient to model the transmission for this simulation study. The input speed may be found by multiplying the output speed by the gear ratio; the input torque may be found by dividing the output torque by the gear ratio and the efficiency.

6.1.3 Consideration of the electric traction motor

The model of the traction motor is more complex than any other component as it involves not only the transmission of power but the conversion of electrical power to mechanical. However the same approach is adopted in that the input power necessary for a given output power is determined, or more specifically the voltage and current necessary to sustain a given torque and speed. These relationships are found for both the series motor and the disc armature motor so it is only necessary to specify torque, speed and the motor being considered for the simulation model to provide the values of voltage and current that will be required. All motor losses are taken into account and as before a value of motor efficiency is available although not actually used itself.

6.1.3.1 Series wound motor

This motor is supplied by the Electro Dynamic Construction Company Ltd. (EDC) and develops 7.5 kW (10 h.p.) at 3400 rev/min. As it is a series wound machine, the working flux will be approximately proportional to armature current until saturation occurs, and constant thereafter. This accounts for the non-linear speed and torque characteristics shown in the performance curves (Fig. 6.8). Although an idealised linear flux/current relationship (Fig. 6.9) is often used to describe the performance of a series wound d.c. motor, in the model developed here an accurate assessment of flux variation is required. To this end, the performance curves in Fig. 6.8 are used in the evaluation of an 'effective working flux', ϕ_{eff} which is defined as:-

$$\phi_{eff} = \frac{60E.a}{n.z.p.} \qquad (6.9)$$

with the other symbols remaining as previously defined. If E is expressed in volts and n in rev/min then ϕ_{eff} will be in Webers. Values of a, z and p are known for the motor and E may be determined from the applied voltage, current, armature resistance and brush voltage drop. Thus by use of the speed v. current curve of Fig. 6.8, ϕ_{eff} may be determined for any given value of current. This value for effective working flux is assumed to include all leakage, loss and secondary effects. A graph of ϕ_{eff} against current is given in Fig. 6.10 and shows a saturation value of 7.3×10^{-3} Wb. Although a linearised version of the curve could be made, the availability of powerful curve-fitting techniques using digital computing facilities allows a good fit to be found using a

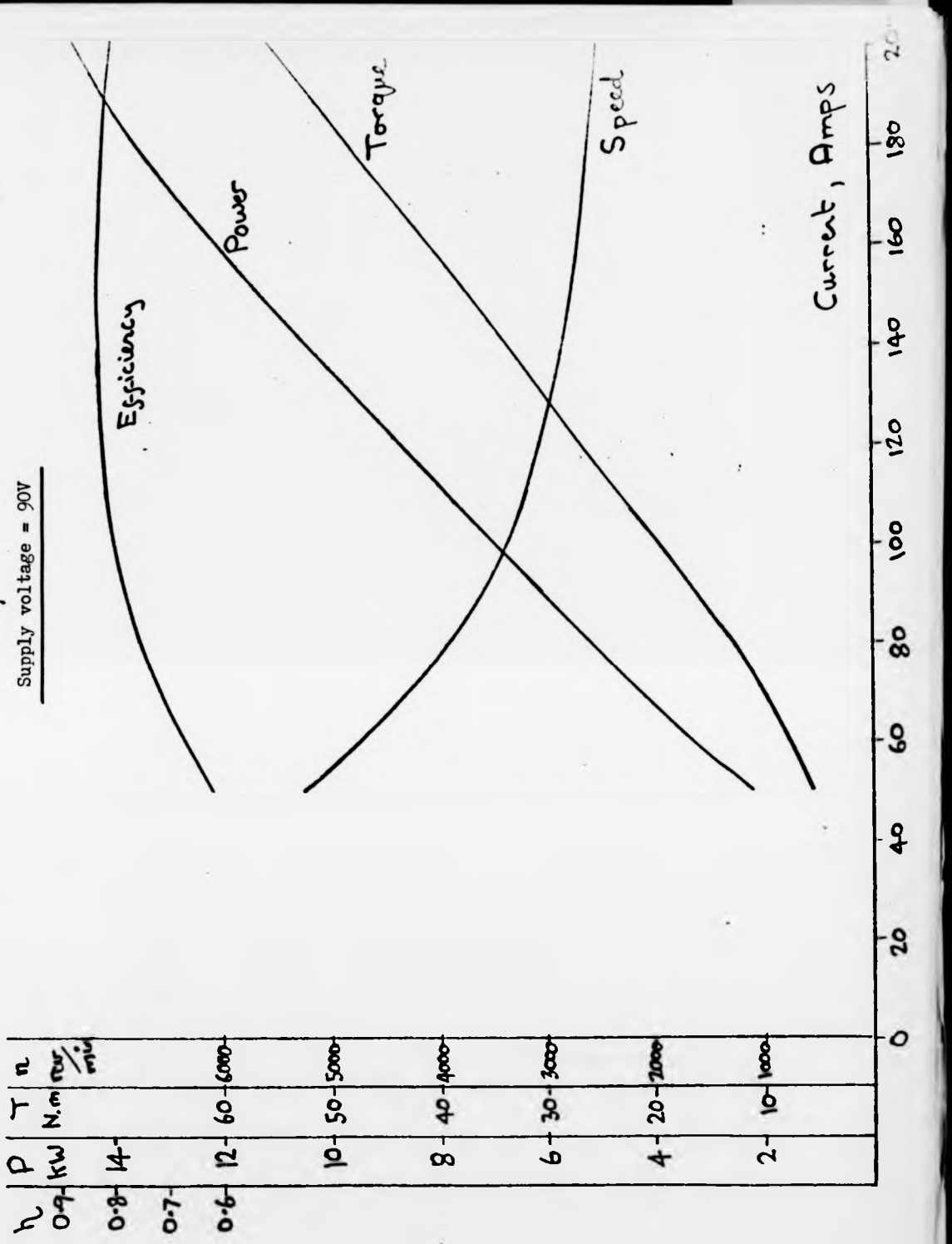

Fig. 6.8 : Performance curves of E.D.C. series wound motor

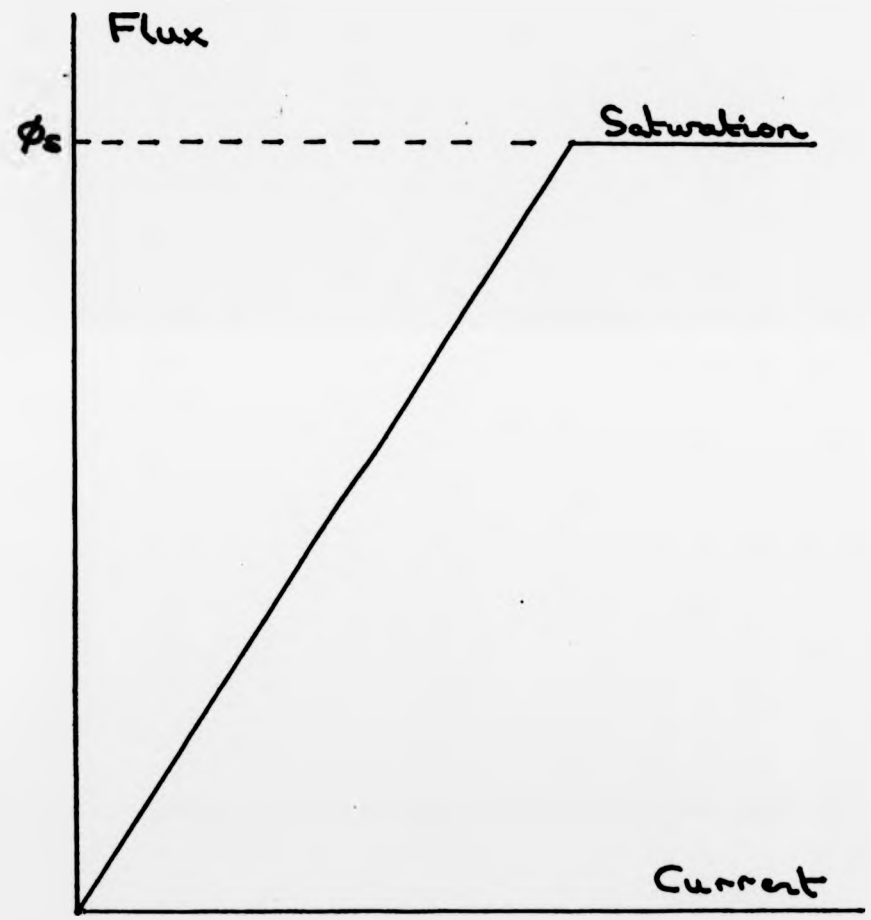

Fig. 6.9 : Idealised linear flux/current relationship

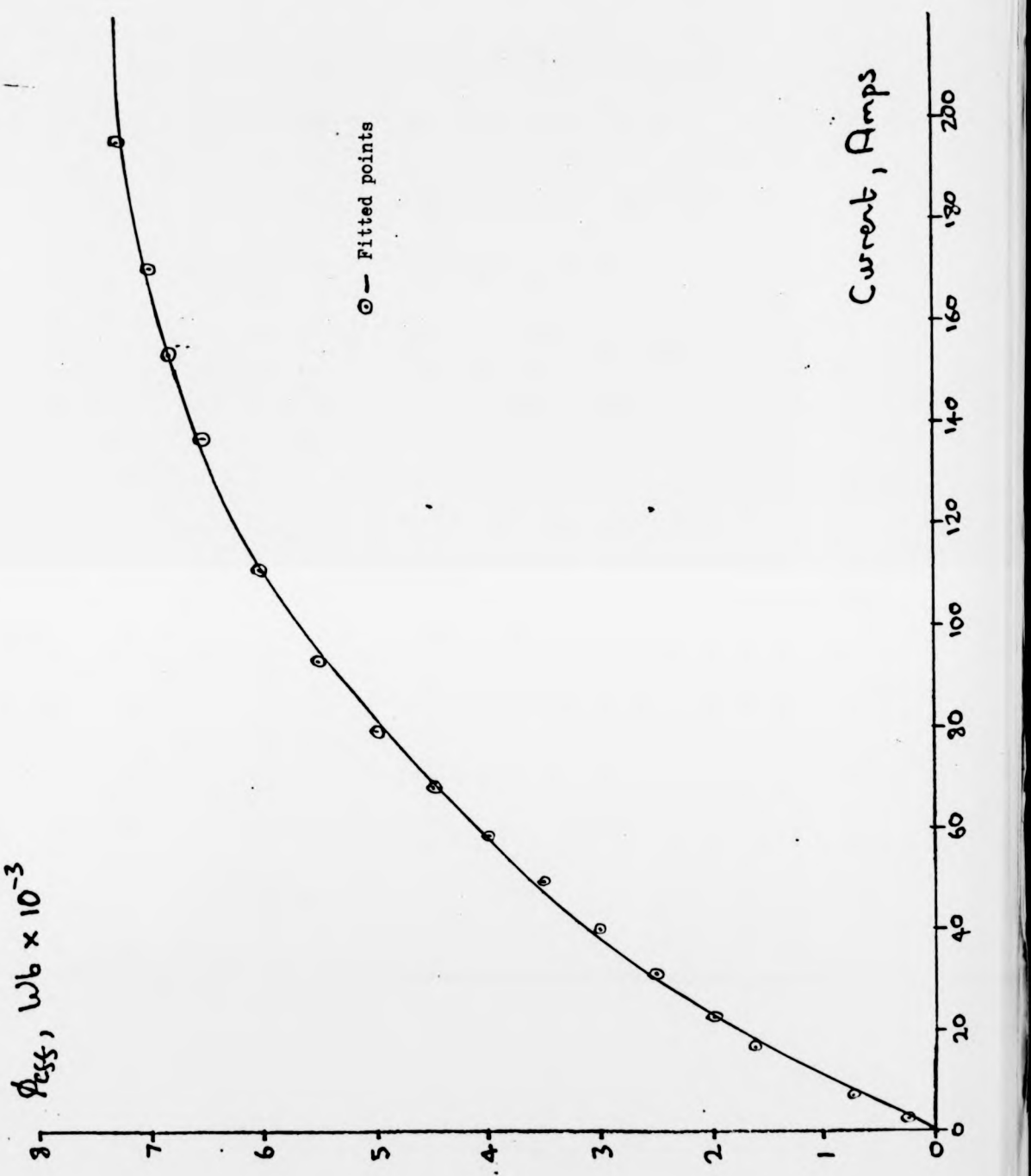

Fig. 6.10 : Effective flux versus current (E.D.C. motor)

polynomial expression. The Time Series Process (TSP) routines available at Warwick are able to perform such curve fitting relatively quickly and easily using a least-squares technique. The majority of the curve in Fig. 6.10 may be expressed as:-

$$I = -2700.19\ \phi_{eff} + 11361900\ \phi_{eff}^{2} - 2676.12 \times 10^{6}\ \phi_{eff}^{3} + 2290 \times 10^{8}\ \phi_{eff}^{4} \qquad (6.10)$$

where I is the current flowing. The equation is valid for values of I between 20A and 200A. Above 200A the flux is assumed constant at 7.3×10^{-3} Wb, and below 20A an alternative equation is used:-

$$I = 4.2658 \times 10^{4}.\phi_{eff}^{1.21} \qquad (6.11)$$

The complete curve fit is shown by discrete points on the curve in Fig. 6.10. Having established the relation between flux and current, it may now be used in the development of a motor model suitable for use in the electric vehicle simulation program. Equation (6.9) may be rearranged into its more usual form:-

$$n = \frac{60E.a}{\phi_{eff}.z.p} \qquad (6.12)$$

with the same notation as before. The power output from the machine may be expressed as:-

$$P_r = E.I - \text{Losses} \qquad (6.13)$$

where P_r is the power output and losses consist of mechanical, iron and brush loss. The mechanical power may also be expressed as:-

$$P_r = \frac{T.n.\pi}{30} \qquad (6.14)$$

where T is in Nm and n in rev/min to yield P_r in watts. Combining equations (6.12) to (6.14) :-

$$\frac{T.n.\pi}{30} = \frac{n.\phi_{eff}.z.p.\ I}{60a} - \text{Losses} \qquad (6.15)$$

$$\text{or} \quad \phi_{eff}.I = \left(\frac{T.n.\pi}{30} + \text{Losses}\right)\left(\frac{60a}{n.z.p}\right) \qquad (6.16)$$

Thus for any value of the output torque and speed, and knowing the losses, the product of the current and flux may be calculated. Combining this with equation (6.10) allows the unique value of each to be found. Equation (6.12) is used to find E and the applied voltage calculated from E, I, the armature resistance and a suitable value for the brush voltage drop. Initial values for the losses are taken from data supplied by the manufacturer although once the speed, voltage and current have been determined, new values may be estimated and substituted in equation (6.16) so that the procedure may be repeated. As the values of the losses are small when compared with the power output of the machine, it has been found that two such repetitions are required to give sufficient accuracy for the simulation. For a given output speed and torque, the required input voltage and current have been determined, and the efficiency may be calculated if required in the usual way.

As a check on the operation of this model, corresponding torque and speed values are taken from the performance curves in Fig. (6.8) and values of V,I and efficiency calculated. These are shown in Fig. (6.11), marked on the original curves, and very close agreement is evident. In all cases, the value of the predicted

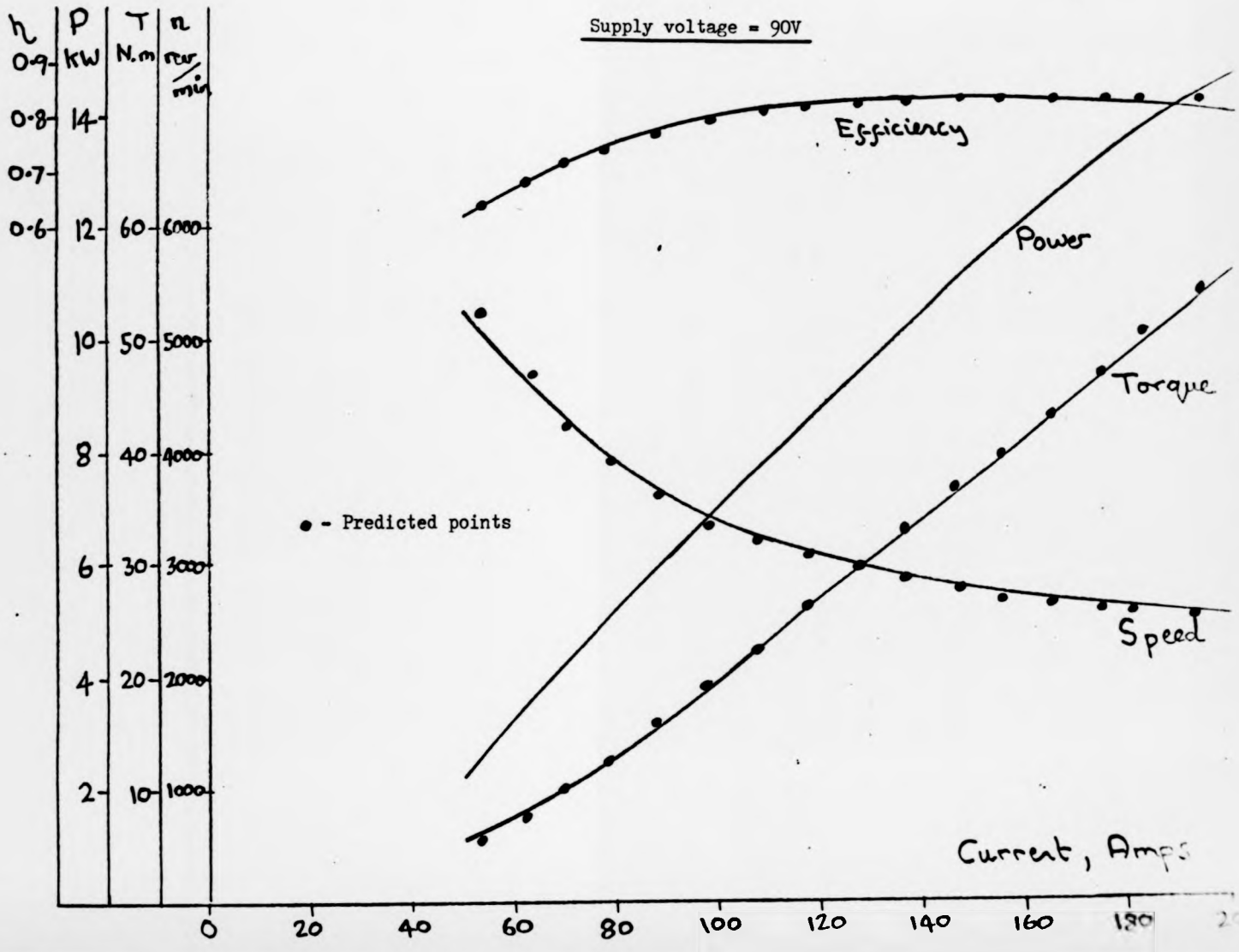

Fig. 6.11 : Performance of E.D.C. motor as predicted by model

required voltage lies within the range 88 to 92 volts.

6.1.3.2 Disc armature motor

Consideration of this machine is considerably easier than the series motor as in this case the flux is constant. The method is derived from that used to predict the performance of disc armature motors which is described in Chapter 4. For a given rotational speed, the generated e.m.f. is found directly from equation (6.12). The mechanical losses are dependent on the speed and machine dimensions are are given by equation (4.14). Having determined these parameters the required armature current is given by:-

$$I = \left(\frac{T.n.\pi}{30} + \text{Losses}\right).\frac{1}{E} \qquad (6.17)$$

where losses include mechanical and brush loss only as there are no iron losses. The applied voltage may be found as before knowing E, I, the armature resistance and a suitable value for the brush voltage drop. Similarly, the motor efficiency at this particular operating point may be calculated.

The methods described above may easily be used to give an 'efficiency map' for each machine. This is a table of efficiency values for given values of torque and speed and such maps are useful in quickly gauging how a motor will be expected to perform under given operating conditions. The efficiency maps for the series machine and the disc armature machine are given in Tables 6.1 and 6.2 respectively, and the superiority of the latter is evident under all operating conditions.

Torque, Nm \ Speed, rev/min	500	1000	1500	2000	2500	3000	3500	4000	4500
5.	0.501	0.628	0.666	0.678	0.678	0.672	0.663	0.652	0.640
10.	0.577	0.701	0.737	0.747	0.747	0.740	0.730	0.718	0.704
15.	0.604	0.729	0.765	0.776	0.775	0.769	0.760	0.749	0.737
20.	0.613	0.741	0.779	0.791	0.792	0.787	0.779	0.769	0.758
25.	0.614	0.746	0.787	0.800	0.803	0.799	0.793	0.784	0.775
30.	0.610	0.747	0.790	0.806	0.810	0.808	0.803	0.795	0.787
35.	0.602	0.746	0.792	0.809	0.815	0.814	0.810	0.804	0.796
40.	0.593	0.742	0.792	0.811	0.818	0.819	0.816	0.811	0.805

Table 6.1 : Efficiency map - E.D.C. series wound motor

Torque, Nm \ Speed, rev/min	500	1000	1500	2000	2500	3000	3500
5.	0.861	0.869	0.864	0.858	0.852	0.846	0.847
10.	0.855	0.892	0.902	0.905	0.906	0.906	0.904
15.	0.825	0.885	0.904	0.913	0.918	0.921	0.922
20.	0.793	0.871	0.898	0.912	0.920	0.925	0.928
25.	0.761	0.854	0.888	0.906	0.917	0.923	0.928
30.	0.732	0.836	0.877	0.898	0.911	0.920	0.926
35.	0.704	0.818	0.865	0.890	0.905	0.915	0.922
40.	0.677	0.801	0.852	0.880	0.898	0.910	0.918

Table 6.2 : Efficiency map - disc armature motor

6.1.4 Consideration of the controller

Controlling the speed of a d.c. motor for battery electric traction has traditionally been achieved by varying the voltage applied to the motor armature and various methods exist to fulfil this basic requirement[57] (battery switching, series resistance, etc.) More recently electronic switching controllers have been specified and developments from these have led to complex microprocessor-based controllers which utilise both armature control and control of a separately excited field[58]. The controller selected for the Reliant Robin project is a modern electronic chopper-type controller intended for use with the disc-armature motor. The chopper controller operates by switching the supply voltage across the motor at frequencies between 600 Hz and 1 KHz. The average voltage seen by the motor depends on the ratio of on-time to off-time which is known as the mark-space ratio. Fig. 6.12 shows how low and high average voltages are achieved. The switching element is usually a thyristor, although recent developments in switching transistor technology have allowed these devices to be used in some chopper circuits. The thyristor has the advantage of being able to handle relatively large currents although it requires additional electronic components to turn it off. The transistor may be turned on and off relatively easily, may operate at higher frequencies but cannot stand such high peak currents.

The main elements of a typical thyristor chopper circuit are shown in Fig. 6.13 and includes the commutating thyristor, T_2, necessary to turn off the main thyristor, T_1. Initially, T_2 is

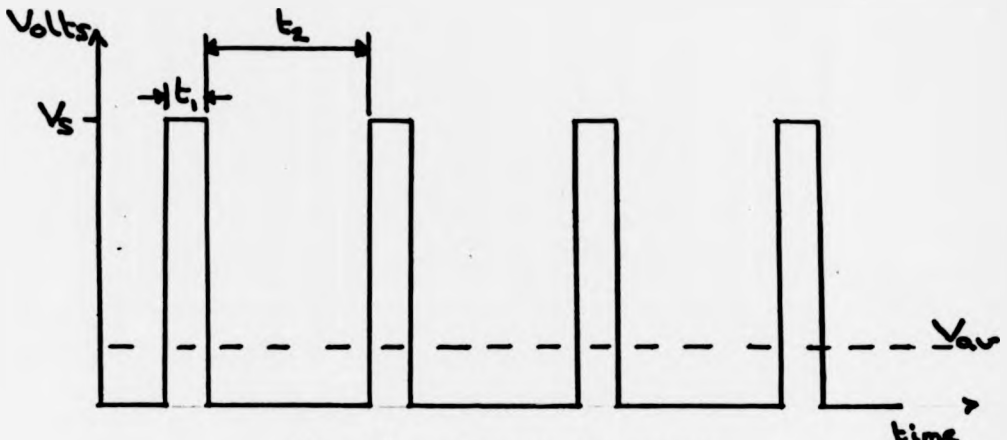

$t_1 < t_2$ - Low average voltage

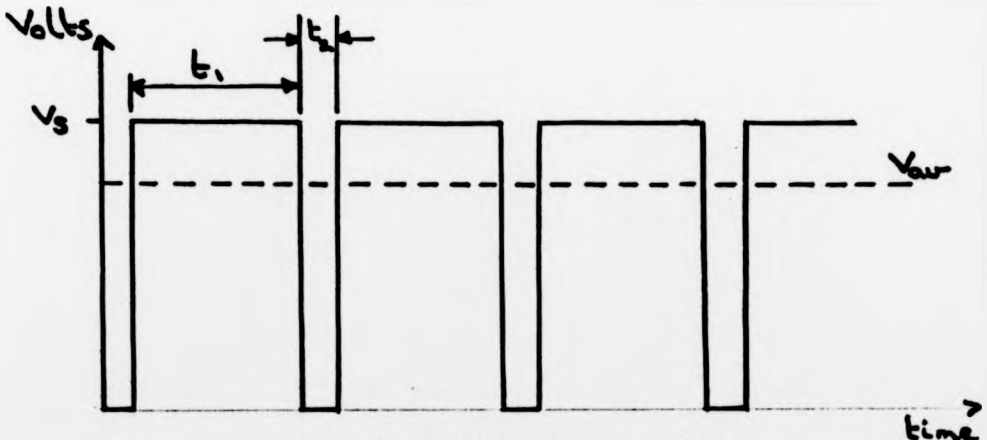

$t_1 > t_2$ - High average voltage

Fig. 6.12 : Operation of chopper controller

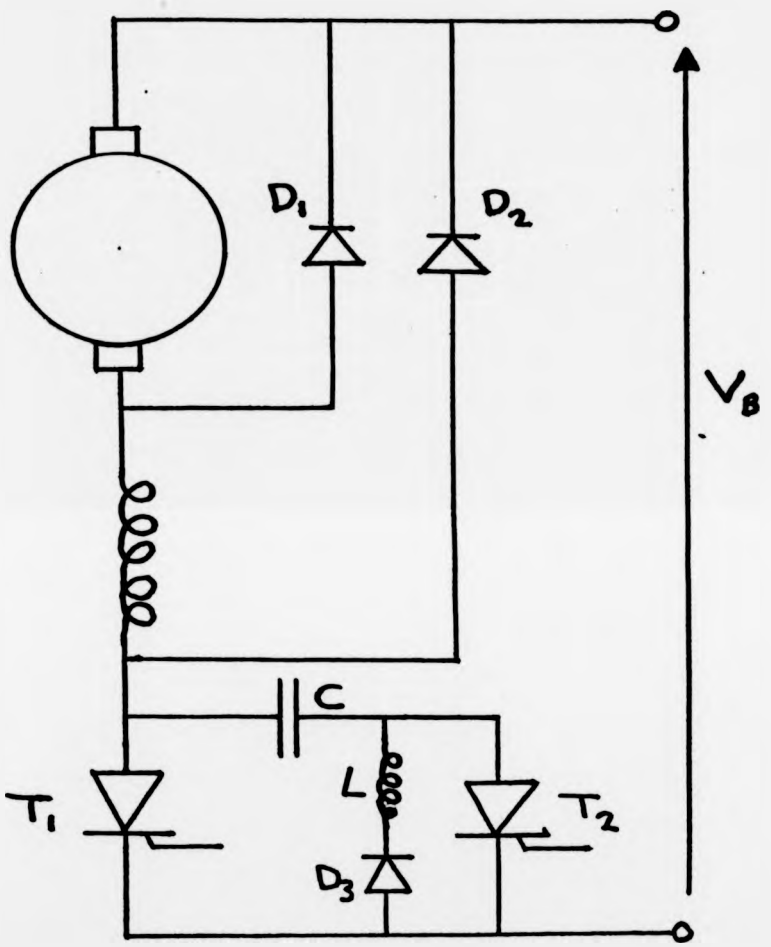

Fig. 6.13 : Typical chopper circuit

switched on and the left hand side of C is charged to the supply voltage through the motor. T_2 turns off naturally when current ceases to flow through it. T_1 is then turned on allowing the full voltage to be applied across the motor, drawing sufficient current to supply the load. In addition, due to LC action, the right hand side of C is now charged to a voltage approaching twice the supply voltage. This is maintained as D_3 is reversed-biased and T_2 is turned off. At the end of the drive pulse it is required to turn off T_1 and this is done by switching on T_2 and applying the voltage on the right hand side of C to T_1 causing it to become reversed biased which turns it off. At the same time, the left hand side of C is charged to the supply voltage ready for the cycle to be repeated.

Diodes are provided across the armature and field windings to permit the continued flow of motor current when the main thyristor is switched off. The inductance of the motor windings helps to sustain a relatively constant current flow through the mtoor. By contrast, the disc armature motor has an extremely low inductance which dictates the use of a much higher switching frequency for the same degree of 'current ripple'. Unfortunately, there are limits to the upper switching frequency of both thyristors and transistors, although no appreciable differences in performance have been noticed in motors tested with transistor chopper controllers (see appendix II).

Very little power is dissipated in such a controller as when the thyristor is on and passing current the voltage across it is small; when it is off, no current is flowing although there is a

large voltage across it. A suitable model of a thyristor chopper controller has been developed by Hind[52] and this will be incorporated into the system model. It is based on a simplified version of Fig. 6.13 and is illustrated in Fig. 6.14. Two conditions are considered, namely when the thyristor is conducting and when it is switched off - periods t_1 and t_2 respectively in Fig. 6.12.

Over the period t_1 when the thyristor is switched on

$$V_B = V_M + V_T \tag{6.18}$$

$$I_B = I_M \tag{6.19}$$

where V_B, V_M and V_T are battery, motor and thyristor voltages respectively while I_B and I_M are the associated battery and motor currents. Over the period t_2:-

$$V_M = -V_{D1} \tag{6.20}$$

$$I_B = 0 \tag{6.21}$$

where V_{D1} is the voltage across the diode. Also, by definition:-

$$D = \frac{t_1}{t_1+t_2} \tag{6.22}$$

where D is known as the duty cycle. Thus taking averages over a complete cycle:-

$$V_{MA} = \frac{(V_B-V_T).t_1}{t_1+t_2} - \frac{V_{D1}.t_2}{t_1+t_2} \tag{6.23}$$

$$= D(V_B - V_T + V_{D1}) - V_{D1} \tag{6.24}$$

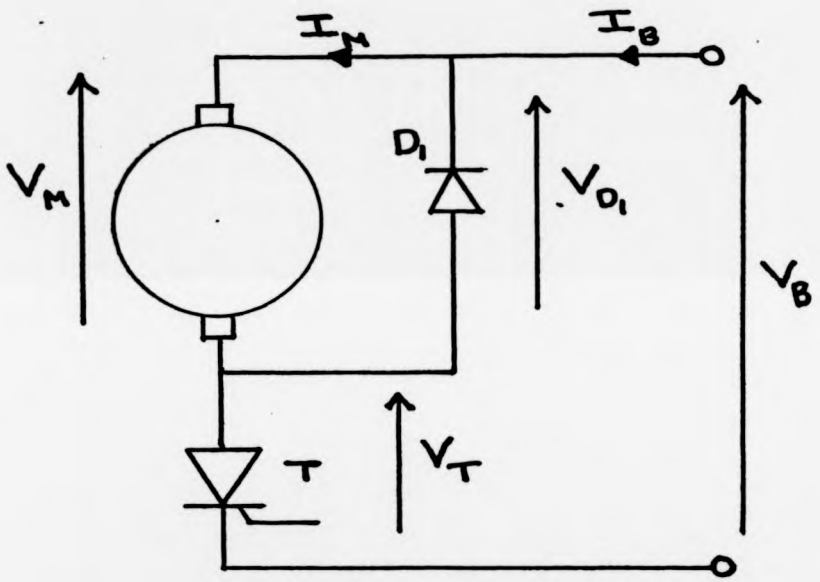

Fig. 6.14 : Model of chopper controller

and thus $$D = \frac{V_{MA} + V_{D1}}{V_B - V_T + V_{D1}} \quad (6.25)$$

Also $$I_{BA} = I_M . D \quad (6.26)$$

where V_{MA} is the average motor voltage and I_{BA} the average battery current. Thus, knowing V_{MA}, V_{D1}, V_B and V_T the value of D may be calculated which in turn is used to find I_{BA}. V_{MA} and I_M are taken from the electric motor model, V_T and V_{D1} may be given suitable values from manufacturers data and V_B is initially taken as the nominal battery voltage. In practice, V_B will depend on I_{BA}, as will be discussed in the next section and this dependence is allowed for by determining a modified value for V_B when the initial value of I_{BA} has been calculated. The modified value of V_B is then used in equation (6.25) to allow a corrected value for I_{BA} to be found, and this is sufficiently accurate for the simulation.

It is assumed in this analysis that average values of voltage and current are sufficient to describe motor and controller behaviour - i.e. a unity form factor is achieved. Further, the assumption is made that the losses associated with the auxiliary components not shown in Fig. 6.14 are negligible by comparison with the components that are considered.

6.1.5 Consideration of the traction battery

In recent years, several alternative storage batteries have been proposed and developed including the high-temperature sodium-sulphur battery and the zinc-chloride battery where superior energy

densities and cycle life over the traditional lead/acid battery have been reported. However, it is widely considered that the lead/acid battery, possibly in an improved form, will be the only realistic choice for battery electric traction for some time to come. Much effort has been expended in studying the performance and behaviour of the lead/acid battery under conditions imposed by electric traction. Although this has resulted in many simulation models of varying complexity, the mathematical modelling of such a battery is not a straightforward process and no universally satisfactory model has yet been found which can cope with the random and irregular demands often made of the battery. It has been widely debated whether electronic chopper controllers have a significant effect on battery performance although a recent study[59] has compared steady discharge with a similar, but chopper driven load, and found no noticeable difference in battery capacity.

In addition to the nominal terminal voltage, the lead acid battery is characterised by the ampere hour capacity at a given discharge rate. For example, a battery with specified capacity 60 Ah at the 20 hour rate will supply 3A for 20 hours before discharge. Because of the high currents involved in traction applications, 5 hour and 2 hour discharge rates are often quoted. It is well-known that the ampere-hour capacity of a battery decreases with increasing discharge current. A simple empirical formula[60] describing the relationship is:-

$$T_m = \frac{C_B}{I_B^N} \qquad (6.27)$$

where T_m is the discharge time, C_B the battery capacity, I_B the discharge current and N a constant.

As well as the relation between battery capacity and output current, there are two further important areas of investigation. These are the variation of terminal voltage with discharge current and remaining capacity. Although it is known that the voltage falls with increasing current and depth of discharge, numerous studies have been made to accurately assess this dependence. A recent study[37] has involved investigating the behaviour of a lead/acid cell when performing a series of charge/discharge cycles as might be encountered in a typical hybrid/electric vehicle application. A bank of batteries is subjected to random current flow in both directions characterised by a different fundamental frequency. A diffusion model is proposed to predict the battery voltage and though agreement between the predicted and actual voltages is excellent, different model coefficients need to be used for each frequency.

For the purposes of the EV simulation model developed here, a simplified battery model is sufficient and this is based on variation of capacity with discharge current, of voltage with discharge current and of voltage with discharge. The variation of capacity with discharge current is relatively straightforward to deal with as this has been the area of much specific investigation and the results of extensive tests are available in textbooks[61] or from manufacturers. For ease of analysis, two parameters are defined - the rated and normalised discharge current:-

$$I_R = \frac{\text{Capacity}}{\text{Specified discharge time}}$$

and $I_N = \frac{I_B}{I_R}$

where I_B is any given discharge current. For example, the rated discharge current of a 60Ah battery specified at the 20 hour rate is 3A, and when discharging at 12 A, $I_N = 4$. The battery capacity is also normalised so that at rated discharge, it is equal to 1. Battery discharge data is collated and a curve produced of normalised capacity against normalised discharge current. (Fig. 6.15). Using curve fitting techniques, a polynomial may be used to express the relationship although this is quite complex and only valid for a range of values of I_N. The prediction of cell terminal voltage with discharge current is dealt with in a similar way except that the discharge current is normalised to the 5 hour discharge rate as most data is presented in this way. The resulting curve and polynomial fit is shown in Fig. 6.16 although this is only true for a fully charged battery. The variation of cell voltage with depth of discharge is shown in Fig. 6.17 and this is true for the specified rated discharge current. Although it is possible to combine the results from Figs. 6.16 and 6.17 to give total voltage dependence, the validation by test of such a relationship is beyond the scope of this work. It will thus be assumed that in all subsequent simulation studies and practical testing that the battery is fully charged, or as near fully charged as to make the difference in voltage negligible. It will be observed from Fig. 6.17 that discharge to 78% of the original capacity is necessary to cause just a 1% change in cell terminal voltage.

Fig. 6.15 : Normalised battery capacity versus normalised discharge current

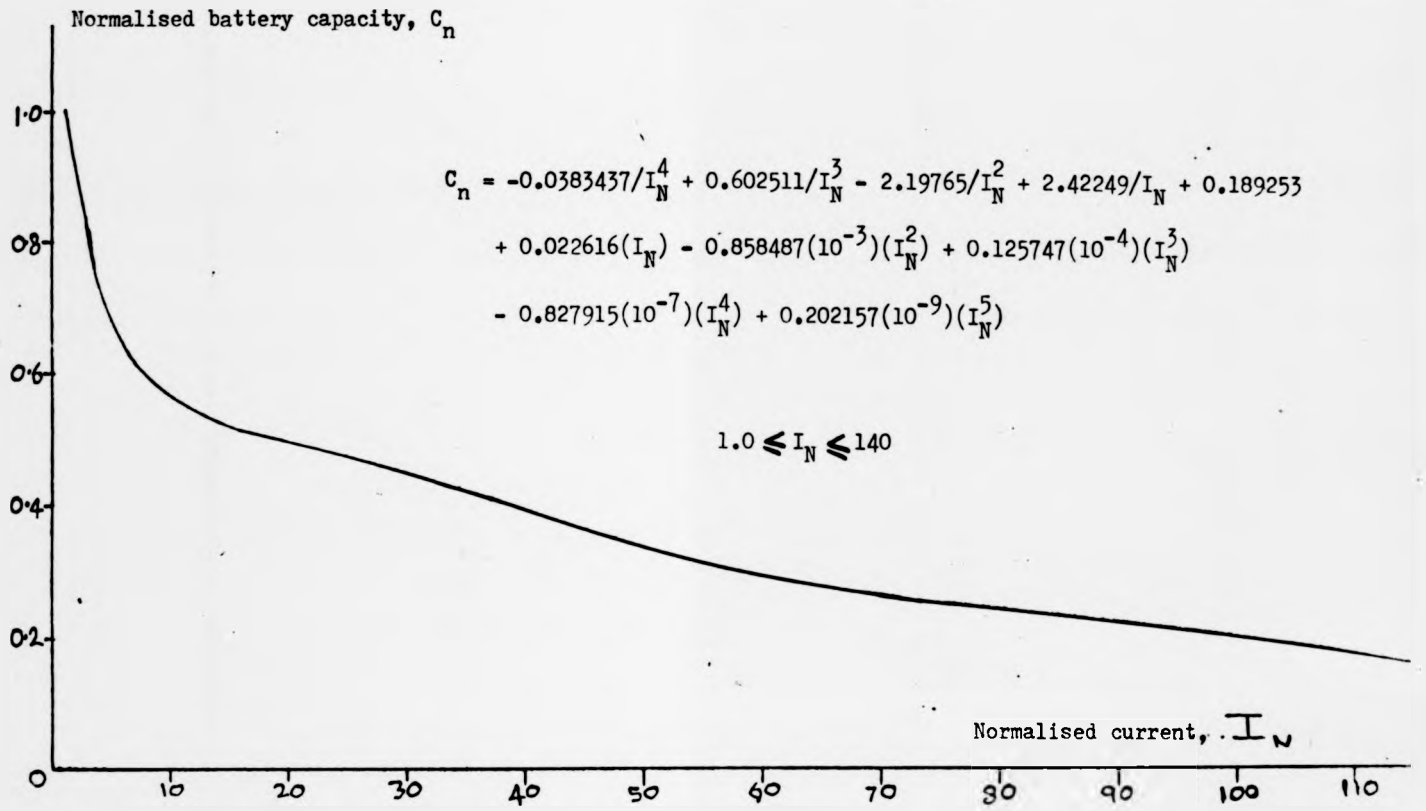

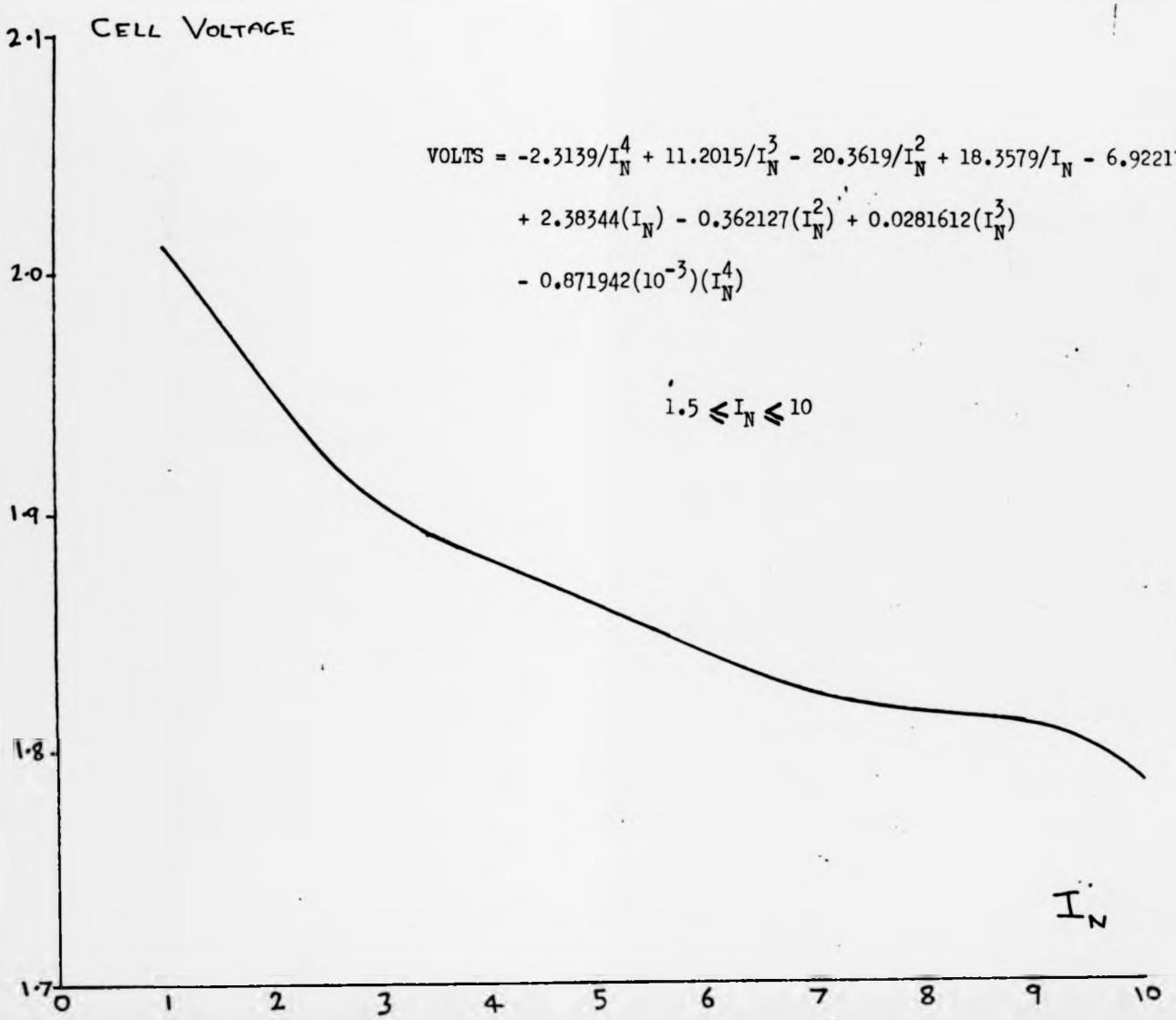

$$\text{VOLTS} = -2.3139/I_N^4 + 11.2015/I_N^3 - 20.3619/I_N^2 + 18.3579/I_N - 6.92217 + 2.38344(I_N) - 0.362127(I_N^2) + 0.0281612(I_N^3) - 0.871942(10^{-3})(I_N^4)$$

$$1.5 \leqslant I_N \leqslant 10$$

Fig. 6.16 : Cell voltage versus normalised discharge current

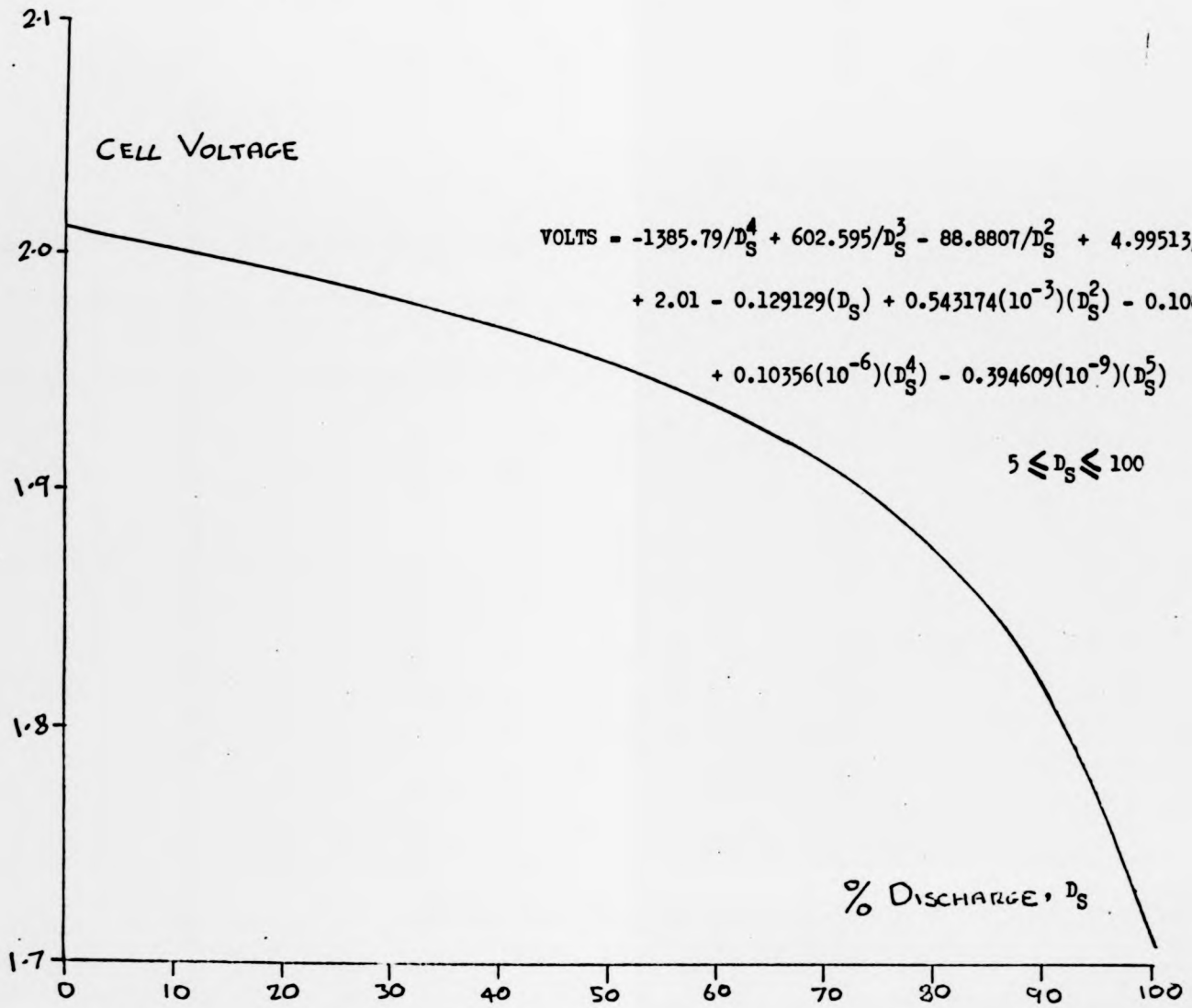

Fig. 6.17 : Cell voltage versus depth of discharge

Fig. 6.15 and 6.16 enable the battery capacity and terminal voltage to be determined for any value of discharge current (within the considered range). The latter is necessary for use in equation (6.25) for the controller model while the former allows an assessment of the expected vehicle range to be made. As the equations are based on steady state discharge characteristics, they are obviously most closely related to the use of the electric vehicle at a constant speed. Although the model does not take account of aging or temperature change, considerable variation can occur in supposedly identical batteries and the generation of a more sophisticated model is outside the scope of this work. However, it will be seen later that the model presented above is sufficient for the analysis of vehicle performance undertaken here.

6.2 Application of the vehicle model

There have been proposed several methods of assessing and comparing the performance of electric vehicles under various operating conditions. They range from determining the vehicle range under steady speed operation to the complex duty cycles that may be encountered in typical urban or city driving. Several such driving cycles are available, some of which have formed the basis for official standards. Probably the most authoritative of these are those incorporated in the SAE/J227 electric vehicle test specification[62]. This standard is intended for use in comparing different vehicles under similar operating conditions and the tests include range (steady speed and repeated cycle), acceleration and

gradeability. As the J227 standard has been widely adopted, it is considered most suitable for application to the electric vehicle model, particularly as two motors are being compared. However, precisely repeatable operating conditions are unlikely to be achieved in practice and thus the most accurate means of comparing vehicle performance without the availability of extensive test apparatus is to use results from constant speed tests.

Having characterised the vehicle components, the complete system model is constructed in the form of a Fortran computer program incorporating the equations and iterations developed in the preceding sections. Input to the program consists of such parameters as vehicle weight, motor weight, battery weight and capacity, etc. Much of the vehicle data is written into the program but there is no reason this could not be changed if necessary. The program will then take each forward gear in turn and for increasing speeds work through the system model calculating the torque, speed, current or voltage associated with each component - in this way the full interdependence of components on one another is taken into account. The required speed is increased until the voltage demanded at the motor is greater than the battery voltage. The vehicle range at a given speed and in a particular gear may be determined, on an energy basis, from the discharge current, effective capacity and speed. An analysis of power flow and dissipation within the vehicle is possible and this can be of great assistance in determining the effect of a change in component or attempting to optimise the vehicle system as a whole[54]. A flowchart of the simulation program is shown in Fig. 6.18

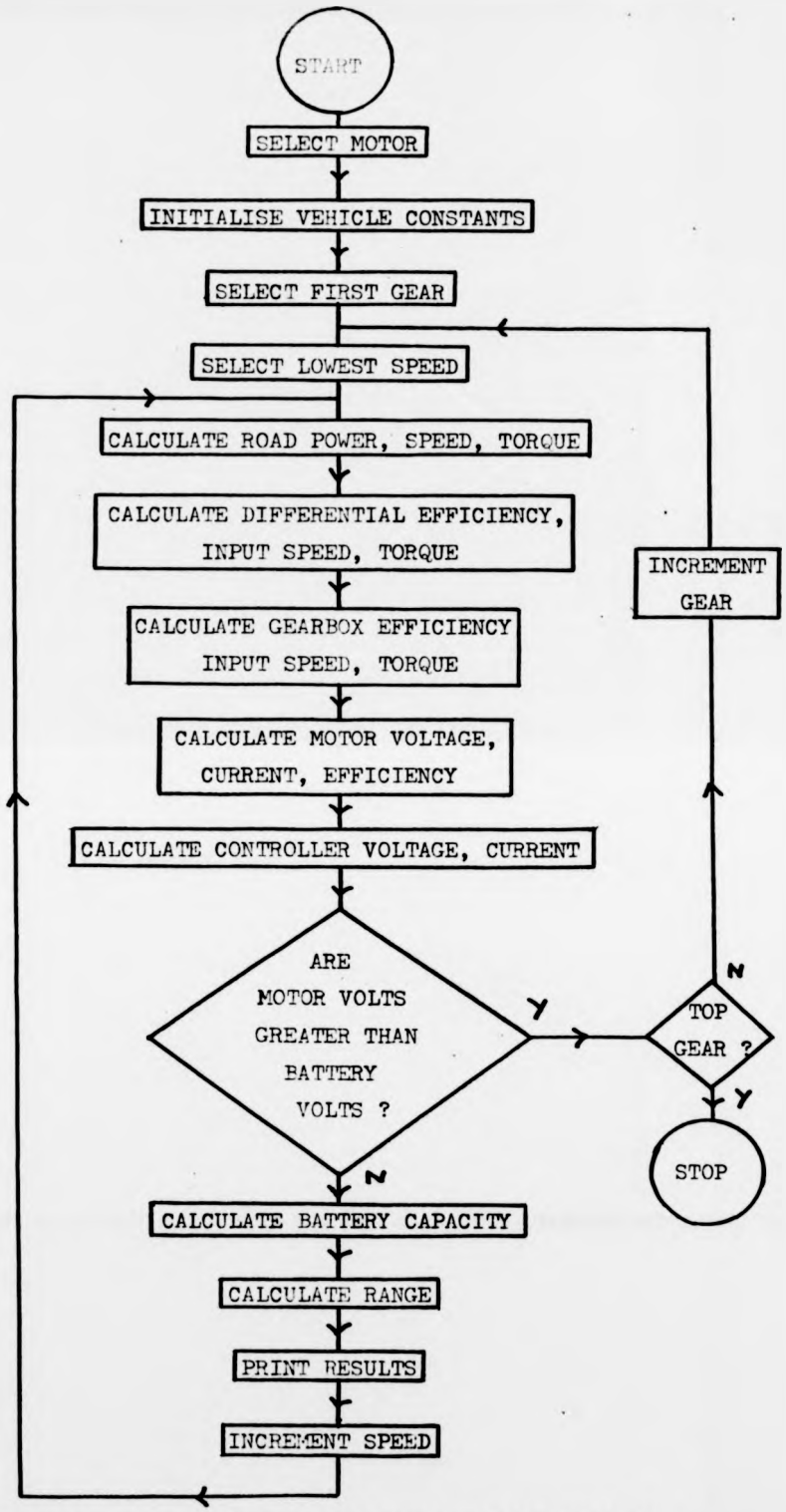

Fig. 6.18 : Flowchart of vehicle simulation program

and the only decision to be made at run time is the selection of the motor to be considered - series wound or disc armature.

Results from the simulation study are presented in Tables 6.3 and 6.4 for the series motor and 6.5 and 6.6 for the disc armature motor. Each gear is used and road speeds from 10 to 30 m.p.h. are used where appropriate. The advantages of the disc armature motor are immediately apparent and the results shown here are particularly valuable for comparison with actual road-test results covered in the next chapter. Although constant speed testing is often considered impractical and unrealistic, it does remain one of the best ways of comparing the performances of a vehicle which uses different drive components.

Gear	1	2	2	2	2	2	3	3
Road Speed, m.p.h.	10	10	15	20	25	30	10	15
Propshaft torque, N.m	9.08	9.08	10.29	11.95	14.09	16.68	9.08	10.29
Propshaft speed, rev/min	608	608	912	1216	1520	1824	608	912
Differential efficiency	0.73	0.73	0.73	0.72	0.72	0.72	0.73	0.73
Gearbox efficiency	0.89	0.90	0.85	0.81	0.77	0.73	0.97	0.97
Motor torque, N.m	2.63	4.93	5.88	7.19	8.94	11.18	7.06	8.07
Motor speed, rev/min	2358	1246	1869	2492	3115	3738	802	1204
Motor voltage, V	30.9	20.9	32.5	46.5	63.2	82.8	16.4	24.4
Motor current, A	36.0	47.6	51.1	56.6	63.5	71.9	57.6	59.9
Motor efficiency	0.59	0.65	0.69	0.72	0.73	0.73	0.64	0.70
Battery voltage, V	96.1	96.3	94.5	91.6	89.9	87.8	96.5	94.9
Battery current, A	12.2	11.1	18.5	29.7	45.9	69.0	10.7	16.4
Predicted range, miles	41.5	47.2	35.2	25.5	19.1	14.3	49.7	41.3

Table 6.3 : Results of computer simulation - E.D.C. motor

Gear	3	3	3	4	4	4	4	4
Road Speed, m.p.h.	20	25	30	10	15	20	25	30
Propshaft torque, N.m	11.95	14.09	16.68	9.08	10.29	11.95	14.09	16.68
Propshaft speed, rev/min	1216	1520	1824	608	912	1216	1520	1824
Differential efficiency	0.72	0.72	0.72	0.73	0.73	0.72	0.72	0.72
Gearbox efficiency	0.96	0.95	0.94	0.99	0.99	0.99	0.99	0.98
Motor torque, N.m	9.5	11.2	13.4	9.1	10.39	12.1	14.3	17.0
Motor speed, rev/min	1605	2006	2407	608	912	1216	1520	1824
Motor voltage, V	33.8	44.6	57.0	14.4	21.1	28.8	37.6	47.5
Motor current, A	64.3	70.1	77.4	66.7	68.4	73.2	79.7	88.0
Motor efficiency	0.74	0.76	0.77	0.61	0.69	0.74	0.76	0.78
Battery voltage, V	92.8	90.8	89.5	96.4	95.0	92.9	91.0	89.8
Battery current, A	24.5	35.7	50.6	11.1	16.3	23.9	34.4	48.1
Predicted range, miles	32.4	25.6	20.5	47.5	41.6	33.5	26.8	21.7

Table 6.4 : Results of computer simulation - E.D.C. motor

Gear	1	2	2	2	2	2	3	3
Road Speed, m.p.h.	10	10	15	20	25	30	10	15
Propshaft torque, N.m	8.80	8.80	9.99	11.65	13.80	*	8.80	9.99
Propshaft speed, rev/min	608	608	912	1216	1520	*	608	912
Differential efficiency	0.73	0.73	0.72	0.72	0.72	*	0.73	0.72
Gearbox efficiency	0.89	0.90	0.85	0.81	0.77	*	0.97	0.97
Motor torque, N.m	2.55	4.77	5.71	7.01	8.75	*	6.83	7.83
Motor speed, rev/min	2358	1246	1869	2492	3115	*	802	1204
Motor voltage, V	66.0	35.5	52.9	70.4	88.0	*	23.5	34.6
Motor current, A	12.5	20.4	24.2	29.3	36.1	*	27.8	31.9
Motor efficiency	0.77	0.86	0.87	0.89	0.90	*	0.88	0.89
Battery voltage, V	97.0	97.3	95.6	93.3	90.8	*	97.4	96.1
Battery current, A	8.7	7.8	13.8	22.7	35.7	*	7.2	12.1
Predicted range, miles	66.5	77.7	52.3	35.8	25.6	*	86.8	63.2

* 30 m.p.h. not available in 2nd gear

Table 6.5 : Results of computer simulation - disc armature motor

Gear	3	3	3	4	4	4	4	4
Road Speed, m.p.h.	20	25	30	10	15	20	25	30
Propshaft torque, N.m	11.65	13.80	16.37	8.80	9.99	11.65	13.80	16.37
Propshaft speed, rev/min	1216	1520	1824	608	912	1216	1520	1824
Differential efficiency	0.72	0.72	0.72	0.73	0.72	0.72	0.72	0.72
Gearbox efficiency	0.96	0.95	0.94	0.99	0.99	0.99	0.99	0.98
Motor torque, N.m	9.21	11.0	13.2	8.9	10.1	11.8	14.0	16.6
Motor speed, rev/min	1605	2006	2407	608	912	1216	1520	1824
Motor voltage, V	46.1	57.6	69.0	18.4	27.0	35.7	44.5	53.4
Motor current, A	37.3	44.1	52.5	35.3	40.2	46.8	55.2	65.4
Motor efficiency	0.90	0.91	0.92	0.87	0.89	0.90	0.91	0.91
Battery voltage, V	94.4	91.9	90.3	97.4	96.1	94.5	92.0	90.4
Battery current, A	18.9	28.5	41.1	7.2	12.0	18.5	27.7	39.8
Predicted range, miles	45.6	33.7	26.0	85.7	64.0	46.8	34.8	27.0

Table 6.6 : Results of computer simulation - disc armature motor

7: PREPARATION AND TESTING OF ROAD VEHICLE

As discussed earlier it is intended to convert a Reliant Robin car to electric drive and then compare the performance of a conventional series wound motor with that of a disc armature motor. The availability of the EDC motor (Fig. 7.1) allowed the first stage of the work, involving preparation of the vehicle and initial testing using the series motor, to be carried out in parallel with the development of the disc armature motor. Owing to difficulties encountered with the disc motor on bench testing a suitable machine has not yet been available for use in the vehicle, although limited performance testing that has been carried out (Chapter 5) has indicated that with the correct armature winding, the specified high performance will be obtained. However, it remains to prove the electric vehicle system model so that a realistic assessment can be made of the improvements to vehicle performance when a disc armature motor is specified. The following sections detail this work and results are presented for the constant speed testing that is more appropriate to the present investigation.

7.1 Vehicle conversion and instrumentation

The Reliant Robin is supplied directly from the manufacturers without the i.c. engine and relevant ancilliary components (fuel system, cooling system, high voltage electrical system, etc.). The gearbox, propellor shaft and rear axle are as fitted to the standard vehicle although as the gearbox is no longer connected to

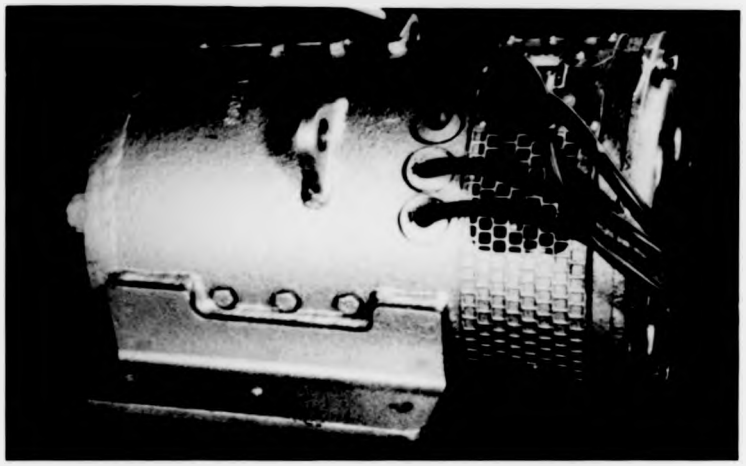

Fig. 7.1 : E.D.C. series wound traction motor

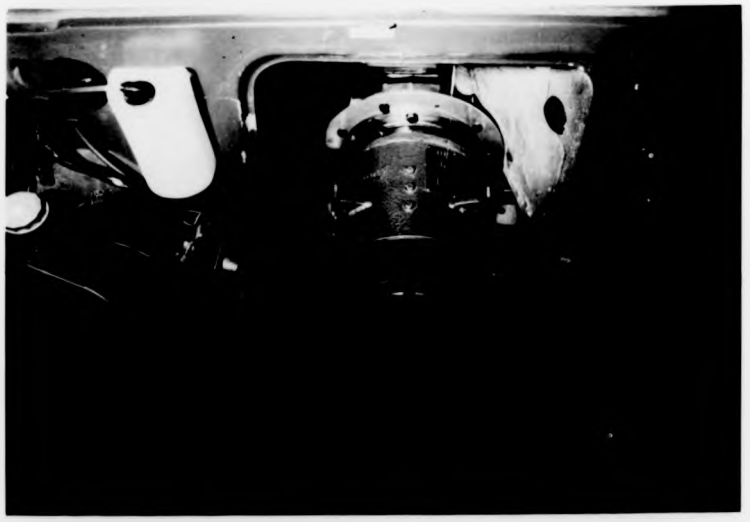

Fig. 7.2 : E.D.C. motor in Reliant vehicle

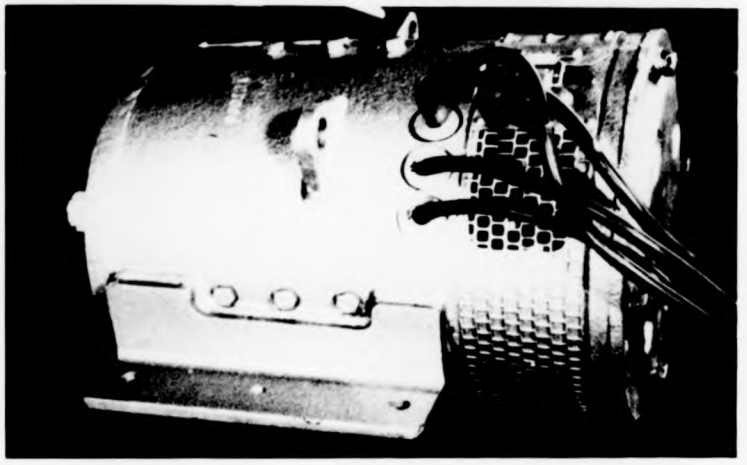

Fig. 7.1 : E.D.C. series wound traction motor

Fig. 7.2 : E.D.C. motor in Reliant vehicle

the engine a suitable supporting bracket is made and welded to the vehicle chassis. The space in front of the gearbox is available for the electric motor and/or other components and the maximum motor diameter is determined to assist in the specification of the disc armature motor (section 3.5.2). The 7.5 kW series motor fits easily into the available space (Fig. 7.2) and is supported at the driving end by the gearbox, and also by brackets welded to the chassis and bolted to each side of the motor. As it is vital to ensure correct alignment between the motor and the clutch/gearbox assembly, a steel mating ring is constructed which is bolted to both motor and gearbox, and is of sufficient length to locate the clutch plates, which are first coupled to the motor shaft, in the correct position on the gearbox splined input shaft. Owing to the intricate nature of this operation, requiring precise measurement and adjustment, it is found most convenient to work on the motor and gearbox external to the vehicle and fix the complete assembly into the vehicle at a later stage (Fig. 7.3). Mechanical alignment and location of the proposed disc armature motor would not be as complex as the shaft length and mounting fixtures are intended for direct location onto the gearbox bell-housing.

Siting of the batteries is the next major task to be undertaken. It was originally intended to retain the vehicle's functional capability as far as possible and thus locate the batteries in the space originally occupied by the fuel tank, with additional space used under the bonnet as necessary. However, it soon became evident that major structural alterations of this nature were beyond the scope of the project and thus the vehicle was reduced to a 2-seater with the space behind the seats to the small

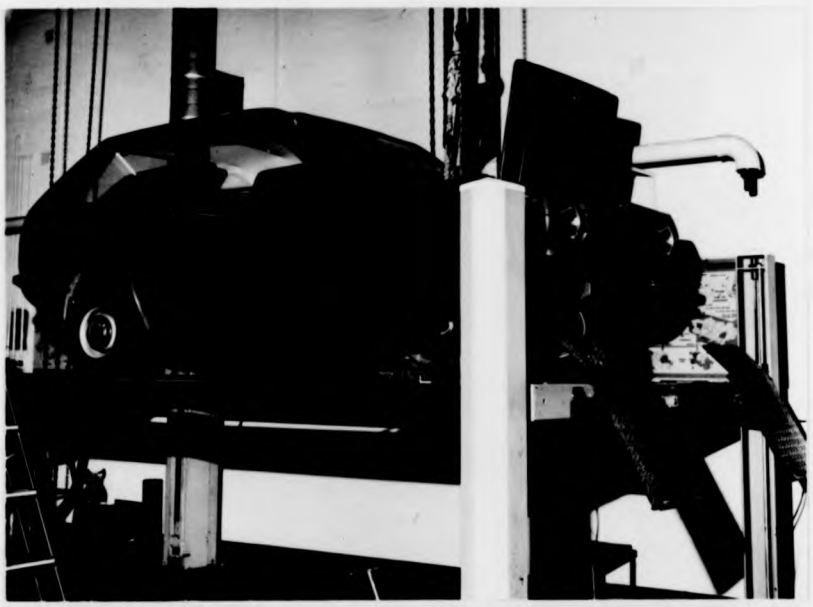

Fig. 7.3 : Fitting the motor into the vehicle

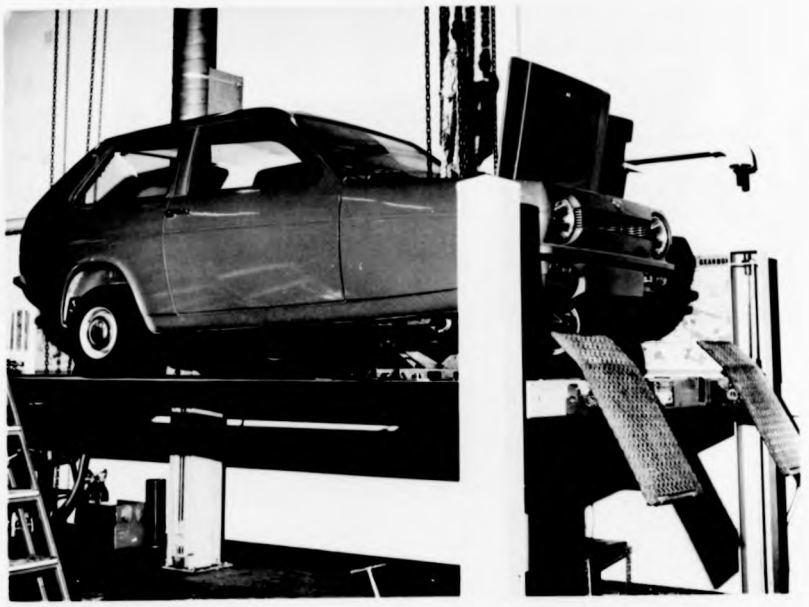

Fig. 7.3 : Fitting the motor into the vehicle

'hatchback-type' rear window of the car utilised. The rear seats are folded forward and a wooden platform is made to the dimensions of the exposed space. This fits on top of the rear wheel arches and is large enough to site the 8 Lucas 66 Ah CP11 heavy-duty SL1 batteries. A cage-type housing is constructed to support the batteries and this is bolted through the platform and car body onto 4 brackets welded to the chassis. The complete assembly is able to restrain the batteries when driving.

As the under-bonnet space contains only the motor, it is possible to locate the electronic controller here. This in fact takes up most of the available space and Fig. 7.4 illustrates the size of a similar controller. The various controller components are bolted to a wooden shelf made to fit over the traction motor. A cable link connects the accelerator pedal to the speed control potentiometer, and although regenerative braking is available, the braking control unit is not connected at this stage. The motor armature and field are connected to the appropriate contactors (allowing electrical reversing) and connections are made through a high current fuse to the batteries at the rear of the vehicle. After taxing, insuring and M.O.T. testing, the Reliant is ready for the road.

In order to assess how the various vehicle components perform under actual operating conditions, instrumentation must be installed which can be used to record the relevant values of voltage, current, torque and speed associated with these components. The instrumentation used on the Reliant Robin allows the following parameters to be measured. Battery voltage and current, motor

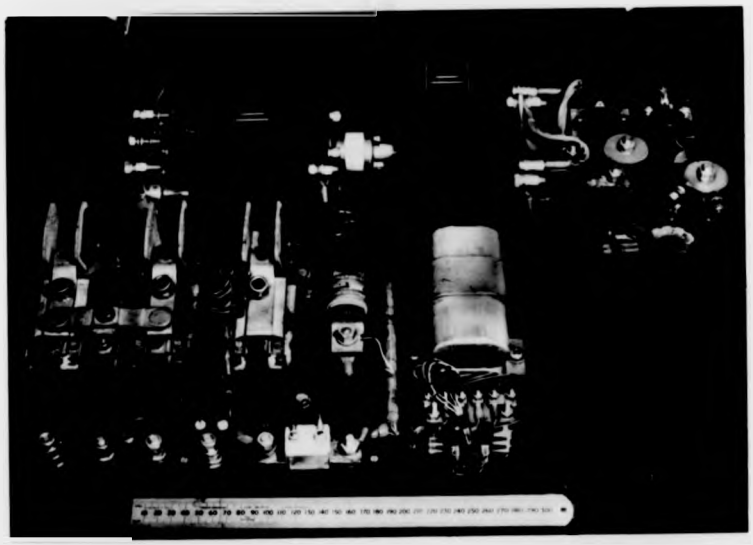

Fig. 7.4 : Typical chopper controller

Fig. 7.4 : Typical chopper controller

voltage and current, propshaft torque and speed. The battery voltage is measured directly and the motor voltage measured between one side of the armature, and the field coils' reversing contactor (i.e. positive voltage is always displayed). Both voltages are monitored on meters within the vehicle. Battery and motor currents are measured by the use of two high-current shunts in the electric circuit. Measurement of the voltages developed across these allows the current to be determined, and the voltages themselves are measured by a battery-powered mean-sensing digital voltmeter carried in the vehicle.

In any electromechanical system, it is important to determine the mechanical power at some point in the drive chain and this is best accomplished on a vehicle such as the Robin by direct measurement of the torque transmitted along the propshaft and its speed of rotation. Fortunately considerable experience in such measurement is available at the University due to a more general involvement in road vehicle technology where the values of such parameters are important to an understanding of i.c. engine behaviour. The speed of rotation of the vehicle propshaft is determined by means of a toothed wheel fitted onto it. A magnetic transducer is used to generate a series of pulses, the frequency of which is proportional to the rotational speed of the propshaft. Determination of the torque transmitted along the propshaft is a more complex problem. Apparatus which is readily available utilises a strain gauge bridge mounted on the propshaft. As the torque increases and the bridge becomes unbalanced, the changing voltage level alters the output frequency of a voltage-

controlled oscillator (V.C.O.) which in turn is amplified and taken to a simple aerial. This complete electronics package must also be fixed to the propshaft and the VCO/transmitter is housed in a small metal case with the batteries in a similar case on the opposite side of the propshaft. The two cases are securely chained to the propshaft and connections made to the strain gauges and the rotating aerial. The strain gauges themselves are aligned along the axis of principal stress which lies at 45° to the propshaft axis. Care is needed in fixing the strain gauge elements to the shaft and extreme cleanliness is necessary. After attaching the leads which are to be connected to the electronics unit, the gauges are protected from the elements by covering with glass fibre matting and a suitable resin. The rotating aerial is a simple brass collar, approximately 40 mm wide, which is fixed around the propshaft but insulated from it. The signal from the transmitter is fed directly to this aerial and picked up using capacitative coupling by a stationary receiver mounted on the vehicle. Finally, the signal passes to the decoding unit on the vehicle which displays a meter reading proportional to the torque transmitted along the propshaft. Calibration of the instrument is required and this is carried out in the laboratory, using a beam and known weights, with the propshaft, aerials and decoding unit removed from the vehicle.

The instrumentation described above is sufficient for an accurate analysis of the vehicle performance and comparison of results with those predicted by the computer simulation model outlined earlier. With proposed operating conditions established, practical testing may be carried out to collect the data necessary for such an analysis.

7.2 Road testing procedure

As discussed earlier, constant speed tests corresponding to the SAE/J227 standard are proposed as these particular tests are most appropriate to the electric vehicle model. Although it is generally not possible to drive a vehicle continuously at constant speed, the range may be determined according to the discharge current at the speed in question. A suitable test route is needed over which values of all the relevant parameters may be measured at constant speed. Fortunately , part of the ring road at Warwick University (essentially a private road) may be utilised as a good portion of this is straight and level, enabling testing to be carried out without significant difficulty. After several initial runs are made to assess the route and ensure the instrumentation is working correctly, a suitable test procedure is established. Two people are needed to perform this safely and accurately - the driver concentrates on controlling the vehicle at the desired speed while the assistant records the values of the voltages, currents and torque. Several runs are carried out, in both directions, and the average values of the measured parameters taken. It is assumed that throughout the tests the battery is fully charged, or very nearly so, and after short periods of testing, the batteries are given a recharge to ensure that this assumption is valid. It is also necessary to zero the torque measuring apparatus before each test to compensate for any frequency drift. The road and weather conditions are chosen to be as good as possible and approximately the same for each set of tests, although this is judged on a

subjective basis. It may be assumed that any discrepancies introduced by the wind and gradient are compensated for by running the vehicle in opposite directions. The weights of the vehicle components and test instrumentation are already known, and the weights of the two people involved in the vehicle testing are measured and recorded for the analysis.

In practice, the proposed test methods prove to be very satisfactory allowing a good and representative sample of measurements to be made. Test speeds of 10 m.p.h., 20 m.p.h. and 30 m.p.h. are taken and each gear used as appropriate - first gear is not used about 10 m.p.h. In order to maintain the batteries in good condition for as long as possible they were never discharged beyond approximately 25% to 30%, and recharging was carried out overnight at a slow rate. To avoid possible high charging currents, the regenerative braking unit was not connected and this would only have been of use if the duty-cycle approach to range assessment was being considered.

7.3 Results from road testing

Although the battery and motor voltages are read directly, the values of currents and torque are initially taken from the relevant meter-readings with the appropriate calibration factors being applied at a later stage. A complete set of results is given in Table 7.1, with an indication of the accuracy of measurement in each case. The figures show the clear benefit of using the higher gears wherever possible, although there are speeds below 10 m.p.h. where the selection of a lower gear enhances the efficiency of the

Gear	1	2	2	2	
Road speed, m.p.h.	10	10	20	30	± 5%
Propshaft torque, N.m	9.5	9.5	13	17	± 1Nm
Motor voltage, V	30	24	49	85	± 2.5V
Motor current, A	39	54	57	71	± 4A
Battery voltage, V	96	96	94	92	± 2.5V
Battery current, A	17	16	35	71	± 4A
Predicted range, miles*	25.6	28.4	21.2	13.9	

Gear	3	3	3	4	4	4
Road speed, m.p.h.	10	20	30	10	20	30
Propshaft torque, N.m	9.5	13	17	9.5	13	17
Motor voltage, V	18	37	55	17	31	50
Motor current, A	60	68	80	66	72	90
Battery voltage, V	96	94	92	96	92	90
Battery current, A	15	30	53	15	29	52
Predicted range, miles*	31.7	25.2	19.2	31.7	26.1	19.8

* see text

Table 7.1 : Test results for electric vehicle

complete vehicle system[54]. The battery current can also be reduced when a lower gear is selected for (initial) acceleration or hill climbing although this effect is not measured in the test programme.

For comparison, Table 7.2 provides values of the measured parameters which have been predicted by the computer simulation model. Agreement is generally good with the largest observed discrepancy being in values of the battery current at the lowest speed. This discrepancy becomes less as the vehicle speed increases and points to possible inaccuracy in the controller model. At lower mark-space ratios, extra switching losses could be incurred which have not been allowed for in the proposed model - an in-depth analysis of the controller behaviour would be needed to resolve this discrepancy. The values of motor current and voltage show very good agreement with predicted values indicating that the proposed motor model is highly suited to this kind of analysis. The good agreement between predicted and actual mechanical output (as determined from propshaft torque) indicates the suitability of the methods used in determining the power flow through the vehicle.

Although it is impractical to determine the vehicle range directly by experiment, an assessment may be made by considering the battery current drawn at a particular speed and the effective battery capacity at this level of current. The battery model described in section 6.1.5 is used here to determine the range in the same way as in the vehicle system model. The discharge current is normalised, the effective capacity found and the total discharge time calculated. Multiplying this by the vehicle speed gives the total range of the vehicle and is presented in the bottom row of

Gear	1	2	2	2
Road speed, m.p.h.	10	10	20	30
Propshaft torque, N.m	9.1	9.1	12.0	16.7
Motor voltage, V	31	21	47	83
Motor current, A	36	48	57	72
Battery voltage, V	96	96	92	88
Battery current, A	12	11	30	69
Predicted range, miles	41.5	47.2	25.5	14.3

Gear	3	3	3	4	4	4
Road speed, m.p.h.	10	20	30	10	20	30
Propshaft torque, N.m	9.1	12.0	16.7	9.1	12.0	16.7
Motor voltage, V	16	34	57	14	29	48
Motor current, A	58	64	77	67	73	88
Battery voltage, V	97	93	90	96	93	90
Battery current, A	11	25	51	11	24	48
Predicted range, miles	49.7	32.4	20.5	47.5	33.5	21.7

Table 7.2 : Theoretical results corresponding to Table 7.1

E.D.C. motor

Table 7.1 for each gear and at the three speeds considered. It must be emphasised that these figures correspond to total battery discharge and are for comparison purposes only, as to continually discharge a battery will place a severe limitation on the useful life expected from it.

For completeness, Table 7.3 gives similar results (including range) for the disc armature motor in the vehicle as predicted by the simulation. These results assume that similar controller efficiencies are likely but do not make any allowance for possible additional losses at low speeds. Comparison of these results with those in Table 7.2 is thus most appropriate. The significant increase in vehicle range under these steady-state driving conditions is a very valuable benefit although it would also be possible to specify a smaller battery for vehicles where the duty cycle is already known.

Gear	1	2	2	2
Road speed, m.p.h.	10	10	20	30
Propshaft torque, N.m	8.8	8.8	11.7	*
Motor voltage, V	66	36	70	*
Motor current, A	13	20	29	*
Battery voltage, V	97	97	93	*
Battery current, A	9	8	23	*
Predicted range, miles	66.5	77.7	35.8	*

* 30 m.p.h. not available in 2nd gear

Gear	3	3	3	4	4	4
Road speed, m.p.h.	10	20	30	10	20	30
Propshaft torque, N.m	8.8	11.7	16.4	8.8	11.7	16.4
Motor voltage, V	24	46	69	18	36	53
Motor current, A	28	37	53	35	47	65
Battery voltage, V	97	94	90	97	95	90
Battery current, A	7	19	41	7	19	40
Predicted range, miles	86.8	45.6	26.0	85.7	46.8	27.0

Table 7.3 : Theoretical results corresponding to table 7.1

Disc armature motor

8: CONCLUSIONS AND SUGGESTIONS FOR FURTHER WORK

A study has been made of the use of disc armature motors for traction applications. A comprehensive design procedure has been developed and with the aid of results from earlier prototypes the performance of a machine with a given set of design parameters can be accurately predicted. The necessary routines to achieve this are contained in a computer program and by the use of the interactive facility the designer can investigate a large number of design alternatives in an extremely short time with varying degrees of freedom on the operation of the program. Machines designed using these methods have been built and tested with close agreement between predicted and actual performance.

As the relatively large number of poles in the machine often dictates a duplex wave arrangement rather than a lap wound armature this type of winding has been of particular interest. It has been shown that in certain cases two alternative connection methods may be adopted for the same winding specification in terms of coils and poles. One such case has been investigated and it is only by careful study of the e.m.f.s generated in the primary and short-circuit armature paths that the optimum configuration may be specified. This is where the short-circuit e.m.f.s developed between like brushes average to approximately zero over a period of rotation. If the optimum winding arrangement is not chosen then significant deterioration in machine performance results which is explained by two mechanisms. The non-zero average value of e.m.f.s short-circuited by the brushgear leads to significant sparking at the brushes, while the lower values of e.m.f. generated in the

primary paths causes a reduction in flux linkages leading to reduced motor speed and torque. These effects have been discussed on a theoretical basis and also demonstrated experimentally. A computer program has been developed which will calculate the values of the primary and short-circuit e.m.f.s in any armature winding for a given pole shape and number of brushes.

The thermal behaviour of the machine is of particular importance in traction applications and rating methods similar to those used in conventional machines (B.S. 1727) are a desirable ideal. Although insufficient testing has been carried out to enable general and extensive rating conditions to be specified results from existing machines that are available enable ratings to be proposed for time periods above 30 minutes.

The use of the motor in a typical battery electric traction application has been investigated with the aid of a simulation model of an electric vehicle and practical road testing. Incorporation of the disc armature motor into the model enables its advantages to be demonstrated. Improved vehicle performance results when such a machine is specified as an alternative to the more conventional series wound motor. This may be taken either as increased range for the same battery capacity or, in a vehicle whose duty cycle is known, a reduced battery requirement.

A continued study of the e.m.f.s generated in the various armature paths forms the basis for further work in this area. In the case of duplex wave windings, alternative arrangements may easily be investigated in order to determine the optimum. For

simple wave windings the procedures developed will be of greatest use in assessing the correlation between the magnitudes of primary and short-circuit e.m.fs and the pole shape, number of coils and number of brushes used. For the particular machine in question, it will be valuable to have an extended set of performance curves to verify that reduced machine performance is apparent over the complete operating range when the non-optimum winding arrangement is selected. This will entail constructing two new armatures and encapsulation using an appropriate grade of material to ensure that low-temperature flexing does not occur.

Investigation of the thermal behaviour of the motor is another area where research must continue. Ideally an accurate thermal model of the motor should be developed as an aid to understanding this behaviour. Comprehensive load/temperature measurements are needed to verify or modify the proposed rating conditions, and if the general standard for rotating electrical machines (B.S. 2613) is to be complied with, the embedded thermocouple technique must be used for these measurements. Of particular interest are the very short-term ratings as specified in B.S. 1727 for battery electric vehicle motors. The effect of forced-cooling the motor should also be assessed. As ferrite materials are likely to be used in the majority of traction applications, the effect of temperature rise on magnet performance must also be studied, and incorporated into the design procedure - possibly as some function of armature current density.

The continued study of motor performance in actual vehicle

operating conditions will enable much valuable information to be gained and highlight areas where improvements or modifications to the design procedures are necessary.

9: REFERENCES

1. Barber, J.M., 'Estimated supplies of transport fuels to the end of the century', 2nd international conference of the Electric Vehicle Development Group, Paper 1.1, May 1978.

2. Chapman, P., Charlesworth, G., and Baker, M., 'Future transport fuels', TRRL report SR 251 1976.

3. Frame, A.G., 'Some aspects of materials and energy in relation to electric powered transport', 3rd international conference of the Electric Vehicle Development Group, Paper 1.1, November 1979.

4. Beagley, T.L., 'Energy and transport', Conference of the Association of District Councils Passenger Transport Operators, October 1979.

5. Odell, P.R., 'The future supply of oil', P.T.R.C. annual conference, University of Warwick 1978.

6. Cluer, A., 'The availability of future fuels - Hydrocarbon liquids from fossil sources', 3rd international conference of the Electric Vehicle Development Group, Paper 1.2, November 1979.

7. Porter and Fitchie, 'Energy for road transport in the U.K.', TRRL report SR 311, 1977.

8. Caudle, P.G., 'The chemical industry and vehicle developments', Electric Vehicle Developments, No. 4, November 1979.

9. Wise, C.E., 'EV revival - Back from oblivion', Machine Design, October 1974.

10. Tomblin, N.H., 'Annual load demand in respect of battery electric vehicles', Electric Vehicle Association report NHT/PMT/E/B. Stat., 1976.

11. Altendorf, J.P., and Kalberlah A., 'Comparison between the primary energy consumption of electric and gasoline powered vehicles', Fourth International Electric Vehicle Symposium, Paper 1.8, 1976.

12. Harding, G.G., 'Developing Electric Vehicles', Ist International Conference ofthe Electric Vehicle Development Group, Paper 4.2, 1977.

13. Goodson, R.E., 'Electric Vehicles - how do they compare with synthetic liquid fuels', 3rd International Conference of the Electric Vehicle Development Group, Paper 3.6, 1979.

14. Jones, I.W., 'Sodium/Sulphur battery design and development for motive power applications', Fourth International Electric Vehicle Symposium, Paper 32.8, 1976.

15. Charkey, A., 'Development of large size nickel-zinc cells for electric vehicles', Fourth International Electric Vehicle Symposium, Paper 32.3, 1976.

16. Duncan, A.S., 'The future of battery electric road vehicles', TRRL report S4UC, 1973.

17. Charlesworth, G., and Baker, M., 'Transport fuels for the post-oil era', Energy Policy, March 1978.

18. Corbett, A.E., and Roerig, C.S., 'Energy utilisation in electric vehicles', Paper to be published.

19. Corbett, A.E., and Mohammad, M.T., 'The disc-armature d.c. motor and its applications', IEE Conference Publication 136, Small Electrical Machines, 59-62, 1976.

20. Carter, A.H., and Corbett, A.E., 'Electric Motor', British Patent 1231782, 1971.

21. Campbell, P., 'The d.c. disc-armature electric motor', Ph.D. Thesis, University of Warwick, 1974.

22. Campbell, P., 'Principles of a permanent magnet axial field d.c. machine', Proc. IEE, 121, pp. 1489-1494, 1974.

23. Stott, G., 'Iron powder compacts for electromagnetic applications', M.Sc. Thesis, University of Warwick, 1971.

24. Corbett, A.E., and Roerig, C.S., 'Selecting permanent magnet materials for disc armature d.c. motors', International Conference on Electrical Machines, SP42, Brussels, 1978.

25. Sommerfeld, A., 'Electrodynamics', Academic Press, P.80, 1952.

26. Campbell, P., 'Permanent magnet motors for electric vehicles', Electric Vehicle Developments, 3, 1979.

27. Turner, A.M., 'Computer-aided design of d.c. disc armature motors', Undergraduate thesis, University of Warwick, 1970.

28. Corbett, A.E., 'A disc armature d.c. motor', EM 70 Conference, Dundee 1970.

29. Corbett, A.E., 'The lawnmower motor', University of Warwick file report, 1970.

30. Corbett, A.E., 'The SSEB motor', University of Warwick file report, 1970.

31. Corbett, A.E., 'The Engineering Society Motor', University of Warwick file report, 1971.

32. Campbell, P., 'A new wheel motor for electric commuter cars', Electrical Review, Vol. 190, No. 10, 1972.

33. Campbell, P., 'Pancake shaped d.c. motor for efficient fan drives', Electrical Review ,Vol. 194, No. 8, 1974.

34. Corbett, A.E., and Mohammad, M.T., 'The disc motor as a control system element', ERA Seminar on selecting small motors for control applications, London, January 1979.

35. 'Electric cars - reports from the builders ', Electrical Review, February 1975.

36. Prigmore, B.J., 'Battery cars today - some theory and some practice', Electronics and Power, June 1975.

37. Dirlik, T., 'Dynamic modelling of lead-acid batteries for automobile propulsion', M.Sc. thesis, University of Warwick, 1976.

38. 'The status of the Flinders University electric vehicle development', Report to the Australian director general of transport, May 1977.

39. 'The Flinders University electric vehicle technology', Licensing package, October 1977.

40. Campbell, P., 'A direct drive wheel motor for electric vehicles', Electrical Review, Vol. 194, No. 8, 1974.

41. Campbell, P., 'The pancake d.c. motor', Electrotechnology, January 1977.

42. Southworth, C.P., 'Ceramic magnets in industrial motors', 1st U.K. Conference on permanent magnets, June 1980.

43. Corbett, A.E., and Roerig, C.S., 'The economic design of disc armature traction motors', Electric Vehicle Developments, No. 5, 1980.

44. Kubo, T., Ohtani, T., Kojima, S., and Kato, N., 'Anisotropic Mn-Al-C alloy permanent magnets can be machined and mass produced', Journal of Electrical Engineering, July 1977.

45. Ohtani, T., et al, 'Magnetic properties of Mn-Al-C permanent magnet alloys', IEEE transactions on magnetics, September 1977.

46. Clayton, A.E., 'The performance and design of direct current machines', Pitman Press, 1952.

47. Tustin, A., and Ward, H., 'The e.m.f.s induced in the armature coils of d.c. machines during commutation', I.E.E. proceedings, 109C, 1962.

48. Tarkanyi, M., Ward, H., and Tustin, A., 'Electronic computers applied to commutation analysis, I.E.E. proceedings, 109C, 1962.

49. Cross, G., and Pratt, J.M.K., Armature conductor eddy current effects in d.c. machine commutation', Fifteenth Universities power engineering conference, March 1980.

50. 'Carbon brushes and electrical machines', Morganite Electrical Carbon Ltd., p. 193 , 1978.

51. Charlesworth, G., 'The energy and resource implications associated with the widespread use of electric vehicles,' Electric Vehicle Development Conference, 1977.

52. Hind, M.A., 'Battery electric vehicle performance evaluation and simulation', Ph.D. thesis, University of Bristol, 1972.

53. White, K.E., 'A digital computer program for simulating electric vehicle performance', SAE technical paper 780216, 1978.

54. Corbett, A.E., and Roerig, C.S., 'Energy utilisation in electric vehicles', Paper submitted for consideration by Electric Vehicle Developments.

55. 'Mechanics of pneumatic tires', (S.K. Clark Ed.), National Bureau of Standards Monograph 122, U.S. Department of Commerce, 1971.

56. Bosworth, J., 'Transmissions for electric vehicles', Undergraduate thesis, University of Warwick, 1978.

57. Murphy, G.J., 'Alternative approaches to speed control in electric vehicles', SAE paper 780292, 1978.

58. Morton, J., Jones, J., and Watson, C., 'Minimisation of electrical losses in a battery electric vehicle', paper presented at the Drive Electric 80 Conference, October 1980.

59. Shepherd, W., and Ahamed, T.V., 'Operation of a lead-acid battery with thyristor chopper burden', Proc. IEE-B, Vol. 127, No. 2, March 1980.

60. Bird, W., 'Report on battery discharge equation', Lucas Internal Report.

61. Smith, G., 'Storage Batteries', Pitman Press, 1971.

62. 'Electric vehicle test procedure - SAE J227a', SAE recommended practice, February 1976.

63. Roganavich, N., 'Speed control of induction motors', Ph.D thesis, University of Warwick 1978.

64. Mohammad, M.T., 'Research and development in axial field motors', Ph.D. thesis, University of Warwick, 1978.

65. 'Specification for motors for battery operated vehicles', B.S. 1727, British Standards Institution, 1971.

66. Corbett, A.E., and Roerig, C.S., 'Motors for electric vehicles', Electric Vehicle Developments, May 1978.

67. Ozpolat, A.M.M., 'An axial-field d.c. electric machine', M.Sc. thesis, University of Warwick, 1980.

68. Campbell, P., 'Performance of a permanent-magnet axial-field d.c. machine', Electric Power Applications, Vol. 2, No. 4, 1979.

APPENDIX I: AN ALTERNATIVE FERRITE DESIGN

The motor described in Chapter 5 was based on a design using Alnico magnets (Hycomax III) in order to achieve a relatively high working flux density and thus good efficiency. However, the recent fluctuations and general upward trend in the world price of cobalt led to Alnico materials becoming much more expensive and prohibitively so for most traction applications. The only feasible economic alternative at present is to use ferrite materials, although the penalties are a low energy product and lower flux densities. Specification of a ferrite material will thus generally require a larger amount of armature copper to be used, with a corresponding increase in the I^2R loss and lowering of motor efficiency. It is, however, possible to obtain some degree of compromise by using a ferrite material well above the BH_{max} point on the demagnetisation curve. This represents inefficient usage of the material and a larger amount will be required than for operation at BH_{max}. However, as ferrites are relatively inexpensive, an economic motor design can generally be produced with an acceptable value of efficiency. To this end, the C.A.D. procedures are used to produce an alternative ferrite design for the 7.5 kW traction application. The same design constraints are imposed in that as the ferrite motor must directly replace the Hycomax III motor the same value of D2 (280 mm) is used. The design parameters for the resulting machine are given in Table A1.1 with the predicted performance curves in Fig. A1.1. It can be seen by comparison with Table 3.4 that in addition to a common value of D2 the length of the magnets used is practically the same, although the flux per

DESIGN NO: 237

DESIGN SPECIFICATION

OUTPUT: 7500. WATTS
VOLTS: 96. V
SPEED: 3400. RPM

DESIGN DATA

D2: 280. MM
D1: 171. MM
POLES: 8.

MAGNETIC CIRCUIT DATA

B1 0.300 TESLA
H1 54000. A/M
LDEFF 1.30
LFACT 1.20
P1I .000835 WEBERS
ALPHA .75
LMAG 62.0 MM
WGTMAG 8.44 KG
THICK 5.53 MM
WGTFRR 3.33 KG
GAP 15.20 MM
MAGDSY 4700. KG/M**3
B1S 1.80 TESLA

ELECTRIC CIRCUIT DATA

PATHS 4.
COILS 57.
TURNS 4.
Z 912.
GAUGE 2.00 MM
WGTWIR 4.60 KG
CRTDSY 7.0 A/MM**2
ARMCRT 89.34 AMPS
LOSS 668.08 WATTS
LAY 4
TEMP 75. DEGREES
SF .35
RARM 0.069 OHMS
ER 98.4% VOLTS

Table A1.1 : Design parameters for 7.5kW ferrite motor

[illegible] 17.97 KG
TOTWGT 33.04 KG
MECHLO 233. WATTS
SPEED 3482.7 RPM
POWER 7493.9 WATTS
TORQUE 20.55 NM
PWRWGT 249.45 WATTS/KG
EFF .884

PERFORMANCE SPECIFICATIONS

CURRENT DENSITY AMP/MM**2.	ARMATURE CURRENT AMPS	SPEED RPM	POWER WATTS	TORQUE NM	EFFICIENCY
1.	12.57	3687.5	833.2	2.16	.691
2.	25.13	3653.6	1992.3	5.21	.826
3.	37.70	3619.6	3129.8	8.26	.865
4.	50.27	3585.6	4245.5	11.31	.880
5.	62.83	3551.7	5339.6	14.36	.885
6.	75.40	3517.7	6412.0	17.41	.886
7.	87.96	3483.8	7462.7	20.46	.884
8.	100.53	3449.8	8491.7	23.51	.880
9.	113.10	3415.8	9499.1	26.56	.875
10.	125.66	3381.9	10484.7	29.61	.869
11.	138.23	3347.9	11448.7	32.66	.863
12.	150.80	3314.0	12390.9	35.70	.856
13.	163.36	3280.0	13311.5	38.75	.849
14.	175.93	3246.0	14210.4	41.80	.841
15.	188.50	3212.1	15087.6	44.85	.834
16.	201.06	3178.1	15943.2	47.90	.826

Table A1.1 (continued) : Design parameters for 7.5kW motor

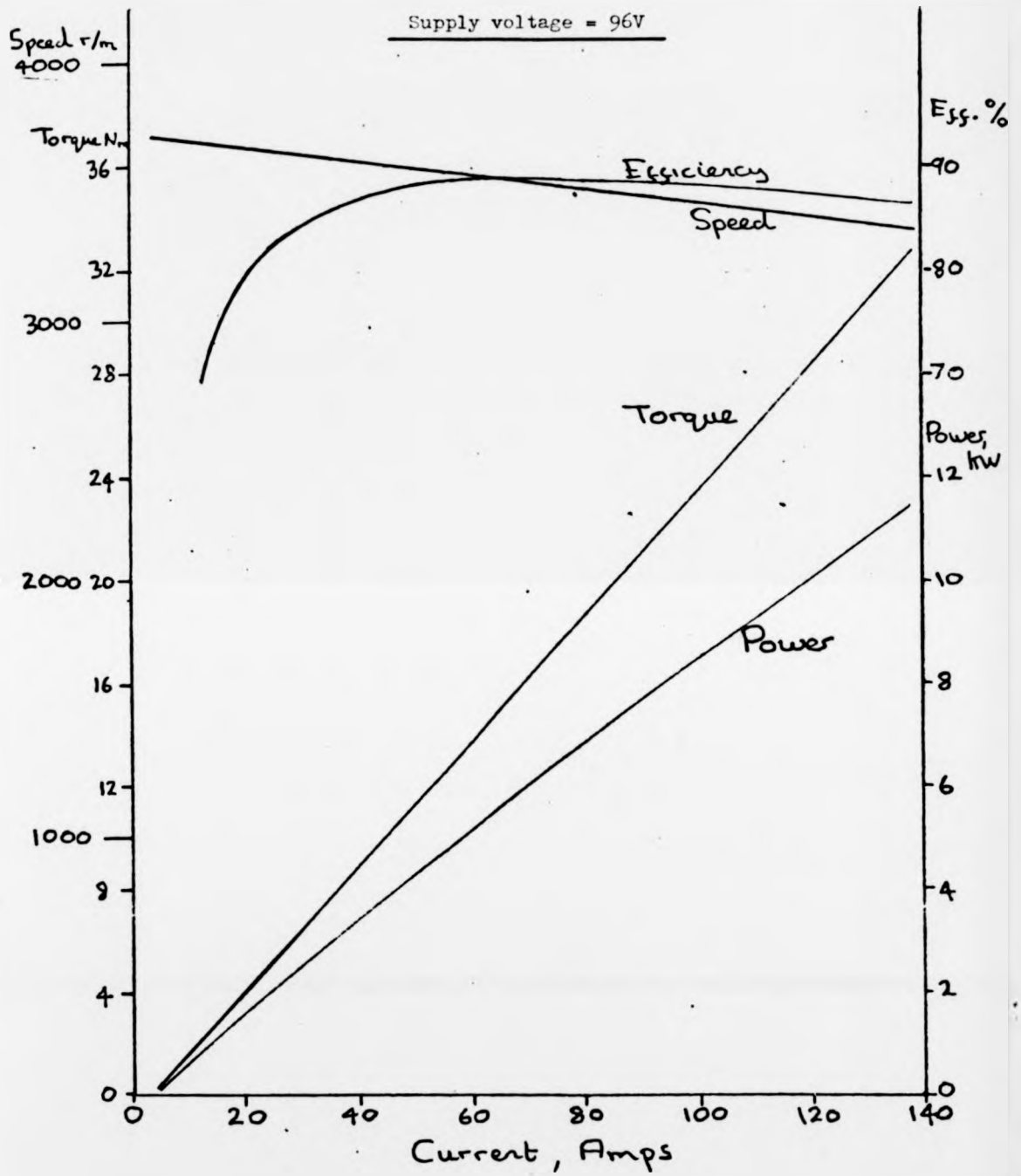

Fig. A1.1 : Predicted performance of 7.5kW ferrite motor

pole in the ferrite motor is only 0.43 times that in the Alnico motor. The armature winding is a 4-layer simple wave arrangement with armature resistance increased by a factor of 1.8 over the Hycomax III motor. However, a slightly reduced current density is necessary for a similar power output at similar speed. The power density of the ferrite design is increased by 25%, the efficiency is approximately 3% less at the specified power output and although this falls off more markedly, it is still acceptable for the application representing a good compromise between cost and performance.

APPENDIX II: FURTHER TRACTION APPLICATIONS

The machines described here have been developed very recently and designed using the CAD procedures developed in Chapter 4. With the need for economic design ferrite materials have been used exclusively and again usually worked well above the BH_{max} point on the demagnetisation curve.

A2.1 The 130W, 2000 rev/min motor

This machine was developed for an invalid wheelchair drive after consultation with a major U.K. manufacturer of such wheelchairs. It was considered that the use of two disc armature motors (per unit) with high efficiency transmissions would offer substantial benefits to the overall performance of the wheelchair. The development program was carried out in conjunction with a small industrial company (Moore Reed and Co. Ltd.) and a successful motor has been designed, built and tested. The design parameters are given in Table A2.1, and it can be seen that the motor operates from a nominal 24 volt supply derived from two lead/acid batteries in series. Predicted performance curves are given in Fig. A2.1 with the measured curves in Fig. A2.2.

A2.2 The 130W, 4000 rev/min motor

The development of this machine follows directly from that described above. It was found that a more efficient motor/transmission system could be achieved by specifying the higher motor speed and a purpose-built gyratory gearbox. The design parameters are given in Table A2.2 and it will be noted that a smaller machine than above

Table A2.1 : Design parameters for 130W, 2000 rev/min motor

DISC-ARMATURE MOTOR DESIGN

DESIGN NO: 400

DESIGN SPECIFICATION

OUTPUT: 130. WATTS
VOLTS: 24. V
SPEED: 2100. RPM

DESIGN DATA

D2: 190. MM
D1: 105. MM
POLES: 8.

MAGNETIC CIRCUIT DATA

BM 0.220 TESLA
HM 115000. A/M
LCOEFF 1.30
LFACT 1.20
PHI .000312 WEBERS
ALPHA .75
LMAG 5.6 MM
WGTMAG 0.39 KG
THICK 2.65 MM
WGTFRR 0.82 KG
GAP 4.00 MM
MAGDSY 4700. KG/M**3
BMS 1.80 TESLA

ELECTRIC CIRCUIT DATA

PATHS 2.
COILS 41.
TURNS 6.
Z 492.
GAUGE 1.00 MM
WGTWIR 0.408 KG
CRTDSY 5.0 A/MM**2
ARMCRT 7.85 AMPS
LOSS 24.07 WATTS
LAY 2
TEMP 75. DEGREES
SF .85
RARM 0.390 OHMS
ER 20.94 VOLTS

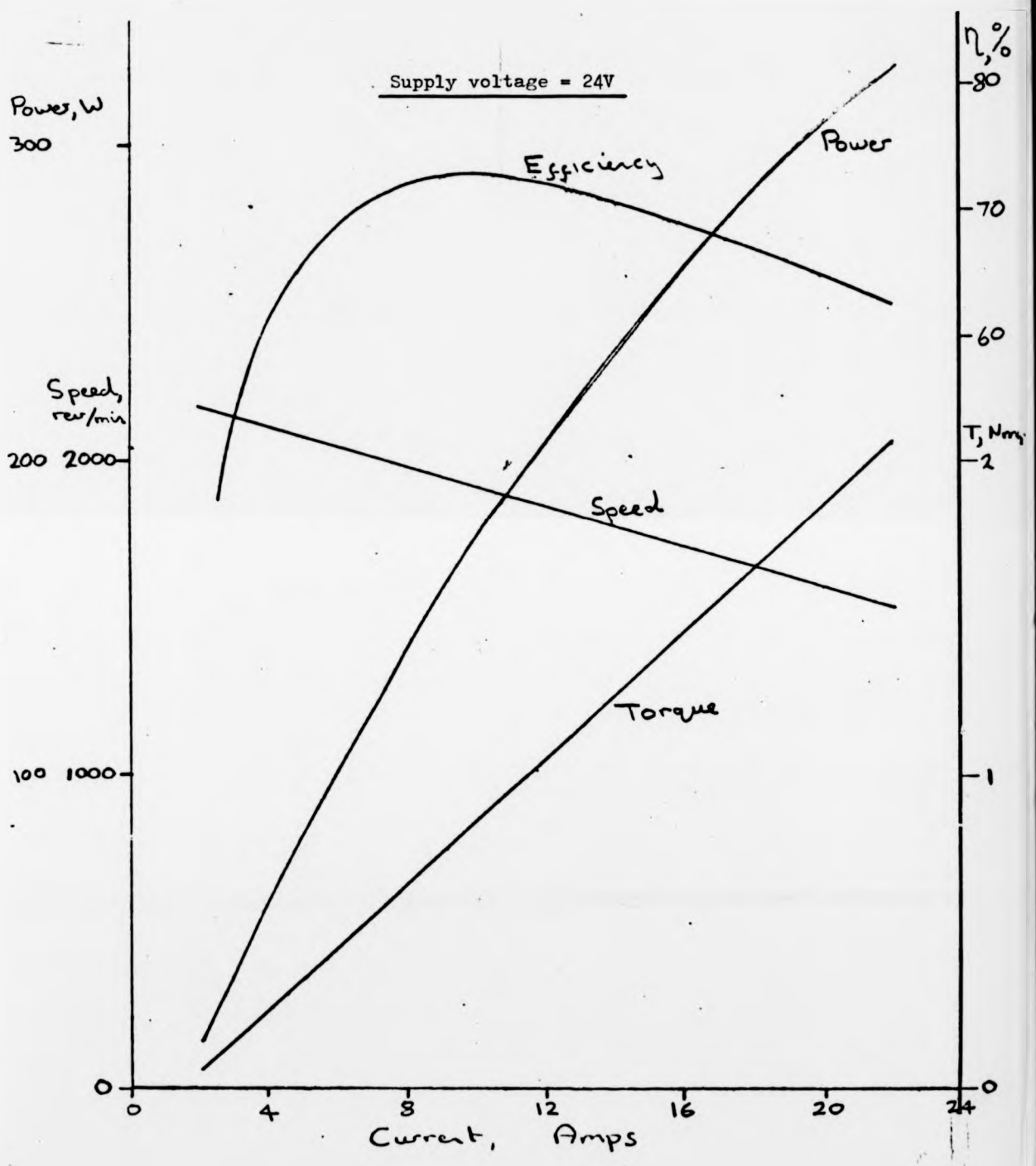

Fig. A2.1 : Predicted performance of 130W, 2000 rev/min motor

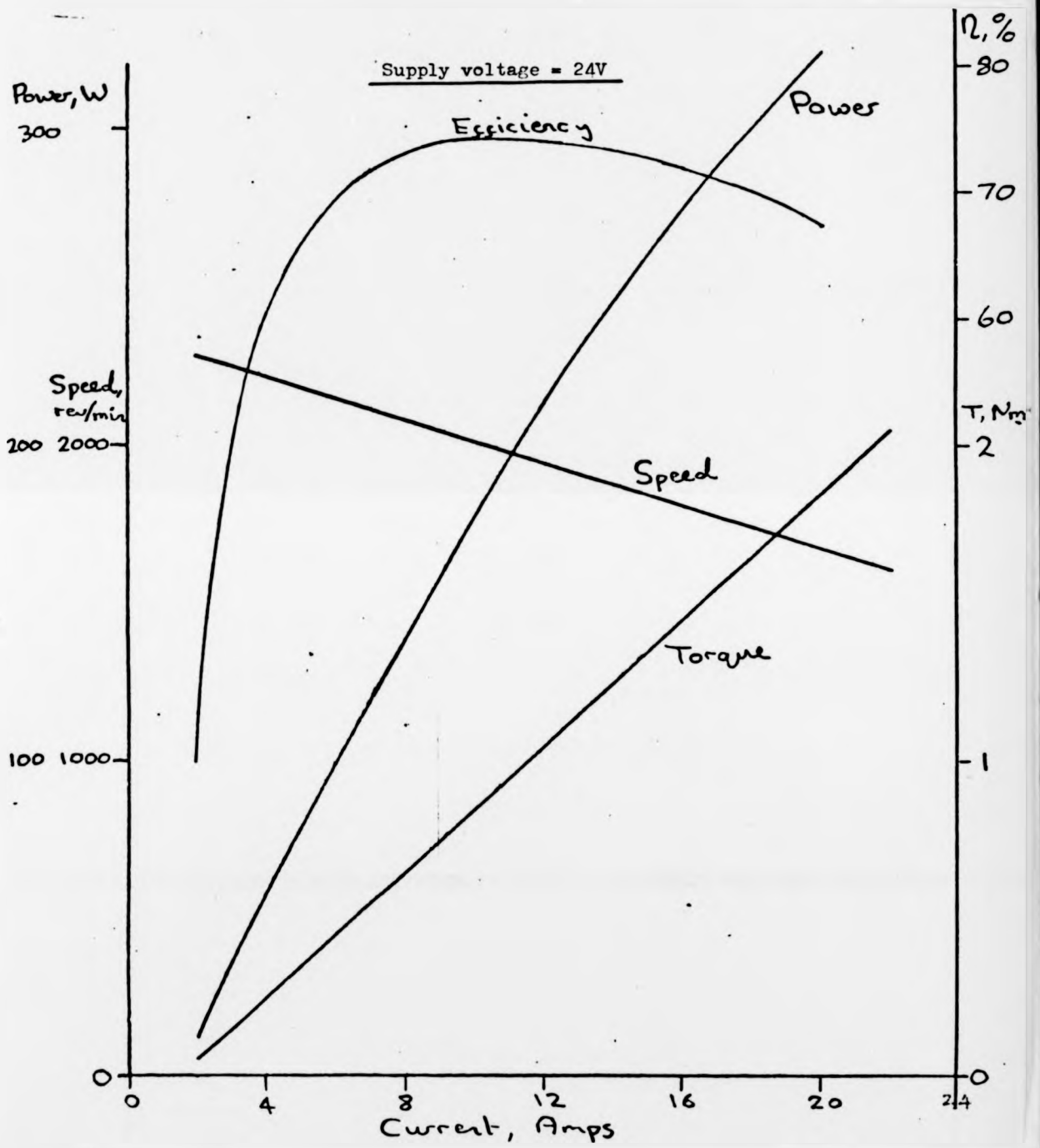

Fig. A2.2 : Measured performance of 130W, 2000 rev/min motor

Table [illegible] : Design parameters for [illegible] rev/min motor

DESIGN SPECIFICATION

OUTPUT: 130. WATTS
VOLTS: 20. V
SPEED: 4190. RPM

DESIGN DATA

D2: 152. MM
D1: 89. MM
POLES: 6.

MAGNETIC CIRCUIT DATA

B1 0.250 TESLA
HM - 92500. A/M
LEOEFF 1.30
LEACT 1.20
PHI .000290 WEBERS
ALPHA .75
LMAG 12.9 MM
WGTMAG 0.55 KG
THICK 3.27 MM
WGTFER 0.62 KG
GAP 6.50 MM
MAGDSY 4700. KG/M**3
BMS 1.80 TESLA

ELECTRIC CIRCUIT DATA

PATHS 2.
COILS 29.
TURNS 5.
Z 290.
GAUGE 1.40 MM
WGTWIR 0.46 KG
CRTDSY 4.5 A/MM**2
ARMCRT 13.85 AMPS
LOSS 42.91 WATTS
LAY 2
TEMP 75. DEGREES
SF .85
RARM 0.115 OHMS
ER 16.90 VOLTS

OUTPUT DATA

Fig. A2.7 : 130W motors, 2000 rev/min (top) and 4000 rev/min

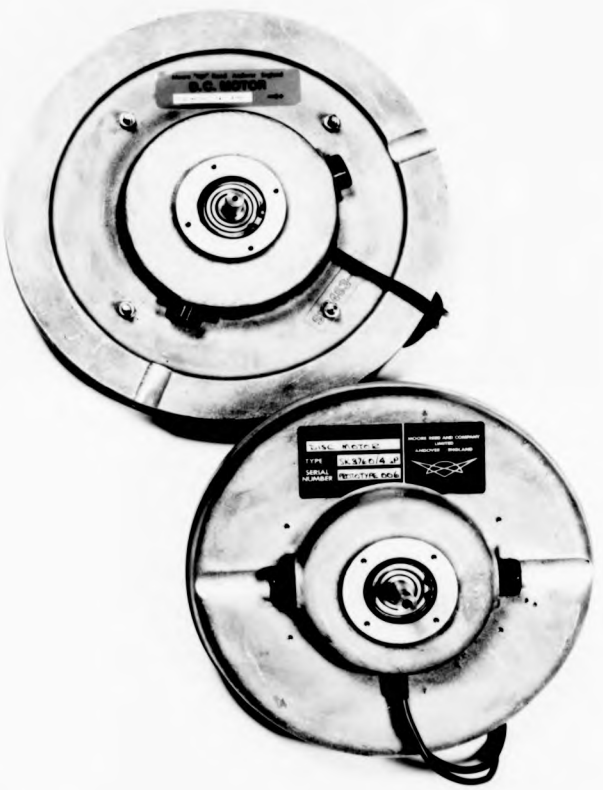

Fig. A2.7 : 130W motors, 2000 rev/min (top) and 4000 rev/min

results with fewer poles. The lower supply voltage of 20V was specified after it was found that significant regulation occurs in the controllers used to drive the wheelchair motors. Predicted and measured performance curves are shown in Figs. A2.3 and A2.4 respectively. This machine has been extensively bench-tested using several chopper controllers and the performance with such a controller is identical to that obtained when using a steady d.c. supply. The development programme is now effectively concluded with the machine at a marketable stage. Evaluation of its use in the envisaged application presently continues.

A2.3 The 20 kW motor

Collaboration with another small industrial company (Lee Dickens Ltd.) led to the development of this more powerful machine. The application is in the drive system of a high-performance hybrid car. The motor itself is unusual in that two electrically independent armatures rotate in a common magnetic circuit (Fig. A2.5) with drive to the vehicle wheels taken via a belt reduction transmission. The design parameters for each 'half' of the motor are given in Table A2.3 with predicted performance in Fig. A2.6. The relatively large amount of ferrite magnet material gives a good working flux with associated high efficiency. Development of this machine continues with bench testing and practical evaluation in progress.

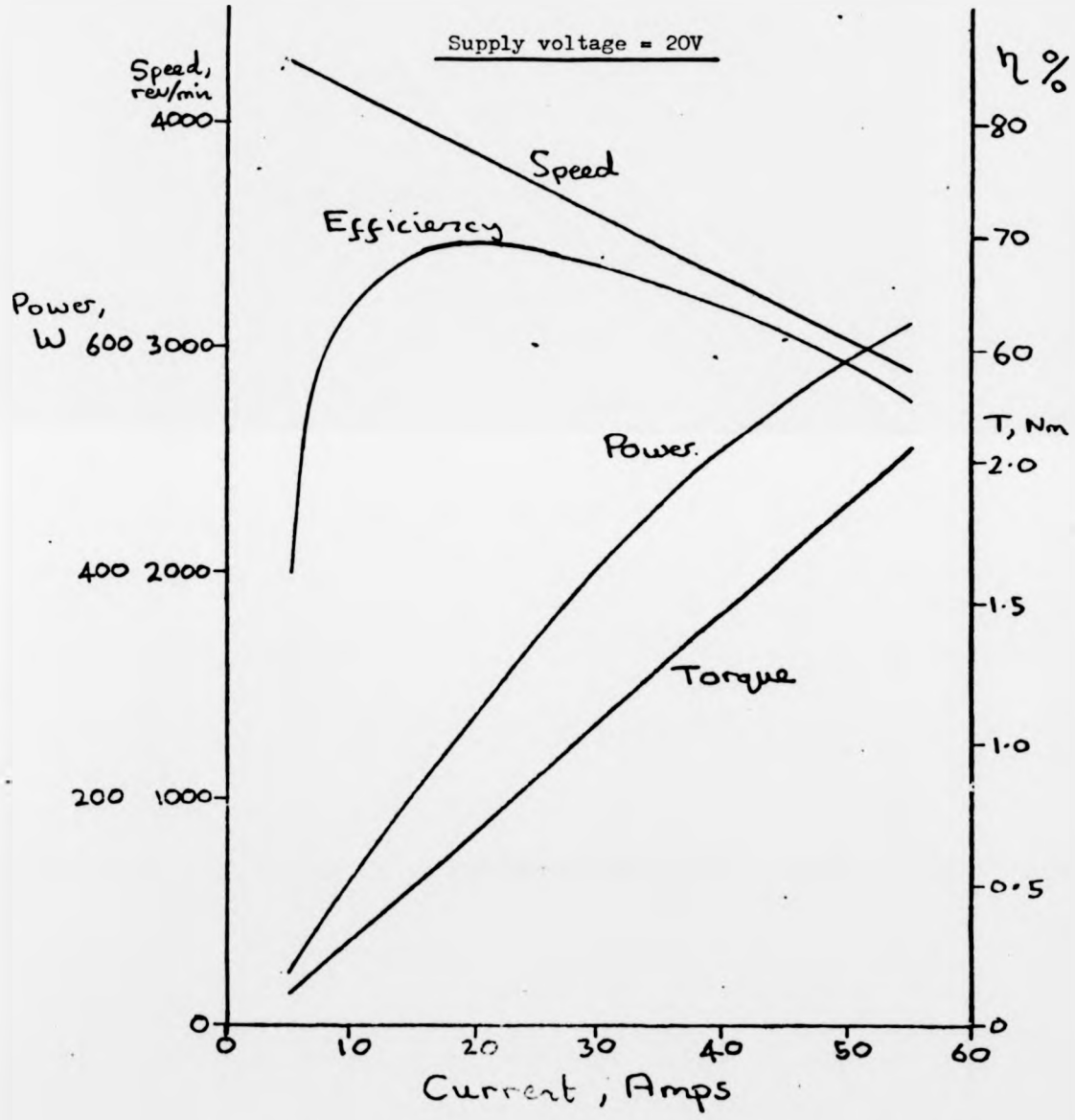

Fig. A2.3 : Predicted performance of 130W, 4000 rev/min motor

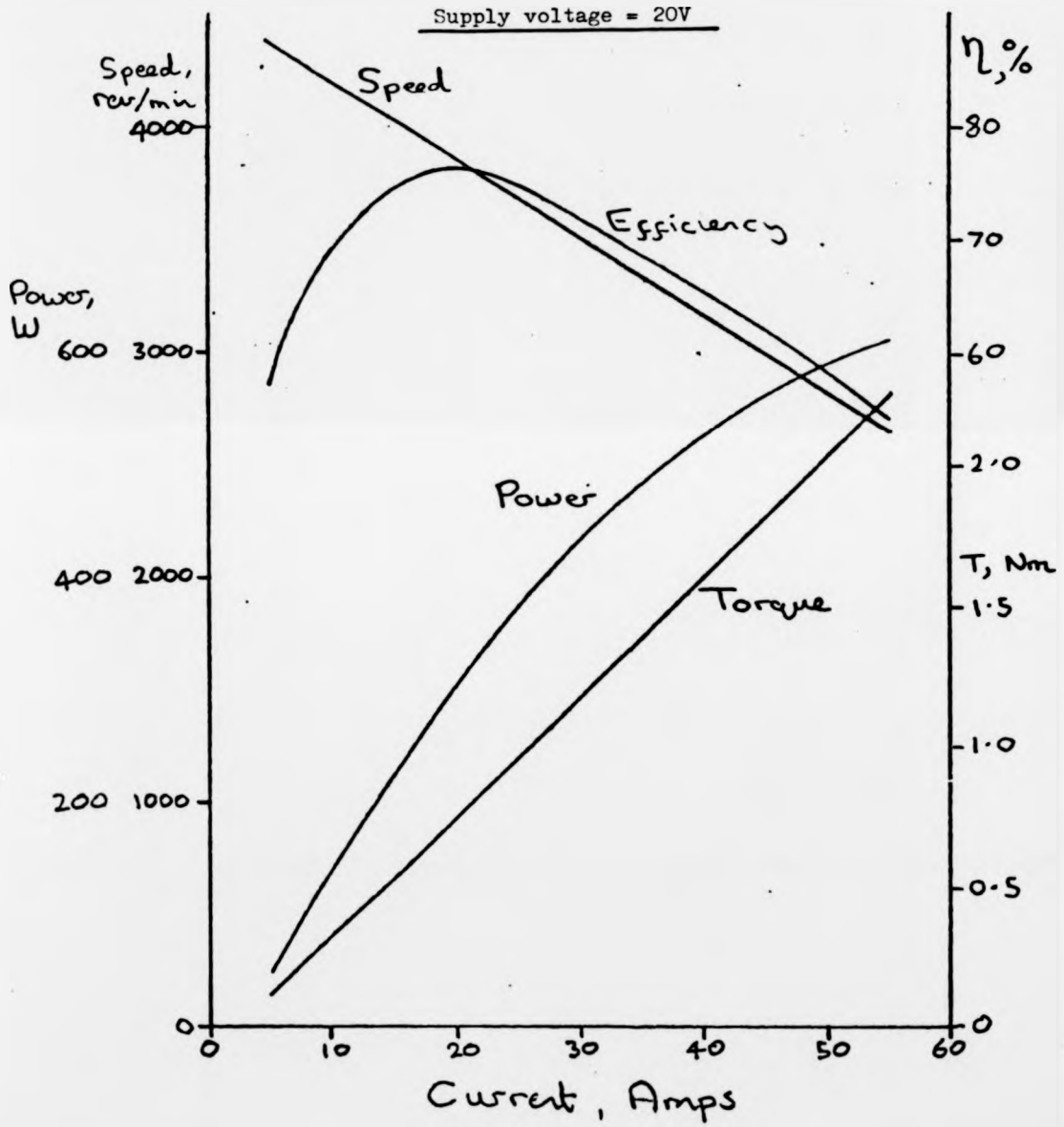

Fig. A2.4 : Measured performance of 130W,. 4000 rev/min motor

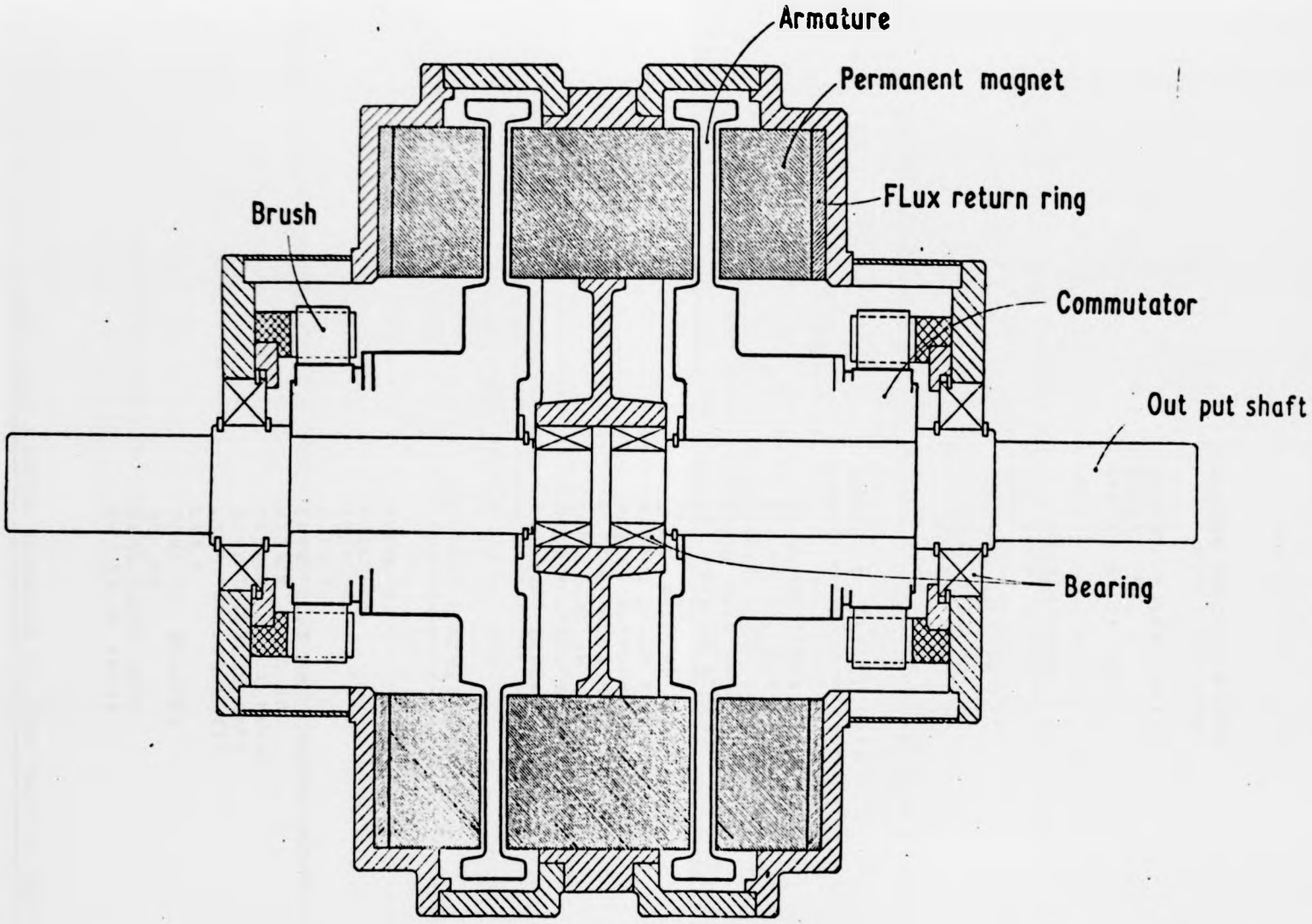

Fig. A2.5 : Disc Armature Twin Rotor Electric Vehicle Traction Motor Unit.

DESIGN NO: 240

DESIGN SPECIFICATION

OUTPUT: 11500. WATTS
VOLTS: 96. V
SPEED: 4000. RPM

DESIGN DATA

D2: 305. MM
D1: 175. MM
POLES: 8.

MAGNETIC CIRCUIT DATA

B4 0.330 TESLA
H4 3500. A/M
LEOEFF 1.30
LFACT 1.20
P4I .001150 WEBERS
ALPHA .75
LMAG 83.1 MM
WGTMAG 14.28 KG
THICK 6.49 MM
WGTFRF 4.94 KG
GAP 12.00 MM
MAGDSY 4700. KG/M**3
B4S 1.80 TESLA

ELECTRIC CIRCUIT DATA

PATHS 8.
COILS 72.
TURNS 8.
Z 1152.
GAUGE 1.63 MM
WGTWIR 4.25 KG
CRTDSY 8.0 A/MM**2
ARMCRT 133.55 AMPS
LOSS 840.94 WATTS
LAY 4
TEMP 75. DEGREES
SF .85
PARM 0.036 OHMS
ER 89.70 VOLTS

Table A2.3 : Design parameters for each 'half' of 2kW rotor

DESIGN NO: 240

DESIGN SPECIFICATION

OUTPUT: 11500. WATTS
VOLTS: 96. V
SPEED: 4000. RPM

DESIGN DATA

D2: 305. MM
D1: 175. MM
POLES: 8.

MAGNETIC CIRCUIT DATA

BM 0.330 TESLA
HM 35000. A/M
LCOEFF 1.30
LFACT 1.20
PHI .001160 WEBERS
ALPHA .75
LMAG 83.1 MM
WGTMAG 14.28 KG
THICK 6.49 MM
WGTFRR 4.94 KG
GAP 12.00 MM
MAGDSY 4700. KG/M**3
BMS 1.80 TESLA

ELECTRIC CIRCUIT DATA

PATHS 8.
COILS 72.
TURNS 8.
Z 1152.
GAUGE 1.63 MM
WGTWIR 4.25 KG
CRTDSY 8.0 A/MM**2
ARMCRT 133.55 AMPS
LOSS 840.94 WATTS
LAY 4
TEMP 75. DEGREES
SF .85
PARM 0.036 OHMS
ER 89.70 VOLTS

Table A2.3 : Design parameters for each 'half' of 20kW motor

[illegible] 15.07 KG
TOTWGT 29.33 KG
MECHLO 520. WATTS
SPEED 4028.5 RPM
POWER 11460.1 WATTS
TORQUE 27.17 NM
PWRWGT 291.41 WATTS/KG
EFF .894

PERFORMANCE SPECIFICATIONS

CURRENT DENSITY AMP/MM**2	ARMATURE CURRENT AMPS	SPEED RPM	POWER WATTS	TORQUE NM	EFFICIENCY
1.	16.69	4217.0	1015.8	2.30	.634
2.	33.39	4190.0	2567.9	5.85	.801
3.	50.08	4163.1	4200.0	9.40	.853
4.	66.78	4136.2	5612.1	12.96	.875
5.	83.47	4109.3	7104.1	16.51	.887
6.	100.16	4082.3	8576.1	20.06	.892
7.	116.86	4055.4	10028.1	23.61	.894
8.	133.55	4028.5	11460.1	27.17	.894
9.	150.24	4001.5	12872.0	30.72	.892
10.	166.94	3974.6	14263.9	34.27	.890
11.	183.63	3947.7	15635.8	37.82	.887
12.	200.33	3920.8	16987.6	41.37	.883
13.	217.02	3893.8	18319.4	44.93	.879
14.	233.71	3866.9	19631.2	48.48	.875
15.	250.41	3840.0	20923.0	52.03	.870
16.	267.10	3813.1	22194.7	55.58	.865

Table A2.3 : Design parameters for each 'half' of 20kW motor

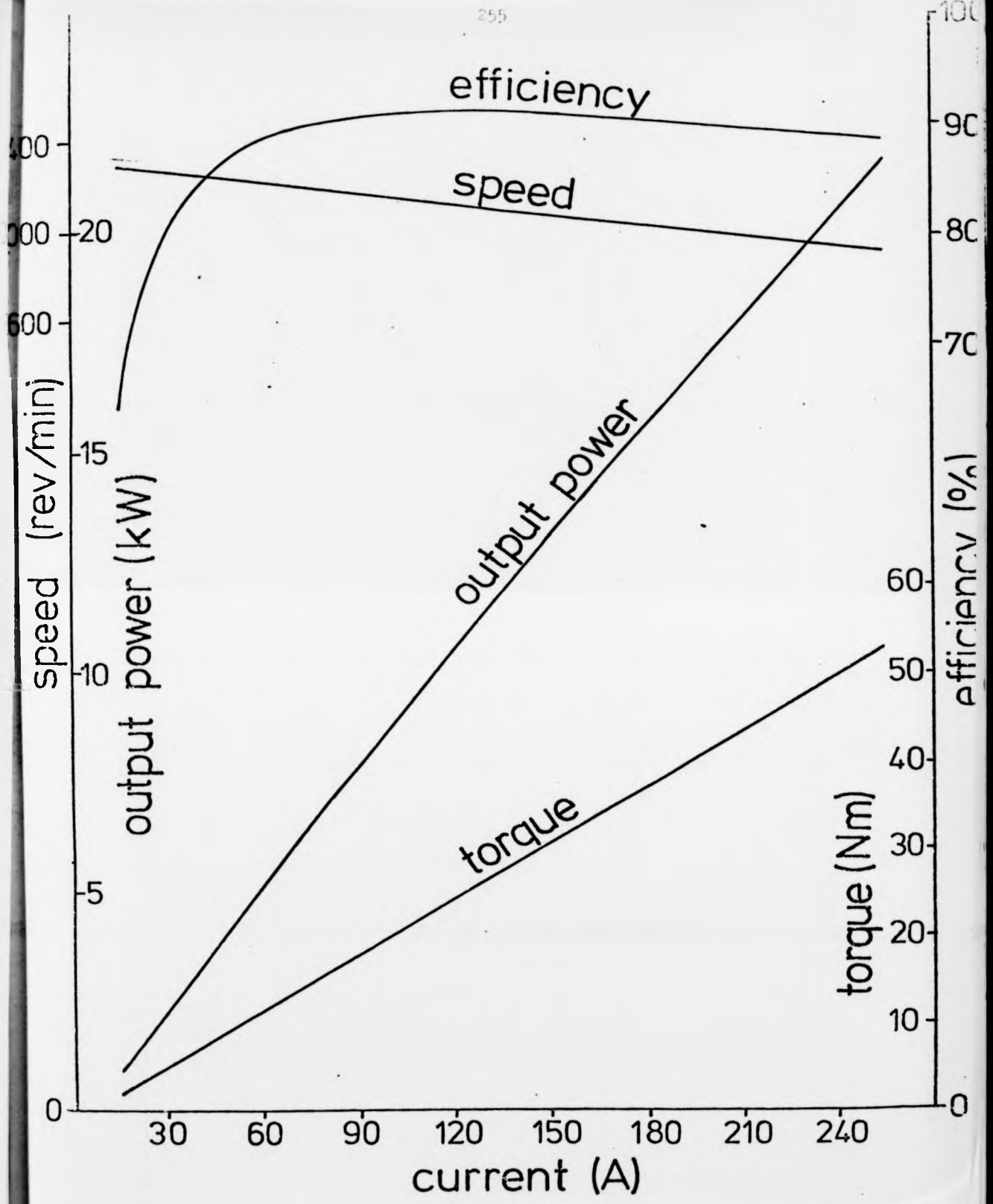

Fig. A2.6 : Predicted performance of 20kW motor at 96V

APPENDIX III: FURTHER APPLICATION OF THE E.M.F. ANALYSIS

Although the method of calculating the e.m.f.s induced in the various armature paths was primarily developed to analyse the alternative duplex arrangements considered earlier, it may be equally well applied to any winding arrangement. As an example, a low speed traction motor developed for bicycle propulsion is investigated particularly as the design involves significant departures from the design principles established here. The machine was designed and built at Cambridge University and has been well documented recently particularly with regard to adverse commutation effects[26,68]. The stator of the machine consists of 10 poles of Alnico material (Hycomax III) but with a ratio of pole-arc to pole pitch of approximately 0.86 compared to the value of 0.75 that has been used in many other designs. Although the flux per pole will be increased, this extension of the pole area has the effect of significantly reducing the neutral area, or commutation zone, between poles. The armature winding is a wave arrangement consisting of only 31 coils (c.f. the minimum of 5 coils per pole specified earlier) and with 10 brushes necessary to carry the full armature current, it is evident that a large number of coils will be short-circuited. Fig. A3.1 shows the connection diagram for this motor and consideration of this reveals that with 10 brushes used in the machine, 18 of the 31 coils are short-circuited by the brushes as the armature rotates. With 4 and 2 brushes used, the numbers of short-circuit coils are 15 and 10 respectively. Further, since the commutation zone is relatively small, many of the short-circuit coils will lie under the influence

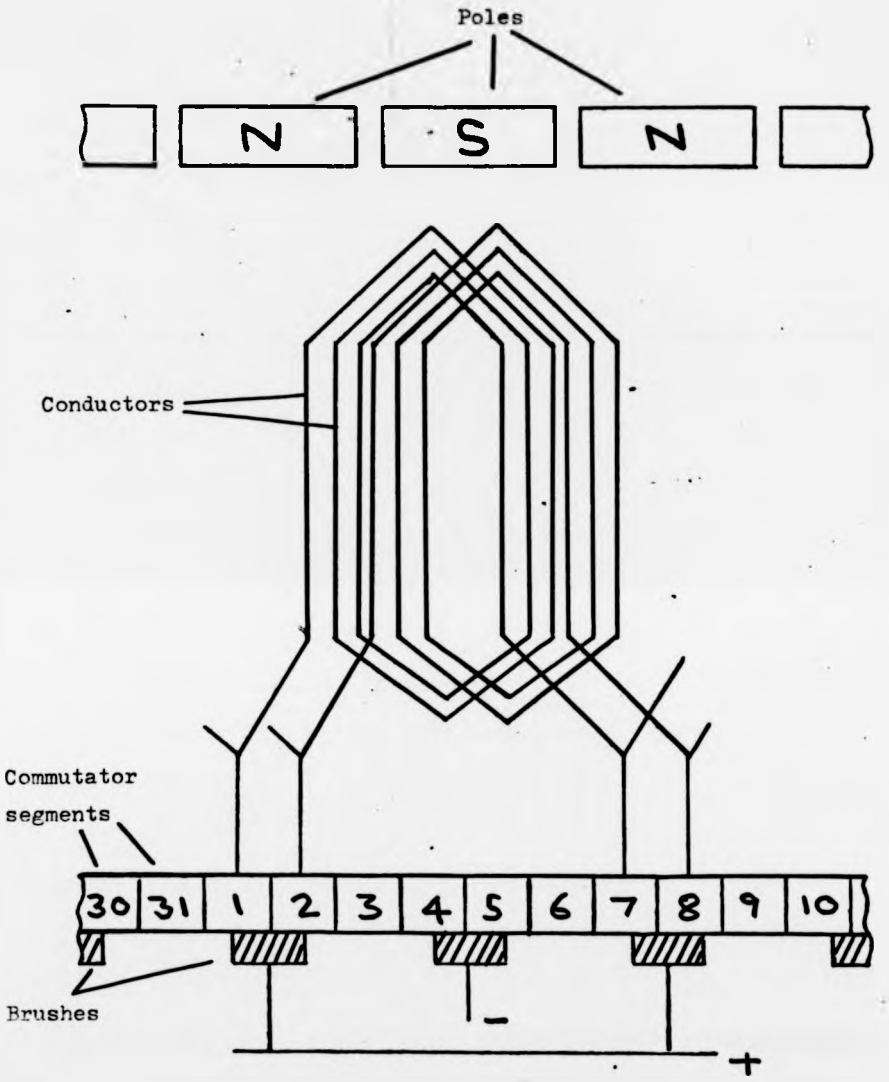

Fig. A3.1 : Connection diagram for 31 coil, 10 pole motor

of one or other of the poles and thus have relatively large e.m.f.s induced in them. This may well lead to adverse commutation conditions and may be investigated further with the aid of the e.m.f. analysis technique developed earlier. Accordingly, the program is run using details of the 31 coil winding and a pole shape similar to that illustrated in Fig. 5.15 but modified to take into account the larger pole-arc to pole-pitch ratio. Results are shown in Figs. A3.2 to A3.4 which illustrate the primary and short-circuit e.m.f.s for 2, 4 and 10 brushes. As before the values of the primary e.m.f.s reduce as the number of brushes is increased although the effect is much more pronounced than in the duplex wave winding considered earlier. Although the short-circuit e.m.f.s average to zero as the armature rotates they represent a very considerable fraction of the primary e.m.f.s. Large peak values are evident when 2 or 4 brushes are used, which, when shorted by the brushes, may well affect the performance of the machine as a whole. With 10 brushes the magnitudes of the short-circuit e.m.f.s are reduced as the paths are formed between adjacent like brushes and thus involve only the e.m.f. generated in a single coil. However, as 18 such paths are formed in the armature it is reasonable to suppose that their combined effect could also possibly lead to an adverse effect on machine performance and symptoms of the kind that have been reported. It is thus clear that with wave windings, and particularly when using multiple brush sets, the effect of the e.m.f.s generated in the short-circuited coils must be carefully considered, especially when using a small number of coils and/or a relatively high ratio of pole arc to pole pitch. The calculation of these e.m.f.s in the manner indicated can be of considerable benefit in assessing this effect.

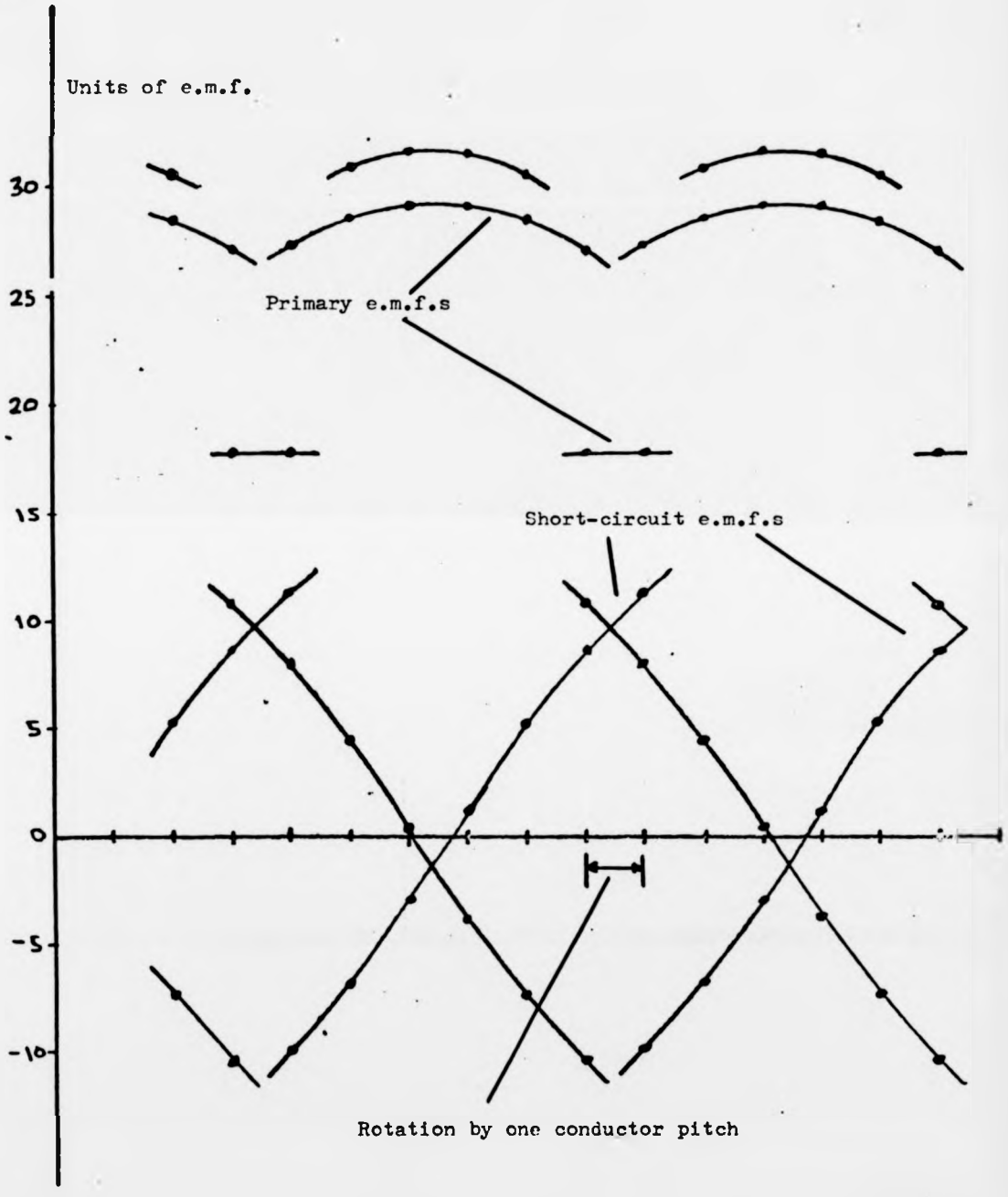

Fig. A3.2 : E.m.f.s generated in 31 coil, 10 pole armature (2 brushes)

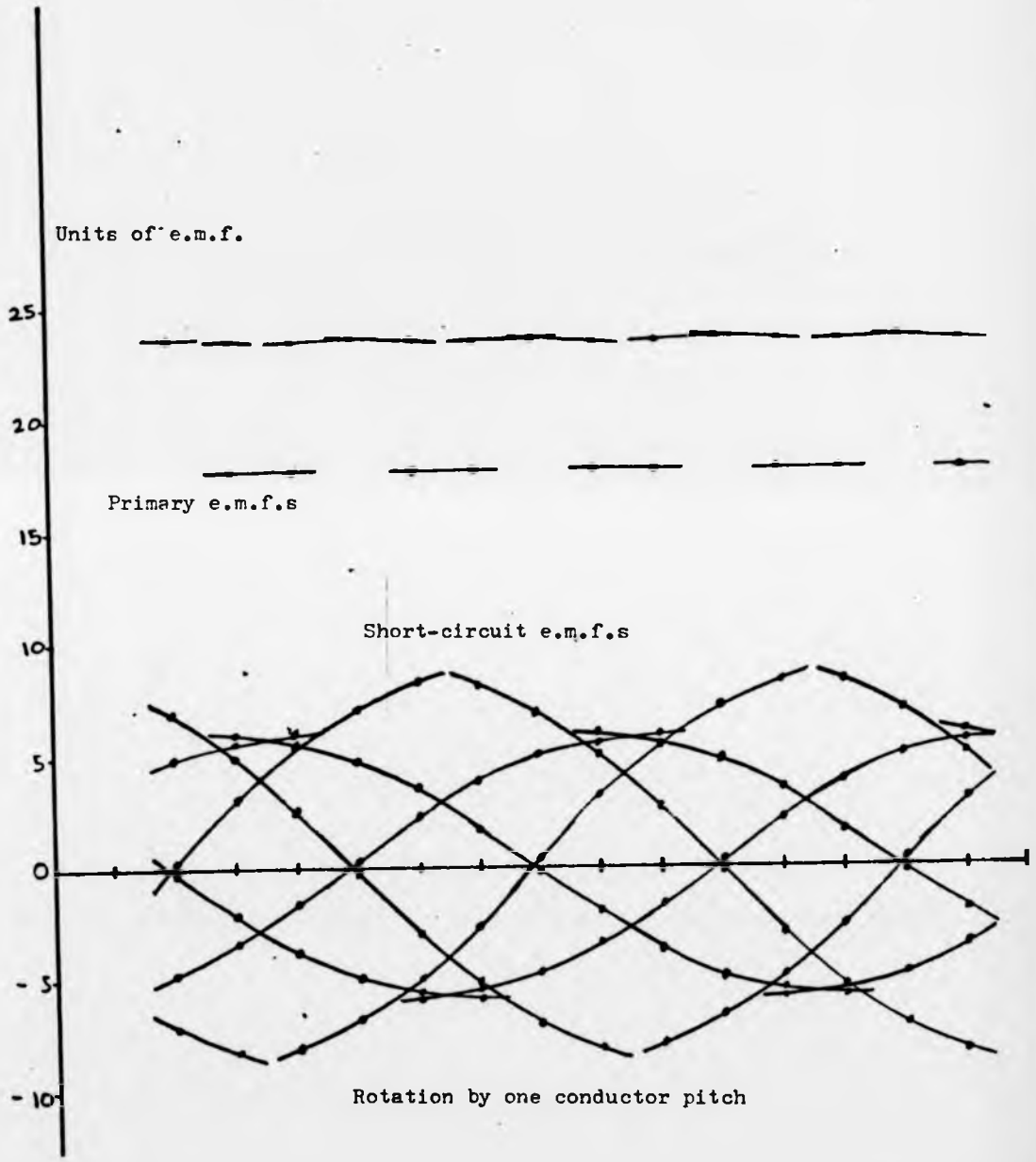

Fig. A3.3 : E.m.f.s generated in 31 coil, 10 pole armature (4 brushes)

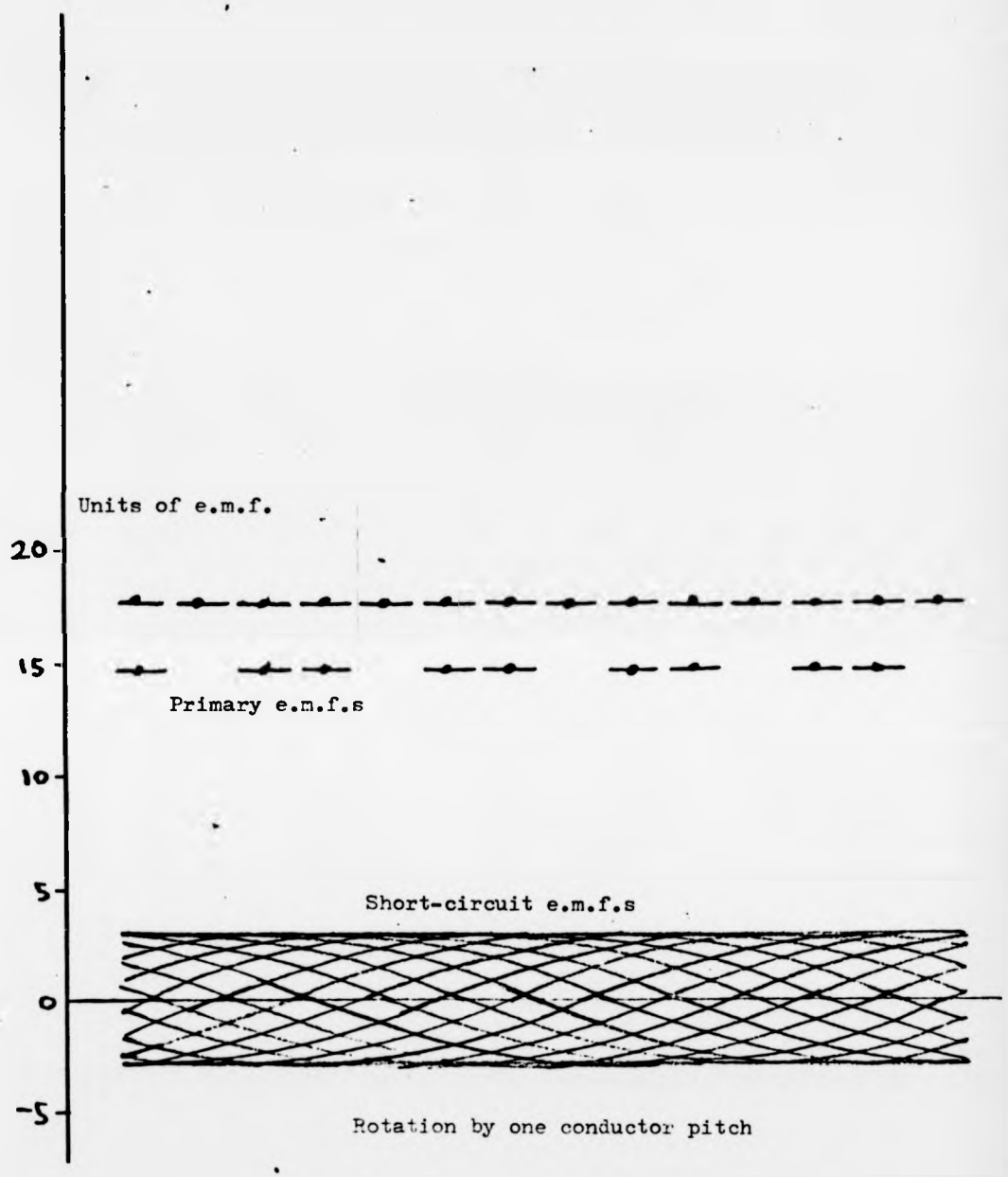

Fig. A3.4 : E.m.f.s generated in 31 coil, 10 pole armature (10 brushes)

APPENDIX IV: SELECTED PUBLISHED PAPERS

The reprints submitted here have been published jointly with the author's supervisor and emanate from or relate to the work described in this thesis. In order, the papers are:-

' Selecting permanent magnet materials for disc-armature d.c. motors' - presented at the International Conference on Electrical Machines, Brussels, 1978.

'The economic design of disc armature traction motors' - published in Electric Vehicle Developments, No. 5, 1980.

'Computer-aided design of permanent magnet motors' - presented at the 1st U.K. Conference on Permanent Magnets, June 1980.

'Disc-armature traction motors' - presented at the Drive Electric 80 Conference, October 1980.

SELECTING PERMANENT MAGENT MATERIALS FOR DISC-ARMATURE D.C. MOTORS

A.E. CORBETT AND C.S. ROERIG

UNIVERSITY OF WARWICK

PAPER PRESENTED AT THE INTERNATIONAL CONFERENCE
ON ELECTRICAL MACHINES, BRUSSELS, 11-13 SEPTEMBER, 1978.

SELECTING PERMANENT MAGNET MATERIALS FOR DISC-ARMATURE D.C. MOTORS

A.E. Corbett and C.S. Roerig,
University of Warwick, Coventry, England.

ABSTRACT

The d.c. disc-armature motor has a disc-shaped ironless armature rotating in a multipolar permanent magnet axial field. The magnetic air-gap length thus includes the thickness of the disc and therefore tends to be longer than that in conventional machines. Although a wide choice of permanent magnet material is currently available the type used depends heavily on the motor application and factors such as efficiency, weight and cost. The long air-gap lends itself to magnetic materials of high coercivity but in many cases size limitations demand a material with high remanence. Here a compromise has to be sought and a computer-aided procedure has been developed to help optimize the design for a given application. The procedure is illustrated with reference to motors being developed for several applications.

INTRODUCTION

Permanent magnets have long been used to supply the field excitation of d.c. machines and developments in recent years have led to a widening of the choice of available materials. In particular, very high energy densities have been achieved with combinations of the rare-earths and these are now specified in place of the more conventional ceramics or alloys in some applications. However in many other applications they must be ruled out on the grounds of cost alone.

When choosing magnets for use in the d.c. disc-armature motor the somewhat longer magnetic air-gap must be carefully considered as it has an important influence on the amount of magnetic material required. The effective use of high-remanence alloy magnets necessitates keeping the air-gap as small as possible thereby limiting the amount of armature copper that can be used. For applications such as low inertia drives this condition of high magnetic loading and low electric loading is very suitable. On the other hand specifying high-coercivity ferrite magnets allows larger air-gaps to be

considered but the relatively low flux density leads to a requirement for more armature copper - precisely the opposite condition to that above. This type of magnet costs less than the alloy type for a given magnetic energy, and its high intrinsic coercive force makes it highly resistant to demagnetisation. It is thus a popular choice for many applications.

In practical terms there exist many variants of the two basic types (alloy and ferrite) and the motor designer needs to be aware of the advantages and limitations of them all. Many magnets used today are anisotropic, i.e. they have a preferred direction of magnetization, and with the continual introduction of new and sometimes more exotic materials the problems involved in magnet selection can become quite complex.

HISTORICAL ASPECTS OF PERMANENT MAGNETS

Development of cobalt steels in the 1920's enabled magnets to be cast to shape in addition to the previous processes of rolling, forging and machining. In the mid-1930's brittle carbon-free alloys were produced which could only be cast, and 1940 saw the advent of the first anisotropic alloys of nickel, aluminium, cobalt, copper and iron - the 'alnico' series. A dramatic improvement in coercivity occurred when ceramic ferrites containing barium, strontium or lead were introduced in the early fifties. This material is produced by pressing and sintering and is available in both isotropic and anisotropic forms. In 1960 magnets became available using cobalt and a rare-earth - in particular samarium[1]. These are usually pressed and sintered and are generally anisotropic. A useful variant of this is where the rare-earth powder is bonded with a polymer to produce a cheaper but easily-machined material. A more recent development was in 1967 when magnets of manganese, aluminium and carbon were made available. The initial material was isotropic and it was not until very recently that an extrusion process was developed to

yield an anisotropic magnet[2,3].

RANGE OF MAGNETIC MATERIALS AVAILABLE

A bewildering range of magnetic materials is available today although the characteristics of many are close enough together to enable just one of a group to be considered. From the motor designer's point of view there are types that he would not normally consider using, again making a choice easier. In this paper a group of five materials is compared although prototype motors have been built using only two of these. It is considered that these five materials cover the available choice at present and one of the groups - the alnico type - has been subdivided to contain two members due to the wide range available. Relevant magnetic and physical properties are shown in Tables 1 and 2 respectively and Fig. 1 illustrates the working demagnetisation curve for each. In order of increasing remanence the materials are barium ferrite, polymer bonded $SmCo_5$, Mn-Al-C alloy, $SmCo_5$, Alnico A and Alnico B. The Mn-Al alloy is not yet available for motor applications but is included for comparison purposes.

Table 1 : Comparison of magnetic properties

Material	Br, Tesla	Hc, kA/M	BH max, kJ/m^3	Max. temp, ^oC	Reversible coeff. of temperature
Barium Ferrite	0.37	240	26	200	0.20%
Polymer $SmCo_5$	0.55	400	55	100	0.03%
Mn-Al-C	0.57	185	44	300	0.12%
$SmCo_5$	0.87	660	152	250	0.04%
Alnico A	1.15	110	89	200	0.02%
Alnico B	1.35	59	60	200	0.02%

Table 2 : Comparison of physical properties

Material	Density, kg/m^3	Machineability
Barium Ferrite	4700	Hard, Brittle-Grinding Only
Polymer $SmCo_5$	5200	Easily Machined and Drilled
Mn-Al-C	5100	Easily Machined and Drilled
$SmCo_5$	8200	Brittle - Grinding Only
Alnico A	7300	Hard, Brittle - Grinding Only
Alnico B	7300	Hard, Brittle - Grinding Only

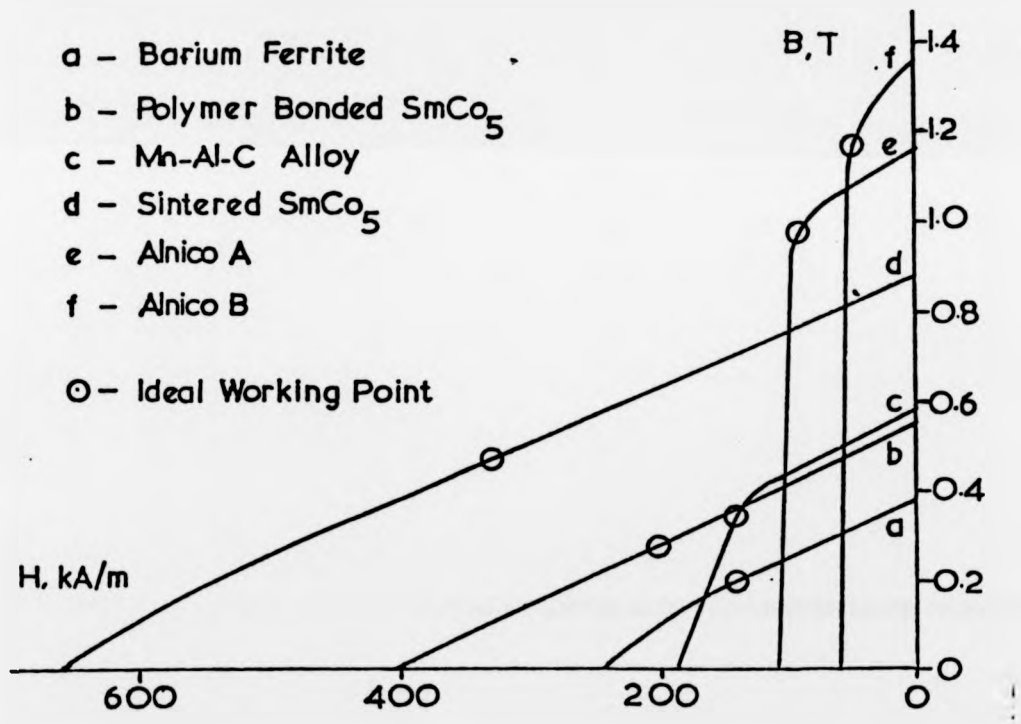

Fig. 1 : Demagnetisation Curves

It is appreciated that many other grades exist but it is felt that this is a representative sample of the best commercially available materials. The relative cost of each material has not been included here as it will be discussed later. It is important to note however that the pressing and sintering process required for ferrite and $SmCo_5$ magnets is more expensive than the casting of alloys and fabrication of polymer-bonded materials, whereas the tooling costs for the former are much higher. The most significant cost difference is in the raw material cost which is much lower for the ferrite materials both on a per unit mass basis and on a per unit energy basis. The optimum working point for each type of magnet is shown in Fig. 1. This represents the most efficient utilization of the material although many designers often work further up the curve, either to achieve an increased working flux or to ensure a greater resistance to demagnetisation. In both cases the penalty is an increase in magnet weight. In spite of a low working flux the very high coercivity and straight-line characteristic of the rare-earth materials allow designs to be contemplated where no flux-return ring is used, thus saving weight. In contrast, the alnico type has a very poor "open circuit" performance and for best utilization needs to be magnetized in situ. Most ferrites can be premagnetized but a flux-return ring is still usually needed.

DESIGN FACTORS IN THE CONSTRUCTION OF DISC-ARMATURE MOTORS

The development of the motor has been described extensively[4,5,6] and it only remains to state that the axial field is produced by a multipolar system of segment-shaped permanent magnets. A complete assembly is shown in Fig. 2. The magnets can be mounted on one or both sides of the armature depending mainly upon the length of magnet involved and the desire to prevent excessive leakage.

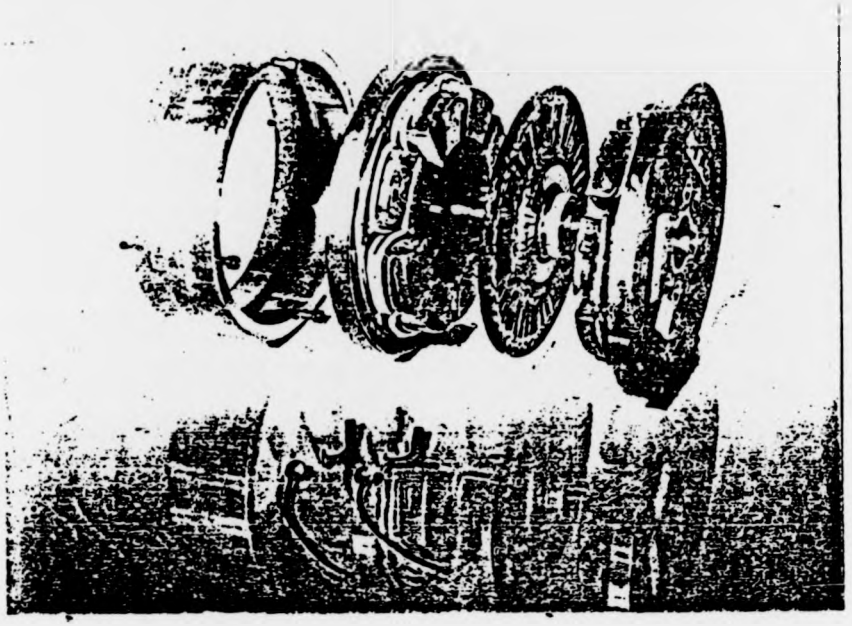

Fig. 2 : Disc-armature motor assembly

The design of a d.c. disc-armature motor is a straightforward process. With reference to Fig. 3 it has been found[5,7] that for maximum power the inner and outer radii of the magnet ring are related by:

$$r_2 = \sqrt{3}\, r_1 \qquad (1)$$

Also the power output of the motor has been found to be proportional to the cube of r_2, and thus for a given magnet material, voltage, speed and power an optimum value for r_2 can be found.

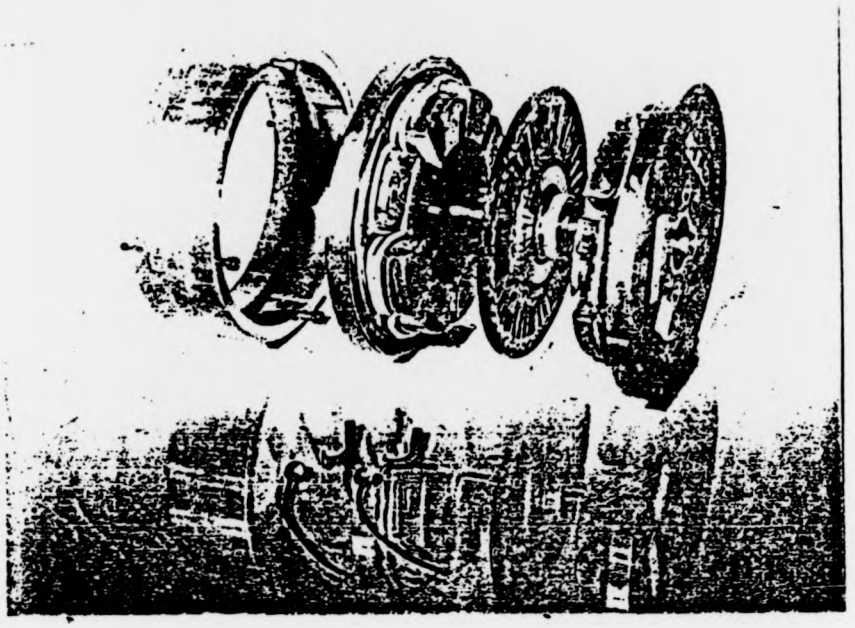

Fig. 2 : Disc-armature motor assembly

The design of a d.c. disc-armature motor is a straightforward process. With reference to Fig. 3 it has been found[5,7] that for maximum power the inner and outer radii of the magnet ring are related by:

$$r_2 = \sqrt{3}\, r_1 \qquad (1)$$

Also the power output of the motor has been found to be proportional to the cube of r_2, and thus for a given magnet material, voltage, speed and power an optimum value for r_2 can be found.

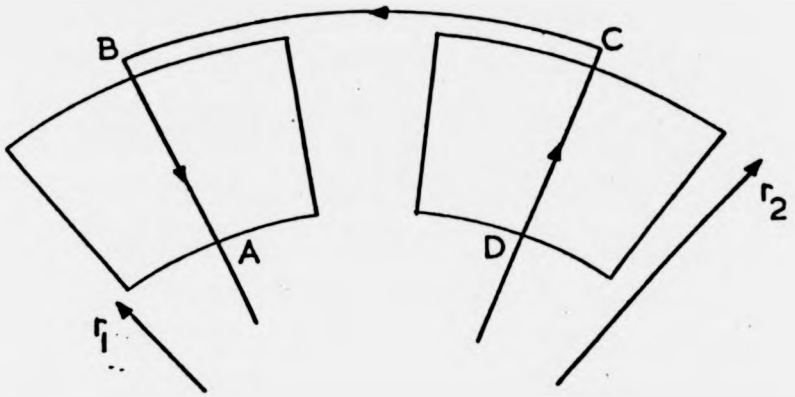

Fig. 3 : Schematic of magnets with a single-turn coil

The difference between r_2 and r_1 is the active-length of a conductor. The number of poles and coils are important factors in the design process. If too few poles are specified, the coil end-windings, represented by BC and DA in Fig. 3, become excessively long and bulky. This leads to high I^2R loss and poor copper utilization. For commutation reasons it is necessary to have a minimum number of coils per pole, and thus as the number of poles increases the number of coils and commutator segments also increase, leading to more costly designs and ultimately to impractical ones. Experience has shown that unless exceptional circumstances warrant it the minimum number of poles should be 6 and the maximum is determined partly by cost and partly by the size of the machine. Several computer routines have been written to assist this choice and these are described later.

CHOOSING THE RIGHT MAGNET MATERIAL FOR THE APPLICATION

A number of prototype motors has been built and evaluated with output powers from 90W to 2200W and speeds in the range 2500 rev/min to 10000 rev/min.

ted in Fig. 1, although some other alnico with lower working flux densities have been used. The applications involved have been varied. A motor for a ride-on lawnmower has been developed using ferrite magnets. This operates from a 12V battery and develops a power output of 950W at a speed of 2500 rev/min. A similar motor but working at 72V has also been constructed.

An electric cooling fan for an automobile engine also uses ferrite magnets. This develops 90W at 2500 rev/min and 14V. Instead of the more usual stationary flux-return ring this motor employs a disc of compressed iron powder fixed to the side of the armature remote from the magnets. This eliminates one of the air-gaps allowing a very compact unit to be constructed as shown in Fig. 4. The motor is actually held together by the attraction of the iron powder ring to the magnets.

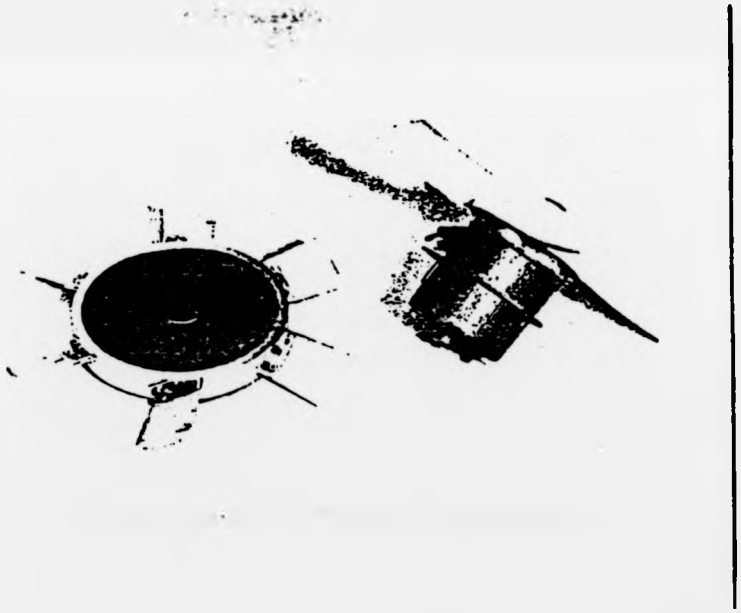

Fig. 4 : Radiator cooling fan motor with a conventional model

An interesting extension of this work is the possibility of loading the armature encapsulating material with iron powder[8]. Although some eddy current and hysteresis loss is introduced the effective air-gap length is considerably reduced.

In the prototypes discussed above the flux density of the ferrite material is suitable for the application involved and machines of short axial length were produced. This was not the case however when a high torque-to-inertia motor was considered. A 90V, 320W motor was required which would accelerate an inertia load from rest to 6000 rev/min in 300 ms and decelerate from this speed to rest in 200 ms. Clearly this performance depends on the inertia of the armature and a very thin armature disc has to be specified. As there is relatively little copper in the armature the highest flux density possible is required and magnets of the Alnico B type were chosen. Due to the low coercivity of this material even a small air-gap needs a long magnet length and Fig. 2 shows how the magnets have been divided so that one half is situated on each side of the armature.

Under construction at present is a high-power disc motor intended for use as a traction motor. It will have an output of 7500 W at 3400 rev/min and operate at 96 V. Its performance is to be evaluated in a small car. Another traction application is a direct-drive wheel motor for an electric moped. A design has been produced to develop an output of 750 W at 600 rev/min and 24 V. In both traction applications a size limitation is imposed necessitating the use of the Alnico-type material. Furthermore, high efficiency which is so important in this field can be more readily achieved using Alnico. In contrast, design studies are also being carried out on automobile accessory applications where low cost is paramount and efficiency is of minor importance. In such conditions no material can compete with the

ferrites.

MAGNET COMPARISON AT THE DESIGN STAGE

To illustrate the differences in magnet materials in a more realistic way a particular motor specification is investigated using each of the above magnets in turn. The design chosen is the low-inertia prototype detailed above i.e. 320 W, 90 V, 6000 rev/min although it is recognized that the acceleration requirement will rarely be met. To make the comparison fairer the ideal magnetic working point is chosen in each case and thus no restriction on size is imposed. Table 3 shows the external diameter, magnet and copper weights, and relative magnet and copper costs of each design, with the cost of barium ferrite magnets represented as 100.

Table 3 : Comparison of magnet costs

Material	Motor Diameter	Copper Weight	Magnet Weight	Copper Cost	Magnet Cost
Barium Ferrite	205 mm	0.30 kg	0.15 kg	163	100
Polymer $SmCo_5$	182 mm	0.18 kg	0.13 kg	97	1800
Mn-Al-C	170 mm	0.17 kg	0.19 kg	92	*
$SmCo_5$	160 mm	0.15 kg	0.14 kg	81	5000
Alnico A	136 mm	0.08 kg	0.60 kg	43	2000
Alnico B	124 mm	0.07 kg	1.15 kg	38	4000

* No reliable information available at present

The magnet costs relate to the finished product and the cost advantage of specifying the ferrite material is immediately apparent although a larger motor results. With all other materials the cost of the copper is negligible in comparison with the magnets. It must be emphasized that the motor

application is of prime importance and the acceleration characteristics required of the low inertia design can only be achieved using Alnico B.

COMPUTER-AIDED DESIGN

The design of an electric motor by hand can be a tedious process, since for optimization purposes it is necessary to consider different numbers of poles, numbers of coils, wire gauges, etc. To overcome this problem several computer programs have been written which considerably ease the burden on the designer. In its most powerful form the program, when given the power, voltage and speed requirement produces a series of alternative designs in any or all of the magnet materials available. These designs encompass wide variations in the numbers of poles and coils, and all of them meet the original specification to within a given tolerance. This is normally the first stage of the procedure.

The designer would study the computer output with due regard to the motor application in terms of size limitation, economics or other factors. He can then return to the computer with more specific requirements including number of poles, magnet material and working point, or gauge of wire to be used. The alternative designs incorporating these restrictions are provided and the final stage of the process is the complete specification of one design with output including a set of predicted performance curves. The procedure is very flexible and has been of great value in the design of these motors. The results presented in Table 3 are all obtained using this process. Instead of spending a considerable time in arithmetic computation the designer is free to concentrate on the many other important aspects of his work.

REFERENCES

1. Bachmann, K., 1971. 'Cobalt-rare earths', International symposium on the properties of electrically conductive, magnetic materials.

2. Kubo, T., Ohtani, T., Kojima, S. and Kato, N., 1977. 'Anisotropic Mn-Al-C alloy permanent magnets can be machined and mass produced', Journal of Electronic Engineering, July 1977, 50-54.

3. Ohtani, T., et al, 1977. 'Magnetic properties of Mn-Al-C permanent magnet alloys', IEEE transactions on magnetics, Vol. May 13, 5 Sept. 1977.

4. Corbett, A.E., 1970. 'A disc-armature d.c. motor', EM70 Conference Publication, University of Dundee, 42.

5. Corbett, A.E., 1970. 'Disc-armature motors', Unpublished report, University of Warwick.

6. Corbett, A.E., and Mohammad, M.T., 1976. 'The disc-armature d.c. motor and its applications', IEE Conference Publication 136, Small Electrical Machines, 59-62.

7. Roerig, C.S., 1977. 'D.C. Disc-Motors', Unpublished report, University of Warwick.

8. Stott, G., 1971. 'Iron powder compacts for electromagnetic applications', M.Sc. thesis, University of Warwick.

Economic design of d.c. disc-armature traction motors

by A.E.Corbett and C.S.Roerig University of Warwick

The use of permanent-magnet material in the field of d.c. motors can often lead to a reduction in size, and therefore an increase in power-to-weight ratio, or in power density. Their use in electric vehicles, where low weight is very important, would thus seem highly appropriate. The d.c. disc-armature motor[1] offers a further advantage in that, as an ironless armature is used, the associated losses can be eliminated, resulting in a very high efficiency maintained over a wide range of operating conditions.

This motor has found various applications,[2] but its use as a traction machine has been the subject of much investigation.[3,4] The selection of magnet material to be used in the machine is often not a straightforward task as this choice can drastically affect the design of a motor of given specification in terms of size, efficiency, power density and cost. The purpose of this article is to highlight the aspects of motor performance and cost which are affected by this choice.

Magnet characteristics and performances

There are many types of permanent-magnet material available today, of widely differing magnetic characteristics and with considerable variation in cost. They range from the cheapest available — the ferrite types, which have the disadvantage of low working flux-density — to the high flux-density Alnicos, to the highly expensive rare-earth materials, for example $SmCo_5$. The selection of suitable material for disc-armature motors has been covered recently,[5] but the performance required from the motor obviously has considerable bearing on this choice.

It is important to recognise, however, particularly in electric ... cost is all-im... when comparing ... internal-combustion ... It is ...

necessary to operate it under conditions where the BH product, or energy product, is a maximum. This entails careful consideration at the design stage of such factors as working flux density, airgap and magnet dimensions. Deviation from this principle can result in the reduction of some aspect of motor performance, although this is sometimes justified. For example, higher efficiency can be obtained at the expense of an increase in magnet weight. This 'nonideal' mode of operation often leads to a more expensive machine as a larger quantity of magnet material will be required. In the disc armature motor the use of high flux-density magnets, such as Alnico, will generally result in higher efficiency, and such materials are often specified for this reason. However, as the motor is intrinsically an efficient machine the difference in efficiency between high and low flux-density motors need not be too pronounced.

Expensive choice

A recent study ...

Economic design of d.c. disc-armature traction motors

by A.E.Corbett and C.S.Roerig University of Warwick

The use of permanent-magnet material in the field of d.c. motors can often lead to a reduction in size, and therefore an increase in power-to-weight ratio, or in power density. Their use in electric vehicles, where low weight is very important, would thus seem highly appropriate. The d.c. disc-armature motor[1] offers a further advantage in that, as an ironless armature is used, the associated losses can be eliminated, resulting in a very high efficiency maintained over a wide range of operating conditions.

This motor has found various applications,[2] but its use as a traction machine has been the subject of much investigation.[3,4] The selection of magnet material to be used in the machine is often not a straightforward task as this choice can drastically affect the design of a motor of given specification in terms of size, efficiency, power density and cost. The purpose of this article is to highlight the aspects of motor performance and cost which are affected by this choice.

Magnet characteristics and performances

There are many types of permanent-magnet material available today, of widely differing magnetic characteristics and with considerable variation in cost. They range from the cheapest available – the ferrite types, which have the disadvantage of low working flux-density – to the high flux-density Alnicos, to the highly expensive rare-earth materials, for example $SmCo_5$. The selection of suitable material for disc-armature motors has been covered recently,[5] but the performance required from the motor obviously has considerable bearing on this choice.

It is important to recognise, however, that, particularly in electric vehicle applications, cost is all-important, especially when comparing such vehicles with internal-combustion-engined counterparts. It is thus the clear duty of the motor designer to minimise the cost of his designs, while maintaining acceptable performance. If a vehicle manufacturer is presented with two alternative motors, one with 5% higher efficiency but costing four times as much, there is little doubt as to which he will choose.

To get the best performance from any permanent-magnet material it is necessary to operate it under conditions where the BH product, or energy product, is a maximum. This entails careful consideration at the design stage of such factors as working flux-density, airgap and magnet dimensions. Deviation from this principle can result in the reduction of some aspect of motor performance, although this is sometimes justified. For example, higher efficiency can be obtained at the expense of an increase in magnet weight. This 'nonideal' mode of operation often leads to a more expensive machine as a larger quantity of magnet material will be required. In the disc-armature motor the use of high flux-density magnets, such as Alnico, will generally result in higher efficiency, and such materials are often specified for this reason. However, as the motor is intrinsically an efficient machine the difference in efficiency between high and low flux-density motors need not be too pronounced.

Expensive choice

A recent study[6] proposed disc-armature motor designs for traction using magnets of the Alnico and rare-earth types, and discounted the cheaper ferrite material. However, the cost penalty in specifying the former materials in traction applications weighs heavily against their use. Fortunately, it is possible to use ferrite material in the 'nonideal' condition outlined above to achieve motor designs of not only comparable performance but which are very much cheaper.

As an example of this technique the design specification used in the study[6] is considered, namely a 10·7 kW, 2630 rev/min motor, working at 240V and with an overall diameter of 420 mm. As indicated earlier it is necessary to use the (ferrite) magnet material inefficiently in order to achieve a higher working flux-density. It is possible, however, to design within the specified diameter a motor with ferrite magnets which has acceptable performance. The armature contains a larger amount of copper, and the overall length is just 20 mm greater than the extremely short rare-earth design.

Performance and cost

The power density of the ferrite design is a very respectable 440 W/kg, second only to the rare-earth motor at 670 W/kg, and 2·5 times that of the Alnico 5-7 design.

The relative costs are difficult to ascertain owing to the fluctuating price of cobalt used in Alnico and rare-earth material. Based on information available at the time of writing, the cost of the ferrite magnets would be £21, that of Alnico 9 £300 and Alnico 5-7 £450, while the rare-earth magnets would cost £430-470. The cost advantage of specifying the ferrite material is immediately apparent.

In terms of efficiency the difference is not so great. All the motors have a very high efficiency (greater than 90%) and as expected Alnico magnets give the highest value. The rare-earth design has a 1% reduction in efficiency compared with Alnico, while the ferrite design yields some 4% less.

Careful design

In conclusion, therefore, it has been shown that far from being discounted for use in traction applications, careful design using ferrite can result in a considerable cost benefit. The small reduction in efficiency is acceptable for most applications and further research and development into disc-armature motors is being undertaken with the expectation that the results will benefit the electric vehicle industry as a whole.

At a time when a common criticism levelled at electric vehicles is one based on economic factors, every attempt must be made to ensure that initial costs as well as running costs are as competitive as possible.

References

1 CARTER, A.H., and CORBETT, A.E.: 'Electric motor'. British Patent 1231782, 1971

2 CORBETT, A.E., and MOHAMMAD, M.T.: 'The disc-armature d.c. motor and its applications'. IEE Conf. Publ. 136, 1976, pp. 59-62

3 CAMPBELL, P., and CORBETT, A.E.: 'The pancake motor' *Automotive Des. Eng.*, July/August 1974

4 CORBETT, A.E., and LEE, G.A.: 'Development of a hybrid electric vehicle using high efficiency disc-motors'. Presented at the International Conference on Electric Vehicle Development, London, November 1979

5 CORBETT, A.E., and ROERIG, C.S.: 'Selecting permanent magnet materials for disc-armature d.c. motors'. Presented at the International Conference on Electrical Machines, Brussels, September 1978

6 CAMPBELL, P.: 'Permanent-magnet motors for electric vehicles', *Electric Vehicle Developments*, September 1979, 3, pp.1-3

Aubrey Corbett and Chris Roerig are with the Department of Engineering, University of Warwick, Coventry CV4 7AL, England

Computer-Aided Design of Permanent Magnet Motors

A.E. Corbett, University of Warwick
C.S. Roerig, Moore Reed and Co. Ltd.

Introduction

Permanent magnets have long been used to supply the field excitation of rotating electrical machines and developments in recent years have led to a widening of the choice of available materials. In particular, very high energy densities have been achieved with combinations of the rare-earths and these are now specified in place of the more conventional ceramics or alloys in some applications. However in many other applications they must be ruled out on the grounds of cost alone. In the field of electric traction or automobile components, for example, cost is a very important factor and the inexpensive ferrite materials are usually specified. On the other hand, a servo system may require a high-performance stepper motor and in this case high energy-density magnets may well be used. Thus, any design routine must be flexible enough to incorporate a wide range of magnet materials and be able to work within the limitations imposed by the application (size, cost, performance etc.) to produce designs which meet the original specification. It must also be able to consider new magnetic materials as they become available and highlight the benefits, if any, of using them. Therefore some means of comparison of designs using both new and existing materials should also be possible.

The modern high-speed digital computer is an ideal base on which to build a design process of this nature and as an example a procedure developed for the design of axial field d.c. machines will be described. These machines have found varied applications (1,2) and are unconventional in that the armature is shaped like a disc and contains no iron (Fig. 1). Thus the magnetic air gap tends to be large compared with conventional machines and this often dictates the choice of magnet material.(3)

Optimum use of Permanent Magnets

Fig. 2 shows the demagnetisation characteristics for several types of magnet material. To achieve the maximum energy from a given volume of material the product of the flux density and magnetising force should be a maximum. This ideal working point, BH_{max}, is shown for each material. It is, however, not always possible to achieve these conditions in practice and a motor specification often dictates some departure from BH_{max}. If a high torque-to-inertia ratio is required an alloy magnet may be used well up the demagnetisation curve simply to achieve the highest possible working flux density. Another example is motors for battery electric traction. The efficiency of such a motor generally increases with the working flux density. As Alnico materials are usually too expensive to be considered in this application ferrite material may often be worked above the BH_{max} point on the curve to give some compromise between cost and good efficiency.

A disadvantage of Alnico is that in order to operate at BH_{max} it must either be magnetised in situ or keepers must be used. This is due to the non-linear characteristic of the demagnetisation curve and as can be seen from Fig. 2, ferrite and rare-earth materials do not suffer from this limitation. Further consideration of the choice of magnetic materials is given in references 3 and 4.

Computer Techniques

The advent of the digital computer not only eliminated many long and tedious hand calculations but also made possible optimisation techniques which were not previously attempted. It is to this type of application, where a set of

calculations may be performed many times over, that the computer is ideally suited. The design parameters of a motor, for example, could be given some initial values; from these the expected performance is calculated and compared with the required performance, and finally the design parameters are modified in some way to try and improve the agreement between required and calculated performance. The whole procedure is then repeated until the agreement is close enough for all practical purposes. Methods of this nature form the basis of many design programs or design 'software'.

When applied to the design of rotating electrical machines an added advantage is that changes in the design parameters (number of poles or coils, wire gauge etc.) may be made readily, and quickly assessed, and it is possible for a program to consider a wide range of these values in the search for the optimum design. The accuracy of the final design obviously depends on the mathematical relations used in the computer program; it is possible to spend many man-years developing software which is sufficiently accurate for general use.

When designing permanent magnet motors there must be some means available of storing data relating to the magnet material to be used, in particular the relevant portion of the B-H characteristic. This could be written into the computer program, although for general usage it will be found more convenient to store this information separately and access the relevant portion when required. Excursions about the BH_{max} point are easily allowed for in this way.

Once the software is written the next step is to run it in the most convenient way. Perhaps the most basic and familiar method is to punch out the program on cards, add cards containing the necessary data inputs (power and speed required, size limitations, etc.) and then allow a computer operator to handle the actual run. Information from the program (the required design parameters) will normally be printed out on the central lineprinter and returned to the designer for consideration. A faster method entailing more user involvement is to write an 'interactive' computer program and then use a remote terminal (Fig. 3). Here, the designer types in his requirements and the program is executed immediately with the results displayed at the terminal screen, and also printed out if required. An important benefit from this technique is the facility to alter any of the design specifications whilst at the terminal - the effect of any change may be assessed a few seconds after it is made. All the software described here is of this interactive nature.

A further advantage in using the computer is its ability for graphical representation. This enables design results to be considered in a more meaningful form and a wealth of software has been written (by others!) and some incorporated into the design procedure which will give the predicted performance curves. Graphical output may be seen at the terminal or, more usually, as hard copy from a plotting device. Of all the benefits that the digital computer can bring to a design process it is the time saved that is most apparent. To consider two or three design alternatives, even with the aid of a calculator, can be a long process. The computer program that has been developed covers some 40 different alternatives in less than seven seconds of computer time, although the hard copy will take slightly longer to produce. With the introduction of low-cost, microprocessor-based desk top computers it may soon be common for even small companies to have such design facilities in-house.

Software Development

The development of computer programs suitable for the design of axial-field d.c. machines has taken place over a period of years with continued refinement and updating of the routines. The first step was to write a program which would determine the performance of a machine when given all the design data. (5) This was a

set of one-off calculations and the onus was very much on the designer in his choice of parameters. There was of course no guarantee that the motor would perform as intended, and usually several attempts were needed to give a satisfactory result. It was decided to improve on this by allowing for parameter change and introducing the interactive facility so that the designer is still able to make changes according to his experience. This is now the second stage of a two-stage procedure and the first stage presents alternative designs encompassing a wide variation in parameters such as poles, coils etc. The only input needed here is the power, voltage and speed required, along with the choice of magnet material. All of the resulting designs will meet the original specification to within a given tolerance. Restrictions may be imposed if necessary and as the program is fully interactive prompts are supplied where appropriate so that the operator need have no working knowledge of computer programming. Selected parameters are varied over a wide range and the results are output as described earlier.

A simplified flowchart of this stage is given in Fig. 4 and although the program necessarily contains much mathematical manipulation the basic relationships may be summarised as follows. With reference to Figs. 4 and 5:-

$$R_2 = f(n,P,V,B_m)$$

where R_2 is the outer active radius, n is the rotational speed, P the power output, V the operating voltage and B_m the flux density on the magnet BH curve.

$$R_1 = R_2/\sqrt{3}$$

where R_1 is the inner active radius. This relation has been found (6) to give maximum power for a given motor diameter.

The initial number of poles depends on the value of R_2, while the wire gauge, number of parallel paths, coils and turns per coil are chosen according to the power, voltage and speed. The airgap is determined from the gauge of wire specified with an allowance made for disc thickness and a suitable running clearance. The magnet dimensions may now be calculated from the number of poles, airgap, R_2 and the operating point on the BH curve.

The predicted power and speed are then calculated and compared with the required values. If agreement is not close enough a correction factor is applied and the entire procedure repeated. When one particular design has been finalised the results are stored and new values of poles and/or coils taken. These values override those set initially. After all variations have been allowed for a complete set of results is output with an indication of the optimum designs in terms of efficiency and power density (power per unit weight). Although this summary is extremely condensed it does represent the iterative nature of the process.

The second stage of the design procedure may be considered even more briefly. Bascially data derived from stage one is input, with the option of modification to any parameter. The performance is calculated and the results output as before with the option of graphics. Additional modifications may then be made and the process repeated. A flowchart is given in Fig. 6. Examples of numerical and graphical results are shown in Figs. 7 and 8, respectively.

Practical Application

Many machines have been designed and built using this process and the applications include a low-inertia drive, automobile cooling fan, low power traction and a 20 kW traction motor illustrated in Fig. 9. The program has been successfully used to design motors with voltages in the range 12-240 V, powers in

the range 20 W - 20 kW, and speeds in the range 200 - 18000 rev/min. The only limitations are those imposed by the initial specification. For example, if a size limit is imposed the computer will try all reasonable means of producing a design, but if it cannot, then a message will be output to this effect.

Although one particular type of motor has been highlighted here, similar methods are applicable to conventional electrical machines. The principal advantages are that a large saving in time can be made, many design alternatives may be compared, excursions along the BH curve are catered for, and an assessment of the relative merits of different magnet materials may easily and quickly be made.

The software is simple enough to be operated by inexperienced personnel and there is also the possibility of using it as a learning tool, as tedious calculation is eliminated allowing concentration on the overall effect of change in design parameters.

References

1. Corbett, A.E., and Mohammad, M.T., 1976.
'The disc-armature d.c. motor and its applications', IEE Conference Publication 136, Small Electrical Machines, 59-62.

2. Ali, M.R.N., Corbett, A.E., Ozpolat, M.A., and Roerig, C.S., 1980.
'Design and performance of disc-armature d.c. motors for traction applications', Fifteenth Universities Power Engineering Conference, 3B2, Leicester.

3. Corbett, A.E., and Roerig, C.S., 1978.
'Selecting permanent magnet materials for disc-armature d.c. motors', International Conference on Electrical Machines, Brussels SP4/2.

4. Corbett, A.E., and Roerig, C.S., 1980.
'The economic design of disc-armature traction motors', Electric Vehicle Developments, 5, p8.

5. Turner, A.M., 1970.
'Computer aided design of d.c. disc-armature motors', Undergraduate thesis, University of Warwick.

6. Corbett, A.E., 1970.
'Disc-armature motors', University of Warwick report.

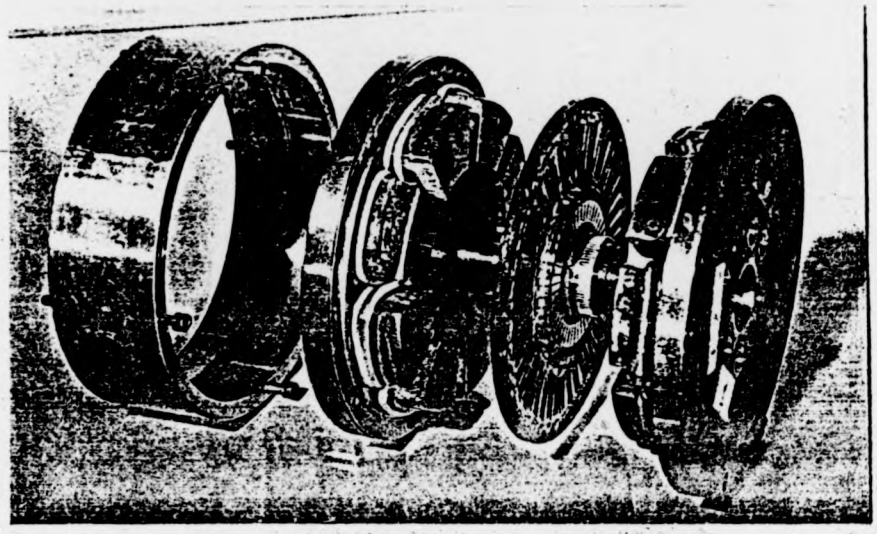

Fig. 1: Exploded view of disc-armature motor

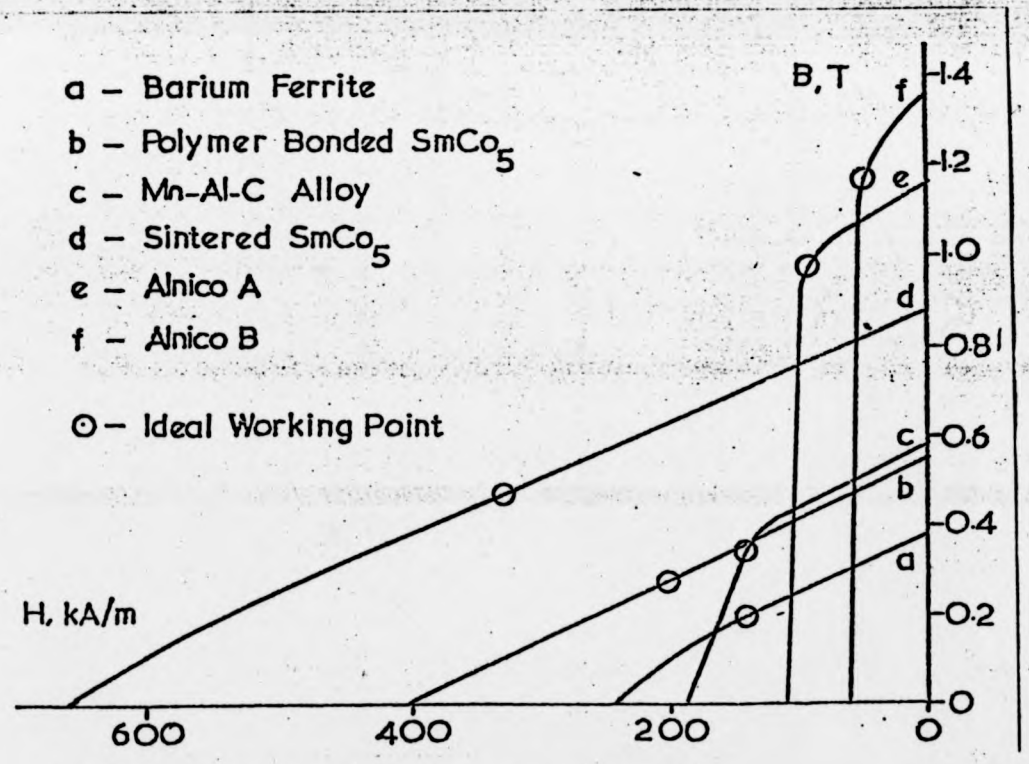

Fig. 2: B-H characteristics of p.m. materials

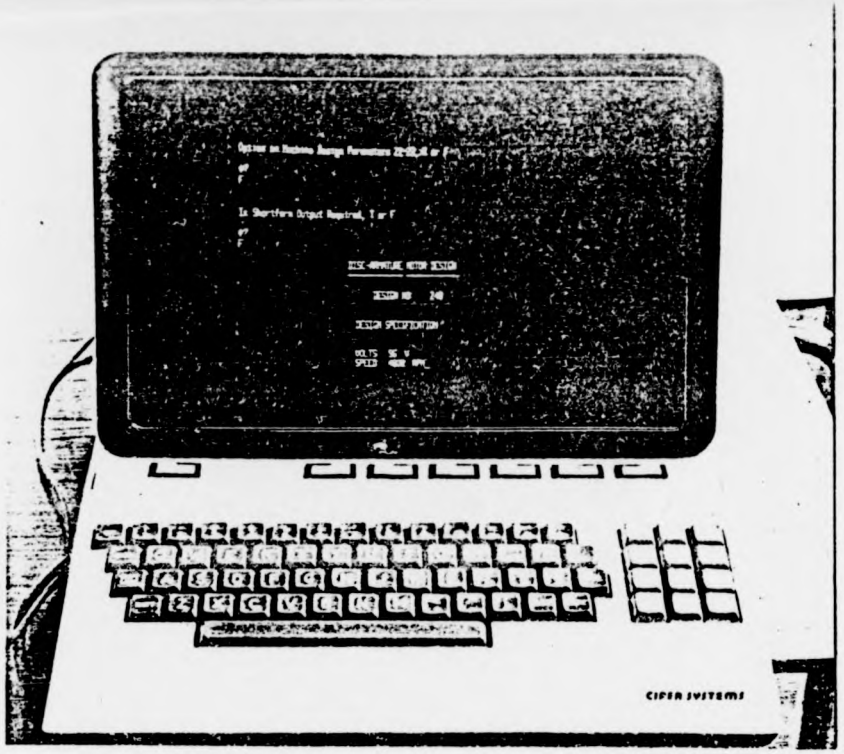

Fig. 3: Computer terminal

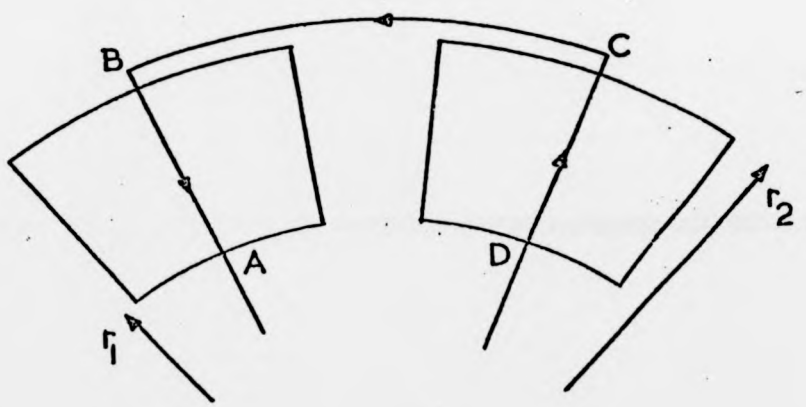

Fig. 5: Schematic of magnets with a single-turn coil

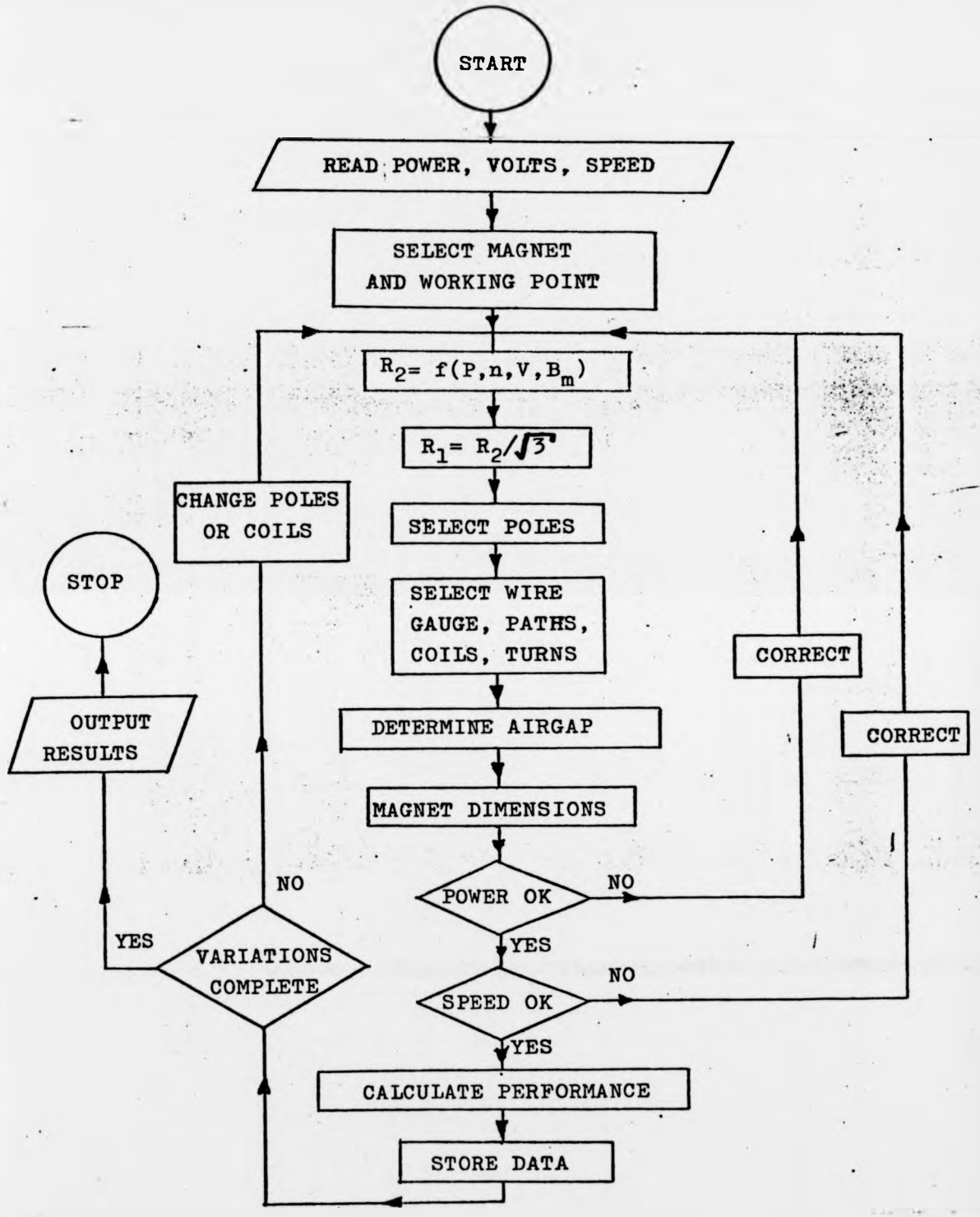

Fig. 4; Flowchart of Stage One Design

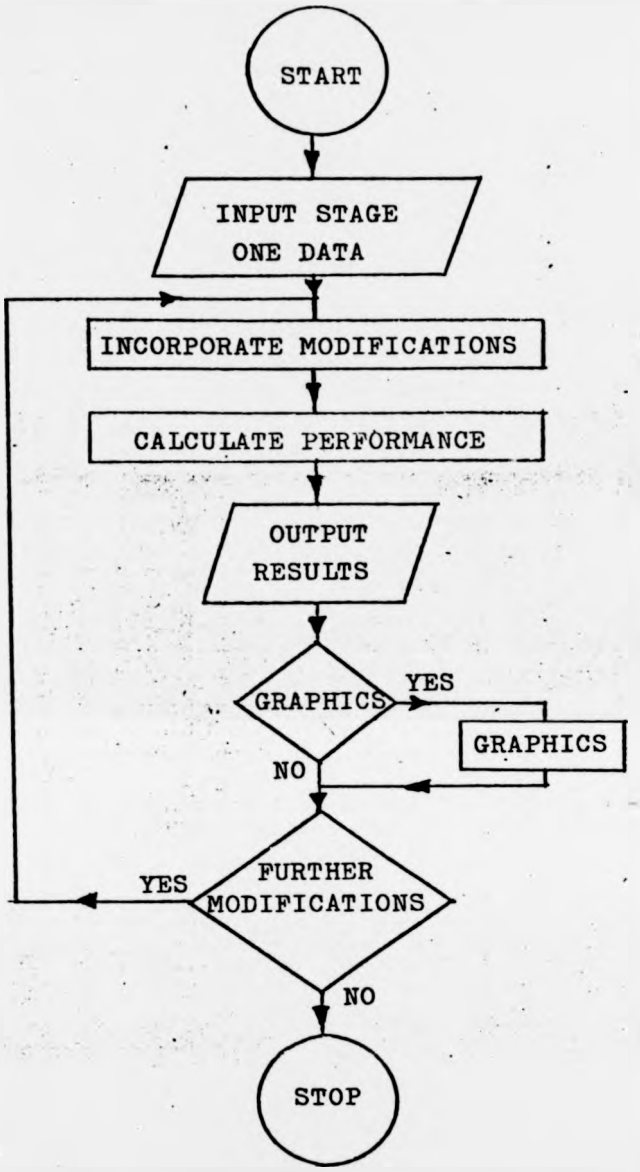

Fig. 6: Flowchart of Stage Two Design

DISC-ARMATURE MOTOR DESIGN

DESIGN NO: 235

DESIGN SPECIFICATION

OUTPUT: 7500. WATTS
VOLTS: 96. V
SPEED: 3400. RPM

DESIGN DATA

D2: 280. MM
D1: 171. MM
POLES: 8.

MAGNETIC CIRCUIT DATA

BM 0.642 TESLA
HM 70722. A/M
LCOEFF 1.30
LFACT 1.20
PHI .001811 WEBERS
ALPHA .76
LMAG 60.0 MM
WGTMAG 12.86 KG
THICK 12.00 MM
WGTFER 7.23 KG
GAP 9.00 MM
MAGDSY 7300. KG/M**3
BMS 1.80 TESLA

ELECTRIC CIRCUIT DATA

PATHS 4.
COILS 46.
TURNS 5.
Z 460.
GAUGE 1.80 MM
WGTWIR 1.83 KG
CRTDSY 8.0 A/MM**2
ARMCRT 81.43 AMPS
LOSS 275.69 WATTS
LAY 2
TEMP 75. DEGREES
SF .85
RARM 0.042 OHMS
ER 92.61 VOLTS

OUTPUT DATA

Fig. 7: Example of Computer Numerical Output

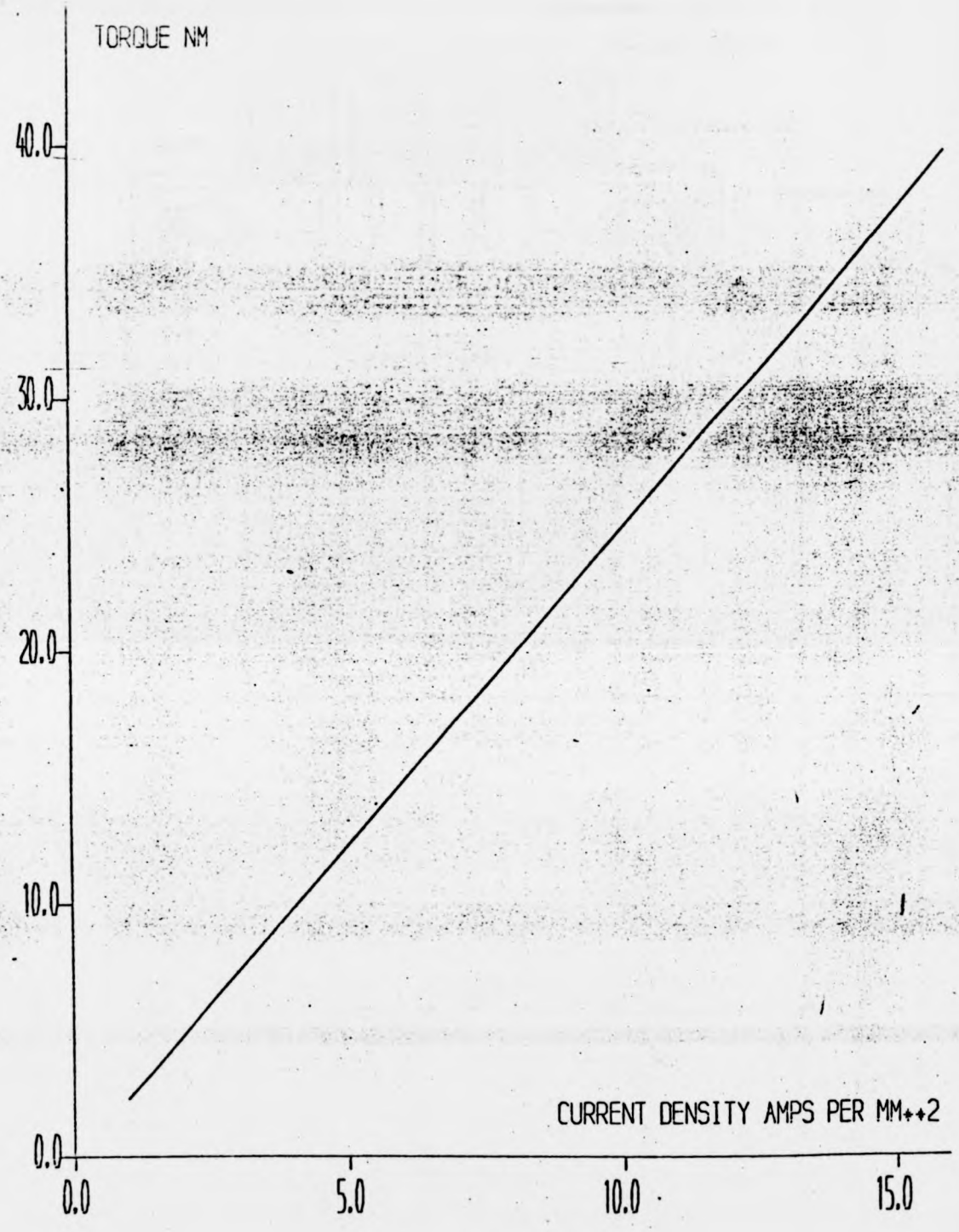

Fig. 8: Example of Computer Graphical Output

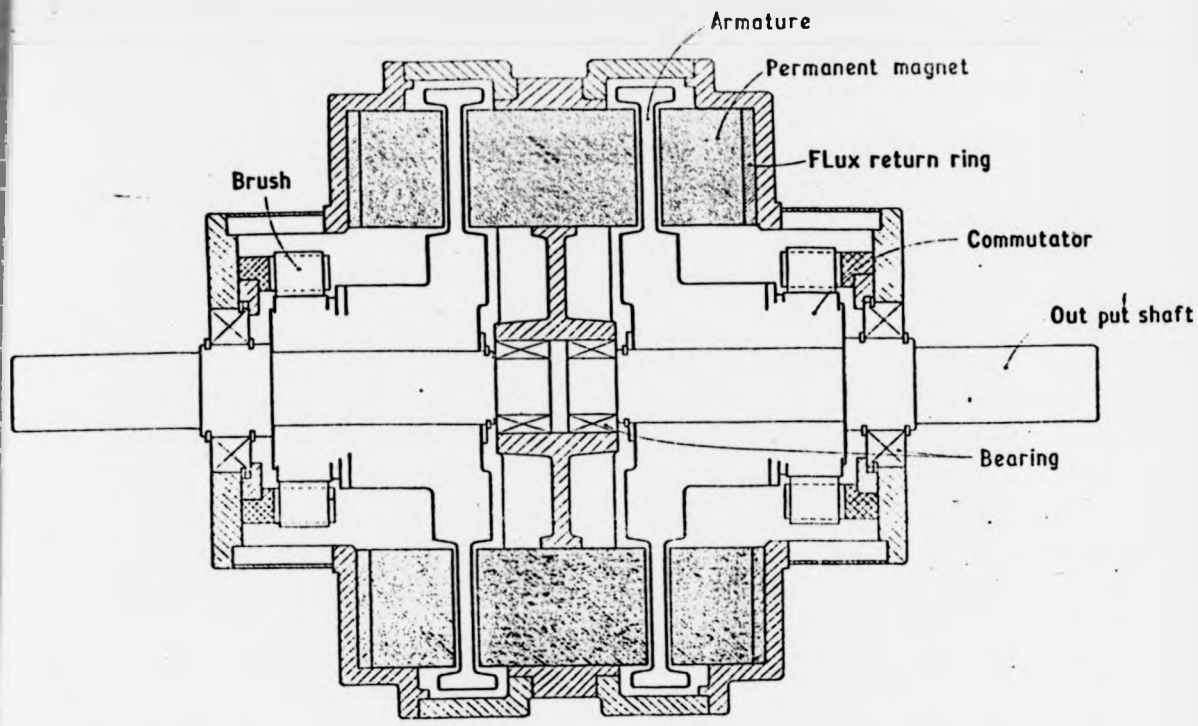

Fig. 9: Twin rotor disc-armature motor for hybrid car drive

DISC ARMATURE TRACTION MOTORS

M.R.N. Ali, C. Anscomb and A.E. Corbett (University of Warwick)
C.S. Roerig (Moore Reed and Co. Ltd.)

1. INTRODUCTION

While the major limitation on electric vehicle performance remains that imposed by the lead/acid battery every effort must be made to ensure the most efficient use of the energy available for vehicle propulsion. On an energy per unit weight basis petrol can have up to 200 times that of a lead/acid traction battery[1] with obvious advantages for road transportation. Two parameters of the electric traction motor which have considerable bearing on the overall vehicle performance are the efficiency and power density (ratio of motor power to motor weight). The disc armature d.c. motor is superior in both respects to the conventional series wound motor which has been an almost universal choice for battery electric traction applications.

The topology of the machine is radically different from conventional machines in that the active conductors run radially and are encapsulated in a plastic material (e.g. epoxy resin) to form a thin disc. It is thus necessary for the working magnetic flux to be oriented in the axial direction. The machine is multipolar with typically 6 to 12 poles. As no iron is contained in the armature the associated losses are eliminated but the magnetic airgap tends to be relatively long which makes it appropriate to use permanent magnets to supply the magnetic field. The elimination of eddy-current and hysteresis losses combined with permanent magnet excitation lead to the high efficiency and power density mentioned above. The machine differs from the printed circuit axial field motor in that wound, multi-turn coils are used with conventional commutator and brushgear. This has the advantage of potentially higher reliability, especially under overload conditions, as the conductors are shielded from the elements. It is also possible to consider all the usual armature winding patterns (lap, wave etc.). After winding the individual coils (Fig. 1) they are nested together, connected to the commutator (Fig. 2) and the complete assembly is then encapsulated in a purpose-built mould. The stator assembly is made by fixing the segment magnets to steel flux-return rings which can form part of the motor case. A complete motor assembly is illustrated in Fig. 3.

2. MAGNET MATERIAL CHOICE

As with any permanent magnet machine the choice of magnet material depends heavily on the machine application[2]. A wide range of materials is available and the characteristic demagnetisation curves of a representative selection are shown in Fig. 4. Machines using materials of higher remanance (or higher working flux) tend to have higher values of efficiency but unfortunately these materials are usually very expensive. The relatively long airgap in the machine, especially in the traction versions, lends itself to materials of high coercivity although these do not provide a high working flux density. Clearly a compromise has to be sought but as the machine is inherently efficient it has been found possible[3] to produce designs using the cheapest material available (Barium Ferrite) which compare very favourably with similar designs[4] using the more expensive materials (Alnico and rare-earth $SmCo_5$). The ferrite material is worked well above the BH_{max} point on the demagnetisation curve (that point corresponding to optimum material utilisation) and although this means a larger amount of magnet material will be required the low cost of the material does not preclude this with the benefit apparent as a higher working flux density. However, as the flux is still less than that obtained using any other material a higher copper content in the armature must be specified to compensate. This in turn will lead to higher copper losses and thus the machine will tend to have a slightly reduced efficiency. While it is difficult to generalise here an impression of the difference in efficiency between an Alnico-magnet disc motor, a ferrite-magnet disc motor and a conventional series wound motor may be gleaned from Fig. 5, and although for the reasons stated the efficiency of the ferrite disc motor will never be as good as the alnico version the improvement over the series machine is quite dramatic. One method of reducing the effective length of the airgap in the machine, and thus the amount of magnet material required is to introduce iron powder into the epoxy resin used for encapsulating the armature[5]. However, this also introduces eddy-current and hysteresis losses and results in magnetic pull between stator and rotor.

3. USE IN BATTERY ELECTRIC TRACTION

In the original patent for the design of the machine[6] electric traction was mentioned as a specific application and the early prototypes were built for this purpose[7,8] although other, very different applications have also been found[9]. Of particular interest is the concept of motorised

wheel units[8] where the electrical machine is situated adjacent to the driven wheel and becomes part of the vehicle unsprung weight (Fig. 6). The unit should be as light as possible and thus the electric motor is designed to have a very high operating speed (in excess of 10,000 rev/min). Suitable gearing must, of course, be interposed between motor and road-wheel. More recent work has employed the more conventional layout of an inboard motor driving the wheels of the vehicle through reduction gearing. (Any solution involving direct drive of the road wheels generally necessitates the specification of a heavy and inefficient machine.)

Various projects have been established to demonstrate the benefits of drives using disc-armature motors. A machine rated at 96 V, 7.5 kW and 3400 rev/min has been built for evaluation in a small electric car based on the Reliant Robin. In this project the disc motor is being compared with an equivalent series-wound motor with both machines designed to drive through the existing 4-speed gearbox and rear axle. The disc motor employs magnets of the alnico type (Hycomax 3) which allow a moderately high air-gap flux density and lead to a very high motor efficiency (Fig. 5). Unfortunately the cost of alnico material has increased quite dramatically during the course of the project owing to a large increase in the world price of cobalt, and it is considered that magnet material of this type will not become widespread in traction motor usage. A machine using ferrite magnets has been developed for use in a hybrid sports car, the Dragonfly Nova (Fig. 7). The motor is rated at 96 V, 20 kW, 4000 rev/min and is novel in that two rotating armatures are used in a common magnetic circuit. The motor has two independent output shafts which power the rear wheels through belt-reduction gearing thereby eliminating the need for a mechanical differential gear. Significant savings in weight and cost result from adopting the twin-rotor arrangement rather than two separate motors. The vehicle also employs a disc-armature generator having many parts which are common to the motor.

Prototypes for lower power traction applications have been produced including machines rated at 12 V, 900 W, 2500 rev/min; 72 V, 1100 W, 2500 rev/min; 24 V, 130 W, 2000 rev/min and 20 V, 180 W, 4000 rev/min.

4. MOTOR PERFORMANCE

Although different in construction the disc armature motor obeys the same fundamental electromagnetic laws as any rotating electrical machine. As permanent magnets are used to provide a constant magnetic field the operating characteristics of the machine are quite straightforward.

Essentially, the rotational speed is proportional to the applied voltage and the torque developed is proportional to the current drawn. At any constant applied voltage the speed falls only slightly as the torque and current increase. The field distortion caused by armature reaction effects is negligible as the air-cored coils and large number of poles means that the demagnetising force per pole is quite small. Similarly, no permanent demagnetisation effects have been recorded with any motor of this type. The low inductance of the armature allows good commutation and thus machines with high rotational speeds may be considered, leading to high specific outputs. As the armature reaction field is negligible the brush position may be set on the neutral axis thus allowing regeneration and motor reversal to be accomplished easily. As can be seen from Fig. 5 the high motor efficiency is maintained over a wide range of power output.

An important factor in traction applications is the thermal behaviour of the motor especially when related to conditions of overload. Conventional motors have a large mass of iron in the rotor to absorb the heat produced by the armature windings. By comparison the heat storage capability of a disc armature motor is poor and the thermal performance must be based upon how quickly heat from the armature can be dissipated. The use of a permanent magnet field means, of course, that there is no heating from field windings. The armature encapsulation material must be able to withstand high temperatures without undue flexing, but it must also be able to accommodate expansion of the copper it surrounds. Good heat transfer results from the armature conductors being close to the surface of the disc and the large surface area presented by the disc geometry. The naturally induced radial airflow can also assist in the cooling process with forced cooling possible under particularly arduous conditions of operation. Extensive tests have been carried out on prototype machines in order to investigate the performance parameters thoroughly and accurately. These include measurement of armature and case temperatures under various loading conditions and it has been found possible[10] to operate the motor with armature temperatures in excess of 100^{o} C. It is necessary however to take into account the reduction in flux density at these temperatures, particularly in the case of ferrite magnets whose reversible coefficient of demagnetisation with temperature is approximately 10 times that of alnico materials.

5. MACHINE DESIGN

The design of a disc armature motor is based upon two fundamental relationships. With reference to Fig. 8 these are:

$$P \propto r_2^3 \qquad (1)$$

where P is the output power and r_2 the outer active radius (the outer radius of the magnet ring).

$$r_2 = \sqrt{3}\, r_1 \qquad (2)$$

where r_1 is the inner active radius. Equation (2) has been found[11] to yield the maximum power output for a given machine diameter. The constant of proportionality in equation (1) depends on such parameters as magnet choice, winding details, operating voltage etc., and it has been found possible[12] to derive an equation relating these factors to yield the optimum value of r_2 for a given motor speed, power, voltage, and magnet material. Having determined r_2 (and thus r_1) in this manner there are still many design possibilities available with wide variation in the number of poles and coils, for example. Specifying too few poles leads to excessively long end-windings thereby increasing the associated I^2R loss. On the other hand, since for commutation reasons, a minimum number of coils per pole must be specified, a large number of poles can result in an excessive number of coils and commutator segments and ultimately in impractical solutions. Also magnetic leakage increases with pole number. It would certainly be a tedious process to design by hand even several of these options for optimisation purposes, but fortunately digital computing techniques can be used to advantage here. Several programs have been written which ease the burden on the motor designer and the most powerful version produces a series of alternative designs when given the power, speed and voltage requirement. In addition, the designs for optimum efficiency and power density are output separately and once a given design has been chosen a set of predicted performance curves may additionally be produced.[13]

6. MOTOR CONTROL

There are several methods of controlling the speed of a battery electric vehicle ranging from the simple but inefficient resistive control to complex and expensive electronic chopper circuits. The choice of

controller rests very much with the envisaged application. For a vehicle which runs for the majority of the time at maximum speed a combination of battery switching and resistive control would probably be the best option; for those intended to operate on public roads alongside conventional i.c. engined vehicles an efficient electronic chopper may well be the most appropriate solution. While battery switching and resistive control may easily be applied to disc armature motors care must be exercised if a chopper controller is to be used. The extremely low value of armature inductance means that a high degree of current ripple will be likely at conventional switching frequencies. This is exactly the opposite condition to that found in the series wound motor whose inductance assists in sustaining a relatively constant motor current. The problem may be overcome by specifying a higher switching frequency although this entails using a power transistor instead of the more usual thyristor. There is, however, a maximum switching rate that may be used with transistors and research is continuing into this important area of application.

7. CONCLUSIONS

The disc-armature motor has been shown to have significant advantages when used in traction applications. The efficiency and power density are improved over comparable d.c. machines and the motor performs well under conditions of overload. The design of such motors is now a straightforward process using CAD procedures and, although selecting control methods requires some care, considerable benefits are nevertheless available for battery electric vehicles.

8. ACKNOWLEDGEMENTS

The authors gratefully acknowledge the support of Cableform Ltd., Electro Dynamic Construction Co. Ltd., Lee-Dickens Ltd., Moore Reed and Co. Ltd., and the Science Research Council.

9. REFERENCES

1. Charlesworth, G., 'The energy and resource implications associated with the widespread use of electric vehicles', 1st International Conference on Electric Vehicle Development, 1, 2 May 1977.

2. Corbett, A.E., and Roerig, C.S., 'Selecting permanent magnet materials for disc-armature d.c. motors', International Conference on Electrical Machines, Brussels, SP4/2 Sept. 1978.

3. Corbett, A.E., and Roerig, C.S., 'The economic design of disc-armature traction motors', Electric Vehicle Developments, 5, March 1980.

4. Campbell, P., 'Permanent-magnet motors for electric vehicles', Electric Vehicle Developments, 3, September 1979.

5. Stott, G., 'Iron powder compacts for electromagnetic applications' M.Sc. thesis, University of Warwick, 1971.

6. Carter, A.H. and Corbett, A.E., 'Electric motor', British Patent 1231782, 1971.

7. Corbett, A.E., 'A disc-armature d.c. motor', EM70 Conference, Dundee, 1970.

8. Campbell, P., 'A new wheel motor for electric commuter cars', Electrical Review, Vol. 190, 1972.

9. Corbett, A.E., and Mohammad, M.T., 'The disc-armature d.c. motor and its applications', IEE Conference Publication 136, Small Electrical Machines, 1976.

10. Ali, M.R.N., Corbett, A.E., Ozpolat, M.A., and Roerig, C.S., 'Design and performance of d.c. disc-armature motors for traction applications', Fifteenth Universities Power Engineering Conference, 3B2, Leicester, March 1980.

11. Corbett, A.E., 'Disc-armature motors', University of Warwick report, 1970.

12. Roerig, C.S., 'D.C. disc-motors', University of Warwick report, 1977.

13. Corbett, A.E., and Roerig, C.S., 'Computer-aided design of permanent magnet motors', First United Kingdom Conference on Permanent Magnets, London, June 1980.

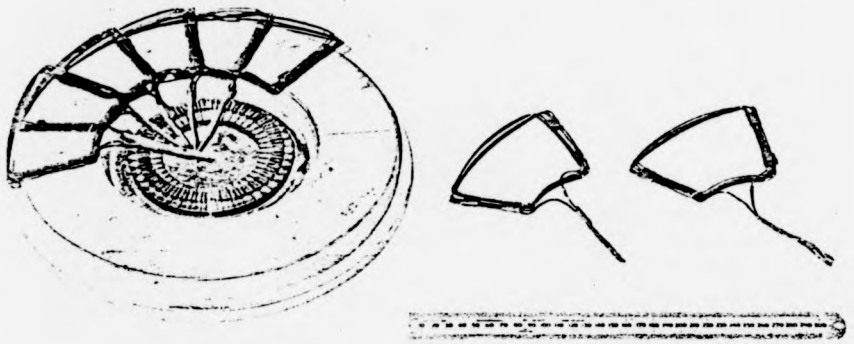

Fig. 1: Coils of armature winding

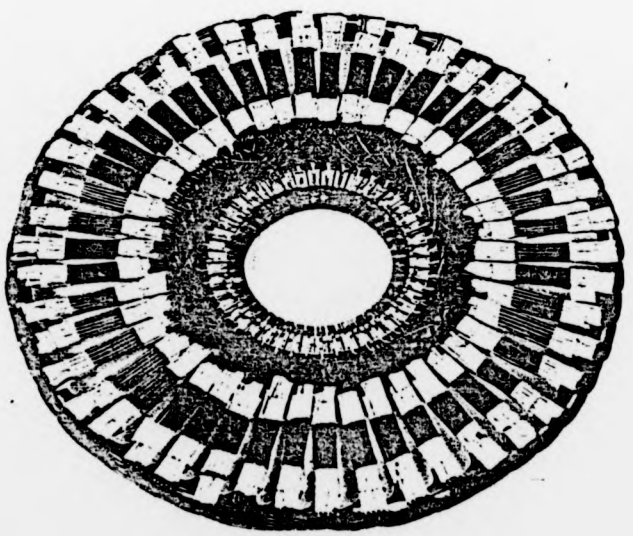

Fig. 2: Armature winding connected to commutator

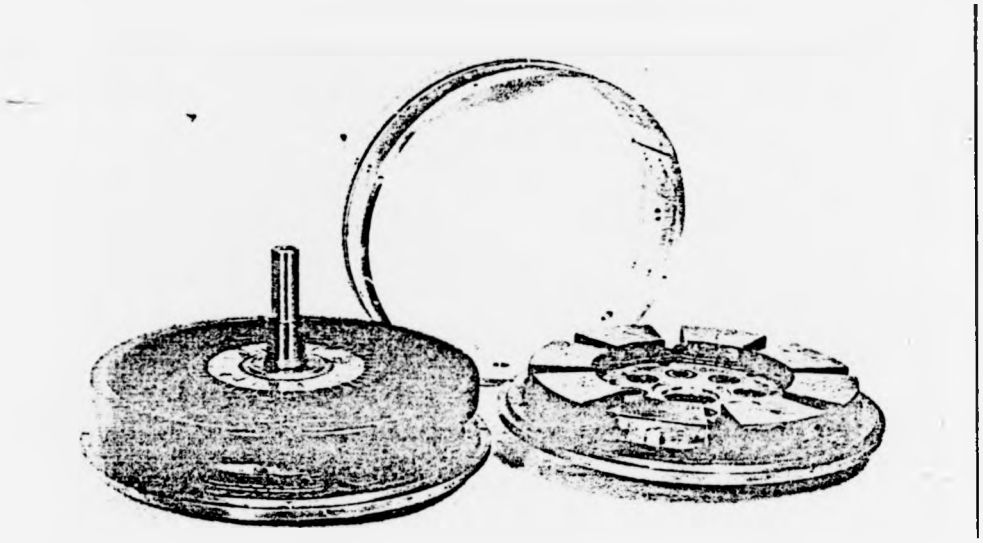

Fig. 3: Components of complete motor

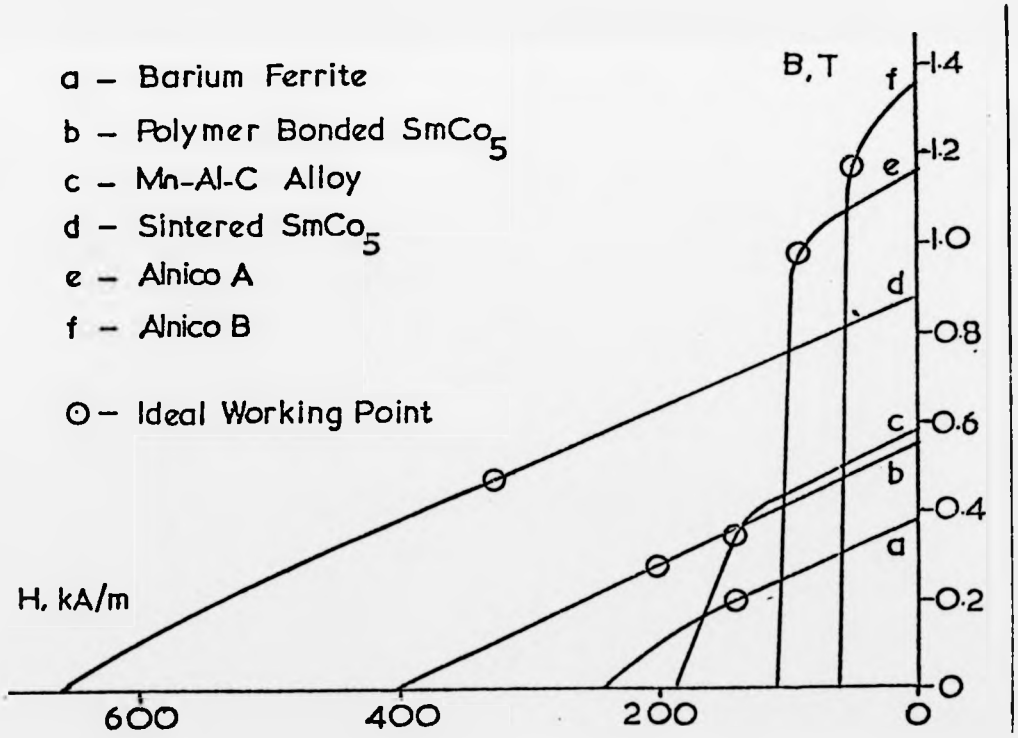

Fig. 4: Characteristics of permanent magnet materials

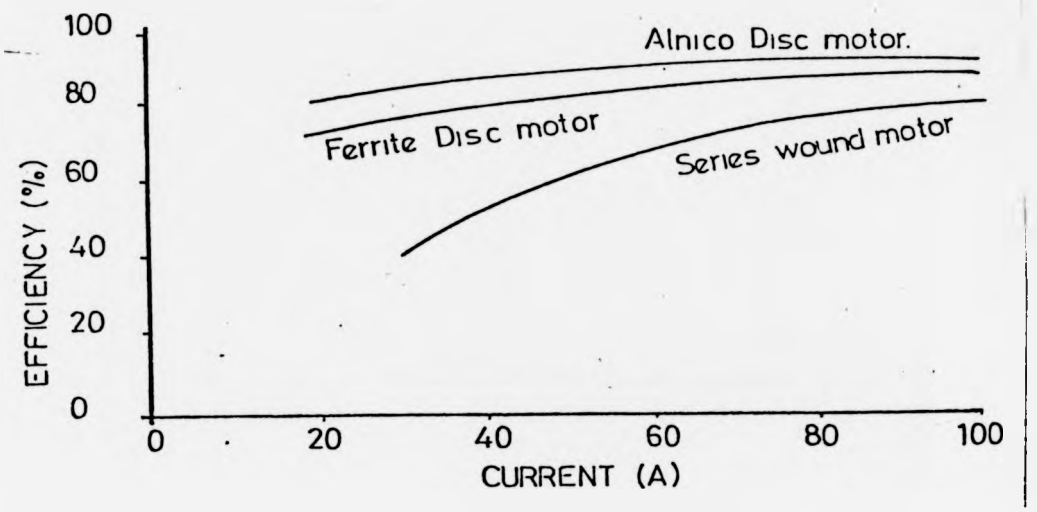

Fig. 5: Comparative motor efficiency characteristics

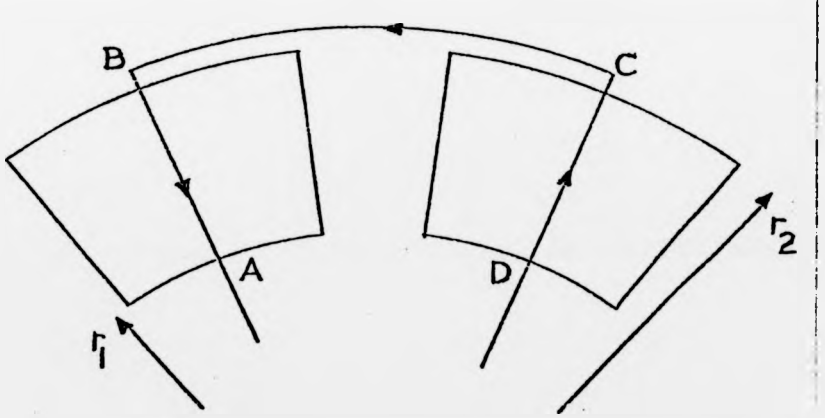

Fig. 8: Schematic of magnets with a single-turn coil

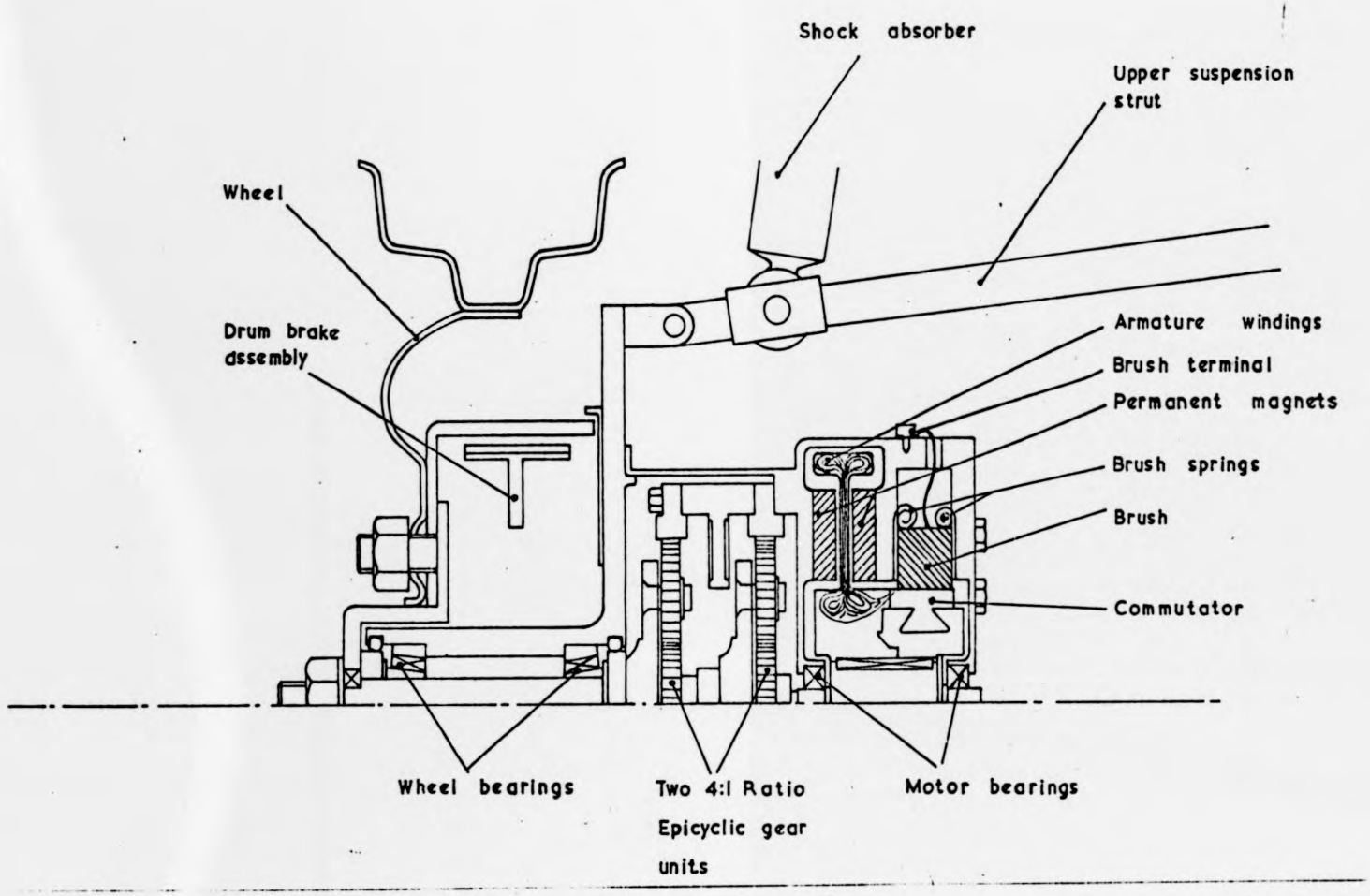

Fig. 6: Motorised wheel unit

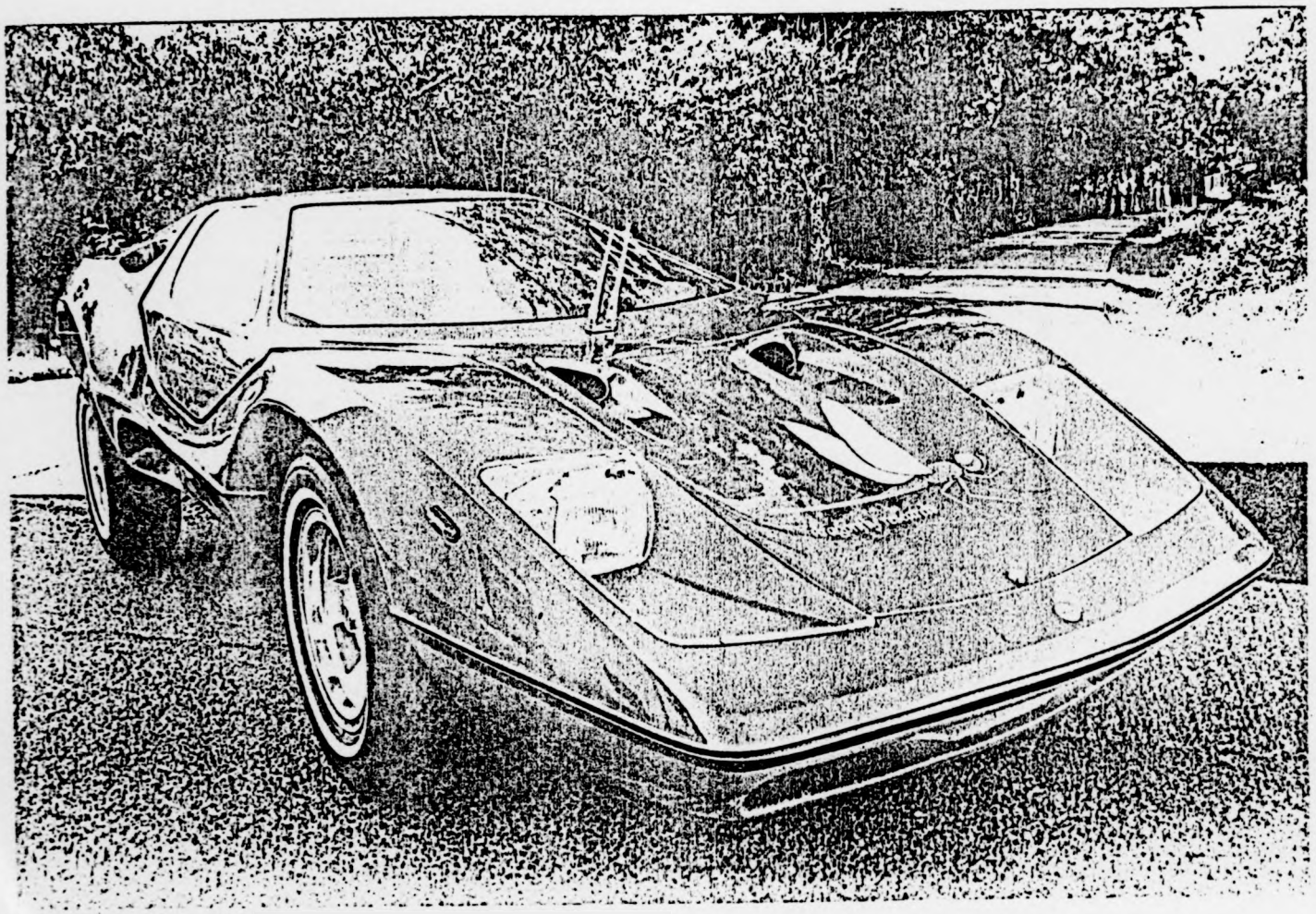

Fig. 7: The Dragonfly Nova hybrid sports car

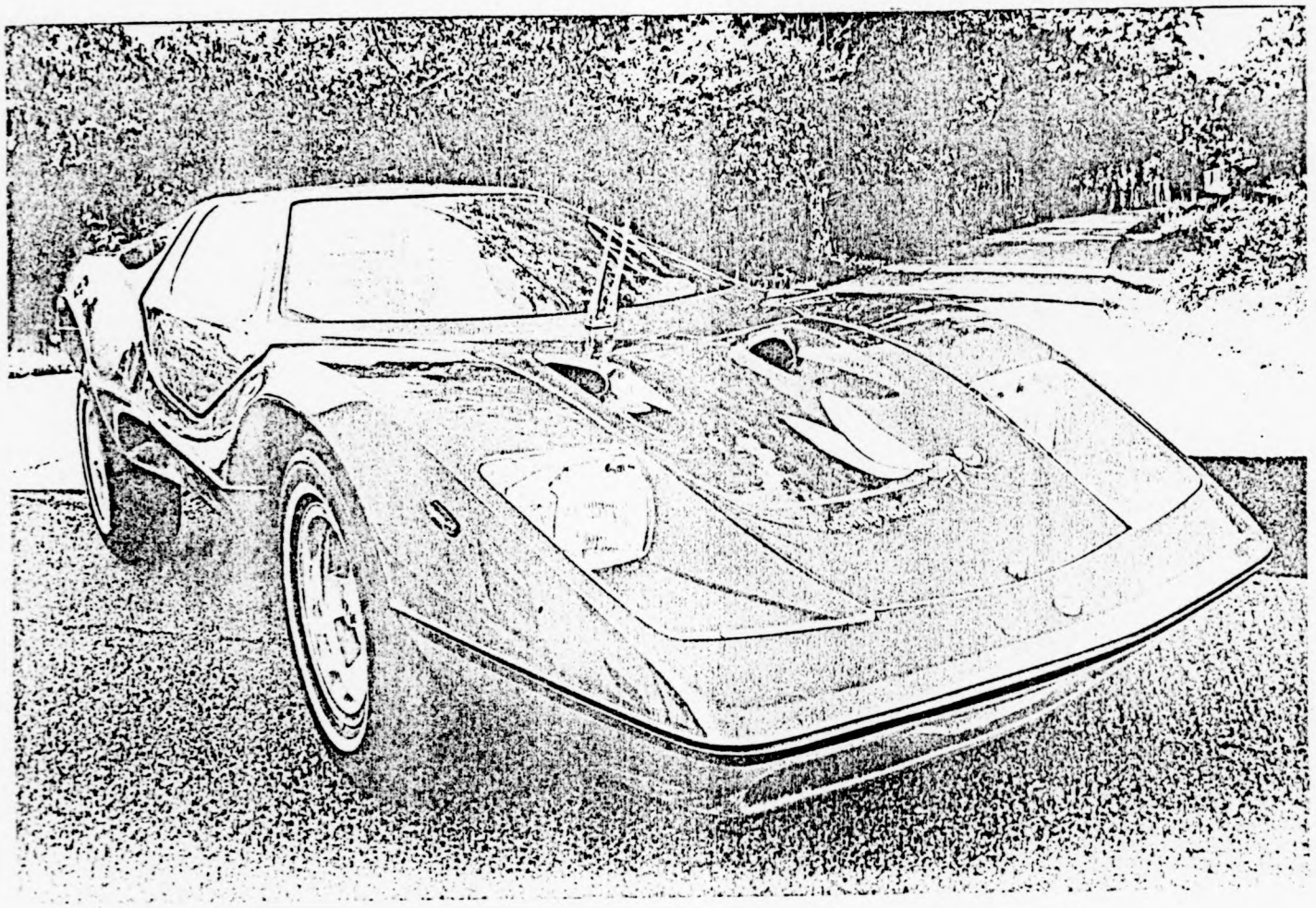

Fig. 7: The Dragonfly Nova hybrid sports car